Aspects of conformal field theories and quantum fields in AdS

Xiang Zhao

Thèse de doctorat

Aspects of Conformal Field Theories and Quantum Fields in AdS

XIANG ZHAO

Composition du Jury :

Christoph KOPPER Professeur, École Polytechnique (Centre de Physique Théorique)	Président
Christopher BEEM Associate Professor, Oxford University	Rapporteur
Nikolay BOBEV Associate Professor, KU Leuven	Rapporteur
Costas BACHAS Directeur de Recherche, École Normale Supérieure (Laboratoire de Physique)	Examinateur
Eric PERLMUTTER Professeur Assistant, CEA-Saclay (Institut de Physique Théorique)	Examinateur
Balt VAN REES Professeur, École Polytechnique (Centre de Physique Théorique)	Directeur de thèse

Acknowledgements

High energy physicists are used to infinities and are trained to deal with them. After four years of doctoral research training, however, my gratitude to my advisor, Balt van Rees, is still beyond any regularisation scheme that I know of.

Whenever I have questions, no matter how vague or trivial they may be, you can always address them lucidly and patiently. The clarity of your explanation and the agility of your thinking are what I could only wish to achieve half as good. Your style of approaching problems has deeply influenced and shaped my understanding of research. The frequent response from you when I explained to you the difficulties I encountered was a simple yet extremely powerful question: *Where does it come from?* It teaches me how to bootstrap myself from the swamp of mistakes and confusions. Your constant and ubiquitous support in my talk preparation, postdoc application and thesis defence arrangement are indispensable for me to come this far. Apart from physics and research skills, you also gave me countless support, help and care in daily life. I really enjoy the dinners and chats with you - we could have had more if there had not been the pandemic. It is of great fortune for me to be your student. You are my 師父(academic father) in the literal sense and beyond.

I would also like to thank my collaborators Shota Komatsu, Edoardo Lauria, Madalena Lemos, Pedro Liendo and Miguel F. Paulos. Edo, thank you for teaching me physics (especially about defects) and helping me throughout research, postdoc application and more. You were always there whenever I need help. Madalena seemed to know that sometimes I was hesitant to ask questions and you encouraged and taught me a lot. I also learned various very useful techniques from Shota's beautiful notes and Mathematica notebooks.

I was also fortunate to have enlightening conversations with other physicists: Stefano Cremonesi, Nabil Iqbal, Marco Meineri, Joao Penedones and Eric Perlmutter.

I want to thank Christoph Beem, Nikolay Bobev, Christoph Kopper, Costas Bachas and Eric Perlmutter for kindly agreeing to be in the committee of my thesis defence.

I am grateful to the secretaries in Ecole Polytechnique, Florence Auger, Fadila Debbou, Malika Lang, and in Durham University, especially Fiona Giblin.

Thanks should also go to my colleagues for interesting, enlightening discussions and wonderful dinners: Theresa Abl, Gabriele Dian, Hongliang Jiang, Daniel Lewis,

Kieran Macfarlane, Nam Nguyen, Davide Polvara, Jiaxin Qiao and Andrew Scoins.

I am fortunate to have a lot of wonderful conversations, interactions and fun with many friends, either known for a long time or newly made since my PhD: Dongyi An, Yang An, Zhiqi Bu, Penghao Cai, Mengzhi Chen, Peng Cheng, Junhuan Feng, Yushan Gao, Shuangli Guo, Yanliang Guo, Jingwei Jiang, Faqiang Li, Luyi Shen, Tinghui Tong and Yat Ho Yiu. I learned a lot and had great joy through playing snooker and pool with Luyi and Yat Ho.

Finally I want to thank my big family for their support, especially my parents and Leasa.

亲爱的爸妈：

我从小就在你们爱的包裹中成长，我的记忆中几乎找不到你们严厉的模样。无论是住在东组团时盒饭附赠的"洗锅水"汤，还是出国读书前的海鲜大餐，我从中品尝到的都是愉快和幸福。

无论大事小事，你们都尊重、支持我的个人选择，让我有充足的空间去探索和成长，却也会在选择是否接收自主招生加分的关键时刻纠正我错误的决定。你们为我取名"翔"，并成为了我展翅起飞前和意外跌落时背后坚固可靠的大地。

充盈且平衡的爱和自由，这是子女能从父母那里收到的最好的礼物。

谢谢你们！

Leasa, thank you for your love, understanding and support throughout the rise and fall of my PhD period and my life. Over the years the colour, warmth, optimism, sweetness and wisdom you have brought to the life of mine and ours are what I relied on to overcome all the difficulties I encountered.

You filled my world with sunshine, breezes and giggles.

You are my angel.

Abstract

This thesis studies the structure and the space of conformal field theories (CFTs), and more generally various properties of conformal correlation functions. It extends into multiple directions, both perturbative and non-perturbative, local and non-local, with and without supersymmetry.

The first aspect concerns the conformal correlation functions in d-dimensional spacetime and their relation to flat-space S-matrices in $(d + 1)$-dimensional spacetime. The connection is built up by considering a quantum field theory (QFT) in a fixed $(d + 1)$-dimensional Anti-de Sitter (AdS) background and sending the radius of the AdS curvature to infinity. That is, the central object to study is the flat-space limit of QFT in AdS. The analysis starts from taking the flat-space limit of the building blocks of Witten diagrams, namely the bulk-boundary and bulk-bulk propagators. This analysis leads to conjectural generic prescriptions to extracting flat-space physics from conformal correlators. Interestingly, the intuitional picture that a Witten diagram simply reduces to the corresponding Feynman diagram does not always hold, and the origin of this discrepancy lies in the bulk-bulk propagators: they could have two different flat-space limits. One of the limits always exists and reduces to Feynman propagator, while the other, when present, can diverge in the flat-space limit. This observation is tested by explicit examples, including four-point scalar contact, exchange and triangle Witten diagrams and the conjectures are expected to work whenever the scattering energy is large enough.

The second aspect studies the classification problem of conformal defects. The goal is to partially answer the question: given a bulk CFT and consistency conditions such as crossing symmetry and unitarity, what are the allowed conformal defects with a non-trivial coupling to the bulk? Analytic bootstrap techniques are applied to study a simplified version of this problem where in the bulk only a single free scalar field is considered. Analysis of various three-point functions among bulk and defect fields leads to the conclusion that almost all the n-point correlation functions of defect fields are completely fixed up to a potentially unfixed one-point function. This analysis also leads to an intermediate result in which it is proven that the n-point correlation functions of a conformal theory with a generalised free spectrum must be those of the generalised free field theory.

The third aspect studies the interplay between analyticity in spin in CFTs and

supersymmetry. Operator spectrum in a general unitary CFT is expected to be captured by a function analytic for spin $\ell > 1$ [1], and the operators are organised into various Regge trajectories. The presence of supersymmetry in general extends the region of analyticity in spin. The $6d$ $\mathcal{N} = (2,0)$ superconformal field theories (SCFTs) is considered as a concrete example, in which analyticity in spin is expected to hold down to $\ell > -3$. Detailed analysis of the four-point function of the the stress tensor supermultiplet uncovers an unexpected interplay between unprotected and protected multiplets: the stress tensor multiplet can be found on a long (unprotected) Regge trajectory when analytically continued to spin $\ell = -2$. In this study a general iterative bootstrap program is also established, which applies to all SCFTs that have a chiral algebra subsector.

Résumé

Cette thèse étudie la structure et l'espace des théories conformes des champs (CFT), et plus généralement diverses propriétés des fonctions de corrélation conformes. Elle s'étend dans de multiples directions, à la fois perturbatives et non perturbatives, locales et non locales, avec et sans supersymétrie.

Le premier aspect concerne les fonctions de corrélation conformes dans l'espace-temps de dimension d et leur relation avec les S-matrices de l'espace plat dans l'espace-temps de $(d + 1)$ dimensions. La connexion est établie en considérant une théorie quantique des champs (QFT) dans un arrière-plan Anti-de Sitter (AdS) de dimension fixe $(d + 1)$ et en envoyant le rayon de la courbure de l'AdS à l'infini. C'est-à-dire que l'objet central à étudier est la limite d'espace plat de QFT dans AdS. L'analyse commence en prenant la limite de l'espace plat des blocs de construction des diagrammes de Witten, à savoir les propagateurs vrac-à-limite et vrac-à-vrac. Cette analyse conduit à des prescriptions génériques conjecturales pour extraire la physique des espaces plats à partir de corrélateurs conformes. Fait intéressant, l'image intuitive qu'un diagramme de Witten réduit simplement au diagramme de Feynman correspondant ne tient pas toujours et l'origine de cet écart réside dans les propagateurs vrac-à-vrac: ils pourraient avoir deux limites d'espace plat différentes. L'une des limites existe toujours et se réduit au propagateur Feynman, tandis que l'autre, lorsqu'elle est présente, peut diverger dans la limite de l'espace plat. Cette observation est testée par des exemples explicites, y compris les diagrammes de Witten de contact scalaire à quatre points, d'échange et de triangle et les conjectures devraient fonctionner chaque fois que l'énergie de diffusion est suffisamment grande.

Le deuxième aspect étudie le problème de classification des défauts CFT. Le but est de répondre en partie à la question: étant donné une CFT du volume et des conditions de cohérence telles que la symétrie de croisement et l'unitarité, quels sont les défauts de conformité autorisés avec un couplage non trivial au volume? Des techniques de bootstrap analytiques sont appliquées pour étudier une version simplifiée de ce problème où, dans l'ensemble, un seul champ scalaire libre est considéré. L'analyse de diverses fonctions à trois points parmi les champs de volume et de défauts conduit à la conclusion que presque toutes les fonctions de corrélation à n points des champs de défauts sont complètement fixées jusqu'à une fonction à un point potentiellement non fixée. Cette analyse conduit également à un résultat

intermédiaire dans lequel il est prouvé que les fonctions de corrélation à n points d'une théorie conforme à spectre libre généralisé doivent être celles de la théorie du champ libre généralisée.

Le troisième aspect étudie l'interaction entre l'analyticité en spin dans les CFT et la supersymétrie. Le spectre des opérateurs dans une CFT unitaire générale devrait être capturé par une analyse de fonction pour le spin $\ell > 1$ [1], et les opérateurs sont organisés en diverses trajectoires de Regge. La présence de supersymétrie étend en général la région d'analyticité en spin. Les $6d$ $\mathcal{N} = (2,0)$ théories des champs superconformes (SCFT) sont considérées comme un exemple concret, dans lequel l'analyticité en spin devrait se maintenir à $\ell > -3$. Une analyse détaillée de la fonction à quatre points du supermultiplet du tenseur des contraintes révèle une interaction inattendue entre les multiplets non protégés et protégés: le multiplet du tenseur des contraintes peut être trouvé sur une longue trajectoire de Regge (non protégée) lorsqu'il continue analytiquement de tourner $\ell = 2$. Dans cette étude, un programme général de bootstrap itératif est également établi, qui s'applique à tous les SCFT qui ont un sous-secteur d'algèbre chirale.

List of Publications

This thesis is based on the following publications, to which all the authors contributed equally.

1. S. Komatsu, M. F. Paulos, B. C. Van Rees, and X. Zhao, *Landau diagrams in AdS and S-matrices from conformal correlators*, *JHEP* **11** (2020) 046, [arXiv:2007.13745]

2. E. Lauria, P. Liendo, B. C. Van Rees, and X. Zhao, *Line and surface defects for the free scalar field*, *JHEP* **01** (2021) 060, [arXiv:2005.02413]

3. M. Lemos, B. C. van Rees, and X. Zhao, *Regge trajectories for the (2,0) theories*, *accepted by JHEP* (12, 2021) [arXiv:2105.13361]

Contents

Chapter 1

Introduction

Symmetry lies at the heart of modern theoretical physics. This thesis focuses on one particular type of spacetime symmetry - *conformal symmetry*, which indicates invariance under Poincaré transformations as well as scale and special conformal transformations (a combination of inversion and translation). Quantum field theories (QFTs) invariant under conformal symmetry are called *conformal field theories* (CFTs). CFT is the central topic of this thesis, but before the detailed discussion perhaps in the first place one wonders: why are CFTs interesting?

1.1 Why Conformal Field Theory?

CFTs play an important role in many areas of physics. They describe the critical phenomena in statistical physics, capture the worldsheet dynamics of string theory, reside on one side of the AdS/CFT correspondence [5–9] and organise a vast territory of the space of QFTs. Here we focus on two main motivations for this thesis.

Signposts in the space of QFTs   Consider the renormalisation group (RG) flow of a QFT. At the infrared (IR) the QFT can either flow to a gapped phase (with a mass or length scale) or a gapless one, and the latter is called an IR *fixed point*. At an IR fixed point the correlation length diverges and the theory becomes scale invariant. In many cases, the scaling invariance gets enhanced to conformal invariance [10] and therefore the long distance dynamics of the theory is captured by a CFT. As the theory flows to the IR fixed point, the irrelevant operators becomes increasingly insignificant and eventually drop out. A generic fact is that most operators are irrelevant. Therefore, many theories distinct at the microscopic level are described by the same CFT in the IR and they belong to the the same *universality class*. Residing at the endpoints of many RG flows, CFTs serve as the signposts of the space of QFTs. Charting out the space of CFTs leads us towards the comprehensive understanding of the long-distance dynamics of almost any QFT that flows to a gapless phase.

Holographic Duality A full-fledged quantum mechanical description of gravity has been a dream of theoretical physicists for decades. The AdS/CFT correspondence provides a non-perturbative definition of quantum gravity in anti-de Sitter (AdS) space in terms of CFTs on the asymptotic boundary. According to the correspondence, the partition function in the bulk is equal to that on the boundary [6, 7]

$$Z_{\text{bulk}}[\phi_0] = Z_{\text{CFT}}[\phi_0],$$

where ϕ_0 denotes collectively the sources of operators in the CFT and boundary conditions of the fields in the bulk. By taking functional derivatives with respect to ϕ_0 and setting them to zero, one obtains equalities between correlation functions in the bulk and in the boundary CFT. Therefore, studying CFTs which have a holographic dual helps us to unveil the shape of quantum gravity.[1]

In addition, within this framework one can consider a scenario where the background AdS geometry is fixed, hence no gravitational dynamics in AdS space and no stress tensor present in the boundary theory. If one also sends the radius of AdS curvature to infinity so that the centre of AdS looks like a flat space, the boundary *conformal* theories (BCTs) will contain information about *non*-conformal flat-space physics in a spacetime of one dimension higher [13]. This can offer a different approach to understand, for example, the analytic structure of flat-space S-matrices from the conformal correlation functions whose analyticity is much better understood.

1.2   The Bootstrap Philosophy

Traditional field theories rely heavily on the Lagrangian formulation. As is taught in graduate courses on QFT, we can perturbatively calculate scattering amplitudes by expanding the interaction term in the Lagrangian, from tree-level amplitudes to higher loop corrections.

The bootstrap philosophy, on the other hand, takes a very different approach. In a very broad sense, the philosophy of the bootstrap is to rely solely on the symmetries and consistency conditions of the theory to solve it non-perturbatively. This has many advantages over the Lagrangian formulation because the power of the latter dims for strongly coupled theories. Moreover, there are intrinsically quantum theories that do not even have a Lagrangian description. These theories automatically fall out of reach of the Lagrangian approach but may still be accessible through the bootstrap approach.

---

[1]See, for example, [11, 12] for discussions on criteria for CFTs to have a holographic dual.

Theories without a Lagrangian A fact in favour of the bootstrap philosophy is the existence of non-Lagrangian theories. For example, the six-dimensional $\mathcal{N} = (2, 0)$ superconformal field theories (SCFTs) do not have any known local Lagrangian description. They were originally defined as the decoupling limit of IIB string theory and the interacting (2,0) theories are labelled by simply-laced Lie algebra $A_{N \geq 1}, D_{N \geq 4}, E_{6,7,8}$ [14].

At large N the (2,0) theories of type A_N and D_N are holographic dual of eleven-dimensional supergravity [5, 15, 16] and for finite N they offer a window into quantum gravity. Through dimensional reduction of (2,0) theories one can construct a vast landscape of lower dimensional supersymmetric field theories and dualities among them. For example, the *AGT correspondence* establishes novel connections between 4d $\mathcal{N} = 2$ class S theories and 2d CFTs [17].

Despite their significance in physics, (2,0) theories are very difficult to study using traditional QFT techniques, because they lack a local Lagrangian. One approach to attack this problem is to view the (2,0) theories as abstract CFTs and constrain them by consistency conditions such as crossing symmetry and unitarity. This approach bears the name of *conformal bootstrap* and we will apply it to study the Regge trajectories of (2,0) theories in Chapter 5. We will explain more about this in Section 2.10 and also apply analytic conformal bootstrap techniques in Chapter 4 to study CFTs with defect.

1.3 Outline

In Chapter 2 we review preliminaries for the main results of the thesis. We discuss the basics of $d > 2$ Euclidean conformal field theories (CFTs), the setup of putting a QFT in a fixed Anti-de Sitter (AdS) background, and the conformal Froissart-Gribov formula (Lorentzian inversion formula) and analyticity in spin.

Chapter 3 is devoted to the establishment of a position-space prescription to extracting flat-space S-matrices in $(d + 1)$-dimensional spacetime from conformal correlation functions in d-dimensional spacetime. The main idea is to put a QFT in a fixed AdS background and send the radius of the AdS curvature to infinity. We start from a heuristic and intuitional analysis of the flat-space limit of the building blocks of Witten diagrams, namely the bulk-boundary and bulk-bulk propagators. This analysis leads to our main conjectural prescriptions to extracting flat-space physics from conformal correlators, which are called *S-matrix conjecture* (3.2.17) and *Amplitude conjecture* (3.2.20). We then focus on the question of *When are the conjectures valid?* and test our conjectures with explicit examples, including contact, scalar exchange and scalar triangle Witten diagrams. At the perturbative level, the main subtlety about the validity region of the conjecture lies in the flat-space limit of the bulk-bulk propagator and we expect the conjectures to work whenever the scattering energy is large enough. In s-channel 2-to-2 scattering of identical scalar

particles, for example, this requires

$$|s - 4m^2| > 4m^2,$$

where s is the Mandelstam variable and m is the mass of external particles. For t and u-channel scattering, s in the above inequality gets replaced by Mandelstam t and u.

Chapter 4 studies the problem of classifying defect CFTs: given a bulk CFT and consistency conditions (crossing symmetry and unitarity), what are the allowed conformal defects with a non-trivial coupling to the bulk? In this chapter we apply analytic bootstrap techniques to study this problem for a single free scalar field living in the bulk. By analysing various three-point functions among bulk and defect fields, we find that almost all the n-point correlation functions of defect fields are completely fixed up to a potentially unfixed one-point function. As an intermediate result, we prove a theorem that the n-point correlation functions of a conformal theory with a generalized free spectrum must be those of the generalized free theory.

Chapter 5 studies the interplay between analyticity in spin in CFTs and supersymmetry. Analyticity in spin in CFTs is established by the Lorentzian inversion formula [1], whose boundary of validity region is controlled by the behaviour of conformal correlators in the Regge limit and is shown to be $\ell > 1$ in general. (See Section 2.14 for more details about this statement.) Adding supersymmetry in general softens the Regge behaviour and extends the analytic region of spin. In this chapter we apply this methodology to the six-dimensional $\mathcal{N} = (2, 0)$ superconformal field theories (SCFTs) and focus on the four-point function of the the stress tensor supermultiplet, for which the analyticity is extended to $\ell > -3$. The analysis of the Regge trajectories of superconformal primary and descendant operators uncovers an unexpected interplay between unprotected and protected multiplets - the stress tensor multiplet can be found on a long (unprotected) trajectory if we analytically continue it to spin $\ell = -2$. We also set up an iterative inversion procedure which can bootstrap CFT data entirely from the protected part of the four-point function. Our results suggest that most of the interacting, physical (2,0) theories should saturate the numerical upper bounds on CFT data given in [18]. However, the iterative inversion procedure does not distinguish between A-type and D-type theories, so we do not know which type of theories are close to being extremal. It would be interesting to improve the method to make the distinction available in the future.

Chapter 2

Preliminaries

In this chapter we discuss aspects of the non-perturbative formulation of conformal field theories (CFTs). We describe the conformal symmetry, both infinitesimal and finite, and examine how it constrains the structure of the theory, in particular the organisation of the local operators and the form of the correlation functions. We then introduce the idea of *conformal bootstrap* which is to carve out the space of theories non-perturbatively using consistency conditions such as crossing symmetry and unitarity. In particular we are interested in the bootstrap in the Lorentzian regime. The data describing the theory can be extracted from the so-called *Lorentzian inversion formula*.

We also discuss the connection between conformal correlation functions and flat-space S-matrices. The relation is built up by considering quantum field theories in Anti-de Sitter space (QFT in AdS) where the correlation functions are related to the conformal correlation functions living on the boundary of AdS. By taking the flat-space limit, the conformal correlation functions morph into S-matrices in flat space.

2.1 Conformal Transformations

2.1.1 Diffeomorphism

Consider a manifold $\mathcal{M}$ equipped with metric g. Under diffeomorphisms generated by the *conformal Killing vector fields* $\epsilon^\mu(x)\partial_\mu$, the metric is invariant up to a rescaling factor. More specifically, under transformation $x^\mu \to \tilde{x}^\mu$ generated by ϵ, the metric transforms as

$$g_{\mu\nu}(x) \to \tilde{g}_{\mu\nu}(\tilde{x}) = \frac{\partial x^\rho}{\partial \tilde{x}^\mu}\frac{\partial x^\sigma}{\partial \tilde{x}^\nu}g_{\rho\sigma}(x) = \Lambda(x)g_{\mu\nu}(x), \qquad (2.1.1)$$

where the spacetime indices $\mu = 1, 2, \ldots, d$.

Unless otherwise specified, in the following we will consider the case $d > 2$ and work in Euclidean space with $g_{\mu\nu}(x) = \delta_{\mu\nu}$. It then follows that the Jacobian of the

transformation (2.1.1) is proportional to an orthogonal matrix

$$\frac{\partial \tilde{x}^{\mu}}{\partial x^{\nu}}(x) = \Omega(x) R^{\mu}{}_{\nu}(x), \quad \Lambda(x) = \Omega(x)^{-2}, \; R^{\mu}{}_{\nu}(x) \in SO(d), \tag{2.1.2}$$

so locally a combination of scaling transformation and rotation.

For an infinitesimal transformation $x^{\mu} \to \tilde{x}^{\mu} = x^{\mu} + \epsilon^{\mu}(x)$, the last equality of (2.1.1) becomes, to the leading order in ϵ,

$$\Lambda(x)\delta_{\mu\nu} = \delta_{\mu\nu} - (\partial_{\mu}\epsilon_{\nu}(x) + \partial_{\nu}\epsilon_{\mu}(x)). \tag{2.1.3}$$

The scaling factor $\Lambda(x)$ can be determined by contracting the indices on both sides with $\delta^{\mu\nu}$ and this leads to the *conformal Killing equation*

$$\partial_{\mu}\epsilon_{\nu} + \partial_{\nu}\epsilon_{\mu} = \frac{2}{d}\partial \cdot \epsilon(x)\,\delta_{\mu\nu}. \tag{2.1.4}$$

The solutions to (2.1.4) are components of the conformal Killing vector fields and they are

$$
\begin{aligned}
\epsilon^{\mu}(x) &= a^{\mu} && \text{(translation)}\\
\epsilon^{\mu}(x) &= m^{\mu}{}_{\nu}x^{\nu} && \text{(rotation)}\\
\epsilon^{\mu}(x) &= \alpha x^{\mu} && \text{(dilatation)}\\
\epsilon^{\mu}(x) &= 2(x \cdot b)x^{\mu} - b^{\mu}x^2 && \text{(special conformal transformation)}
\end{aligned}
\tag{2.1.5}
$$

where $a^{\mu}, m^{\mu}{}_{\nu}, \alpha, b^{\mu}$ are constants and $m^{\mu}{}_{\nu}$ is antisymmetric. Exponentiating gives the finite transformations $x^{\mu} \to \tilde{x}^{\mu}(x)$ with

$$
\begin{aligned}
\tilde{x}^{\mu}(x) &= x^{\mu} + a^{\mu} && \text{(translation)}\\
\tilde{x}^{\mu}(x) &= R^{\mu}{}_{\nu}x^{\nu} && \text{(rotation)}\\
\tilde{x}^{\mu}(x) &= \alpha x^{\mu} && \text{(dilatation)}\\
\tilde{x}^{\mu}(x) &= \frac{x^{\mu} - b^{\mu}x^2}{1 - 2(b \cdot x) + b^2 x^2} && \text{(special conformal transformation)}
\end{aligned}
\tag{2.1.6}
$$

In particular, special conformal transformations (SCT) can also be written as

$$\frac{\tilde{x}^{\mu}}{\tilde{x}^2} = \frac{\tilde{x}^{\mu}}{x^2} - b^{\mu}, \tag{2.1.7}$$

which means SCT is a combination of inversion ($x^{\mu} \to x^{\mu}/x^2$), translation and inversion again.

Under transformation (2.1.1) local operators simply transform as tensors

$$
\begin{aligned}
\mathcal{O}^a(x) \equiv \mathcal{O}^{\mu_1\dots\mu_m}{}_{\nu_1\dots\nu_n}(x) &\to \tilde{\mathcal{O}}^{\mu_1\dots\mu_m}{}_{\nu_1\dots\nu_n}(\tilde{x}) \\
&= \frac{\partial \tilde{x}^{\mu_1}}{\partial x^{\rho_1}} \cdots \frac{\partial \tilde{x}^{\mu_m}}{\partial x^{\rho_m}} \frac{\partial x^{\sigma_1}}{\partial \tilde{x}^{\nu_1}} \cdots \frac{\partial x^{\sigma_n}}{\partial \tilde{x}^{\nu_n}} \mathcal{O}^{\rho_1\dots\rho_m}{}_{\sigma_1\dots\sigma_n}(x) \quad (2.1.8) \\
&= \Omega(x)^{m-n} \rho^a{}_b(R^\mu{}_\nu(x)) \mathcal{O}^b(x),
\end{aligned}
$$

where a is a shorthand notation for all the indices of $\mathcal{O}$, $\rho^a{}_b(R^\mu{}_\nu(x))$ is in the representation ρ in which $\mathcal{O}^a$ lives.

2.1.2 Scale and Weyl Transformation

Let us consider a generic metric in this subsection and discuss scale and Weyl transformations. Infinitesimal scale transformations are defined as rescaling of the metric

$$
g_{\mu\nu}(x) \to (1 + 2\lambda) g_{\mu\nu}(x), \tag{2.1.9}
$$

plus a transformation of the local operators

$$
\delta_\lambda \mathcal{O}^a(x) = \lambda(-\Delta - m + n) \mathcal{O}^a(x), \tag{2.1.10}
$$

where Δ is the *scaling dimension* of operator $\mathcal{O}^a$ and as in (2.1.8) m and n are the number of upper and lower indices of $\mathcal{O}^a$.

By promoting the constant parameter λ to a function of positions we obtain the *Weyl transformations*. In other words, Weyl transformations are local scale transformations. Setting $\lambda = \lambda(x)$ and exponentiating (2.1.10) gives the finite Weyl transformation of $\mathcal{O}^a$

$$
\mathcal{O}^a(x) \to \tilde{\mathcal{O}}^a(\tilde{x}) = \sigma(x)^{-\Delta - m + n} \mathcal{O}^a(x), \tag{2.1.11}
$$

and the metric also gets rescaled

$$
g_{\mu\nu}(x) \to \sigma(x)^2 g_{\mu\nu}(x). \tag{2.1.12}
$$

2.1.3 Conformal Transformation

By combining diffeomorphisms generated by conformal Killing vector fields with Weyl transformations one can keep the metric invariant. These combined transformations are called *conformal transformations*. More explicitly, we set $\Omega(x)$ in (2.1.8) and $\sigma(x)$ in (2.1.11) equal and this leads to

$$
g_{\mu\nu}(x) = \delta_{\mu\nu} \to \delta_{\mu\nu},
$$
$$
\mathcal{O}^a(x) \to \tilde{\mathcal{O}}^a(\tilde{x}) = \Omega(x)^{-\Delta} \rho^a{}_b(R^\mu{}_\nu(x)) \mathcal{O}^b(x), \quad R^\mu{}_\nu(x) \in SO(d). \tag{2.1.13}
$$

To be conformally symmetric is to be invariant under both diffeomorphisms generated by conformal Killing vector fields and the corresponding Weyl transformations which cancel the metric rescaling.

2.2 Conformal Ward Identity and Conserved Charges

Correlation functions of operators $\mathcal{O}$, either fundamental or composite, can be defined through path integrals as

$$\langle \mathcal{O}_1(x_1) \ldots \mathcal{O}_n(x_n) \rangle_g = \frac{1}{Z[g]} \int [\mathcal{D}\phi]_g \, e^{-S[\phi,g]} \mathcal{O}_1(x_1) \ldots \mathcal{O}_n(x_n), \qquad (2.2.1)$$

where ϕ denotes fundamental fields and g is the metric. The partition function is

$$Z[g] = \int [\mathcal{D}\phi]_g \, e^{-S[\phi,g]}. \qquad (2.2.2)$$

Assuming the absence of diffeomorphism and Weyl anomalies, conformal symmetry at the level of correlation functions dictates that

$$\langle \tilde{\mathcal{O}}_1(\tilde{x}_1) \ldots \tilde{\mathcal{O}}_n(\tilde{x}_n) \rangle = \langle \mathcal{O}_1(\tilde{x}_1) \ldots \mathcal{O}_n(\tilde{x}_n) \rangle, \qquad (2.2.3)$$

where both sides are evaluated under the flat metric and at the same points. The infinitesimal form of (2.2.3) leads to a useful differential equation called the *Ward identity*.

Let us define symmetry generators as the change of an operator under an infinitesimal transformation *at the same point*

$$\tilde{\mathcal{O}}(x) - \mathcal{O}(x) \equiv \omega_a G_a \mathcal{O}(x), \qquad (2.2.4)$$

where ω_a is a position independent small parameter and a denotes abstractly a collection of indices. By promoting ω_a to a function of position, one finds that the variation of the action has to take the form

$$\delta S = \int d^d x \, \partial_\mu \omega_a(x) J_a^\mu(x). \qquad (2.2.5)$$

Integrating by parts and considering expansion of (2.2.3) under (2.2.4) up to the leading order in ω_a we get the *Ward identity*

$$\partial_\mu \langle J_a^\mu(x) \mathcal{O}_1(x_1) \ldots \mathcal{O}_n(x_n) \rangle = -\sum_i \delta(x - x_i) \langle \mathcal{O}_1(x_1) \ldots G_a \mathcal{O}_i(x_i) \ldots \mathcal{O}_n(x_n) \rangle.$$

$$(2.2.6)$$

For conformal transformations, the infinitesimal parameter ω_a and the current $J_a^\mu(x)$ are replaced respectively by conformal Killing vectors $\epsilon_\nu(x)$ in (2.1.5) and the stress tensor $T^{\mu\nu}(x)$. Then we obtain the *conformal Ward identity*.

Each conformal Killing vector allows us to define a conserved charge operator through the conformal Ward identity

$$Q_\epsilon(\Sigma) \equiv - \int_\Sigma dS_\mu \epsilon_\nu(x) T^{\mu\nu}(x), \tag{2.2.7}$$

where Σ is an oriented boundary (codimension one) of a spacetime region V. $Q_\epsilon(\Sigma)$ acts on all the operators inside V.

At the classical level the conservation of the charge operator $Q_\epsilon(\Sigma)$ follows from the conserved current $\partial_\mu T^{\mu\nu}(x) = 0$, the conformal Killing equation (2.1.4) and the tracelessness condition for the stress tensor $T^\mu_{\ \mu} = 0$.

To see the conservation at the quantum level, we consider the correlation function

$$\langle Q_\epsilon(\Sigma) \mathcal{O}_1(x_1) \dots \mathcal{O}_n(x_n) \rangle$$

and use Stokes' theorem, the conformal Killing equation (2.1.4) and the conformal Ward identity. Because of the Dirac delta functions on the RHS of the conformal Ward identity, the correlation function is invariant under the deformation of Σ as long as it does not cross any operator insertions. This is the sense in which $Q_\epsilon(\Sigma)$ is conserved. (By choosing Σ as a spatial slice and deforming it along the time direction, one can recover the more conventional charge conservation which says the time derivative of the charge operator vanishes.) Operators like $Q_\epsilon(\Sigma)$ are also called *topological surface operators*.

The generator G_a and the conserved charge Q_ϵ are directly related through (2.2.6). Consider a deformation of Σ which cross a single operator $\mathcal{O}(x)$

$$\Sigma_1 \to \Sigma_2, \quad x \in V_1, x \notin V_2 \tag{2.2.8}$$

and define the difference between the two boundaries as

$$\Sigma_\mathcal{O} = \Sigma_1 - \Sigma_2, \tag{2.2.9}$$

where $-\Sigma$ denotes the same hypersurface with orientation reversed. By construction $\Sigma_\mathcal{O}$ only encloses operator $\mathcal{O}(x)$ and nothing else. Compare the difference between the action of $Q_\epsilon(\Sigma_1)$ and $Q_\epsilon(\Sigma_2)$ we have[1]

$$\langle Q_\epsilon(\Sigma_\mathcal{O}) \mathcal{O}(x) \dots \rangle = \epsilon_a \langle G_a \mathcal{O}(x) \dots \rangle. \tag{2.2.10}$$

---

[1]The relation between ϵ_μ and ϵ_a will be made explicit shortly in the next section.

Since Σ's are topological surfaces, we can quantise the theory[2] and deform the surfaces such that Σ_1 and Σ_2 coincide with constant time surfaces. Then a correlation function becomes a time-ordered expectation value and we get[3]

$$\langle 0|T\{[Q_\epsilon, \mathcal{O}(x)]\ldots\}|0\rangle = \epsilon_a \langle G_a \mathcal{O}(x)\ldots\rangle, \qquad (2.2.11)$$

This means Q_ϵ is just the operator formulation of the generator $\epsilon_a G_a$.

2.3 Conformal Algebra

By considering the conformal Killing vectors (2.1.5) explicitly we can obtain in total four generators $P_\mu, M_{\mu\nu}, D, K_\mu$ for conformal transformations.

Translation

$$P^\mu = -\int_\Sigma dS_\mu T^{\mu\nu}(x). \qquad (2.3.1)$$

Rotation

$$\begin{aligned}
m_{\nu\rho} M^{\nu\rho} &= -\int_\Sigma dS_\mu m_{\nu\rho} x^\rho T^{\mu\nu}(x) \\
&= -\int_\Sigma dS_\mu m_{\nu\rho} \frac{1}{2}\left(x^\rho T^{\mu\nu}(x) - x^\nu T^{\mu\rho}(x)\right) \\
\rightarrow M^{\nu\rho} &= -\int_\Sigma dS_\mu \frac{1}{2}\left(x^\rho T^{\mu\nu}(x) - x^\nu T^{\mu\rho}(x)\right),
\end{aligned} \qquad (2.3.2)$$

where in the second line we have used the antisymmetry $m_{\nu\rho} = -m_{\rho\nu}$.

Dilatation

$$D = -\int_\Sigma dS_\mu x_\nu T^{\mu\nu}(x). \qquad (2.3.3)$$

---

[2]By quantisation we mean choosing a time direction and a foliation of the spacetime orthogonal to the time direction. Operators in correlation function will be time ordered. We will discuss more about quantisation in Section 2.6.

[3]Now Q_ϵ is an operator acting on the Hilbert space associated to the quantisation and does not explicitly depend on Σ.

Special conformal transformation

$$b_\nu K^\nu = -\int_\Sigma dS_\mu (2(x \cdot b)x_\nu - b_\nu x^2)T^{\mu\nu}(x)$$

$$= -\int_\Sigma dS_\mu b_\nu \left(2x^\nu x_\rho T^{\mu\rho}(x) - x^2 T^{\mu\nu}(x)\right) \qquad (2.3.4)$$

$$\rightarrow K^\nu = -\int_\Sigma dS_\mu \left(2x^\nu x_\rho T^{\mu\rho}(x) - x^2 T^{\mu\nu}(x)\right).$$

The nonzero commutation relations among the generators are:

$$\begin{aligned}
[M_{\mu\nu}, P_\rho] &= \delta_{\nu\rho} P_\mu - \delta_{\mu\rho} P_\nu, \\
[M_{\mu\nu}, K_\rho] &= \delta_{\nu\rho} K_\mu - \delta_{\mu\rho} K_\nu, \\
[M_{\mu\nu}, M_{\rho\sigma}] &= \delta_{\nu\rho} M_{\mu\sigma} - \delta_{\mu\rho} M_{\nu\sigma} + \delta_{\nu\sigma} M_{\rho\mu} - \delta_{\mu\sigma} M_{\rho\nu}, \\
[K_\mu, P_\nu] &= 2\delta_{\mu\nu} D - 2M_{\mu\nu}, \\
[D, P_\mu] &= P_\mu, \\
[D, K_\mu] &= -K_\mu.
\end{aligned} \qquad (2.3.5)$$

This is the *conformal algebra*. By rewriting the generators as

$$L_{\mu\nu} = M_{\mu\nu}, \quad L_{-1,0} = D, \quad L_{0,\mu} = \frac{P_\mu + K_\mu}{2}, \quad L_{-1,\mu} = \frac{P_\mu - K_\mu}{2}, \qquad (2.3.6)$$

with $L_{ab} = -L_{ba}$ and $a, b = \{-1, 0, 1, \ldots, d\}$, one can show that L_{ab} satisfy the commutation relations of $SO(d+1, 1)$, which is the rotation group in $d+2$ dimension with Lorentzian signature.

2.4 Primary and Descendant Operators

Using the conformal algebra (2.3.5) we can construct corresponding irreducible representations and organise operators accordingly. Since dilatation and rotation generators commute, we can diagonalise them simultaneously and label operators by their eigenvalues, the scaling dimension Δ and the spin ℓ.[4]

The last two equations in (2.3.5) indicates that P_μ and K_μ raise and lower the scaling dimension by one unit. For physically sensible theories the spectrum (the scaling dimension in this case) should be bounded from below, thus we can define a *conformal primary operator* as the lowest weight operator, such that it is annihilated by K_μ

$$[K_\mu, \mathcal{O}^a(0)] = 0 \qquad \text{(primary operator)}. \qquad (2.4.1)$$

---

[4]Here we only consider symmetric traceless representations of $SO(d)$ so a single label ℓ suffices.

For a given primary operator, acting on it with P_μ generates a tower of operators with higher scaling dimensions

$$\{[P_{\mu_1}, \mathcal{O}^a(0)], [P_{\mu_1}[P_{\mu_2}, \mathcal{O}^a(0)]], \ldots\}. \tag{2.4.2}$$

These operators descending from the primary operator are called *descendant operators*. Each tower of operators forms a *conformal multiplet*.

For other generators the primary operators satisfy

$$[D, \mathcal{O}^a(0)] = \Delta \mathcal{O}^a(0), \tag{2.4.3}$$

$$[M_{\mu\nu}, \mathcal{O}^a(0)] = (\mathcal{S}_{\mu\nu})^a{}_b \mathcal{O}^b(0), \tag{2.4.4}$$

$$[K_\mu, \mathcal{O}^a(0)] = 0, \tag{2.4.5}$$

where $(\mathcal{S}_{\mu\nu})^a{}_b = \rho^a{}_b(M_{\mu\nu})$ is in the representation ρ in which $\mathcal{O}^a$ lives. For operators away from the origin, using $\mathcal{O}(x) = e^{x \cdot P} \mathcal{O}(0) e^{-x \cdot P}$ and the conformal algebra (2.3.5) one obtains

$$[P^\mu, \mathcal{O}^a(x)] = \partial^\mu \mathcal{O}^a(x), \tag{2.4.6}$$

$$[D, \mathcal{O}^a(x)] = (x^\mu \partial_\mu + \Delta) \mathcal{O}^a(x), \tag{2.4.7}$$

$$[M_{\mu\nu}, \mathcal{O}^a(x)] = M_{\mu\nu} e^{x \cdot P} \mathcal{O}^a(0) = \left(m_{\mu\nu} + (\mathcal{S}_{\mu\nu})^a{}_b\right) \mathcal{O}^a(x), \tag{2.4.8}$$

$$[K_\mu, \mathcal{O}^a(x)] = \left(k_\mu + 2\Delta x_\mu - 2x^\nu (\mathcal{S}_{\mu\nu})^a{}_b\right) \mathcal{O}^a(x), \tag{2.4.9}$$

where $m_{\mu\nu} = x_\nu \partial_\mu - x_\mu \partial_\nu$, $k_\mu = 2x_\mu(x \cdot \partial) - x^2 \partial_\mu$.

2.5 Conformal Correlation Functions

Conformal correlation functions are the central objects of CFTs. As mentioned before, they are invariant under conformal transformations. Using (2.2.3) and (2.1.13) we have the following Ward identity of finite transformation

$$\langle \mathcal{O}_1^{a_1}(\tilde{x}_1) \ldots \mathcal{O}_n^{a_n}(\tilde{x}_n) \rangle = \Omega(x_1)^{-\Delta_1} \cdots \Omega(x_n)^{-\Delta_n} \left\langle \rho^{a_1}_{b_1}(R(x_1)) \mathcal{O}_1^{b_1}(x_1) \cdots \rho^{a_n}_{b_n}(R(x_n)) \mathcal{O}_n^{b_n}(x_n) \right\rangle, \tag{2.5.1}$$

where again both sides are evaluated in the flat metric. This equation imposes strong constraints on the form of correlation functions, as we will now discuss.

In the rest of this section we focus on two, three and four-point functions. For simplicity we will only consider scalar operators.

2.5.1 Two-point Function

The Ward identity (2.5.1) completely fixes two-point functions to be

$$\langle \mathcal{O}_1(x_1)\mathcal{O}_2(x_2) \rangle = \frac{C\delta_{\Delta_1\Delta_2}}{|x_{ij}|^{2\Delta_1}}, \tag{2.5.2}$$

where $x_{ij} \equiv x_i - x_j$. We can normalise the operators such that $C = 1$.

2.5.2 Three-point Function

As for three-point functions we get

$$\langle \mathcal{O}_1(x_1)\mathcal{O}_2(x_2)\mathcal{O}_3(x_3) \rangle = \frac{f_{123}}{|x_{12}|^{\Delta_1+\Delta_2-\Delta_3}|x_{23}|^{\Delta_2+\Delta_3-\Delta_1}|x_{31}|^{\Delta_3+\Delta_1-\Delta_2}}, \tag{2.5.3}$$

where the *three-point function coefficient* f_{123} cannot be scaled away once we fix the two-point function coefficient and it is not determined by conformal symmetry.

2.5.3 Four-point Function

For four-point functions we define the *conformal cross ratios* as

$$u = z\bar{z} = \frac{x_{12}^2 x_{34}^2}{x_{13}^2 x_{24}^2}, \quad v = (1-z)(1-\bar{z}) = \frac{x_{14}^2 x_{23}^2}{x_{13}^2 x_{24}^2}, \tag{2.5.4}$$

where $x_{ij} \equiv x_i = x_j$.

In Euclidean region where all operators are spacelike separated, z and $\bar{z}$ are complex conjugate of each other and live on the complex plane. Using conformal transformations one can reach the following configuration

$$x_1 = (0,0,0,\ldots), \quad x_2 = (x,y,0,\ldots), \quad x_3 = (1,0,0,\ldots), \quad x_4 = \infty, \tag{2.5.5}$$

then one finds that $z = x + iy$. We will discuss Lorentzian and generic complex-time configurations in Section 2.13.

Conformal symmetry constrains the four-point functions to only depend on the cross ratios up to a universal kinematic prefactor

$$\langle \mathcal{O}_1(x_1)\mathcal{O}_2(x_2)\mathcal{O}_3(x_3)\mathcal{O}_4(x_4) \rangle = \left|\frac{x_{24}}{x_{14}}\right|^{\Delta_{12}} \left|\frac{x_{14}}{x_{13}}\right|^{\Delta_{34}} \frac{g(z,\bar{z})}{|x_{12}|^{\Delta_1+\Delta_2}|x_{34}|^{\Delta_3+\Delta_4}}, \tag{2.5.6}$$

where $\Delta_{ij} \equiv \Delta_i - \Delta_j$. It can be checked that (2.5.6) satisfies (2.5.1) for any function $g(z,\bar{z})$. The function $g(z,\bar{z})$ is the main object of study in CFTs and we will discuss it in more detail in Section 2.11.

2.6 Radial Quantisation and the State-Operator Correspondence

In this thesis we define quantisation to be a choice of foliation of the spacetime. Each quantisation defines a direction of time and each leaf of the foliation, orthogonal to the time direction, has its own Hilbert space of states. The time evolution moves the states from one leaf to another. The most familiar quantisation is widely used in Poincaré invariant theories in $\mathbb{R}^d$ where the time evolution is generated by the Hamiltonian P^0. In conformally invariant theories it is convenient to foliate the spacetime by S^{d-1} spheres of various radii centred at the origin and time evolution is generated by the dilatation operator D. This is called the *radial quantisation*.

Using radial quantisation we can show that in CFT local operators at the origin are in one-to-one correspondence with states. In a general QFT, local operators are defined at points in the spacetime while states span over the entire spatial slice. In a CFT, however, scaling invariance allows to us shrink a spherical spatial slice into the point at the origin, where a state can be identified with a local operator at that point.

In the path integral language, states living on a sphere (Hilbert space) are generated by inserting operators inside the sphere and performing the path integral. For a given sphere, a general state can be decomposed in to basis states

$$|\psi\rangle = \int \mathcal{D}\phi_b |\phi_b\rangle\langle\phi_b|\psi\rangle, \tag{2.6.1}$$

where ϕ_b denotes field configurations on the sphere. The coefficients can be calculated by path integral. When there is an operator insertion $\mathcal{O}(x)$ in the path integral, the coefficients are

$$\langle\phi_b|\mathcal{O}(x)|0\rangle = \int_{\phi=\phi_b} \mathcal{D}\Phi e^{-S[\Phi]}\mathcal{O}(x), \tag{2.6.2}$$

where Φ denotes field configurations in the ball and ϕ denotes the boundary value of Φ on the sphere. Therefore, the operator $\mathcal{O}(x)$ creates a state

$$\mathcal{O}(x)|0\rangle = \int \mathcal{D}\phi_b |\phi_b\rangle \int_{\phi=\phi_b} \mathcal{D}e^{-S[\Phi]}\mathcal{O}(x). \tag{2.6.3}$$

In particular, an operator at the origin creates an eigenstate of the dilatation operator

$$D\mathcal{O}(0)|0\rangle = [D,\mathcal{O}(0)]|0\rangle + \mathcal{O}(0)D|0\rangle = \Delta\mathcal{O}(0)|0\rangle. \tag{2.6.4}$$

On the other hand, given an eigenstate of the dilatation operator $|\mathcal{O}_i\rangle$ we can construct a local operator at the origin $\mathcal{O}_i(0)$ through its correlation functions with other

local operators

$$\langle 0|\phi_1(x_1)\phi_2(x_2)\ldots\mathcal{O}_i(0)|0\rangle := \langle 0|\phi_1(x_1)\phi_2(x_2)\ldots|\mathcal{O}_i\rangle. \tag{2.6.5}$$

Therefore, we have an identification between eigenstates of D and local operators at the origin

$$\mathcal{O}(0) \leftrightarrow \mathcal{O}(0)|0\rangle \equiv |\mathcal{O}\rangle. \tag{2.6.6}$$

This is called *the state-operator correspondence*. For operators away from the origin, it can be written as a infinite sum of primary and descendant operators at the origin and thus corresponds to a linear combination of eigenstates of D.

2.6.1 Map to Cylinder

Under a Weyl transformation, i.e. a rescaling of the metric, the radial quantisation can be mapped to a conventional quantisation on a cylinder. This can be seen by writing down the metric explicitly

$$ds^2_{\mathbb{R}^d} = dr^2 + r^2 ds^2_{S^{d-1}} = e^{2\tau}\left(d\tau^2 + ds^2_{S^{d-1}}\right) = e^{2\tau} ds^2_{\mathbb{R}\times S^{d-1}}, \tag{2.6.7}$$

where

$$r = e^{\tau} \tag{2.6.8}$$

and time translation on the cylinder is related to the dilatation in the flat space.

Under Weyl transformations $g_{\mu\nu}(x) \rightarrow \Omega^2(x)g_{\mu\nu}(x)$ the correlation functions transform as[5]

$$\langle \mathcal{O}_1(x_1)\ldots\mathcal{O}_n(x_n)\rangle_{\Omega^2 g} = \frac{\langle \mathcal{O}_1(x_1)\ldots\mathcal{O}_n(x_n)\rangle_g}{[\Omega(x_1)]^{\Delta_1}\ldots[\Omega(x_n)]^{\Delta_n}}. \tag{2.6.9}$$

Applying this to the cylinder map (2.6.8), we can define operators on the cylinder by

$$\mathcal{O}_{\text{cyl.}}(\tau, \mathbf{n}) \equiv e^{\Delta\tau}\mathcal{O}_{\text{flat}}(r, \mathbf{n}), \quad \mathbf{n} \in S^{d-1}, \tag{2.6.10}$$

such that

$$\langle \mathcal{O}_{\text{cyl.},1}(\tau_1, \mathbf{n}_1)\ldots\mathcal{O}_{\text{cyl.},n}(\tau_n, \mathbf{n}_n)\rangle = \langle \mathcal{O}_{\text{flat},1}(r_1, \mathbf{n}_1)\ldots\mathcal{O}_{\text{flat},n}(r_n, \mathbf{n}_n)\rangle. \tag{2.6.11}$$

---

[5]In even dimensions the trace of the stress tensor does not vanish in general. As a result the partition function is not invariant under Weyl transformation and the theory has a *Weyl anomaly*. The Weyl anomaly does not play a role in this thesis and we will not discuss it.

2.7 Reflection Positivity and Unitarity

In Lorentzian signature, unitarity requires the norm of states in the Hilbert space to be non-negative. In Euclidean signature the notion of unitarity becomes *reflection positivity*

$$\langle\phi|\phi\rangle = \langle 0|\mathcal{O}_{E,n}^\dagger \ldots \mathcal{O}_{E,1}^\dagger \mathcal{O}_{E,1} \ldots \mathcal{O}_{E,n}|0\rangle \geq 0, \tag{2.7.1}$$

where "E" denotes Euclidean and for scalar operators

$$\mathcal{O}_E^\dagger(t_E, \mathbf{x}) = \mathcal{O}_E^*(-t_E, \mathbf{x}). \tag{2.7.2}$$

The Euclidean counterpart of Hermitian operators satisfy

$$\mathcal{O}_E(t_E, \mathbf{x})^\dagger = \mathcal{O}_E(-t_E, \mathbf{x}), \tag{2.7.3}$$

and are called *real* operators. It can be shown that the coefficients of three-point functions λ_{ijk} of real operators are real.

It has been established in [19] that from a reflection-positive CFT we can reconstruct a unitary Lorentzian CFT by analytic continuation.

Unitarity bound The unitarity condition imposes constraints on the spectrum of CFTs. They are captured by lower bounds on the scaling dimensions of the operators

$$\Delta = 0 \text{ (unit operator)}$$
$$\Delta \geq \begin{cases} \frac{d-2}{2}, & \ell = 0 \\ \ell + d - 2, & \ell > 0 \end{cases} \tag{2.7.4}$$

These are called the *unitarity bounds*.

2.8 The Operator Product Expansion

Using radial quantisation and the state-operator correspondence, we can show the following operator equation

$$\mathcal{O}_i(x_i)\mathcal{O}_j(x_j) = \sum_k \frac{\lambda_{ijk}}{|x_{ij}|^{\Delta_i+\Delta_j-\Delta_k}} C_a(|x_{ij}|, \partial_k)\mathcal{O}_k^a(x_k), \tag{2.8.1}$$

where C_a is understood as a power series in ∂_k and is completely fixed by conformal symmetry. (2.8.1) is valid inside any correlation function as long as all other operators $\mathcal{O}_l(x_l)$ satisfy

$$|x_{lk}| > \max(|x_{ik}|, |x_{jk}|). \tag{2.8.2}$$

In words, this means that the product of two local operators can be rewritten as an infinite sum of other local operators and is called the *operator product expansion* (OPE). In particular, by considering the correlation function of both sides of (2.8.1) with another operator $\mathcal{O}_l$, one finds that λ_{ijk} is just the three-point function coefficient. Hence λ_{ijk} is also called the *OPE coefficient*.

To show the OPE we use radial quantisation originated at x_k, insert the operators $\mathcal{O}_i(x_i)$ and $\mathcal{O}_j(x_j)$ inside a ball centred at the origin and perform the path integral over the interior of the ball to generate a state $|\psi\rangle$ on the sphere. Then we decompose $|\psi\rangle$ into dilatation eigenstates, which by the state-operator correspondence are in one-to-one correspondence to primary or descendant operators at the origin. This produces an equation which is just (2.8.1) with both sides acting on the vacuum state and by removing the vacuum state we obtain (2.8.1).

Note that we can choose x_k and the corresponding radial quantisation freely as long as (2.8.2) is satisfied. This means (in the Euclidean region) the OPE (2.8.1) converges whenever we can use a sphere to separate $\mathcal{O}_i(x_i), \mathcal{O}_j(x_j)$ from all other operators.

2.9 QFT in AdS and Boundary Conformal Theory

In this section we consider the setup where QFT is placed in *fixed* Anti-de Sitter (AdS) space, which is a maximally symmetric spacetime with a negative cosmological constant. For a more comprehensive and pedagogical introduction to this subject we refer to [20].

2.9.1 QFT in AdS: motivation

There are various motivations to consider putting a QFT in AdS [21–23]. First, it is the leading order semi-classical approximation to quantum gravity in the sense that gravitational fluctuation is considered as negligible. Therefore any sensible theory of quantum gravity has to reduce to QFT in AdS when the gravitational dynamics is turned off. Another motivation follows from the fact that AdS space provides an IR cutoff which preserves the symmetry [21]. This is useful to study dynamics in QFT otherwise plagued by IR divergences. Lastly, the motivation for this thesis is to consider the flat-space limit of QFT in AdS.

For a QFT living in $(d + 1)$-dimensional AdS space which preserve its isometries, the theory is constrained by the conformal group $SO(d, 2)$ and we can define *boundary correlation functions* as correlation functions of local bulk operators whose insertion points are pushed towards the conformal boundary [8, 9].[6] The full set of

---

[6]Alternatively boundary correlation functions can be defined as functional derivatives of the bulk partition function with respect to the boundary conditions [6, 7]. For discussions on the equivalence between the two definitions, see *e.g.* [24].

correlation functions then defines a conformally invariant theory living on the boundary. This is similar to the AdS/CFT correspondence, but with one notable difference, namely there is no graviton in the bulk and no stress tensor on the boundary. Such conformally invariant (boundary) theory without a stress tensor is called a *boundary conformal theory* (BCT) to be distinguished from the full-fledged conformal field theory [13]. Apart from the absence of a stress tensor, a BCT behaves just like a CFT. Most notably it also has unitarity (or reflection positivity for Euclidean signature), the state-operator correspondence and convergent OPE.

The duality between the bulk and the boundary allows one to study QFTs in AdS using techniques established in CFT. Furthermore, one can take the *flat-space limit* of QFT in AdS, for which the curvature radius R and scaling dimensions in BCT are sent to infinity [25–27]. Intuitively, the centre of AdS space in this limit becomes a flat space and one expects to be able to extract the S-matrix of the flat-space QFT, either gapped or gapless, from the boundary conformal correlation functions. This provides an alternative approach to study the (especially non-perturbative) analytic structure of flat-space S-matrix, because CFTs are more constrained and their analytic structure is better understood.

2.9.2 QFT in AdS: setup

Let us discuss the setup of putting a QFT in AdS in more details. This subsection mainly follows the discussion in [13].

AdS space can be described equivalently by several different coordinates. Here we consider the $d + 1$ dimensional Euclidean AdS space, denoted as AdS_{d+1}, and discuss three coordinates which will be useful later.

In *Poincaré coordinates* the metric is

$$ds^2 = R^2 \frac{dz^2 + dr^2 + r^2 d\Omega_{d-1}^2}{z^2}, \qquad z > 0, \tag{2.9.1}$$

where R is the radius of AdS curvature, r and Ω^i ($i = 1, \ldots, d$) are radial and angular coordinates of a d-dimensional flat space. This shows that AdS_{d+1} is conformal to $\mathbb{R}^+ \times \mathbb{R}^d$ and the conformal boundary consists of a copy of $\mathbb{R}^d$ at $z = 0$ and a single point at $z = \infty$.

Alternatively, we can make the change of coordinates $z = e^\tau \cos\lambda, r = e^\tau \sin\lambda$ to obtain the *global coordinates*

$$ds^2 = R^2 \frac{d\tau^2 + d\lambda^2 + \sin^2\lambda \, d\Omega_{d-1}^2}{\cos^2\lambda}. \tag{2.9.2}$$

This shows that AdS_{d+1} is conformal to a solid cylinder whose boundary at $\lambda = \frac{\pi}{2}$ is conformal to $\mathbb{R} \times S^{d-1}$. This is the cylinder-to-flat-space map discussed in Section 2.6.1.
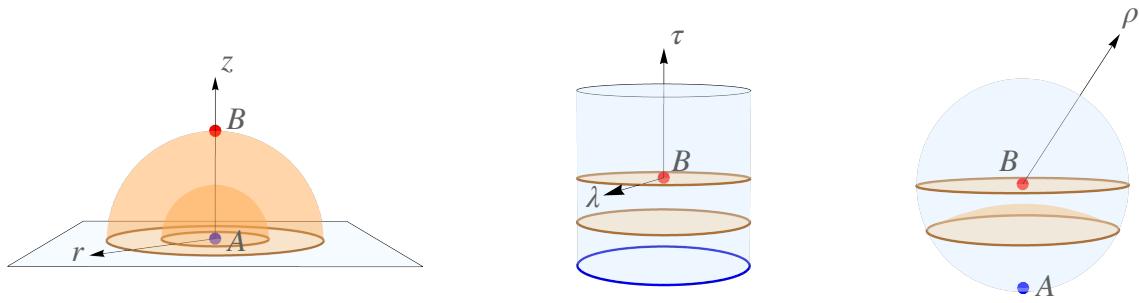
Figure 2.1. AdS space in Poincaré coordinates, global coordinates and spherical coordinates. The red points and orange surfaces (each with its own Hilbert space) are identified among the figures. The blue points in Poincaré and spherical coordinates are identified with the blue circle in global coordinates, which is the $\tau \to -\infty$ conformal boundary.

Finally in *spherical coordinates* the metric is

$$ds^2 = d\rho^2 + R^2 \sinh^2\left(\frac{\rho}{R}\right) d\Omega_d^2. \tag{2.9.3}$$

Thus AdS_{d+1} can also be regarded as an open ball with the conformal boundary being a sphere at $\rho = \infty$.

Boundary Operator-Bulk State Correspondence   Similar to the argument in CFTs, using radial quantisation one obtains a one-to-one correspondence between a state living in the bulk and an operator at the origin of the conformal boundary. On the one hand, an operator inserted at point A in figure 2.1 creates a state on the Hilbert space. On the other hand, a state on the Hilbert space can be propagated backwards to infinite past and reach the boundary point A, which defines a local operator on the boundary. The bulk states can be labelled by eigenvalues of the dilatation operator D and $SO(d)$ rotation generator $M_{\mu\nu}$. For $SO(d)$ scalars we have the familiar relation between the scaling dimension Δ of boundary primary operator and the mass m of the single particle state in the bulk as

$$\Delta(\Delta - d) = m^2 R^2. \tag{2.9.4}$$

To obtain gapped theories in the flat-space, the limit to take is sending both R and Δ to infinity while holding their ratio fixed

$$R \to \infty, \quad \Delta \to \infty, \quad \lim_{R \to \infty} \frac{\Delta}{R} = m \text{ fixed.} \tag{2.9.5}$$

In the flat-space limit, the ratio is just the mass of the single particle state.

Bulk-Boundary Operator Expansion   The boundary operator-bulk state correspondence also induces a *bulk-boundary operator expansion*. The argument is again

similar to that of OPE in CFTs. A local operator in the bulk (for example at point B in figure 2.1) creates a state in the Hilbert space. This state can be decomposed into eigenstates of the dilatation operator D and by boundary operator-bulk state correspondence these eigenstates are in one-to-one correspondence to boundary operators with definite scaling dimensions, namely, primary or descendant operators. Therefore a bulk operator can be written as a linear combination of primary and descendant operators at the boundary

$$\phi_i(z,x) = \sum_j b_{ij} z^{\Delta_j} C_a(x, \partial_x) \mathcal{O}_j^a(x), \tag{2.9.6}$$

where the index a again labels $SO(d)$ representations. By taking the limit $z \to 0$, one obtains a boundary operator by pushing the bulk operator to the boundary[7]

$$\mathcal{O}(x) = \lim_{z \to 0} z^{-\Delta_{\mathcal{O}}} \phi(z,x), \tag{2.9.7}$$

and the boundary correlation function is [9]

$$\langle \mathcal{O}_1(x_1) \dots \mathcal{O}_n(x_n) \rangle_{\text{boundary}} = \lim_{z \to 0} z^{-\sum_{i=1}^{n} \Delta_i} \langle \phi_1(x_1, z) \dots \phi_n(x_n, z) \rangle_{\text{bulk}} \tag{2.9.8}$$

Boundary Operator Product Expansion   Operators on the conformal boundary satisfy the usual OPE as in CFTs

$$\mathcal{O}_i(x_i)\mathcal{O}_j(x_j) = \sum_k \frac{\lambda_{ijk}}{|x_{ij}|^{\Delta_i + \Delta_j - \Delta_k}} C_a(x_k, \partial_k) \mathcal{O}_k^a(x_k). \tag{2.9.9}$$

The argument is completely analogous to that in Section 2.8. Using radial quantisation, the operator insertions $\mathcal{O}_i(x_i)$ and $\mathcal{O}_j(x_j)$ create a state in the Hilbert space of the QFT in AdS through path integral. This state can be decomposed into dilatation eigenstates, each of which corresponds to a local operator at the origin determined by the quantisation. Hence the OPE holds.

2.9.3   Assumptions for the Flat-space Limit

To discuss the flat-space limit of QFT in AdS on a firm ground we need to make the following assumptions:

---

[7]This relation can be understood by considering as an example a single scalar field in AdS. Since in (AdS) Feynman diagrams each external operator is connected to a bulk-bulk propagator, we can equivalently study the limit for the bulk-bulk propagator where one of the bulk points is pushed to the boundary. In this limit the bulk-bulk propagator becomes the bulk-boundary propagator [9, 28]. To obtain the operator on the boundary one needs to approach the boundary away from the source points [29]. The prefactor, *i.e.* one, in front of $\mathcal{O}(x)$ follows from our definition of the bulk-boundary propagator (3.2.4), whose normalisation absorbs the holographic renormalisation factor $(2\Delta - d)$ first pointed out in [30]. This can be seen explicitly by comparing the definitions of bulk-boundary propagator between (3.2.4) and that in [30].

Assumption 1. *The boundary conditions and the curvature couplings (if any) preserve the AdS isometries at the quantum level. As the radius of curvature R increases, this continues to hold.*

As a result of this assumption the conformal symmetry of the boundary correlation functions is also preserved for any R all the way to the flat-space limit.

Assumption 2. *The Hilbert space of the QFT in AdS approaches that of the generalised free field (GFF) theory when R is large, and coincides with the flat-space Hilbert space when $R \to \infty$.*

As we will see later in Chapter 3, the GFF spectrum is related to the identity (non-interacting) part of the flat-space S-matrix.

More generally, these two assumptions lead to our conjecture that relates d-dimensional conformal correlation functions and $(d + 1)$-dimensional flat-space S-matrix

$$\lim_{R \to \infty} \langle \mathcal{O}_1 \dots \mathcal{O}_a \mathcal{O}_{a+1} \dots \mathcal{O}_{a+b} \rangle_R \sim \langle k_1 \dots k_a | \hat{S} | p_1 \dots p_b \rangle. \qquad (2.9.10)$$

Chapter 3 is devoted to details of this conjecture and we will see to what extent and precisely how it holds.

2.10 CFT Data and Conformal Bootstrap

Conformal symmetry completely fixes two-point functions. Three-point functions are fixed up to the OPE coefficient. In general, an n-point function can be reduced to an infinite sum of $(n - 1)$-point functions using the OPE. By doing this iteratively, any n-point function can be reduced to three-point functions which are fixed up to the OPE coefficient.[8] Therefore, with the knowledge of the spectrum and the OPE coefficients one can completely determine any n-point conformal correlation functions. The set {spectrum, OPE coefficients} is called the *CFT data*.

Knowing the CFT data amounts to a complete understanding of the local degrees of freedom of the theory, for example OPE structure and correlation functions of local operators. However, this is highly non-trivial because the CFT data cannot be arbitrary. Consider any three local operators in an n-point function ($n > 3$), one can use the OPE between $\mathcal{O}_1$ and $\mathcal{O}_2$ and then between O_3 and the expansion operators from $\mathcal{O}_1 \times \mathcal{O}_2$; or one can first use the OPE between $\mathcal{O}_2$ and $\mathcal{O}_3$ and then fuse with

---

[8]The rigorous justification of this iterative procedure relies on proving the infinite sums from OPEs can be exchanged (otherwise performing OPEs in different ordering gives different results), which has not been done so far. In this thesis we focus on four-point functions, for which the OPE convergence has been rigorously established [31].

$\mathcal{O}_1$. These two options give naively different expressions, but they must agree as long as the OPEs converge. Schematically, this is

$$\langle \overbrace{\mathcal{O}_1 \mathcal{O}_2} \mathcal{O}_3 \dots \mathcal{O}_n \rangle = \langle \mathcal{O}_1 \overbrace{\mathcal{O}_2 \mathcal{O}_3} \dots \mathcal{O}_n \rangle \tag{2.10.1}$$

This is the *associativity of the OPE* and it imposes non-trivial constraints on the CFT data.

The program of exploiting these constraints with the goal to reduce or even identify the space of consistent CFT data is call the *conformal bootstrap* program. As explained in Section 2.9, apart from studying properties of CFTs, we also have in mind the goal to study flat-space physics through understanding conformal correlation functions using the conformal bootstrap methods.

2.11 Four-point Functions, Conformal Blocks and the Crossing Equation

In this section let us examine the four-point functions in more detail. Define a complete basis as

$$\mathbf{1} = \sum_{\mathcal{O}} |\mathcal{O}| \equiv \sum_{\mathcal{O}} \left(\sum_{\alpha = \mathcal{O}, P\mathcal{O}, PP\mathcal{O}, \dots} (\langle \alpha | \alpha \rangle)^{-1} |\alpha \rangle \langle \alpha| \right) \tag{2.11.1}$$

where $\mathcal{O}$ denotes conformal primary operators and $|\mathcal{O}|$ is a projector onto the conformal multiplet of $\mathcal{O}$. By construction, the projector $|\mathcal{O}|$ commutes with all conformal generators.[9]

Using radial quantisation and inserting this basis in the four-point function we get

$$\langle \mathcal{O}_1(x_1) \mathcal{O}_2(x_2) \mathcal{O}_3(x_3) \mathcal{O}_4(x_4) \rangle = \left| \frac{x_{24}}{x_{14}} \right|^{\Delta_{12}} \left| \frac{x_{14}}{x_{13}} \right|^{\Delta_{34}} \frac{g(z, \bar{z})}{|x_{12}|^{\Delta_1 + \Delta_2} |x_{34}|^{\Delta_3 + \Delta_4}}$$

$$= \sum_{\mathcal{O}} \langle 0 | \mathcal{O}_1(x_1) \mathcal{O}_2(x_2) | \mathcal{O} | \mathcal{O}_3(x_3) \mathcal{O}_4(x_4) | 0 \rangle . \tag{2.11.2}$$

The fact that $|\mathcal{O}|$ commutes with conformal generators means each summand in (2.11.2) satisfies the Ward identity (2.5.1) and, just like the correlator itself, is a function of cross ratios z and $\bar{z}$. This leads to the definition of the *conformal block*

---

[9]This follows from the obvious commutation between the conformal generators Q and the identity operator and the fact that the actions of Q simply reorganise local operators within the same conformal multiplet.

as the projection of the four-point function onto a certain conformal multiplet[10]

$$
\left|\frac{x_{24}}{x_{14}}\right|^{\Delta_{12}} \left|\frac{x_{14}}{x_{13}}\right|^{\Delta_{34}} \frac{f_{12\mathcal{O}}f_{34\mathcal{O}}G_{\Delta_{\mathcal{O}},\ell_{\mathcal{O}}}^{\Delta_{12},\Delta_{34}}(z,\bar{z})}{|x_{12}|^{\Delta_1+\Delta_2}\,|x_{34}|^{\Delta_3+\Delta_4}} := \langle 0\,|\mathcal{O}_1(x_1)\mathcal{O}_2(x_2)|\,\mathcal{O}\,|\mathcal{O}_3(x_3)\mathcal{O}_4(x_4)|\,0\rangle\,,
$$

$$(2.11.3)$$

where the OPE coefficients come from applying the OPE between $\mathcal{O}_1(x_1) \times \mathcal{O}_2(x_2)$ and $\mathcal{O}_3(x_3) \times \mathcal{O}_4(x_4)$, respectively. Stripping off the kinematic prefactor, the correlator $g(z,\bar{z})$ has the following *conformal block decomposition*

$$
g(z,\bar{z}) = \sum_{\Delta_{\mathcal{O}},\ell_{\mathcal{O}}} f_{12\mathcal{O}}f_{34\mathcal{O}}\, G_{\Delta_{\mathcal{O}},\ell_{\mathcal{O}}}^{\Delta_{12},\Delta_{34}}(z,\bar{z}). \tag{2.11.4}
$$

This is called the *s*-channel block decomposition because it converges when $\mathcal{O}_1$ is close to $\mathcal{O}_2$. Alternatively there are two other different ways to apply the OPEs among operators

$$
\langle \mathcal{O}_1(x_1)\mathcal{O}_2(x_2)\mathcal{O}_3(x_3)\mathcal{O}_4(x_4)\rangle \qquad (t\text{-channel}), \tag{2.11.5}
$$

$$
\langle \mathcal{O}_1(x_1)\mathcal{O}_2(x_2)\mathcal{O}_3(x_3)\mathcal{O}_4(x_4)\rangle \qquad (u\text{-channel}), \tag{2.11.6}
$$

By identifying s and t-channel block decomposition, we obtain the following *crossing equation*

$$
\sum_{\Delta_{\mathcal{O}},\ell_{\mathcal{O}}} f_{12\mathcal{O}}f_{34\mathcal{O}}\, G_{\Delta_{\mathcal{O}},\ell_{\mathcal{O}}}^{\Delta_{12},\Delta_{34}}(z,\bar{z}) = \frac{(z\bar{z})^{\frac{\Delta_1+\Delta_2}{2}}}{((1-z)(1-\bar{z}))^{\frac{\Delta_2+\Delta_3}{2}}} \sum_{\Delta_{\mathcal{O}'},\ell_{\mathcal{O}'}} f_{23\mathcal{O}'}f_{14\mathcal{O}'}\, G_{\Delta_{\mathcal{O}'},\ell_{\mathcal{O}'}}^{\Delta_{32},\Delta_{14}}(1-z,1-\bar{z})
$$

$$(2.11.7)$$

or schematically

$$
\sum_{\mathcal{O}} \;\;\begin{matrix}\mathcal{O}_1 & & \mathcal{O}_4 \\ & \mathcal{O} & \\ \mathcal{O}_2 & & \mathcal{O}_3\end{matrix}\;\; = \;\; \sum_{\mathcal{O}'} \;\;\begin{matrix}\mathcal{O}_1 & & \mathcal{O}_4 \\ & \mathcal{O}' & \\ \mathcal{O}_2 & & \mathcal{O}_3\end{matrix} \tag{2.11.8}
$$

It is also called the *bootstrap equation* because the idea of conformal bootstrap is directly implemented through this equation.

---

[10]Conformal blocks can also be calculated by solving the conformal Casimir equations, up to normalisation.

2.12 The Conformal Partial Wave Expansion

Besides conformal block decomposition (2.11.4), the conformal correlator also has the *conformal partial wave expansion* [32]

$$g(z, \bar{z}) = \sum_{\ell=0}^{\infty} \int_{d/2-i\infty}^{d/2+i\infty} \frac{d\Delta}{2\pi i} c(\Delta, \ell) F_{\Delta,\ell}^{\Delta_{12},\Delta_{34}}(z, \bar{z}) + \text{(non-norm.)}. \qquad (2.12.1)$$

The function $c(\Delta, \ell)$ is called the *OPE density* and is the key object. It encodes all the dynamical information about the correlator. The function $F_{\Delta,\ell}(z, \bar{z})$ is called the *conformal partial wave* and is given by a conformal block with dimension Δ plus a *shadow conformal block* with dimension $\tilde{\Delta} \equiv d - \Delta$,

$$F_{\Delta,\ell}^{\Delta_{12},\Delta_{34}}(z, \bar{z}) = \frac{1}{2} \left(G_{\Delta,\ell}^{\Delta_{12},\Delta_{34}}(z, \bar{z}) + \frac{K_{d-\Delta,\ell}}{K_{\Delta,\ell}} G_{d-\Delta,\ell}^{\Delta_{12},\Delta_{34}}(z, \bar{z}) \right), \qquad (2.12.2)$$

where the coefficient $K_{\Delta,\ell}$ reads

$$K_{\Delta,\ell}^{\Delta_{12},\Delta_{34}} = \frac{\Gamma(\Delta - 1)}{\Gamma(\Delta - \frac{d}{2})} \kappa_{\Delta+\ell}^{\Delta_{12},\Delta_{34}},$$

$$\kappa_{\Delta+\ell}^{\Delta_{12},\Delta_{34}} = \frac{\Gamma\left(\frac{\Delta+\ell+\Delta_{12}}{2}\right) \Gamma\left(\frac{\Delta+\ell-\Delta_{12}}{2}\right) \Gamma\left(\frac{\Delta+\ell+\Delta_{34}}{2}\right) \Gamma\left(\frac{\Delta+\ell-\Delta_{34}}{2}\right)}{2\pi^2 \Gamma(\Delta+\ell-1)\Gamma(\Delta+\ell)}. \qquad (2.12.3)$$

The conformal partial waves with integer spin and unphysical dimension, $\Delta \in d/2 + i\mathbb{R}$ form a complete basis for normalisable functions and satisfy the orthogonality relation which schematically reads

$$\left(F_{\Delta,\ell}^{\Delta_{12},\Delta_{34}}, F_{\Delta',\ell'}^{\Delta_{12},\Delta_{34}} \right) \sim \delta_{\ell,\ell'} \delta(\Delta - \Delta'). \qquad (2.12.4)$$

There are, however, contributions to the correlator which are non-normalisable and they are denoted as "(non-norm.)" in (2.12.1). The most notable example of non-normalisable contribution is the identity operator. Details about non-normalisable contributions are discussed in Appendix B of [33].

From (2.12.2) it is obvious that $K_{\Delta,\ell} F_{\Delta,\ell}(z, \bar{z})$ is invariant under $\Delta \leftrightarrow \tilde{\Delta}$ and this is called *shadow symmetry*. As a result we can assume $c(\Delta, \ell)/K_{\Delta,\ell}$ to be also shadow symmetric (because the anti-symmetric part, if any, does not contribute to (2.12.1))

$$\frac{c(\Delta, \ell)}{K_{\Delta,\ell}^{\Delta_{12},\Delta_{34}}} = \frac{c(d - \Delta, \ell)}{K_{d-\Delta,\ell}^{\Delta_{12},\Delta_{34}}}. \qquad (2.12.5)$$

The shadow symmetry allows us to rewrite (2.12.1) as an integral over conformal

blocks only

$$g(z, \bar{z}) = \sum_{\ell=0}^{\infty} \int_{d/2-i\infty}^{d/2+i\infty} \frac{d\Delta}{2\pi i} \, c(\Delta, \ell) G_{\Delta,\ell}^{\Delta_{12},\Delta_{34}}(z, \bar{z}) + \text{(non-norm.)}. \qquad (2.12.6)$$

Then by deforming the integral contour over Δ to the right half plane and picking up the poles in $c(\Delta, \ell)$ we recover the conformal block expansion (2.11.4).[11] Therefore, the OPE density encodes the CFT data through the location and the residue of its poles

$$f_{12\mathcal{O}} f_{34\mathcal{O}} = -\operatorname{Res}_{\Delta'=\Delta_{\mathcal{O}}} c(\Delta', \ell_{\mathcal{O}}). \qquad (2.12.7)$$

Using the orthogonality condition of the conformal partial waves one can extract the OPE density by integrating both sides of (2.12.1) against another conformal partial wave.[12] This gives the *Euclidean inversion formula*

$$c(\Delta, \ell) = n_{\Delta,\ell} \int_{\mathbb{C}} dz d\bar{z} \, \mu(z, \bar{z}) F_{\Delta,\ell}^{\Delta_{12},\Delta_{34}}(z, \bar{z}) g(z, \bar{z}), \qquad (2.12.8)$$

where the integration runs over the Euclidean region, namely the entire complex plane with $\bar{z} = z^*$. The integration measure is

$$\mu(z, \bar{z}) = \left| \frac{z - \bar{z}}{z\bar{z}} \right|^{d-2} \frac{((1-z)(1-\bar{z}))^{\frac{\Delta_{34}-\Delta_{12}}{2}}}{(z\bar{z})^2}. \qquad (2.12.9)$$

We leave the normalisation factor $n_{\Delta,\ell}$ implicit because it is not important for the discussion. Note that the Euclidean inversion formula is valid only for integer spins.

2.13 Euclidean, Lorentzian and Complex Kinematic Regions

So far we have been considering Euclidean CFTs where operators are spacelike separated. For four-point functions in cross ratio space, this means $\bar{z} = z^* \in \mathbb{C}$. If the operators are analytically continued to a Lorentzian configuration, then $z, \bar{z} \in [0, 1]$ and are independent of each other. More generally, (during analytic continuation) z and $\bar{z}$ can be viewed as two independent complex variables.

Regge Limit   For example, to reach the (*t*-channel) *Regge limit* described in [34, 35], one needs to continue $\bar{z}$ around 1 and then send both z and $\bar{z}$ to 0 while keeping their ratio fixed.

---

[11]A subtlety related to this statement is that conformal blocks also have poles in Δ, which originate from the zeros in the projector defined in (2.11.1), through which the conformal block is defined. These poles are cancelled by the spurious poles in $c(\Delta, \ell)$ such that the conformal block decomposition is indeed recovered. For more details see [33].

[12]The non-normalisable terms should be first subtracted and later added back after integration.
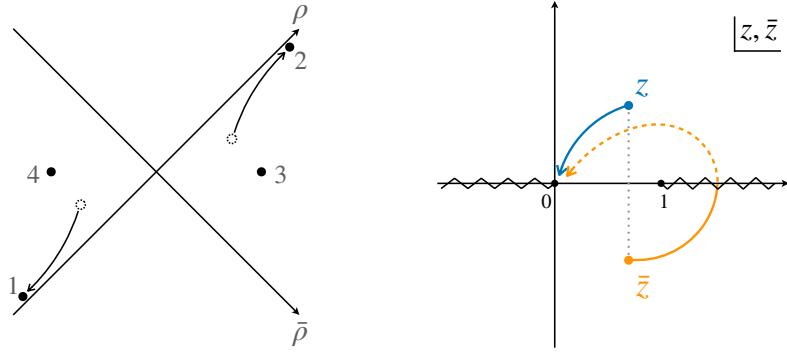
Figure 2.2. Regge limit in position space starting from a Lorentzian configuration (left) and cross ratio space starting from a Euclidean configuration (right).

By introducing a new pair of cross ratios $\rho, \bar{\rho}$ defined through

$$z = \frac{4\rho}{(1+\rho)^2}, \quad \bar{z} = \frac{4\bar{\rho}}{(1+\bar{\rho})^2}, \qquad (2.13.1)$$

the Regge limit can also be parametrised as

$$\rho = \sigma w = \sigma e^{i\theta}, \quad \bar{\rho} = \frac{\sigma}{w} = \sigma e^{-i\theta},$$
$$w \to 0, \quad \sigma \text{ fixed, or } \quad \theta = it + \epsilon, \quad t \to \infty, \qquad (2.13.2)$$

where $\sigma \in [0,1]$, θ is real in Euclidean signature and imaginary in Lorentzian signature and t is called the boost parameter. As $t \to \infty$, x_1 and x_2 are sent to infinity along the lightlike direction. One can check that (2.13.2) indeed agrees with the Regge limit, with which we have $z \sim 4w\sigma, \bar{z} \sim 4w\sigma^{-1}$ and the $i\epsilon$ prescription dictates the direction of analytic continuation across the lightcones.

The Regge limit can also be visualised in position space starting from a Lorentzian configuration, in which $\rho, \bar{\rho}$ are real and independent of each other. By putting four operators respectively at

$$x_1 = (-\rho, -\bar{\rho}), \quad x_2 = (\rho, \bar{\rho}), \quad x_3 = (1,1), \quad x_4 = (-1,-1), \qquad (2.13.3)$$

we see that in the Regge limit (2.13.2) operator 1 and 2 are sent to infinity along the lightcone. This is illustrated in figure 2.2.

As we will see in Chapter 3, in the flat-space limit, the CFT Regge limit corresponds to high energy scattering limit (QFT Regge limit) in the t-channel.

Lightcone limit on the second sheet Similar to the Regge limit, the lightcone limit on the second sheet (LLSS) also corresponds to continuing $\bar{z}$ around 1 and sending z to 0. The difference is that $\bar{z}$ is now fixed and finite.

Both Regge limit and LLSS are important for the discussion in the next section which

we will now turn to.

2.14 The Lorentzian Inversion Formula

By analytically continuing the Euclidean inversion formula (2.12.8) to the Lorentzian regime, one obtains Caron-Huot's Lorentzian inversion formula [1],[13] which dictates that the OPE density is a combination of two functions analytic in spin[14]

$$c(\Delta, \ell) = c^t(\Delta, \ell) + (-1)^\ell c^u(\Delta, \ell),$$

$$c^t(\Delta, \ell) = \frac{\kappa_{\Delta+\ell}^{\Delta_{12},\Delta_{34}}}{4} \int_0^1 dz d\bar{z} \mu(z,\bar{z}) G_{\ell+d-1,\Delta-d+1}^{\Delta_{12},\Delta_{34}}(z,\bar{z}) \mathrm{dDisc}_t \left[g(z,\bar{z}) \right],$$

$$c^u(\Delta, \ell) = \frac{\kappa_{\Delta+\ell}^{\Delta_{12},\Delta_{34}}}{4} \int_{-\infty}^0 dz d\bar{z} \mu(z,\bar{z}) G_{\ell+d-1,\Delta-d+1}^{\Delta_{12},\Delta_{34}}(z,\bar{z}) \mathrm{dDisc}_u \left[g(z,\bar{z}) \right]. \tag{2.14.1}$$

The most important factors appearing above are the *double discontinuities*, which for a generic function $g(z,\bar{z})$ read

$$\mathrm{dDisc}_t[g(z,\bar{z})] = \cos\left(\pi \frac{\Delta_{34} - \Delta_{12}}{2}\right) g(z,\bar{z}) - \frac{1}{2} e^{\mathrm{i}\pi \frac{\Delta_{34}-\Delta_{12}}{2}} g\left(z, 1-(1-\bar{z})e^{-2\pi\mathrm{i}}\right)$$

$$- \frac{1}{2} e^{-\mathrm{i}\pi \frac{\Delta_{34}-\Delta_{12}}{2}} g\left(z, 1-(1-\bar{z})e^{2\pi\mathrm{i}}\right).$$

$$\mathrm{dDisc}_u[g(z,\bar{z})] = \cos\left(\pi \frac{\Delta_{34} - \Delta_{12}}{2}\right) g(z,\bar{z}) - \frac{1}{2} e^{\mathrm{i}\pi \frac{\Delta_{34}-\Delta_{12}}{2}} g\left(z, \bar{z}e^{2\pi\mathrm{i}}\right)$$

$$- \frac{1}{2} e^{-\mathrm{i}\pi \frac{\Delta_{34}-\Delta_{12}}{2}} g\left(z, \bar{z}e^{-2\pi\mathrm{i}}\right). \tag{2.14.2}$$

In words, the $t(u)$-channel double discontinuity operation takes a function and subtracts from it its analytic continuations around $\bar{z} = 1(\infty)$ in both directions. Also notice that the conformal block appearing in the integration kernel has swapped dimension and spin.

In the Regge limit each conformal block (with $\ell \geq 2$) scales as

$$G_{\Delta,\ell}(z,\bar{z}) \sim (z\bar{z})^{\frac{1-\ell}{2}}, \tag{2.14.3}$$

---

[13]The Lorentzian inversion formula was derived in both cross ratio space [1] and position space [33]. Here we only state the final result.

[14]The analyticity in spin can be rigorously established only for (most part of) the leading Regge trajectory so far. Regge trajectories correspond to singularities in $c(\Delta, \ell)$, and since the integrals in (2.14.1) diverge at this point it is unclear how to extend analyticity beyond (*e.g.* fixing ℓ and increasing Δ) the leading trajectory. Nevertheless, the Lorentzian inversion formula has been largely successful in explaining the smoothness of the numerically obtained CFT spectra even beyond the leading trajectory (see *e.g.* [36]). Therefore, in this thesis we will use the phrase 'analyticity in spin' while keeping in mind that it is not fully rigorous in the mathematical sense.

therefore the s-channel block decomposition diverges in the Regge limit. This is not surprising because to reach Regge limit one needs to send $\bar{z}$ around 1 (see figure 2.2) and the s-channel block decomposition stops to converge. The Lorentzian inversion formula in principle allows for analytically continuing spin in (2.12.1) to complex values with small or negative real part (implemented by the Sommerfeld-Watson transform), such that the divergence issue faced by s-channel OPE is overcome. This then allows one to derive the asymptotic behaviour of the correlator in the Regge limit (and the LLSS).[15] This series of ideas largely resembles the Regge theory in QFT[16] and is therefore called the *conformal Regge theory* [35, 38–40].

The validity of the Lorentzian inversion formula depends on the behaviour of the correlator in both the Regge limit and the LLSS. Following the conformal Regge theory prescription, one finds that in general the Regge behaviour has the form[17]

$$\lim_{w \to 0} (g(z, \bar{z}) - 1) \sim w^{1-\ell_*}, \tag{2.14.4}$$

where ℓ_* is the intercept of the leading Regge trajectory (*i.e.* the trajectory on the $\Delta - \ell$ plane with the largest spin for any given dimension) with the shadow symmetric line $\Delta = d/2$. The potential divergence of the Lorentzian inversion formula is embodied in the integral

$$\oint_0 dw\, w^{\ell - \ell_* - 1}, \quad |w| \to 0, \tag{2.14.5}$$

thus $\ell > \ell_*$ is needed for convergence. The Regge boundedness of conformal correlators leads to the upper bound on the intercept $\ell_* \leq 1$, thus in general the Lorentzian inversion formula is valid and establishes analyticity in spin for $\ell > 1$. A similar analysis indicates (but does not prove rigorously) that in the LLSS the correlator scales as

$$\lim_{z \to 0} (g(z, 1 - (1 - \bar{z})e^{2\pi i} - 1) \sim z^{\frac{\tau_0}{2}}, \tag{2.14.6}$$

where τ_0 is the lowest twist ($\Delta - \ell$) above the identity operator. Using the unitarity bound (2.7.4) one again obtains that the inversion formula converges for $\ell > 1$.

In Chapter 5 we will see that the presence of supersymmetry softens the Regge behaviour of the correlator and thus analyticity in spin gets extended further. We will also discuss along the way practical applications of the Lorentzian inversion

---

[15]This derivation is not fully rigorous because, as mentioned in footnote 14, the analyticity in spin has not been fully established.

[16]In QFT, the Froissart-Gribov formula (see *e.g.* Section 2 of [37] for a review) establishes analyticity in spin and applying the Sommerfeld-Watson transform to the partial wave expansion of the scattering amplitude determines its high energy behaviour. In fact the Lorentzian inversion formula was originally called the conformal Froissart-Gribov formula.

[17]Here we assume the only non-normalisable term to be the identity operator.

formula.

Chapter 3

Landau Diagrams in AdS and S-matrices from Conformal Correlators

3.1 Introduction

In this chapter we continue and expand the discussion in Section 2.9 on QFT in AdS and its flat-space limit.

Let us first briefly review the setup and we refer to Section 2.9 for more details. Consider a quantum field theory on a fixed $(d+1)$-dimensional AdS background. In this setup, take a correlation function of local operators and push its insertion points all the way to the conformal boundary, inserting scaling factors to obtain a finite answer, as in (2.9.8). This LSZ-like limit gives rise to what we call *boundary correlation functions*. If the AdS isometries are preserved then these obey all the useful axioms of usual CFT correlation functions: conformal invariance in d dimensions, a large domain of analyticity and a convergent conformal block decomposition. All this is of course familiar from AdS/CFT; the only difference is that there is no stress tensor in the boundary spectrum because the bulk metric is not dynamical.

Our main interest lies with the behaviour of these boundary correlation functions in the *flat-space limit*. (We will write it as $R \to \infty$ with R the curvature radius of AdS.) Supposing that it exists, it is a natural expectation that the *S-matrix* of the bulk theory is encoded in the flat-space limit of the boundary correlation functions. This idea has a long history, especially in the context of AdS/CFT (starting with [26, 27, 41–44]) where one can try to extract string theory amplitudes from CFT correlators. Until recently comparatively little attention has been given to the setup where the bulk theory is gapped and does not contain gravity, but see [13, 23, 45–52] for works in that direction. It is nevertheless an extremely interesting subject. This is because scattering amplitudes are rather mysterious objects with an interplay

of analyticity and unitarity that appears to be at most partially understood. But via the QFT in AdS construction we can obtain amplitudes as a limit of conformal correlation functions, and it is natural to expect that the well-established properties of the latter can clarify some of the mysteries surrounding the former.

As for the precise map from correlator to amplitude there exist several proposals. Two concrete proposals were written down in [13]: one in Mellin space and a phase shift formula. In other work mention was made of a Fourier space algorithm [53]. In this work we propose a *position-space* limit, which refines and generalizes the idea proposed in [54] for AdS$_2$. One might wonder why we need yet another formula given we already have concrete proposals. The main reason is because the existing proposals have their own shortcomings: for instance, the phase shift formula has a drawback that it can only be defined in a physical kinematics and relies on averaging over the OPE data, which is sometimes difficult to perform in practice. On the other hand, the Mellin approach involves integral transforms of some correlators which make it hard to discuss their analytic properties at the nonperturbative level. In fact the existence of the Mellin-space representation of the correlators was established only quite recently in [55] and yet, its analyticity is not fully understood. Another, more technical issue is that there are singularities of the flat-space amplitudes which are not well-understood in the Mellin approach. One representative example are anomalous thresholds, which come from on-shell propagations of particles in several different channels. Such singularities are hard to see from the Mellin approach since the poles of the Mellin representation of the correlator are normally associated with the operator product expansion in a single channel.

By contrast, our position-space approach has the distinguishing feature that it requires no OPE data manipulation or integral transforms: instead the position-space correlator *becomes* the S-matrix element. We propose, for example, that two-point functions $|x - y|^{-2\Delta}$ become single-particle norms, $\langle \vec{k} | \vec{p} \rangle \propto \delta^{(d)}(\vec{k} - \vec{p})$, that contact diagrams in AdS become momentum-conserving delta functions, and more generally that

$$\lim_{R \to \infty} \langle \mathcal{O}_1(x_1) \mathcal{O}_2(x_2) \ldots \mathcal{O}_n(x_n) \rangle = \langle \vec{k}_1 \vec{k}_2 \ldots | \ldots \vec{k}_n \rangle \,, \qquad (3.1.1)$$

with a suitable normalization of the operators. To make the above formula work a map is needed from boundary positions to on-shell momenta, which indeed both have d components. It turns out that this map is not without i's, and for physical kinematics we need to move the x_i to complex positions. This is maybe to be expected, since in real Lorentzian AdS massive particles cannot reach the boundary. The precise map is given in section 3.2.3. For a four-point function of identical operators it implies a relation between cross-ratios and Mandelstam invariants as given in equation (3.2.32).

Another distinguishing feature of our proposal is that it fails to work in certain kinematic regions. Starting with the exchange diagram, which is discussed in detail

in section 3.3.3, we find that there are regions in the complex Mandelstam planes
where the flat-space limit of the correlation function diverges, even after stripping off
the momentum-conserving delta function, and therefore does not equal the scattering
amplitude. As we explain qualitatively in section 3.2, this is due to the possibility
of exchanged particles going on-shell and propagating over distances of the order of
the ever-growing AdS scale.[1] Such a separation of the interaction vertices in a given
diagram is of course reminiscent of flat-space Landau diagrams which can be used
to deduce the location of potential singularities in flat-space scattering amplitudes.
In AdS with finite R the infrared is regulated and these Landau singularities do not
exist, but that does not mean that they cannot spoil the flat-space limit. To un-
derstand them better we formulate in section 3.4 the general AdS Landau equations
and compare them with their flat-space counterpart. We will argue that they are
indicators of singularities in the flat-space amplitude, since, it appears that every
flat-space Landau singularity is surrounded by a region in the Mandelstam planes
where the flat-space limit does not work. This would imply that the AdS Landau
equations can reproduce anomalous thresholds in the flat-space limit; to demonstrate
this we include a numerical analysis of the triangle diagram in section 3.4.2.

In sections 3.5 and 3.6 we compare our proposal with the Mellin space and phase
shift proposals of [13], respectively. We will find that the Mellin space proposal can
be recovered from our proposal (for Mellin-representable correlation functions) via
a saddle point analysis, and can understand the divergences from the AdS Landau
singularities as originating from a contribution of Mellin poles that are picked up by
moving the original integration contour to the steepest descent contour. (Conversely,
it is natural to suspect that anomalous thresholds cannot appear if no poles are picked
up.) Conformal blocks will really only enter our discussion in section 3.6, where we
will make contact with the phase shift formula of [13] and formulate a condition on
the OPE data such that the flat-space limit amplitude obeys unitary conditions. We
will also see that in that context the singularities arise from divergent contributions
of conformal blocks corresponding to "bound states" in the flat space limit. The
results in this section should be viewed as a first exploration into the implications of
the existence of an OPE for scattering amplitudes — we hope to report more results
in this direction in the near future.

---

[1]Landau diagrams in AdS were discussed also in [56], but there are several important differences
from our work. In [56], the authors only considered trajectories of massless particles in Lorentzian
AdS which interact at a single bulk point. Such diagrams give rise to singularities of the boundary
correlation functions even before the flat-space limit is taken. On the other hand, in this chapter we
discuss Landau diagrams of massive particles in a complexified AdS space that interact at widely
separated bulk points and which are responsible for singularities of the S-matrix in the flat-space
limit.

3.2 The flat-space limit in position space

In this section, we present our conjectural position-space recipe for obtaining flat-space scattering amplitudes from the conformal boundary correlation functions of a QFT in AdS. In order to motivate the conjectures, we first explain how the building blocks of AdS Witten diagrams, namely the bulk-boundary propagator and the bulk-bulk propagator, morph into their counterparts in flat space. Our main result will be that the bulk-boundary propagator becomes very simple in the flat-space limit and essentially reduces to a factor like e^{ipx} with an on-shell momentum p while the bulk-bulk propagator becomes the Feynman propagator $1/(p^2 + m^2)$.

After presenting our position-space formulas, we discuss briefly its physical implications including a direct relation between the conformal cross ratios and the Mandelstam variables. We also give a heuristic argument on why such a formula may fail to work in certain kinematic regions. Understanding the details of why and how the formula fails is the main subject of the rest of this chapter and that is what will lead us to propose the AdS analogue of Landau diagrams in section 3.4.

3.2.1 The flat-space limit setup

Let us first specify the setup in more details. We consider massive quantum scalar fields ϕ_i with mass m_i. The corresponding boundary operators $\mathcal{O}_i$ which can be obtained by pushing ϕ_i to the conformal boundary have scaling dimensions Δ_i and they satisfy $\Delta_i(\Delta_i - d) = m_i^2 R^2$. The exact meaning of the flat-space limit is sending both AdS curvature radius R and scaling dimension Δ_i to infinity while keeping the ratios fixed

$$R \to \infty, \ \Delta_i \to \infty, \ \lim_{R,\Delta_i \to \infty} \frac{\Delta_i}{R} = m_i \text{ fixed.} \tag{3.2.1}$$

3.2.2 Motivating the conjecture

To motivate the conjecture, let us consider the flat-space limit of the bulk-boundary and bulk-bulk propagators.

Bulk-boundary propagator

We follow the conventions of [43]. This means that we will describe Euclidean AdS$_{d+1}$ using embedding space coordinates X living in $d + 2$ dimensional Minkowski space which obey:

$$-(X^0)^2 + \sum_i (X^i)^2 = -R^2, \quad X^0 > 0$$

and points on the conformal boundary of AdS are labelled by $d + 2$ dimensional
points P on the projective null cone:

$$- (P^0)^2 + \sum_i (P^i)^2 = 0, \quad P \sim \lambda P \ (\lambda \in \mathbb{R}^*) \tag{3.2.2}$$

We can resolve the constraints and 'gauge fix' as follows:

$$X = \left(R \cosh \left(\frac{\rho}{R} \right), \ R \sinh \left(\frac{\rho}{R} \right) n_X \right),$$
$$P = (1, \ n_P),$$

Where we introduced our choice of local coordinates for AdS_{d+1}: a radial coordinate
ρ and a $d+1$ dimensional unit norm vector n^μ which obeys $n^\mu n^\nu \delta_{\mu\nu} = 1$. The metric
reads:

$$ds^2 = d\rho^2 + R^2 \sinh^2 \left(\frac{\rho}{R} \right) d\Omega_d^2, \tag{3.2.3}$$

and therefore the flat-space limit in these coordinates is very simple: we just send
$R \to \infty$ holding all of the coordinates fixed. The standard Euclidean coordinate x
is then:

$$x = \rho n_X.$$

Now consider the bulk-boundary propagator. It reads:

$$G_{B\partial}(X, P) = \frac{\mathcal{C}_\Delta}{R^{(d-1)/2}(-2P \cdot X/R)^\Delta}$$
$$= \frac{\mathcal{C}_\Delta}{2^\Delta R^{(d-1)/2}} e^{-\Delta \log(-P \cdot X/R)} \tag{3.2.4}$$

where

$$\mathcal{C}_\Delta = \frac{\Gamma(\Delta)}{2\pi^h \Gamma(\Delta - h + 1)}, \qquad h = \frac{d}{2}, \qquad \Delta(\Delta - d) = m^2 R^2.$$

Substituting

$$- P \cdot X/R = \cosh \left(\frac{\rho}{R} \right) - \sinh \left(\frac{\rho}{R} \right) n_P \cdot n_X \tag{3.2.5}$$

straightforwardly yields that

$$\boxed{G_{B\partial}(X, P) \xrightarrow{R \to \infty} \frac{m^{h-1}}{2^{mR+1} \pi^h R^{1/2}} e^{m n_P \cdot x}.} \tag{3.2.6}$$

This can be compared this with an external leg in a flat-space Feynman diagram,
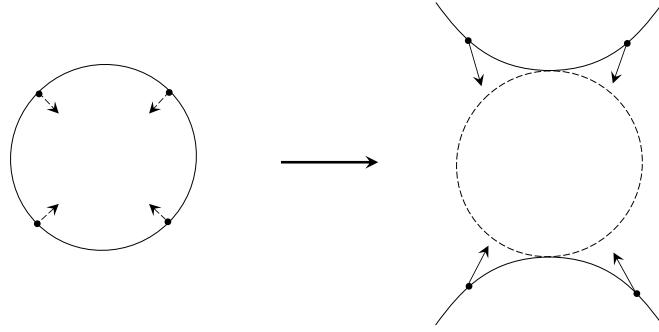
Figure 3.1. Analytic continuation of the boundary points. We start from a CFT on S^d and analytically continue the insertion points of operators to complex values in order to recover the flat-space S-matrix. Geometrically this corresponds to going from a sphere to a hyperboloid.

which would simply read

$$\frac{1}{\sqrt{Z}} e^{i\eta_{\mu\nu} k^\mu y^\nu}. \tag{3.2.7}$$

with k^μ an on-shell Lorentzian momentum (so $k^2 = -m^2$), y^ν a Lorentzian position, $\eta_{\mu\nu} = \text{diag}(-++\ldots+)$, and, because we work in conventions where all momenta are ingoing, $k^0 > 0$ or $k^0 < 0$ for an ingoing or outgoing momentum, respectively.

Clearly we find the normalization factor

$$\frac{1}{\sqrt{Z}} = \frac{\mathcal{C}_\Delta}{2^\Delta R^{(d-1)/2}} \xrightarrow{R\to\infty} \frac{m^{h-1}}{2^{mR+1}\pi^h R^{1/2}}, \tag{3.2.8}$$

whereas the exponents are matched as follows. First we recognize that (3.2.6) was derived with a Euclidean signature bulk metric, so the contraction $n_P \cdot x$ is really equal to $\delta_{\mu\nu} n_P^\mu x^\nu$, and similarly $\delta_{\mu\nu} n_p^\mu n_p^\nu = 1$. On the other hand (3.2.7) requires Lorentzian signature, so if we write $y^\mu = (y^0, \underline{y})$ and $x^\mu = (x^0, \underline{x})$ then the standard *bulk* analytic continuation dictates that[2]

$$y^0 = -ix^0, \qquad \underline{y} = \underline{x}, \tag{3.2.9}$$

and therefore a match can be obtained if the *boundary* points do something entirely different, namely we need to set

$$n_p^0 = -k^0/m \qquad \underline{n}_p = i\underline{k}/m. \tag{3.2.10}$$

We conclude that physical S-matrix momenta correspond to complex boundary positions! More precisely, the above equation shows that if we start from real bound-

---

[2]There is no real freedom here: the bulk point x is integrated over and should be continued in accordance with the desired Wick rotation.

ary coordinates in Euclidean signature (so real n_p^μ), then we need to continue the
spacelike components $\underline{n}_p$ to purely imaginary values, whereas the zero-component
remains real but obeys $|n_p^0| > 1$ because $|k^0| > m$. Pictorially this corresponds to
analytically continue the boundary sphere to a hyperboloid, see figure 3.1. Alterna-
tively, supposing we start from real boundary coordinates in Lorentzian signature,
which according to the bulk analytic continuation (3.2.9) corresponds to real $\underline{n}_p$ but
purely imaginary n_p^0, then we find that we need to continue *all* the components to
purely imaginary values. We should also note that these continuations always re-
spect $1 = \delta_{\mu\nu} n_p^\mu n_p^\nu = -\eta_{\mu\nu} k^\mu k^\nu / m^2$, so we are automatically on the mass shell. The
analytic continuation will be discussed in more detail below.

Bulk-bulk propagator

Next we consider the bulk-bulk propagator $G_{BB}(X_1, X_2)$. Its defining equation reads

$$\left(\Box_g - \Delta(\Delta - d)\right) G_{BB}(X_1, X_2) = \frac{1}{\sqrt{g}} \delta^{(d+1)}(X_1 - X_2). \qquad (3.2.11)$$

For the computations that are to follow it turns out that the most convenient solution
is the split representation of [43] where[3]

$$G_{BB}(X_1, X_2) = \int_{-i\infty}^{i\infty} \frac{dc}{2\pi i} \frac{2c^2}{c^2 - (\Delta - h)^2} \int_{\partial AdS} dQ \frac{R^{1-d} \mathcal{C}_{h+c} \mathcal{C}_{h-c}}{(-2Q \cdot X_1/R)^{h+c}(-2Q \cdot X_2/R)^{h-c}}$$
$$(3.2.12)$$

In the large R limit we send $\Delta \to \infty$ but we have to give some thought to the scaling
of X_1 and X_2. In the spherical AdS coordinates introduced above we have

$$X_1 = \left(R \cosh\left(\frac{\rho_1}{R}\right), R \sinh\left(\frac{\rho_1}{R}\right) n_{X_1}\right),$$
$$X_2 = \left(R \cosh\left(\frac{\rho_2}{R}\right), R \sinh\left(\frac{\rho_2}{R}\right) n_{X_2}\right),$$
$$Q = (1, n_Q).$$

and the integration measure dQ is the usual one on the d-dimensional sphere. In the
flat-space limit we keep ρ fixed as we send $R \to \infty$. The substitution

$$c \equiv iKR, \qquad K \in \mathbb{R} \qquad (3.2.13)$$

---

[3]The solutions can also be written as $G_{BB}(X_1, X_2) = \frac{R^{1-d} \mathcal{C}_\Delta}{u^\Delta} {}_2F_1\left(\Delta, \Delta - d/2 + 1, 2\Delta - d + 1; -4/u\right)$ with $u = (X_1 - X_2)^2/R^2$. In this case the two limits discussed later in this section yield, respectively, the familiar Bessel function expression for the position-space Klein-Gordon propagator and an expression which is familiar from the large Δ limit of a one-dimensional conformal block.

$$\overset{R\gg 1}{\sim} \int \frac{d^{d+1}k}{(2\pi)^{d+1}} \frac{e^{ik(x_1 -}}{k^2 + m}$$

$$\overset{R\gg 1}{\sim} \; e^{-\Delta d(X_1, X_2)}$$
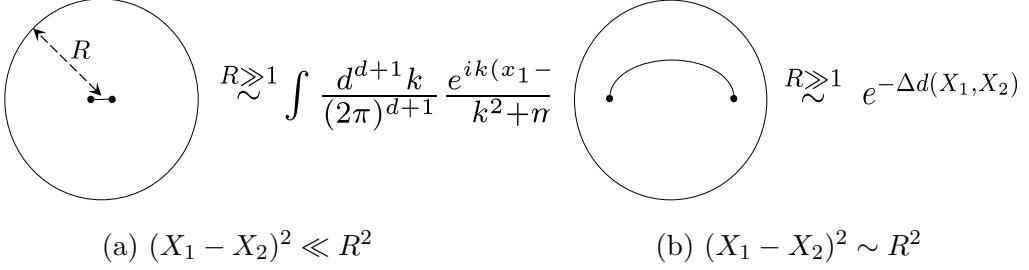
(a) $(X_1 - X_2)^2 \ll R^2$ (b) $(X_1 - X_2)^2 \sim R^2$

Figure 3.2. Two different limits of the bulk-bulk propagator. (a) If the two bulk points are close to each other $(X_1 - X_2)^2 \ll R^2$, the large R limit gives a propagator in flat space. (b) If the two bulk points are kept apart, the limit is described by a geodesic in AdS which connects the two points. In this case, the propagator falls off exponentially $e^{-\Delta d(X_1, X_2)}$ where $d(X_1, X_2)$ is a geodesic distance between the two points.

yields

$$\frac{1}{(\Delta - h)^2 - c^2} \qquad \to \qquad \frac{1}{R^2} \frac{1}{m^2 + K^2} \tag{3.2.14}$$

with $\Delta(\Delta - d) = m^2 R^2$ as before, and with the appropriate large R limits of the other building blocks we find that

$$G_{BB}(X_1, X_2) \to \int_0^\infty \frac{K^d dK}{(2\pi)^{d+1}} \int d\Omega_d \frac{e^{iK\left(\rho_1 n_Q \cdot n_{X_1} - \rho_2 n_Q \cdot n_{X_2}\right)}}{m^2 + K^2}$$

$$= \int \frac{d^{d+1}k}{(2\pi)^{d+1}} \frac{e^{ik \cdot (x_1 - x_2)}}{m^2 + k^2}, \tag{3.2.15}$$

where the integral over the AdS boundary coordinate Q simply becomes an integral over a d-dimensional unit sphere, and we have made the identification $Kn_Q^\mu \to k^\mu$. Notice that we get the right answer on the nose: unlike the bulk-boundary propagator there are no relative factors of i or normalization issues. See also figure 3.2a.

In the above flat-space limit, we implicitly assumed that the two bulk points are close to each other, $(X_1 - X_2)^2 \ll R^2$. Although this would be appropriate for the flat-space limit, there also exists a pure *large Δ limit* of the propagator where the bulk points are kept apart. To find the behaviour in this limit we can close the c contour in the appropriate right or left half plane to pick up the pole at $c = \pm(\Delta - h)$. The Q integral can then be done via a saddle point approximation (which is easy after choosing a specific frame) and results in

$$G_{BB}(X_1, X_2) \to \exp(-\Delta \tilde{\rho}) = \exp(-\Delta \operatorname{arccosh}(-X_1 \cdot X_2 / R^2)) \tag{3.2.16}$$

up to a prefactor and other non-exponential terms in Δ that will not matter below. Note that what appears in the exponent is a geodesic distance between the two points X_1 and X_2, so in this limit we recover a classical particle travelling along the geodesic between these two points (see figure 3.2b).

In order for the flat-space limit to work all the interactions must take place at distances below the AdS scale. In the integrals over the bulk vertices X_1 and X_2 it is therefore essential that these large Δ limits are always suppressed for the correlation functions that we want to analyse. This is a nontrivial condition since the points X_1 and X_2 are integrated over in a Witten diagram and in principle both limits must be included. As we see in the subsequent sections, this large Δ limit is precisely what sometimes obstructs us from taking the flat-space limit in position space. For now, we proceed to present our conjectures on the flat-space limit relegating detailed discussions about possible subtleties to subsection 3.2.4.

3.2.3 S-matrix conjecture and amplitude conjecture

Any Witten diagram is a combination of bulk-bulk and bulk-boundary propagators which are connected at vertices to be integrated over all of AdS_{d+1}. In the preceding section we have seen that the flat-space limit of these building blocks (when holding the bulk coordinates ρ and n^μ fixed) reduces them to the corresponding flat-space expression, and in particular bulk-boundary propagators reduce to the usual external leg factors for position-space Feynman diagrams after a suitable analytic continuation. It is then natural to formulate the

S-matrix conjecture :

$$\langle \tilde{\underline{k}}_1 \ldots \tilde{\underline{k}}_a | S | \underline{k}_1 \ldots \underline{k}_b \rangle \overset{?}{=} \lim_{R \to \infty} \left(\sqrt{Z} \right)^{a+b} \langle \mathcal{O}(\tilde{n}_1) \ldots \mathcal{O}(\tilde{n}_a) \mathcal{O}(n_1) \ldots \mathcal{O}(n_b) \rangle|_{\text{S-matrix}}$$

$$(3.2.17)$$

where the boundary correlator should be evaluated in the round metric on the boundary S^d and analytically continued to the 'S-matrix' configurations which in unit vector coordinates $\delta_{\mu\nu} n^\mu n^\nu = \delta_{\mu\nu} \tilde{n}^\mu \tilde{n}^\nu = 1$ correspond to the values

$$(n^0, \underline{n}) = (-k^0, i\underline{k})/m \,, \tag{3.2.18}$$

and similarly for the tilded variables, with $k^0 > 0$ for 'in' and $\tilde{k}^0 < 0$ for 'out' states. The normalization factor $\sqrt{Z}$ was given in (3.2.8).[4]

Notice that the object on the left-hand side of equation (3.2.17) is an S-matrix element and therefore includes possible disconnected components as well as an overall

---

[4]This is the right normalization factor when operators are normalized as $\langle \mathcal{O} | \mathcal{O} \rangle = \mathcal{C}_\Delta$. For unit normalized operators one should replace Z by $\tilde{Z} = \mathcal{C}_\Delta^2 Z$ in (3.2.17). Notice also that in our conventions $\mathcal{O} = \mathcal{O}^{(\text{can})}/(2\Delta - d)$ where $\mathcal{O}^{(\text{can})}$ would be the operator dual to a canonically normalized scalar field in AdS, a common normalization convention in the holographic renormalization literature [57].

momentum-conserving delta function. Schematically we can write:

$$\langle \tilde{\underline{k}}_1 \ldots \tilde{\underline{k}}_a | S | \underline{k}_1 \ldots \underline{k}_b \rangle = (\text{disconnected})$$
$$+ (2\pi)^{d+1} i \, \delta^{(d+1)} \left(\sum_{j=1}^{a} \tilde{k}_j + \sum_{i=1}^{b} k_i \right) \mathcal{T}(\tilde{k}_1 \ldots \tilde{k}_a; k_1 \ldots k_b)$$

$$(3.2.19)$$

where the scattering amplitude $\mathcal{T}(\ldots)$ normally has no further delta-function singularities. To obtain $\mathcal{T}(\ldots)$ we can consider the *connected* correlation function which we then divide by the contact diagram to get rid of the momentum-conserving delta function. This leads us to the

Amplitude conjecture :

$$\mathcal{T}(\tilde{k}_1 \ldots \tilde{k}_a; k_1 \ldots k_b) \stackrel{?}{=} \lim_{R \to \infty} \frac{\langle \mathcal{O}(\tilde{n}_1) \ldots \mathcal{O}(\tilde{n}_a) \mathcal{O}(n_1) \ldots \mathcal{O}(n_b) \rangle_{\text{conn}}}{D(\tilde{n}_1, \ldots, \tilde{n}_a, n_1, \ldots, n_b)} \Bigg|_{\text{S-matrix, cons}}$$

$$(3.2.20)$$

with $D(\tilde{n}_1, \ldots, \tilde{n}_a, n_1, \ldots, n_b)$ denoting the contact diagram in AdS, which is most easily defined as the function that is a constant in Mellin space.[5] Notice also that, as indicated by the subscript, we not only continue the momenta to the S-matrix configuration as in (3.2.18) but we also evaluate it on the support of the momentum-conserving delta function in (3.2.19).

Validity of the conjectures We now make two important comments on our conjectures. First, precisely speaking these conjectures are valid only in certain kinematic regions. At the level of Witten diagrams, this is basically due to the large Δ limit of the bulk-bulk propagator, which we discussed at the end of the last subsection. We will give a heuristic explanation of why they can fail in subsection 3.2.4 and discuss in more detail when the conjectures hold in the rest of this chapter. Second, although here we motivated the conjectures by the analysis of perturbative Witten diagrams, one can arrive at the same conclusion from the conformal block expansion once one makes certain assumptions on the OPE coefficients. We will present a first exploration in this direction in section 3.6 while a more detailed analysis will be presented in a future work.

Comparison between the conjectures Although the expressions look similar, there is an important difference between the S-matrix conjecture in (3.2.17) and the amplitude conjecture in (3.2.20). The former in its most general form only really makes sense for real (on-shell) momenta, because only in that case can we make sense of various delta functions. The latter has no such restriction and can be

---

[5]The masses of the external particles in the contact diagram should be taken to be the physical masses in the interacting theory.

applied to complex values of the momenta. Because of this feature, one might think that the amplitude conjecture is more useful in practice. However we emphasize that being able to reproduce the momentum-conserving delta function is not merely of academic interest but is necessary in certain situations in order to capture the correct physics of scattering amplitudes. The best place to see this is the scattering amplitude in integrable field theories in two dimensions. Owing to the existence of higher conserved charges, the (higher-point) scattering amplitudes in integrable field theories come with extra factors of delta functions, one for each pair of incoming and outgoing momenta, $\propto \prod_j \delta^{(2)}(\tilde{k}_j + k_j)$. As we see in the next section, the momentum-conserving delta function in general come from a certain exponentially growing piece of the boundary CFT correlator. This suggests that the higher-point correlation functions in integrable field theories in AdS_2 grow much faster than the corresponding counterparts in non-integrable field theories when we take the flat-space limit. This feature is arguably what distinguishes integrable field theories from non-integrable field theories in AdS_2. It would be interesting to make this precise and check it in explicit examples[6].

Connections to previous results   The S-matrix conjecture (3.2.17) would lead to an elegant way to obtain scattering amplitudes directly from the correlation function in position space. A similar conjecture was published for AdS$_2$ in [54], where it was claimed that the Euclidean amplitude could be obtained as a limit of the position-space expression. The derivation in that paper however required a more involved wave-packet analysis, and the momentum-conserving delta function was left implicit. In unrelated work, the paper [13] presented both a Mellin space formula and a phase shift formula that could be used in certain cases to extract a flat-space scattering amplitude from CFT data. A detailed comparison with these two prescriptions will be presented in section 3.5 and 3.6, respectively. Finally our conjectures are rather closely related to a recent proposal in [53]. Although we do not see the need to perform any Fourier transforms as was proposed in that work, the underlying picture is quite appealing — both to explain the complexification of the boundary positions and to highlight potential issues with the conjectures.

3.2.4 Potential subtleties

We now present a heuristic explanation on why the conjectures can fail in certain kinematic regions. For this purpose it is useful to connect our conjectures to a 'cylinder with caps' picture put forward in [53] (see figure 3.3) [7]. This picture involves the complexification of the boundary positions and naturally ties the 'real-time AdS/CFT' prescriptions of [63, 64] to the extraction of scattering amplitudes from

---

[6]See recent works [51, 52, 58–62] on integrable (or solvable) theories on AdS_2.

[7]We thank João Penedones for pointing out the relevance of this picture for our formulae.
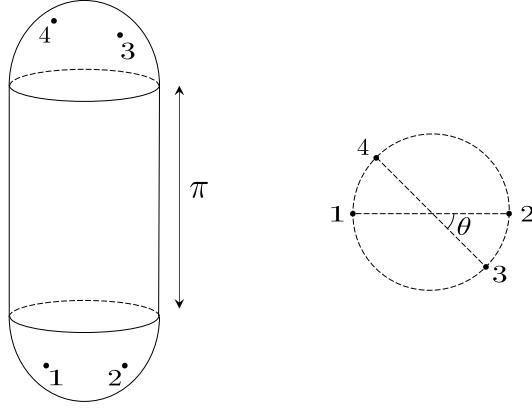
Figure 3.3. A 'cylinder with caps' configuration discussed in [53]. We consider two Euclidean hemispheres and connect them by a Lorentzian cylinder of length π. We then insert two operators on the upper cap and the remaining two operator on the lower cap. The right figure shows a configuration of operator when viewed from the bottom of the lower cap. The angle θ depicted in the figure becomes a scattering angle in the flat-space limit.

conformal correlation functions. To see this, introduce new coordinates as:

$$X = (R\cosh(r/R)\cosh(\tau), R\cosh(r/R)\sinh(\tau), R\sinh(r/R)\underline{n}') \qquad (3.2.21)$$

with $\underline{n}'$ a new unit norm vector. Next we set $\tau = it$ so we are in Lorentzian signature and the metric becomes:

$$ds^2 = dr^2 - R^2\cosh^2(r/R)dt^2 + R^2\sinh^2(r/R)\,d\Omega_{d-1}^2 \qquad (3.2.22)$$

These are the standard global coordinates for Euclidean AdS. The map between old boundary coordinates n^μ and the new boundary coordinates $(\tau, \underline{n}')$ is easily found, and (3.2.18) then implies that we need to set:

$$\tanh(\tau) = -\frac{k^0}{m}, \qquad \frac{\underline{n}'}{\cosh(\tau)} = i\frac{\underline{k}}{m} \qquad (3.2.23)$$

to obtain an S-matrix element with external momentum k^μ. In terms of the Lorentzian coordinate t this means that we can take:

$$\begin{aligned} \text{in state with } k^0 > 0: \quad & t = -\pi/2 + i\operatorname{arccoth}(\,k^0\,/m), \quad & \underline{n}' = -\frac{\underline{k}}{|\underline{k}|} \\ \text{out state with } k^0 < 0: \quad & t = +\pi/2 - i\operatorname{arccoth}(|k^0|/m), \quad & \underline{n}' = -\frac{\underline{k}}{|\underline{k}|} \end{aligned} \qquad (3.2.24)$$

Notice that with our in-going conventions it is entirely reasonable that $\underline{n}'$ points in the opposite direction of $\underline{k}$. What is more interesting is the behaviour of t: when

41

(a)   (b)   (c)
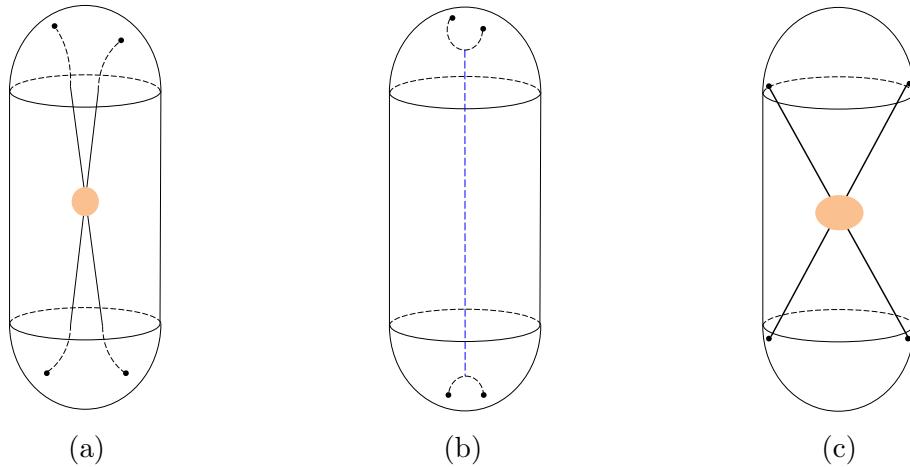
Figure 3.4. Geodesic configurations and flat-space scattering. (a) The geodesics that
describe the flat-space scattering in the large R limit. Two particles emitted from the
operators in the lower Euclidean cap first tunnel to the Lorentzian cylinder, then scatter
at the centre of AdS and tunnel back to the upper Euclidean cap. (b) The geodesics that
give a dominant contribution when two operators are close to each other. Two operators
in the lower cap are directly connected by a Euclidean geodesic, and so are the operators
in the upper cap. These two geodesics can also be connected by an exchange of some light
particle (denoted by a blue dashed line). (c) The geodesics relevant for the bulk point
limit which corresponds to $|k^0| \to \infty$ in our setup. When two operators are close to the
edge of the lower cap, the dominant contribution is given by geodesics which connect four
operators in the Lorentzian cylinder.

tracing it in the complex time plane we see that we arrive exactly at the complex
time contour sketched already in figures 1 and 2 in [63], the essential bits of which
we reproduced in figure 3.3. The idea is that a Lorentzian segment, now with a
length in global time of exactly π, is sandwiched between two Euclidean 'caps' that
are responsible, via operator insertions on their conformal boundary, for the initial
and final state of the scattering event. Modulo Fourier transforms, this is exactly
the same picture as transpired from [53].

   We can now use the 'caps' picture to explain potential subtleties of our conjec-
tures. To simplify the discussion we will consider a four-point function with two
operators in the upper cap and the remaining two in the lower cap as in figure 3.3.

AdS as a particle accelerator   As discussed previously, particles dual to CFT
operators become classical in the flat space limit and travel along geodesics inside
AdS. In the present case, we have to find a geodesic in a mixed-signature spacetime
since the bulk geometry consists of the Euclidean part and the Lorentzian part.
To understand such a geodesic, let us start with the two operators inserted in the
lower cap, see figure 3.4a. The particles emitted from these operators first need to
'tunnel' to the Lorentzian cylinder following the Euclidean geodesics. In order to
smoothly connect them to the Lorentzian geodesics, these two particles must have

42

zero velocities when they emerge into the Lorentzian cylinder from below. Once they appear at the bottom of the cylinder, they then start to accelerate and approach each other owing to an attractive potential coming from the AdS curvature. In this sense, the AdS spacetime acts like a *particle accelerator*. Eventually, these particles collide at the centre of AdS and scatter. Since the Compton wavelengths of these particles ($\propto 1/\Delta$) are much smaller than the AdS radius, the scattering process must be described by the flat-space S-matrix. The energy of the collision is determined by how far apart the particles were at the bottom of the cylinder; the farther they were, more they get accelerated. After the collision, the particles move away from each other and eventually reach the top of the cylinder and then tunnel into the upper Euclidean cap.

Other geodesics The discussion so far seems to support our conjectures on the flat-space limit. There is however one important subtlety: *the geodesic configuration described above is not the only one that contributes to the four-point function.* To understand this, let us consider a limiting case in which the two operators in the lower cap are very close to each other. In this case, we should take into account a Euclidean geodesic which directly connects these two operators (see figure 3.4b). This latter geodesic has a smaller Euclidean action than the one described above and therefore gives a dominant contribution.

On the other hand, if we separate the two operators in the Euclidean cap, this latter geodesic tends to have a larger Euclidean action and therefore can be neglected. In particular, if we consider the so-called bulk-point limit [56] which in this picture corresponds to inserting the two operators at the edge of the cap, the former geodesic becomes entirely Lorentzian while the latter geodesic is Euclidean and is therefore suppressed. See figure 3.4c.

These considerations suggest that the validity of our conjectures depends on the kinematics. Of course, it is hard to tell just from this heuristic argument when precisely they work. The purpose of the rest of this chapter is to perform a more careful analysis and delineate the kinematic region in which they are supposed to hold.

3.2.5 Conformal Mandelstam variables and kinematics

In this subsection we discuss some important aspects of the kinematical relation (3.2.18) between real Lorentzian momenta and complexified boundary positions. More details and technical derivations can be found in appendix 3.A.

Conformal Mandelstam variables

Let us first say a few words about cross ratios. In terms of the spherical coordinates on the boundary of AdS, we have

$$-P_i \cdot P_j = 1 - n_i \cdot n_j = 1 + \frac{k_i \cdot \eta \cdot k_j}{m_i m_j} \tag{3.2.25}$$

This equation immediately implies the following relation between conformal cross ratios and momenta:

$$\frac{(P_i \cdot P_j)(P_k \cdot P_l)}{(P_i \cdot P_k)(P_j \cdot P_l)} = \frac{(m_i m_j + k_i \cdot \eta \cdot k_j)(m_k m_l + k_k \cdot \eta \cdot k_l)}{(m_i m_k + k_i \cdot \eta \cdot k_k)(m_j m_l + k_j \cdot \eta \cdot k_l)} . \tag{3.2.26}$$

By further imposing the momentum conservation[8]

$$\sum_i k_i = 0 , \tag{3.2.27}$$

one can rewrite the right hand side of (3.2.26) in terms of Mandelstam invariants.

It is instructive to work out the relation explicitly for four-point functions of identical scalar operators. The familiar cross ratios are then:

$$u := \frac{P_{12} P_{34}}{P_{13} P_{24}} , \qquad v := \frac{P_{14} P_{23}}{P_{13} P_{24}} , \qquad \left(P_{ij} := -2 P_i \cdot P_j \right) , \tag{3.2.28}$$

but it will sometimes be better to use either the Dolan-Osborn variables $(z, \bar{z})$ [65, 66] or the radial coordinates $(\rho, \bar{\rho})$ [67]:

$$u = z \bar{z} , \quad v = (1 - z)(1 - \bar{z}) , \quad z = \frac{4\rho}{(1 + \rho)^2} , \quad \bar{z} = \frac{4\bar{\rho}}{(1 + \bar{\rho})^2} . \tag{3.2.29}$$

---

[8]Interestingly, there always exists a conformal transformation that places the external points P_i such that $\sum_i k_i = 0$ and therefore $s + t + \tilde{u} = 4m^2$ in terms of Mandelstam invariants. This is why, in the equations below, there are never three independent Mandelstam invariants which would be too many to match against the two independent cross ratios.

$$\rho, \bar{\rho} \qquad\qquad\qquad\qquad\qquad\qquad s$$

$$s = 4m^2 \left(\frac{1-\sqrt{\rho\bar{\rho}}}{1+\sqrt{\rho\bar{\rho}}}\right)^2 \qquad\qquad 4m^2$$
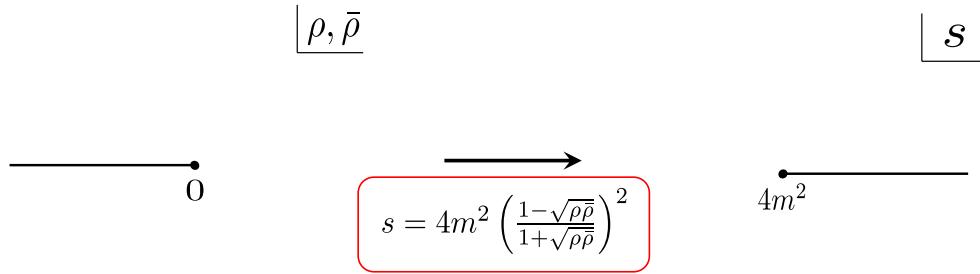
Figure 3.5. The analytic structure of the four-point function in CFT and the flat-space S-matrix. The conformal Mandelstam variables map the branch-cut singularities of the four-point function to a two-particle threshold of the S-matrix.

We then get the relation[9]

Conformal Mandelstam variables :

$$
\begin{aligned}
s &:= -(k_1 + k_2)^2 = 4m^2 \left(\frac{1 - \sqrt{\rho\bar{\rho}}}{1 + \sqrt{\rho\bar{\rho}}}\right)^2 , \\
t &:= -(k_1 + k_4)^2 = 4m^2 \left(\frac{\sqrt{\rho} + \sqrt{\bar{\rho}}}{1 + \sqrt{\rho\bar{\rho}}}\right)^2 , \\
\tilde{u} &:= -(k_1 + k_3)^2 = -4m^2 \left(\frac{\sqrt{\rho} - \sqrt{\bar{\rho}}}{1 + \sqrt{\rho\bar{\rho}}}\right)^2 .
\end{aligned}
\tag{3.2.30}
$$

(Here we used $\tilde{u}$ instead of the conventional notation u in order to distinguish it from the cross ratio u.) These equations (3.2.30) are a new parametrization of the conformal cross ratios of the boundary CFT correlators, chosen precisely such that they become the Mandelstam variables of the scattering amplitudes in flat space. For AdS$_2$ this relation was derived previously in [54] and the result here generalizes it to arbitrary dimensions.

The above equations map the Euclidean CFT kinematics where ρ and $\bar{\rho}$ are complex conjugates to the *Euclidean region* where $0 < s, t, \tilde{u} < 4m^2$, which is the orange triangle in the centre of figure 3.6 shown below. To reach physical kinematics of scattering amplitudes, or indeed any other region, some careful analytic continuations are needed and we will discuss those below. One interesting initial observation is that the expected two-particle branch cut at $s = 4m^2$ is built in from the beginning: according to equation (3.2.30) we just inherit it from the branch cuts at $\rho, \bar{\rho} = 0$

---

[9]While preparing this work, [68] appeared in arXiv in which a similar relation between the cross ratios and the Mandelstam variables was discussed. It also discusses the relation between the momentum conservation and the saddle-point equation, which we explain in section 3.2. As acknowledged in that paper, the results in this work were obtained prior to the publication of [68].

that exist in any correlation function, even before taking the flat-space limit.[10] We
illustrated this in figure 3.5. This behaviour should perhaps be contrasted with the
Mellin space prescriptions: in Mellin space the idea is that infinite sequences of poles
condense into cuts and it is for example impossible to explore other Riemann sheets
before taking the flat-space limit. On the other hand, whereas our prescription nicely
yields the two-particle threshold there is no sign of any further cuts or poles (at least
on the first sheet) because conformal correlation functions are always perfectly ana-
lytic in the Euclidean region. In section 3.3 and beyond we will see that this is very
much related to the subtleties already discussed in section 3.2.4.

Analytic continuations

By conformal invariance, the n-point boundary correlation functions in the flat Eu-
clidean boundary metric depend only on the combinations $-P_i \cdot P_j$. Contact or
light-cone singularities arise when there are i, j such that $-P_i \cdot P_j = 0$. These
singularities correspond to the end points of branch cuts of position-space CFT cor-
relators, which extend to infinity along the negative real axis in the complex plane
of $-P_i \cdot P_j$. From the last expression in equation (3.2.25) we find that

$$
\begin{aligned}
i \text{ in, } j \text{ out or vice versa:} \qquad & -P_i \cdot P_j|_{\text{S-matrix}} \geq 2 \\
i, j \text{ both in or both out:} \qquad & -P_i \cdot P_j|_{\text{S-matrix}} \leq 0
\end{aligned}
\qquad (3.2.31)
$$

with the inequalities holding by virtue of the fact that all the k_i^μ/m_i are unit norm
timelike vectors with $|k_i^0| \geq m_i$. The second continuation precisely lands us on a
branch cut. To see how we should approach the branch cut, recall that in flat space
one requires the corresponding Mandelstam invariants like $s_{ij} = -(k_i+k_j)\cdot\eta\cdot(k_i+k_j)$,
to have a small *positive* imaginary part. In terms of such variables $-2m_i m_j P_i \cdot P_j =
(m_i + m_j)^2 - s_{ij}$, so we will need to give a small *negative* imaginary part to $-P_i \cdot P_j$
when i and j are either both 'in' or both 'out'.

Let us return to the cross ratios for the four-point functions of identical operators.
With the $i\epsilon$ prescription understood, it is not hard to deduce (see appendix 3.A) that
reaching physical kinematics in the s-channel means that we should set the $(\rho, \bar{\rho})$
variables to:

$$
\rho = \frac{\sqrt{s} - 2m}{\sqrt{s} + 2m} e^{i(\theta - 2\pi)}, \qquad \bar{\rho} = \frac{\sqrt{s} - 2m}{\sqrt{s} + 2m} e^{-i\theta} \qquad (3.2.32)
$$

where θ is the scattering angle defined through

$$
t = \frac{1}{2}(4m^2 - s)(1 - \cos(\theta)), \qquad \tilde{u} = \frac{1}{2}(4m^2 - s)(1 + \cos(\theta)). \qquad (3.2.33)
$$

---

[10]This simply follows from the fact that the operator product expansion generally gives terms like
$(\rho\bar{\rho})^\Delta$ with Δ being noninteger. Therefore if we view the correlator as a function of two independent
parameters ρ and $\bar{\rho}$, it has a branch cut at $\rho, \bar{\rho} = 0$.

The factor $2\pi i$ indicates that ρ should be evaluated on the second sheet obtained by circling around zero in a clockwise fashion whereas $\bar{\rho}$ remains on the first sheet.
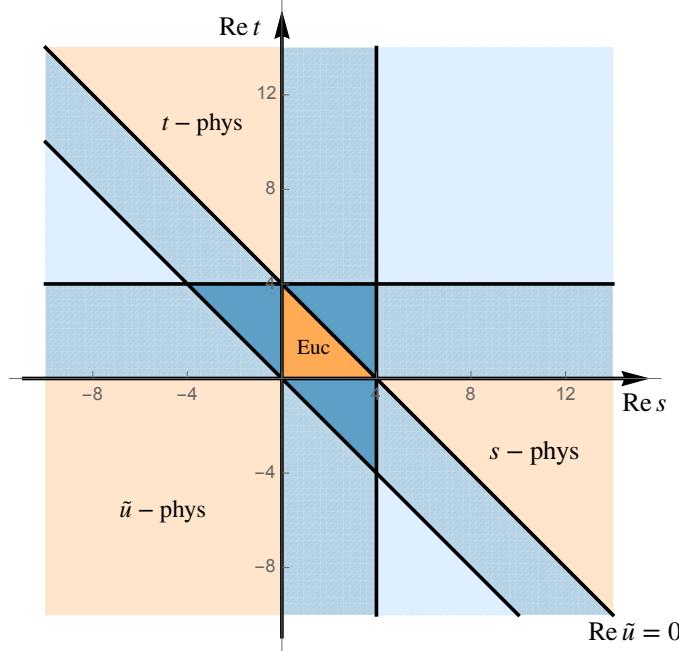

Figure 3.6. The Mandelstam (s, t) plane, coloured according to the analytic continuation necessary to reach each region. The main distinction is orange versus blue: in the former one should take ρ and $\bar{\rho}$ to be complex conjugates and in the latter they are real and independent. A refinement is the dark versus light shading. In the darkest central triangles ρ and $\bar{\rho}$ should be taken to live on the first sheet, and passing to lighter shades corresponds to one or two analytic continuations of either ρ or $\bar{\rho}$ around either 0 or 1. Exactly which sheet corresponds to which region is detailed in appendix 3.A.

We can also consider the Mandelstam plane more generally and to find the analytic continuations in the cross ratios that are necessary to reach all its different regions. This is done in detail in appendix 3.A and we summarize a few essential fact in figure 3.6.

Kinematic limits

The conformal Mandelstam variables allow us to relate kinematic limits of the CFT correlator to those of the scattering amplitude. Here we summarize the correspondence relegating more details including the derivations to appendix 3.A.

OPE limit Let us first analyse the s-channel OPE limit in which both ρ and $\bar{\rho}$ approach zero: $\rho, \bar{\rho} \to 0$. Using the conformal Mandelstam variables (3.2.30), we can immediately see that this limit corresponds to the low-energy limit, or more precisely

the near-threshold limit

$$s \sim 4m^2 \,, \qquad t, \tilde{u} \sim 0 \,. \tag{3.2.34}$$

Regge limit We next consider the Regge limit of the CFT correlator discussed in [34, 35, 56, 69]. Following [35], we write the cross ratios as

$$u = \sigma^2 \,, \qquad v = (1 - \sigma e^\rho)(1 - \sigma e^{-\rho}) \simeq 1 - 2\sigma \cosh \rho \,. \tag{3.2.35}$$

Then, to get to the Regge limit, we first analytically continue v as

$$v \to e^{2\pi i} v \,, \tag{3.2.36}$$

and send $\sigma \to 0$ while keeping ρ fixed. In this limit, the conformal Mandelstam variables scale as

$$s \sim 4m^2 \left(1 - \frac{1}{\cosh^2 \frac{\sigma}{2}}\right) \,, \qquad t \sim -\tilde{u} \sim \frac{4m^2}{\sigma} \frac{1}{\cosh^2 \frac{\sigma}{2}} \gg 1 \,. \tag{3.2.37}$$

This in fact corresponds to the Regge limit of scattering amplitudes (in the t-channel). This is of course expected from various results in the literature but the virtue of the conformal Mandelstam variables is that it makes the relation transparent.

Bulk-point limit Another interesting limit is the so-called bulk-point limit studied in [56]. This limit corresponds to the following analytic continuation[11] of the radial coordinates ρ,

$$\rho = e^{-i\pi-\epsilon} e^{i\varphi} \,, \qquad \bar{\rho} = e^{-i\pi-\epsilon} e^{-i\varphi} \,. \tag{3.2.38}$$

Here ϵ is the regularization parameter, which will be sent to 0 in the bulk-point limit. In this limit, the conformal Mandelstam variables scale as

$$s \to \infty \,, \qquad t \to -\infty \,, \qquad \tilde{u} \to -\infty \,, \tag{3.2.39}$$

while the scattering angle θ is finite. This is a fixed-angle high energy scattering limit, which was studied by Gross and Mende [70] in string theory.

Massless limit Although this is not a kinematic limit, it is interesting to discuss the massless limit $m \to 0$. If we naively take this limit, the conformal Mandelstam variables (3.2.30) all vanish. In order to have finite Mandelstam variables, we need to approach the bulk-point limit as we send m to 0. This is consistent with the results in the literature on the flat-space limit of the massless scattering, all of which involve taking the bulk-point limit. It would be interesting to clarify the precise relation

---

[11]Here we are following the definition of the bulk-point limit in [56]. To relate it to the analytic continuation to physical scattering kinematics discussed above (3.2.32), we need to perform a further Euclidean rotation $\rho \to e^{-\pi i}\rho$ and $\bar{\rho} \to e^{\pi i}\bar{\rho}$.

between our proposal and those results, in particular the position-space approach to the massless scattering discussed in [42]. We leave it for future investigations.

Double lightcone limit   Finally let us briefly mention the double lightcone limit, which corresponds to

$$u = \epsilon(1 - \eta) , \qquad v = (1 - \epsilon)\eta , \tag{3.2.40}$$

with $\epsilon \ll \eta \ll 1$. In this limit, we obtain

$$s \sim 4m^2(1 - 2\sqrt{\epsilon}) , \quad t \sim 4m^2(1 - 2\sqrt{\eta}) , \quad \tilde{u} \sim -4m^2(1 - 2(\sqrt{\epsilon} + \sqrt{\eta})) . \tag{3.2.41}$$

To our knowledge, this limit does not correspond to a well-studied limit of scattering amplitudes. However, given the role the double lightcone limit played in the development of the analytic conformal bootstrap, it might be worth studying this limit in the flat-space scattering.

3.3   Illustrative examples

We now test our conjectures in several simple and illustrative examples: two-point functions, contact diagrams and four-point exchange diagrams. The goal of this section is threefold. First, we explain the details of how the formula works in simple cases. Second, we point out that the saddle-point equations for the geodesic networks in AdS can be interpreted as the momentum conservation at each bulk vertex. We also see a natural connection with the flat-space limit of the Mellin amplitude, which we explore more in section 3.5. Third, we discuss how and when our formula stops working using the exchange diagram as an illustrative example. In section 3.4 below, we combine the latter two observations and propose the AdS analogue of Landau diagrams, which delineate the kinematic regions in which the position-space recipe for the flat-space limit gives a divergent answer.

3.3.1   Two-point functions

The easiest example for which we can test (3.2.17) is the two-point function. In our normalization

$$\langle \mathcal{O}(n_1)\mathcal{O}(n_2) \rangle = \frac{\mathcal{C}_\Delta 2^{-\Delta}}{(1 - n_1 \cdot n_2)^\Delta} \tag{3.3.1}$$

We multiple by the factor Z and use the continuation in (3.2.18) to move particle 1 to the 'in' position, so $(n_1^0, \underline{n}_1) = (-q_1^0, i\underline{q}_1)/m$ and particle 2 to the 'out' position, which we can write as $(n_2^0, \underline{n}_2) = (q_2^0, -i\underline{q}_2)/m$, with $q^0 \geq 0$ and $q^2 = -m^2$ in both cases. This yields

$$Z\langle \mathcal{O}(n_1)\mathcal{O}(n_2) \rangle|_{\text{S-matrix}} = \frac{Z\,\mathcal{C}_\Delta 2^{-\Delta}}{(1 + q_1^0 q_2^0/m^2 - \underline{q}_1 \cdot \underline{q}_2/m^2)^\Delta} = \frac{2^\Delta \mathcal{C}_\Delta^{-1} R^{d-1}}{(-\eta_{\mu\nu}(q_1 + q_2)^\mu (q_1 + q_2)^\nu/m^2)^\Delta} \tag{3.3.2}$$

49

This expression is best understood by going to a frame where $q_1 = (m, \underline{0})$. We get

$$\frac{2^\Delta \mathcal{C}_\Delta^{-1} R^{d-1}}{\left(1 + \sqrt{1 + \underline{q}_2^2/m^2}\right)^\Delta} \tag{3.3.3}$$

and we observe that for large Δ this function starts to look like a delta function singularity, in the sense that it becomes a positive 'bump' with support contracting to the point where $\underline{q}_2 = 0$. To check that all the factors come out right we can integrate:

$$\int d^d \underline{q} \frac{2^\Delta \mathcal{C}_\Delta^{-1} R^{d-1}}{\left(1 + \sqrt{1 + \underline{q}^2/m^2}\right)^\Delta} = 2(2\pi m R)^d \frac{\Delta \Gamma(\Delta - d)}{\Gamma(\Delta)} \xrightarrow{R \to \infty} 2m(2\pi)^d \tag{3.3.4}$$

which demonstrates that, more generally,

$$Z\langle \mathcal{O}(n_1)\mathcal{O}(n_2)\rangle|_{\text{S-matrix}} \xrightarrow{R \to \infty} 2E_1 (2\pi)^d \delta^{(d)}(\underline{q}_1 - \underline{q}_2) \tag{3.3.5}$$

thus proving our general formula (3.2.17) for single-particle states.

3.3.2 Contact diagram and momentum conservation

For our next example we consider n-point contact diagrams, which according to our conjectures should give rise to the momentum-conserving delta function in the flat-space limit. The diagram can be written as

$$G_c(P_i) = \int dX \prod_{i=1}^n G_{B\partial}(X, P_i) = \frac{1}{R^{n(d-1)/2}} \int dX \prod_{i=1}^n \mathcal{C}_{\Delta_i} 2^{-\Delta_i} e^{-\Delta_i \log(-P_i \cdot X/R)} \tag{3.3.6}$$

Vertex momenta and vertex Mandelstam invariants

We will analyse the Euclidean correlator for now, which means that the integral over X is over the hyperboloid $X^2 = -R^2$ and $X^0 > 0$. In the flat-space limit all the scaling dimensions become large and we can use a saddle point approximation for the integral. The relevant function to extremise is then

$$f_c(X) = -\sum_i \Delta_i \log(-P_i \cdot X/R) + \lambda(X^2 + R^2) \tag{3.3.7}$$

with λ a Lagrange multiplier. In more detail, we define the integrals as

$$\int_{\text{AdS}} dX = 2R \int_{-\infty}^\infty d^{d+2}X \, \theta(X^0)\delta(X^2 + R^2) = 2R \int_{-i\infty}^{i\infty} \frac{d\lambda}{2\pi i} \int_{-\infty}^\infty d^{d+2}X \, \theta(X^0) e^{\lambda(X^2 + R^2)} \tag{3.3.8}$$

with the factor $2R$ inserted so the volume element agrees with the one given by the metric in equation (3.2.3). The saddle point equation becomes:

$$\sum_i \Delta_i \frac{P_i}{P_i \cdot X} - 2\lambda X = 0 \tag{3.3.9}$$

which we can contract with X to yield

$$\lambda = -\frac{1}{2R^2} \sum_i \Delta_i \,. \tag{3.3.10}$$

and substituting this back we obtain that

$$\sum_i \Delta_i \left(\frac{P_i}{P_i \cdot X/R} + X/R \right) = 0 \,. \tag{3.3.11}$$

Now comes a crucial observation: We can interpret (3.3.11) as a momentum-conservation condition at the interaction vertex in AdS. To see this, introduce κ_i defined as

$$\kappa_i := \frac{\Delta_i}{R} \left(\frac{P_i}{P_i \cdot X/R} + X/R \right) \,. \tag{3.3.12}$$

In terms of these variables, the saddle-point equation (3.3.11) indeed takes the form of the momentum conservation

$$\sum_i \kappa_i = 0 \,. \tag{3.3.13}$$

In addition, they are on-shell (in the Euclidean sense) and tangent vectors to AdS, i.e.,

$$\kappa_i^2 = m_i^2, \qquad X \cdot \kappa_i = 0 \,. \tag{3.3.14}$$

For these reasons, we call these variables 'vertex momenta'. Geometrically these vectors measure the momenta of particles at the position of the interaction vertex in AdS (see figure 3.7). The fact that the saddle-point equation for the geodesics coincides with the momentum conservation was first pointed out in [71] for three-point functions. Our analysis provides a simple generalization of that statement to higher-point functions.

It is instructive to introduce also the 'vertex Mandelstam invariants'. If we set

$$\sigma_{ij} := -\frac{\Delta_i \Delta_j}{\sum_k \Delta_k} \frac{P_i \cdot P_j}{(P_i \cdot X/R)(P_j \cdot X/R)} = \frac{\Delta_i \Delta_j}{\sum_k \Delta_k} \left(1 - \frac{\kappa_i \cdot \kappa_j}{m_i m_j} \right) \tag{3.3.15}$$

then the saddle point equations (3.3.11), contracted with P_j, can be written as:

$$\sum_j \sigma_{ij} = \Delta_i \,. \tag{3.3.16}$$

51
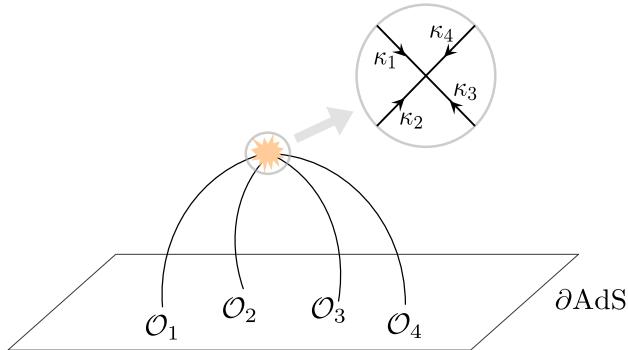
Figure 3.7. Vertex momenta and their conservation. The saddle-point equation for the
contact diagram can be interpreted as the momentum conservation of 'vertex momenta'
(denoted by κ_j's), which are momenta of particles measured at a point where all particles
meet. Since the particles follow curved trajectories, these momenta in general do not
coincide with the boundary momenta introduced in section 3.2.

Note furthermore that for $n \geq 4$ the relation between the σ_{ij} and the P_i is constrained
via their cross ratios,

$$\frac{\sigma_{ij}\sigma_{kl}}{\sigma_{ik}\sigma_{jl}} = \frac{(P_i \cdot P_j)(P_k \cdot P_l)}{(P_i \cdot P_k)(P_j \cdot P_l)} \, . \tag{3.3.17}$$

Namely the cross ratios of the vertex Mandelstam invariants coincide with the confor-
mal cross ratios of CFT. The previous two equations give precisely enough constraints
to completely determine the σ_{ij}. The beauty of using the vertex Mandelstam vari-
ables is that they turn the saddle-point equations, which are originally constraints
on $(d + 2)$-component vectors, into simple algebraic equations (3.3.16) and (3.3.17)
for σ_{ij}. Once they are determined, one can compute X from

$$P_i \cdot X/R = -\frac{\Delta_i}{\sqrt{\sum_k \Delta_k}} \sqrt{-\frac{\sigma_{jk}}{\sigma_{ij}\sigma_{ik}} \frac{(P_i \cdot P_j)(P_i \cdot P_k)}{P_j \cdot P_k}} \, . \tag{3.3.18}$$

Readers familiar with the Mellin space description of a correlator [43, 72] would
immediately notice an interesting similarity: if one replaces σ_{ij} in (3.3.16) with the
Mellin variables γ_{ij}, equation (3.3.16) coincides with the familiar constraint on γ_{ij}.
There is indeed a more precise connection. In section 3.5 we will explain that the
Mellin representation in the flat-space limit can be evaluated via the saddle point
method, and at the saddle point the γ_{ij} become equal to the σ_{ij} and therefore in
particular obey equation (3.3.17). In the remainder of this section we will however
stick to the position-space description and discuss the explicit solutions to the saddle-
point equations and their physical implications.

Boundary momenta vs. vertex momenta

So far, we have introduced two different notions of momenta for the CFT correlators. First there are the boundary momenta k_i that we used in section 3.2 to state our conjecture. In Euclidean kinematics it is better to momentarily forget about the i's in equation (3.2.18) and set:

$$k_j^\mu = -\frac{\Delta_j}{R} n_{P_j}^\mu, \qquad \text{where } P_j = (1, n_{P_j}). \tag{3.3.19}$$

These momenta are on-shell, $k_j^2 = m_j^2$, but it is not at all necessary for them to be conserved since we are free to choose arbitrary values of the n_P. Physically the k_j^μ measure the momenta of particles at the boundary of AdS, and the relative minus sign means that they are ingoing.

A second set of momenta are the vertex momentum κ_i which measure the momenta of particles at the position of the interaction vertex in AdS and were introduced in the previous subsection. Like the boundary momenta these are also on-shell, but unlike the boundary momenta they always satisfy the momentum conservation condition. This indicates that the vertex and boundary momenta do not agree in general.

The discrepancy arises, of course, because the hyperbolic space is not flat and particles move along curved trajectories.[12] For given P_i the saddle point equations select the particular bulk point X such that the particles interact at the vertex in a *locally* momentum-conserving fashion. The relation between P_i and X is, especially for higher-point functions, quite complicated, and it is therefore not always easy to determine the vertex momenta. Nevertheless, there is a simple and beautiful relation between these two momenta if we are in a special kinematics in which the *boundary momenta k_i* are also conserved. To see this, let us take a closer look at the momentum conservation condition for the boundary momenta $\sum_i k_i = 0$. Using (3.3.19), we can rewrite it into

$$\frac{1}{\sum_k \Delta_k} \sum_i \Delta_i P_i = C := (1, 0, 0, \dots). \tag{3.3.20}$$

Now, for this particular choice of the boundary points, the saddle-point equation for the vertex momenta (3.3.11) becomes trivial to solve: we find that $X = RC$ does the job since $P_i \cdot C = -1$. It immediately follows that $\kappa_i = (0, k_i)$, so bulk and vertex momenta agree, and therefore the Mandelstam invariants for the boundary momenta also coincide with the vertex Mandelstam invariants σ_{ij}.

Restricting the P_i to the support of the momentum conserving delta function would be sufficient to extract the amplitude $\mathcal{T}(\dots)$ as follows from our amplitude

---

[12]The k_i and κ_i are normalized tangent vectors to the geodesic, so the contraction with any Killing vector field is conserved along the trajectories. But this is not relevant for the component-wise comparison in these paragraphs.

conjecture. That said, we should remember that important information is lost if we impose the boundary momentum conservation from the outset: our S-matrix conjecture states that the contact diagram, when suitably continued to Lorentzian signature, becomes a momentum-conserving delta function. To verify this, we need to start with a more general configuration in which the boundary momenta are *not* conserved and carefully analyze what happens if we approach the support of the momentum-conserving delta function. This analysis turns out to be quite complicated in general. So we will consider only $n = 3$ and $n = 4$ in what follows.

General momenta, $n = 3$

As a warm up, let us consider the three-point function, $n = 3$. In this case, we can solve the saddle point equation (3.3.11) even in the absence of the conservation of the boundary momenta. Specifically we try an ansatz of the form

$$X/R = \sum_j c_j P_j \qquad (3.3.21)$$

and the saddle point equations then determine the coefficients

$$c_1 = \sqrt{-\frac{P_2 \cdot P_3}{2(P_1 \cdot P_2)(P_1 \cdot P_3)} \frac{\Delta_{12|3}\Delta_{13|2}}{\Delta_{23|1}\sum_k \Delta_k}} \qquad (3.3.22)$$

with $\Delta_{12|3} = \Delta_1 + \Delta_2 - \Delta_3$, and cyclic permutations thereof. The vertex momenta obey

$$\sigma_{12} = \frac{1}{2}\Delta_{12|3}. \qquad (3.3.23)$$

Note that, for the three-point function, (3.3.23) immediately follows from the saddle-point equation written in terms of the vertex Mandelstam variables, (3.3.17).

The analysis of the three-point function is certainly a simple and instructive exercise but unfortunately there is not much more we can say, since there are no physical three-point scattering processes and we cannot really see the emergence of the delta-function. Thus we will not work out the details of the flat-space limit any further.

Instead let us briefly mention two specific limits of the Δ_i variables for later reference. First we can take the limit where $\Delta_2 = \Delta_3$ and send Δ_1 to 0. In that case c_1 goes to zero, so X becomes a linear combination of P_2 and P_3 which means that X lies on the geodesic between P_2 and P_3 in AdS. Another possible limit is the 'decay' limit where we send, say $\Delta_{23|1}$ to zero so particle 1 can (almost) decay into particles 2 and 3. In that case c_1 blows up whereas c_2 and c_3 go to zero, which means that X approaches P_1. These are drawn in figure 3.8.

(a) $\Delta_1 \to 0$ (b) $\Delta_{23|1} \to 0$
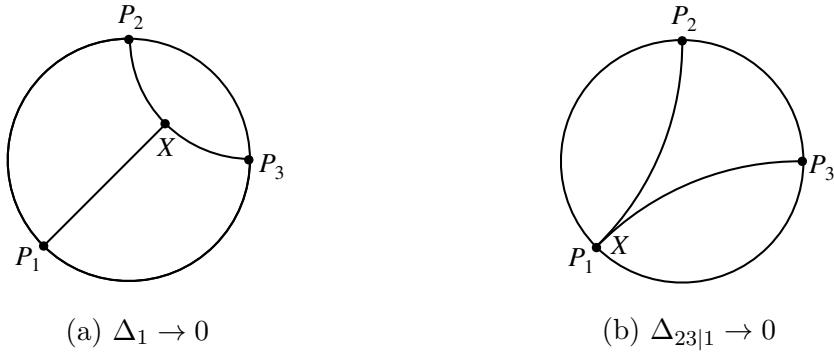
Figure 3.8. Two different limits of the three-point diagram with $\Delta_2 = \Delta_3$.

General momenta, $n = 4$

Let us now consider a more physically interesting example, the contact diagram for four identical particles. We will do a detailed analysis and show that the momentum-conserving delta function appears from the saddle point value of the diagram, in accordance with our S-matrix conjecture. Let us first determine the σ_{ij} by solving the algebraic equations (3.3.16) and (3.3.17). The result is given purely in terms of the conformal cross ratios (3.2.29) as

$$
\begin{aligned}
\sigma_{12} = \sigma_{34} &= \Delta \frac{\sqrt{u}}{1 + \sqrt{u} + \sqrt{v}} , \\
\sigma_{13} = \sigma_{24} &= \Delta \frac{1}{1 + \sqrt{u} + \sqrt{v}} , \\
\sigma_{14} = \sigma_{23} &= \Delta \frac{\sqrt{v}}{1 + \sqrt{u} + \sqrt{v}} .
\end{aligned}
\tag{3.3.24}
$$

One can then define corresponding vertex Mandelstam invariants via $s := 4m^2 - \frac{8}{\Delta}\sigma_{12}$, $t := 4m^2 - \frac{8}{\Delta}\sigma_{13}$ and $u := 4m^2 - \frac{8}{\Delta}\sigma_{14}$. In equation (3.2.30) we wrote an expression for the conformal (or boundary) Mandelstam invariants which was valid on the support of the momentum-conserving delta function; one can verify that it agrees precisely with equation (3.3.24).

With the σ_{ij} in hand we can determine X via equation (3.3.18). The bulk point is most easily described as a linear combination of the boundary points as in equation (3.3.21). With a little work we find that (3.3.18) reduces to:

$$
P_i \cdot X = -\frac{R}{4c_i} .
\tag{3.3.25}
$$

and that

$$
c_1 = \frac{\alpha}{(P_{12}P_{13}P_{14})^{1/2}}
\tag{3.3.26}
$$

with others obtained through cyclic permutations of the indices. The common factor

α is given by

$$\alpha = \frac{(P_{12}P_{13}P_{14}P_{23}P_{24}P_{34})^{1/4}}{\sqrt{2}\left(\sqrt{P_{12}P_{34}} + \sqrt{P_{13}P_{24}} + \sqrt{P_{14}P_{23}}\right)^{1/2}}. \tag{3.3.27}$$

The on-shell value of $f_c(X)$ reads:

$$f_c(X) = \Delta \sum_{i=1}^{4} \log(4c_i) \tag{3.3.28}$$

To compute the full saddle-point approximation we need to compute the determinant of the Hessian. The second derivatives are given by:

$$\frac{\partial^2 f_c(X)}{\partial X_\mu \partial X_\nu} = \sum_{i=1}^{4} \Delta \frac{P_i^\mu P_i^\nu}{(P_i \cdot X)^2} + 2\lambda \eta^{\mu\nu} = \frac{4\Delta}{R^2}\left(\sum_{i=1}^{4} 4c_i c_i P_i^\mu P_i^\nu - \eta^{\mu\nu}\right)$$

$$\frac{\partial^2 f_c(X)}{\partial X_\mu \partial \lambda} = 2X^\mu = \sum_{i=1}^{4} 2c_i P_i^\mu \tag{3.3.29}$$

$$\frac{\partial^2 f_c(X)}{\partial \lambda^2} = 0$$

After introducing the vectors

$$\tilde{P}_i = 2c_i P_i \tag{3.3.30}$$

one uses the matrix determinant lemma for

$$\left|\begin{matrix} -\eta + \sum_i \tilde{P}_i(\tilde{P}_i)^T & \sum_i \tilde{P}_i \\ \sum_i (\tilde{P}_i)^T & 0 \end{matrix}\right| = (-1)^d 4 \det_{ij}\left[\delta_{ij} - (\tilde{P}_i)^T \tilde{P}_j - \frac{1}{4}e_{ij}\right]$$

$$= (-1)^d \frac{32\sqrt{P_{12}P_{13}P_{14}P_{23}P_{24}P_{34}}}{\left(\sqrt{P_{12}P_{34}} + \sqrt{P_{13}P_{24}} + \sqrt{P_{14}P_{23}}\right)^3} \tag{3.3.31}$$

where $e_{ij} = 1$ for all i and j. Mopping up all the other factors ultimately gives

$$G_c(P_i) \xrightarrow{R\to\infty} R^{-d+3} 2^{2\Delta - d/2 - 6} \pi^{-3d/2 + 1/2} \Delta^{3d/2 - 9/2} \frac{\left(\sqrt{P_{12}P_{34}} + \sqrt{P_{13}P_{24}} + \sqrt{P_{14}P_{23}}\right)^{-2\Delta + 3/2}}{(P_{12}P_{13}P_{14}P_{23}P_{24}P_{34})^{1/4}} \tag{3.3.32}$$

As expected, this is a manifestly crossing symmetric function of the positions that also obeys the right conformal transformation properties for a four-point function of identical operators.

Now, according to the prescription dictated by the 'S-matrix' conjecture (3.2.17), we should obtain a momentum conserving delta function if we multiply the contact diagram $G_c(P_i)$ by the normalization factor $\sqrt{Z}$, analytically continue to the 'S-matrix' configuration and then take the flat-space limit. In equations this means

that

$$Z^2 G_c(P_i)|_{\text{S-matrix}} \xrightarrow{R\to\infty} i(2\pi)^{d+1}\delta^{(d+1)}(k_1 + k_2 + k_3 + k_4) \tag{3.3.33}$$

should hold, with the momenta k_i related to the boundary points P_i through (3.3.19). In appendix 3.C we prove that this is indeed the case.[13]

3.3.3 Exchange diagram and geodesic networks

We now discuss the next-to-simplest Witten diagram for the four-point functions, namely the exchange diagram. By analysing its flat-space limit, we encounter an interesting obstruction against the position-space recipe for the flat-space limit. This naturally leads us to propose the notion of Landau diagrams in AdS, which will be the subject of the next section.

The exchange diagram is given by

$$G_e(P_i) = \int dX dY G_{B\partial}(X, P_1) G_{B\partial}(X, P_2) G_{BB}(X, Y) G_{B\partial}(Y, P_3) G_{B\partial}(Y, P_4) \tag{3.3.34}$$

We will set all the external dimensions equal $\Delta_1 = \Delta_2 = \Delta_3 = \Delta_4 = \Delta$ and the dimension of the exchanged particle equal to Δ_b for simplicity. Using the split representation for the bulk-bulk propagator this becomes

$$G_e(P_i) = \int_{-i\infty}^{i\infty} \frac{dc}{2\pi i} \frac{2c^2}{c^2 - (\Delta_b - h)^2} \int dQ \int dX dY \frac{R^{3-3d}\mathcal{C}_{h+c}\mathcal{C}_{h-c}}{(-2Q \cdot X/R)^{h+c}(-2Q \cdot Y/R)^{h-c}}$$
$$\times \frac{(\mathcal{C}_\Delta)^4}{(-2P_1 \cdot X/R)^\Delta(-2P_2 \cdot X/R)^\Delta(-2P_3 \cdot Y/R)^\Delta(-2P_4 \cdot Y/R)^\Delta} \, . \tag{3.3.35}$$

Contribution from the saddle

In the flat space limit, we expect this integral to be dominated by the saddle point. After introducing the Lagrange multipliers $\lambda_{Q,X,Y}$ and θ_Q, the function to extremise becomes

$$f_e(X, Y, Q, c) = -c\left[\log(-Q \cdot X/R) - \log(-Q \cdot Y/R)\right]$$
$$-\Delta\left[\sum_{j=1,2}\log(-P_j \cdot X/R) + \sum_{j=3,4}\log(-P_j \cdot Y/R)\right] \tag{3.3.36}$$
$$+\lambda_Q Q^2 + \theta_Q(Q^0 - 1) + \lambda_X(X^2 + R^2) + \lambda_Y(Y^2 + R^2) \, .$$

---

[13]In particular, the seemingly random and certainly lengthy prefactor in equation (3.3.32) is essential to reproduce the correct normalization in equation (3.3.33).

Imposing

$$\frac{\partial f_e}{\partial c} = \frac{\partial f_e}{\partial Q} = \frac{\partial f_e}{\partial \lambda_Q} = \frac{\partial f_e}{\partial \theta_Q} = \frac{\partial f_e}{\partial \lambda_X} = \frac{\partial f_e}{\partial \lambda_Y} = 0\,, \tag{3.3.37}$$

we find that the two bulk points must coincide at the saddle point; namely $X = Y$ (and $\lambda_Q = \theta_Q = 0$). The remaining saddle point equations reduce to

$$c\frac{Q}{Q \cdot X} + \Delta \sum_{j=1,2} \frac{P_j}{P_j \cdot X} - 2\lambda_X X = 0\,,$$
$$-c\frac{Q}{Q \cdot X} + \Delta \sum_{j=3,4} \frac{P_j}{P_j \cdot X} - 2\lambda_Y X = 0\,. \tag{3.3.38}$$

Contracting these equations with X, we get

$$\lambda_X = -\frac{1}{2R^2}(2\Delta + c)\,, \qquad \lambda_Y = -\frac{1}{2R^2}(2\Delta - c)\,. \tag{3.3.39}$$

Now, to understand the physical meaning of the saddle-point equations, it is again useful to use the vertex momenta

$$\kappa_j := \frac{\Delta_j}{R}\left(\frac{P_j}{P_j \cdot X/R} + X/R\right)\,, \qquad \chi := \frac{c}{R}\left(\frac{Q}{Q \cdot X/R} + X/R\right)\,. \tag{3.3.40}$$

Here χ is a vertex momentum associated with the exchanged particle. Unlike the external vertex momenta, it is *off-shell*, meaning that $\chi^2 \neq m_b^2$ with $m_b := \Delta_b/R$. In terms of these variables, the saddle-point equation again takes the form of the momentum conservation

$$\kappa_1 + \kappa_2 + \chi = 0\,, \qquad \kappa_3 + \kappa_4 - \chi = 0\,. \tag{3.3.41}$$

This in particular means that the vertex momenta of the external particles are conserved, $\sum_j \kappa_j = 0$. Note that (3.3.41) matches our expectation in the flat-space limit: the momentum conservation holds at each vertex but the internal particle is off-shell.

To determine the saddle-point values of c, Q, and $X(= Y)$ we can again consider the vertex Mandelstam variables. Owing to the momentum conservation of the external particles $\sum_j \kappa_j = 0$, σ_{ij}'s are given by the same expressions as the contact diagram (3.3.24) and so is X. On the other hand, if we use the momentum conservation at each interaction vertex (3.3.41), we obtain alternative expressions

$$c^2 = 4\Delta^2 - 8\Delta\sigma_{12} = 4\Delta^2 - 8\Delta\sigma_{34} \tag{3.3.42}$$

With (3.3.24) this yields[14]

$$c^2 = 4\Delta^2 \frac{-\sqrt{P_{12}P_{34}} + \sqrt{P_{13}P_{24}} + \sqrt{P_{14}P_{23}}}{\sqrt{P_{12}P_{34}} + \sqrt{P_{13}P_{24}} + \sqrt{P_{14}P_{23}}} \qquad (3.3.43)$$

In terms of the vertex momenta, or in terms of the boundary momenta on the support of the momentum-conserving delta function, this expression is actually much simpler:

$$c^2 = R^2 s \,, \qquad (3.3.44)$$

with s the conformal Mandelstam variable (3.2.30). This is simply a manifestation of the fact that c^2 measures the energy of the exchanged particle. We can then determine Q solving (3.3.38). The result reads

$$Q \propto \lambda_Y \sum_{j=1,2} c_j P_j - \lambda_X \sum_{k=3,4} c_k P_k \,, \qquad (3.3.45)$$

where c_j's are given by (3.3.26) and $\lambda_{X,Y}$ given by (3.3.39). Not written is an unimportant proportionality factor that fixes the gauge $Q^0 = 1$.

With $X = Y$ it is immediate that the on-shell value of f_e coincides with that of the contact diagram, so we find again that

$$f_e = \Delta \sum_{i=1}^{4} \log(4c_i) \,. \qquad (3.3.46)$$

As is the case with the contact diagram, we also need the one-loop fluctuation around the saddle point to reproduce the correct flat-space limit. It turns out that the computation is most efficiently done if we first perform integration of X, Y and Q exactly and then compute the fluctuation around the saddle point of c (3.3.43). Relegating the details to Appendix 3.D, here we display the final result

$$G_e(P_i) \xrightarrow{R\to\infty} G_c(P_i)\big|_{R\to\infty} \times \frac{R^2}{\Delta_b^2 - c^2} \,, \qquad (3.3.47)$$

where the first factor $G_c(P_i)\big|_{R\to\infty}$ is the flat-space limit of the contact diagram (3.3.32). Thus, once we multiply $G_e(P_i)$ with the normalization factors $\sqrt{Z}$ and perform the analytic continuation, we recover the result for the exchange diagram in the flat-space limit including the momentum conserving delta function:

$$Z^2 G_e(P_i)\big|_{\text{S-matrix}} \xrightarrow{R\to\infty} i(2\pi)^{d+1}\delta^{(d+1)}(k_1 + k_2 + k_3 + k_4)\frac{1}{(k_1+k_2)^2 + m^2} \,. \qquad (3.3.48)$$

---

[14]The sign of c is arbitrary, since the equations are invariant under $c \to -c$ and $Q \to X + Q/(2Q \cdot X)$.
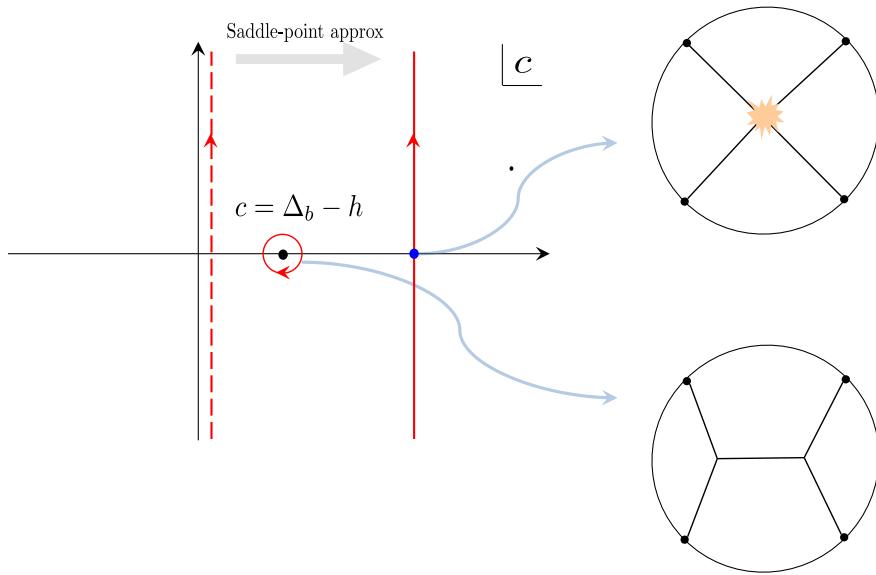
Figure 3.9. The contributions from the saddle point and the pole for the exchange diagram. To evaluate the exchange diagram using the saddle-point approximation of the c-integral, we need to deform the original contour (the red dashed line) to a steepest descent contour (the solid red line) that goes through the saddle point (the blue dot). Upon doing so, the contour sometimes needs to cross the poles of the integrand and this produces an additional contribution. Physically, the contribution from the saddle-point corresponds to a scattering process in which the four-particles meet at a point while the contribution from the pole corresponds to a geodesic network. The former is related to a flat-space S-matrix while the latter is not.

Contribution from the pole

We have seen above that the contribution from the saddle point beautifully reproduces the flat-space limit of the exchange diagram. There is however one subtlety in the argument above: initially the contour of integration of c is placed along the imaginary axis. In order to evaluate the integral using the saddle-point approximation, we need to shift the contour so that it goes through the saddle point given by (3.3.44). Upon doing so, the contour sometimes crosses poles in the integrand of (3.3.35), namely the poles at $c = \pm(\Delta_b - h)$. When this happens, the full contribution in the large R limit is given by a sum of two terms, the saddle-point contribution determined above, and the contribution from the residue of the pole (see figure 3.9).

Let us for now discuss the contribution from the pole in the right half plane,

$c = \Delta_b - h$. Evaluating the integral (3.3.35) at the pole we get

$$
\begin{aligned}
G_e(P_i)|_{\text{pole}} = & (h - \Delta_b) \int dQ \int dX dY \, \frac{R^{3-3d} \mathcal{C}_{\Delta_b} \mathcal{C}_{d-\Delta_b}}{(-2Q \cdot X/R)^{\Delta_b}(-2Q \cdot Y/R)^{d-\Delta_b}} \\
& \times \frac{(\mathcal{C}_\Delta)^4}{(-2P_1 \cdot X/R)^\Delta(-2P_2 \cdot X/R)^\Delta(-2P_3 \cdot Y/R)^\Delta(-2P_4 \cdot Y/R)^\Delta} \, .
\end{aligned}
\tag{3.3.49}
$$

To analyse the rest of the integral, we can again use the saddle-point approximation. This is a safe manipulation since the integrand is not singular (for generic P_j's). Now the function to extremise is

$$
\begin{aligned}
f_{e,\text{pole}}(X, Y, Q) = & -\Delta_b \left[\log(-Q \cdot X/R) - \log(-Q \cdot Y/R) \right] \\
& - \Delta \left[\sum_{j=1,2} \log(-P_j \cdot X/R) + \sum_{j=3,4} \log(-P_j \cdot Y/R) \right] \\
& + \lambda_Q Q^2 + \theta_Q(Q^0 - 1) + \lambda_X(X^2 + R^2) + \lambda_Y(Y^2 + R^2) \, .
\end{aligned}
\tag{3.3.50}
$$

Since the integration variable c in (3.3.36) is replaced by a fixed number Δ_b, the saddle-point equations do not set the two bulk points to be coincident, so generically $X \neq Y$. Instead we obtain

$$
\Delta_b \frac{Q}{Q \cdot X} + \Delta \sum_{j=1,2} \frac{P_j}{P_j \cdot X} - 2\lambda_X X = 0 \,, \qquad -\Delta_b \frac{Q}{Q \cdot Y} + \Delta \sum_{j=3,4} \frac{P_j}{P_j \cdot Y} - 2\lambda_Y Y = 0 \,,
$$
$$
-\Delta_b \frac{X}{Q \cdot X} + \Delta_b \frac{Y}{Q \cdot Y} + 2\lambda_Q Q = 0 \,,
\tag{3.3.51}
$$

where $\lambda_{X,Y}$ are given by

$$
\lambda_X = -\frac{1}{2R^2}(2\Delta + \Delta_b) \,, \qquad \lambda_Y = -\frac{1}{2R^2}(2\Delta - \Delta_b) \,.
\tag{3.3.52}
$$

The first two equations can be recast into the momentum conservations at the two bulk vertices X and Y. To see this, we introduce internal vertex momenta

$$
\chi_1 := \frac{\Delta_b}{R} \left(\frac{Q}{Q \cdot X/R} + X/R \right) \,, \qquad \chi_2 := \frac{\Delta_b}{R} \left(\frac{Q}{Q \cdot Y/R} + Y/R \right) \,.
\tag{3.3.53}
$$

Then the first two equations in (3.3.51) can be rewritten as

$$
\kappa_1 + \kappa_2 + \chi_1 = 0 \,, \qquad \kappa_3 + \kappa_4 - \chi_2 = 0 \,.
\tag{3.3.54}
$$

There are two important differences compared to equation (3.3.41): first the two internal momenta $\chi_{1,2}$ are in general different, and second, unlike χ in (3.3.41) the
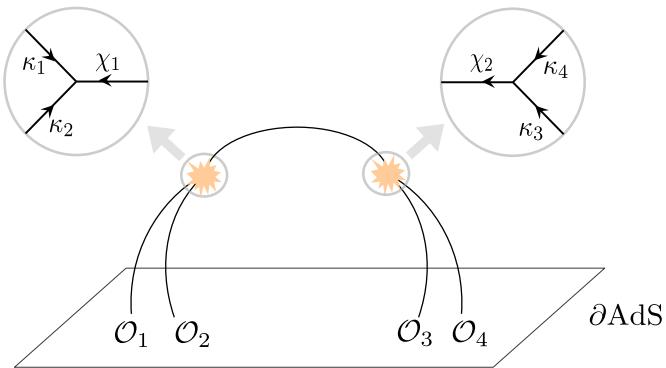
Figure 3.10. Geodesic network. The contribution from the pole $c = \Delta_b$ corresponds to a network of geodesics in which the conservation of momenta holds at each vertex. Here $\chi_{1,2}$ are internal vertex momenta while κ_j's are external vertex momenta.

internal momenta $\chi_{1,2}$ are on-shell, i.e. $\chi_1^2 = \chi_2^2 = m_b^2$. Geometrically, these features reflect the fact that the contribution from the pole describes a network of geodesics in which two interaction points are macroscopically separated in AdS.[15] This is also consistent with the analysis in section 3.2, which showed that the pole contribution to the bulk-to-bulk propagator corresponds to a geodesic connecting two bulk points (see also figure 3.10). This is reminiscent of Landau diagrams in flat space, which correspond to trajectories of on-shell particles in complexified Minkowski space. In section 3.4, we will use this observation to propose the AdS version of Landau diagrams.

There are two different ways to evaluate the saddle-point value of $f_{e,\text{pole}}$. The first approach is to explicitly determine the saddle point by solving all the equations (3.3.51) and then to evaluate $f_{e,\text{pole}}$ on that saddle point. The second approach is to perform the integrals of X, Y and Q in (3.3.49) exactly and use the asymptotic form of the conformal block. As explained in appendix 3.D, the second approach turns out to be simpler and the result reads

$$f_{e,\text{pole}} = -\Delta \log\left(\frac{P_{12}P_{34}}{16}\right) + g\left(\Delta_b\right) . \tag{3.3.55}$$

with

$$g(x) := -4\Delta \log(\Delta) + (2\Delta + x)\log(\Delta + \tfrac{x}{2}) + (2\Delta - x)\log(\Delta - \tfrac{x}{2}) + x\log\left(\frac{2m - \sqrt{s}}{2m + \sqrt{s}}\right), \tag{3.3.56}$$

where s is the Mandelstam variable.

---

[15]Unlike the 'geodesic Witten diagram' introduced in [73], here the bulk vertices do not lie on the geodesic connecting the boundary points (as long as $m_b > 0$). Both constructions do reduce to a conformal block at large Δ, albeit with different normalizations.
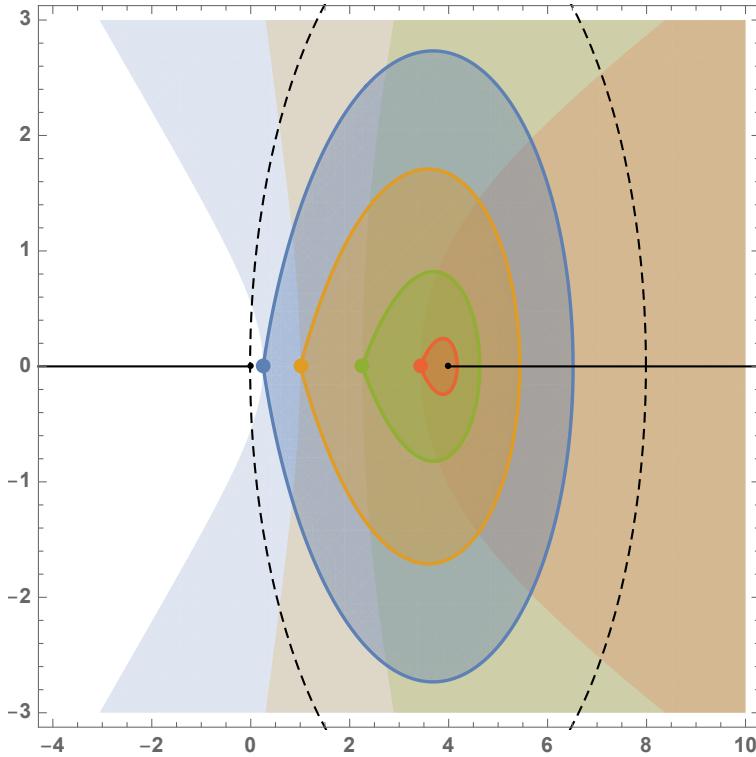
Figure 3.11. Regions in the complex s plane where the pole at $c = \Delta_b$ is picked up (lighter shaded) and the smaller subregion where the flat-space limit diverges (darker shaded). The different colours correspond to $m_b = 0.5, 1, 1.5, 1.85$ and we have set $m = 1$. The problematic region for the exchange diagram always lies within the disk given by $|s - 4m^2| < 4m^2$. We assumed that the external momenta are chosen such that momentum conservation holds.

Exchange of dominance

We have seen that the exchange diagram receives two different contributions, the one associated with the saddle point of c and the other associated with the pole of c. As discussed above, the first contribution correctly reproduces the flat-space limit while the second contribution corresponds to a network of geodesics in which the two bulk points are macroscopically separated in AdS. Therefore the large R limit of the exchange diagram gives the flat-space result if and only if the second contribution can be neglected.

Clearly the most interesting configuration is when we are on the support of the momentum-conserving delta function so the external momenta obey $\sum_{i=1}^4 k_i = 0$. In that case the algorithm is the following (see figure 3.9).

1. Compare the position of the steepest descent contour through the saddle point at $c = R\sqrt{s}$ and the position of the pole at $c = \Delta_b$. If the steepest descent contour is to the left of the pole, the flat space limit gives the correct answer.

2. If the steepest descent contour is to the right of the pole, compare the real parts of the exponents (3.3.46) and (3.3.55). In fact, if $\sum_{i=1}^{4} k_i = 0$ then the value of f_e at the saddle point value vanishes and so we simply need to check the sign of the real part of (3.3.55): if it is positive then the flat-space limit diverges, and if it is negative then the flat-space limit gives the correct answer.

In figure 3.11, we plotted the region in which the flat-space limit works/fails in the complex s-plane. As one can see there, the bound-state pole $s = m_b^2$ is at the edge of a larger 'blob' where the flat-space limit gives a divergent answer. The size of the region grows as we decrease the mass of the bound state, and when it becomes massless $m_b \to 0$, the region is given by a disk of radius $4m^2$ centred at the two-particle threshold $s = 4m^2$. Therefore, if we are agnostic about m_b then the flat-space limit of the exchange diagram is only guaranteed to be finite for $|s - 4m^2| > 4m^2$. We furthermore observe that the bad region vanishes entirely as $m_b \to 2m$, and that for any $0 \le m_b < 2m$ it always includes at least a little bit of the physical line $s > 4m^2$.

3.4 Landau diagrams in AdS

In section 3.2 we discussed two large Δ_b limits of the bulk-bulk propagator $G_{BB}(X, Y)$: one where the distance between X and Y becomes much smaller than the AdS radius R, which reproduced the flat-space Klein-Gordon propagator, and one where this distance is kept finite in units of R, which reproduced the simple exponential $G_{BB}(X, Y) \sim \exp(-\Delta_b d(X, Y))$ with $d(X, Y) = \text{arccosh}(-X \cdot Y/R^2)$ the geodesic distance between X and Y (in units of the AdS radius).

In the flat-space analysis of Witten diagrams the bulk points X and Y are integrated over and in the large Δ analysis their locations are dynamically determined by the saddle point equations. It is therefore not entirely surprising that both behaviours of the bulk-bulk propagator can play a role. As was exemplified by the exchange diagram of the previous subsection, for a propagator in a generic Witten diagram the saddle point equations read:

$$\frac{\partial f}{\partial c} = 0 \qquad \Longrightarrow \qquad \log(-Q \cdot X) - \log(-Q \cdot Y) = 0 \qquad (3.4.1)$$

$$\frac{\partial f}{\partial Q} = 0 \qquad \Longrightarrow \qquad -c\left(\frac{X}{Q \cdot X} - \frac{Y}{Q \cdot Y}\right) + 2\lambda_Q Q = 0 \qquad (3.4.2)$$

Together they yield $Y = X$, and with all the bulk vertices close together we reproduce the flat space result because all the interactions take place at a distance much smaller than the AdS radius. The only potential hiccup in this procedure are the poles in the complex c plane: if the steepest descent contour through the saddle point in the c plane passes on the wrong side of one of these poles then its residue needs to be

taken into account, resulting in unwanted additional contributions that can spoil the extraction of an amplitude from the position-space correlator.

An *AdS Landau diagram* can be defined as a network of geodesics in AdS such that vertex momentum is conserved at every interaction point. We recall that the vertex momentum for each external leg is

$$\kappa_i = \frac{\Delta_i}{R} \left(\frac{P_i}{P_i \cdot X/R} + X/R \right) , \qquad (3.4.3)$$

and for each internal leg it is

$$\chi_i = \frac{\Delta_i}{R} \left(\frac{Q_i}{Q_i \cdot X/R} + X/R \right) , \qquad (3.4.4)$$

where for every bulk-bulk propagator $G_{BB}(X, Y)$ the value of Q is determined through momentum conservation and

$$2\lambda_Q Q = \Delta_b \left(\frac{X}{Q \cdot X} - \frac{Y}{Q \cdot Y} \right) \qquad (3.4.5)$$

and $Q^2 = 0$ and $Q^0 = 1$. Notice that the first equation in (3.4.1) no longer needs to be obeyed because c is fixed to one of its poles; for definiteness we chose the pole at $c = \Delta_b$ but we will discuss this further below. Clearly the AdS Landau diagrams extremise the 'action'

$$
\begin{aligned}
f = &- \sum_{\langle ik \rangle \in \text{Ext}} \Delta_i \log(-P_i \cdot X_k) - \sum_{\langle kl \rangle \in \text{Int}} \Delta_{\langle kl \rangle} \left(\log(-Q_{\langle kl \rangle} \cdot X_k) - \log(-Q_{\langle kl \rangle} \cdot X_l) \right) \\
&+ \sum_k \lambda_k (X_k^2 + R^2) + \sum_{\langle kl \rangle \in \text{Int}} \left(\lambda_{\langle kl \rangle} Q_{\langle kl \rangle}^2 + \theta_{\langle kl \rangle} (Q_{\langle kl \rangle}^0 - 1) \right)
\end{aligned}
$$

$$(3.4.6)$$

where $\langle ik \rangle$ runs over the set of external legs between the boundary points P_i and bulk points X_k connected by a bulk-boundary propagator, and $\langle kl \rangle$ labels all pairs of internal legs, so legs connected by a bulk-bulk propagator. We will call the saddle point equations the *AdS Landau equations* and the on-shell value of this action then gives the contribution of the AdS Landau diagram to the flat-space limit of the Witten diagram.

Notice that an alternative action can be obtained by eliminating Q and simply using the large Δ expression for the bulk-bulk propagator:

$$\tilde{f} = - \sum_{\langle ik \rangle \in \text{Ext}} \Delta_i \log(-P_i \cdot X_k) - \sum_{\langle kl \rangle \in \text{Int}} \Delta_{\langle kl \rangle} \, d(X_k, X_l) + \sum_k \lambda_k (X_k^2 + R^2) \quad (3.4.7)$$

with $d(X_k, X_l) = \text{arccosh}(-X_k \cdot X_l/R^2)$ as above. In this sense an AdS Landau

diagram is a sort of 'minimal distance' diagram: the Δ's provide a 'spring constant' that determines how much the action decreases if we pull points further apart, and the external leg factors provide a 'renormalized distance' between bulk and boundary points.

Returning to our conjectures we see that we can divide the configuration space of all values of the Mandelstam invariants into different regions as follows. We first look at the original saddle point equations and determine the integration contours for the c variables in the correct flat space limit. If poles have been crossed in deforming the original integration contour to this steepest descent contour then the corresponding leg is 'freed' and the bulk points are allowed to separate. For each region we can construct the AdS Landau diagram with the corresponding free internal legs, demanding that all the non-free internal legs are contracted to a point. In regions where the number of free legs is not zero, our conjectures have a chance of working only if the on-shell value of the action is subleading compared to the contact diagram.[16]

3.4.1 Comparison with flat space Landau diagrams

Much like flat space Landau diagrams, our AdS Landau diagrams correspond to classical on-shell particles propagating over large distances with momentum conservation holding at the vertices. Let us compare the equations in a bit more detail.

In flat space the Landau conditions can be formulated as follows [74, 75].[17] Suppose the external momenta are q_i^μ. One then associates a momentum k_r^μ and a parameter α_r to each internal leg r and a position x_s^μ to each vertex s. Then for the internal leg between position x^μ and y^μ we impose that any non-zero propagation is physical, so

$$x^\mu - y^\mu = \alpha k^\mu \tag{3.4.8}$$

Now either α is zero, the leg is contracted and the diagram said to be *reduced*, or the propagation needs to be on-shell. In equations, for every leg we need that:

$$\alpha(k^2 + m^2) = 0 \tag{3.4.9}$$

---

[16]In fact, for the contact diagram on the support of the momentum conserving delta function the on-shell action is zero. Therefore the condition for the conjectures to hold becomes $\text{Re}(f) < 0$.

[17]A priori all the positions and momenta here are to be understood in Minkowski space with a metric with mostly plus signature. More interesting singularities can be obtained by complexification. In particular, to obtain singularities in the 'Euclidean domain' where s, t, u are all positive (and below threshold), we can analytically continue the spacelike components of k^μ and x^μ to purely imaginary values (for example, in the centre of mass frame $s = 4m^2 + 4\vec{p}^2$ so $s < 4m^2$ requires $\vec{p}^2 < 0$). Absorbing the signs in a redefinition of the metric, this is commonly described as a configuration with all minus signature metric and real momenta. However our conjectures carry additional factors of i. More precisely, equation (3.2.18) informs us that imaginary $\vec{p}$ corresponds to real n^μ, which means that standard Euclidean AdS is appropriate for the Euclidean domain in the Mandelstam invariants.

The last condition is momentum conservation for each vertex. If we ignore signs corresponding to in- or outgoing momenta then this can be schematically written as:

$$\sum_r k_r^\mu + \sum_i q_i^\mu = 0 \qquad (3.4.10)$$

with the sum running over all legs, both external and internal (and both contracted and not contracted), that end on the given vertex. The parameter α is interesting here: for a large range of values of the Mandelstam invariants (in particular, all the physical values as well as the Euclidean region) the only possible singularities have $\alpha \geq 0$. Singularities with other values of α can appear on other sheets. More extensive reviews of the Landau equations can be found, for example, in [76–78].

From the preceding discussions one can distil a nearly perfect analogy with the AdS equations: the conservation of the on-shell momenta in flat space becomes simply the conservation of the on-shell vertex momenta in AdS, and equation (3.4.5) fixes the direction of the 'momentum' Q^μ to be a linear combination of X and Y such that the relevant vertex momenta at X and Y are tangential to the geodesic between X and Y. This latter condition is precisely the expected AdS analogue of flat-space propagation with a fixed momentum.

An final subtlety is the parameter α in the flat-space Landau equations. Its AdS analogue is λ_Q since that is the natural relative parameter between the momentum through a leg and its displacement. In particular, $\lambda_Q = 0$ if the leg is contracted which corresponds to $\alpha = 0$ in flat space. But in flat space we can furthermore deduce that $\alpha \geq 0$ for singularities corresponding to physical or Euclidean kinematics, and it is not immediately clear that the sign of λ_Q is similarly important. To see this we will consider the defining equation for λ_Q, which is

$$\lambda_Q = \frac{\Delta_b}{4} \left(\frac{1}{(Q \cdot Y)^2} - \frac{1}{(Q \cdot X)^2} \right) \qquad (3.4.11)$$

To see the relevance of the sign of λ_Q we first have to discuss the irrelevance of the sign of c. Consider then a solution of the AdS Landau equations for a given value of c. We claim that there must exist a solution at the opposite value $-c$ with Q pointing in the opposite direction. To see this, notice that we can always choose a frame where we only need to consider the $\mathbb{R}^2$ spanned by X and Y, implying that we can take $X = (\cosh(\rho_X), \sinh(\rho_X))$, $Y = (\cosh(\rho_Y), \sinh(\rho_Y))$. Since Q is a linear combination of X and Y which obeys $Q^2 = 0$ and $Q^0 = 1$, it must be that $Q = (1, \pm 1) =: Q_\pm$ and that correspondingly

$$\lambda_Q^\pm = \frac{c}{4} \left(e^{\pm 2\rho_Y} - e^{\pm 2\rho_X} \right) \qquad (3.4.12)$$

The choice between the '+' and the '−' sign is not fixed in our partial analysis, but it

(a) Normal diagram with $\lambda_Q > 0$ (b) 'Flipped' diagram with $\lambda_Q < 0$
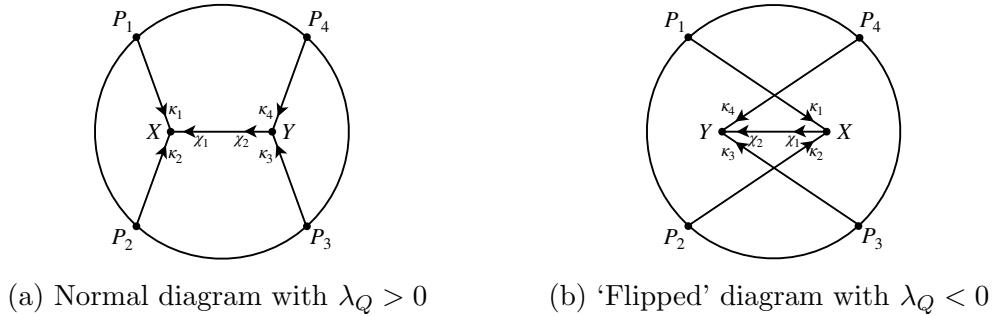
Figure 3.12. Normal and 'flipped' scalar exchange diagram.

will be fixed by the vertex momentum conservation equations which given c provide a definite direction to Q. However, we also notice that the momentum conservation equations are invariant under sending $c \to -c$ and exchanging Q^+ and Q^-. Doing so sends[18]

$$\lambda_Q^\pm \to -\frac{c}{4}\left(e^{\mp 2\rho_Y} - e^{\mp 2\rho_X}\right) = e^{\mp 2(\rho_X + \rho_Y)}\lambda_Q^\pm. \tag{3.4.13}$$

So, no matter whether the original solution had Q_+ or Q_- at $+c$, if λ_Q was positive at $+c$ then it is also positive at $-c$, and vice versa. In summary: the sign of λ_Q does not depend on the choice between picking up the pole at $+\Delta_b$ or $-\Delta_b$. Suppose then that we set $c = \Delta_b$. To see that positive λ_Q is the 'correct' direction, note that from equations (3.4.4) and (3.4.5) it follows that the corresponding vertex momentum points inward at X and outward at Y. This is exactly in agreement with the relative minus signs in vertex momentum conservation equations like equation (3.3.54), where all the other vertex momenta are defined to point inward.

To conclude the analogy we just need to deduce that saddle points with $\lambda_Q < 0$ are unimportant in Euclidean configuration. Clearly something is amiss with them, since they would correspond to 'flipped' solutions where particles propagate in the direction opposite to their vertex momenta. This is illustrated in figure 3.12 using the scalar exchange diagram as an example. In equations what happens is the following. If $\lambda_Q < 0$ and $c = +\Delta_b$ then $(-Q \cdot Y) > (-Q \cdot X)$, implying that the action can be reduced by decreasing c. We take this as an indication that the saddle point in the c plane lies to the *left* of the pole, much like in the unshaded region in figure 3.11 for the exchange diagram. This means that the pole is not picked up and indeed the solution with $\lambda_Q < 0$ is unimportant.

Let us stress that this argument was restricted to Euclidean kinematics. Note that in flat space Landau singularities with non-positive α can become important when considering more involved analytic continuations in the Mandelstam variables, for example by passing onto other sheets. In AdS the same observation holds: such continuations may force a deformation of the c integration contour which forces one

---

[18]The gauge constraint $Q^0 = 1$ introduces some non-covariance in the expression for λ_Q. This is why λ_Q is not completely invariant.

to take into account a contribution of the pole independently of the location of the saddle point. It would be interesting to see if a criterion similar to the positivity of λ_Q can be formulated for general complex values of the Mandelstam invariants.

Finally let us stress the most striking difference between the flat space and AdS Landau equations appears to be that the latter can be solved much more generally than the former. In fact, if we do not require the λ_Q variables to be positive then it appears that the AdS Landau equations have a solution for *any* values of the external momenta. This is not because the number of equations has changed but rather because of the more permissive nature of the AdS Landau equations. Most importantly, conservation of the vertex momenta can be achieved by moving the bulk point X to a suitable location – something which is impossible in flat space because of translation invariance.

Of course the AdS Landau diagrams are only important if (1) the poles are picked up, and (2) the on-shell value of the action (3.4.6) has positive real part. As we have seen above, this leads to 'blobs' where our conjectures are not valid because the flat-space limit diverges. It is our expectation that there is always a large region where the conjectures work and the AdS Landau diagrams do not dominate, and it would be interesting to find such a region. For four-point functions we can use the conformal block decomposition and some initial steps in this direction are discussed in section 3.6. It would also be worthwhile to further investigate the natural conjecture that the support for flat-space Landau diagrams lies within the closure of the divergent blobs for AdS Landau diagrams.

3.4.2 Anomalous thresholds and the triangle diagram

It is worthwhile to illustrate the general discussion of AdS Landau diagrams with the example of the triangle diagram, which is the simplest diagram exhibiting an anomalous threshold, i.e. a singularity in the Mandelstam s plane not directly attributable to an intermediate physical state. In more detail, we will consider an all-scalar triangle diagram with equal external masses m, equal internal masses μ, and a momentum configuration as in figure (3.13). In flat space the loop integral is easily written down and one finds that for

$$\frac{1}{2}m < \mu < \frac{\sqrt{2}}{2}m, \qquad 0 < s < 2m^2, \tag{3.4.14}$$

there is a cut in the Mandelstam s variable on the physical sheet starting at

$$s^{\mathrm{anom}} = 4m^2 - \frac{m^4}{\mu^2}. \tag{3.4.15}$$

Since this is less than the natural physical threshold $4\mu^2$, the singularity is said to be anomalous. Our aim in this section is to reproduce this anomalous threshold from
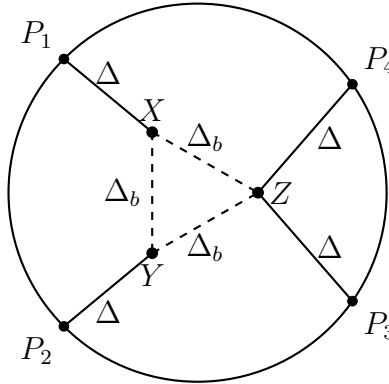
Figure 3.13. The triangle diagram in AdS.

the corresponding Witten diagram.

In AdS the triangle Witten diagram reads

$$G_t(P_i) = \int dX dY dZ G_{B\partial}(X, P_1) G_{B\partial}(Y, P_2) G_{B\partial}(Z, P_3) G_{B\partial}(Z, P_4)$$
$$\times G_{BB}(X, Y) G_{BB}(Y, Z) G_{BB}(X, Z). \tag{3.4.16}$$

with scaling dimensions $\Delta \sim mR$ and $\Delta_b \sim \mu R$ for the propagators as given in figure 3.13. As per the previous discussion, the action of the AdS Landau diagram to extremise is:

$$\tilde{f}_t(X, Y, Z) = - \Delta \log(-P_1 \cdot X/R) - \Delta \log(-P_2 \cdot Y/R)$$
$$- \Delta \log(-P_3 \cdot Z/R) - \Delta \log(-P4 \cdot Z/R)$$
$$- \Delta_b d(X, Y) - \Delta_b d(Y, Z) - \Delta_b d(X, Z), \tag{3.4.17}$$

with $d(X, Y) = \text{arccosh}(-X \cdot Y/R^2)$. We will again assume that we are on the support of the momentum conserving delta function and will also pass to the centre of mass frame. Then the symmetries of the problem dictate the following ansatz:

$$P_1 = (1, \cos(\theta_P), \sin(\theta_P)), \qquad P_2 = (1, \cos(\theta_P), -\sin(\theta_P)),$$
$$P_3 = (1, -\cos(\theta_P), \sin(\theta_P)), \quad P_4 = (1, -\cos(\theta_P), -\sin(\theta_P)),$$
$$X = \left(R \cosh\left(\frac{\rho_X}{R}\right), R \sinh\left(\frac{\rho_X}{R}\right) \cos(\theta_X), R \sinh\left(\frac{\rho_X}{R}\right) \sin(\theta_X)\right), \tag{3.4.18}$$
$$Y = \left(R \cosh\left(\frac{\rho_X}{R}\right), R \sinh\left(\frac{\rho_X}{R}\right) \cos(\theta_X), -R \sinh\left(\frac{\rho_X}{R}\right) \sin(\theta_X)\right),$$
$$Z = \left(R \cosh\left(\frac{\rho_Z}{R}\right), R \sinh\left(\frac{\rho_Z}{R}\right), 0\right).$$

Although we wrote equations for AdS_2, the diagram does not depend on Mandelstam

t so our result is actually valid for any spacetime dimension. The only independent parameters are ρ_X, ρ_Z and θ_X and the remaining AdS Landau equations can be found from:

$$\frac{\partial \tilde{f}_t}{\partial \rho_X} = \frac{\partial \tilde{f}_t}{\partial \rho_Z} = \frac{\partial \tilde{f}_t}{\partial \theta_X} = 0 \,, \tag{3.4.19}$$

whereas the Mandelstam s variable is related to θ_P as:

$$\theta_P = -\frac{1}{2} \arccos\left(\frac{s - 2m^2}{2m^2}\right) + \pi \,. \tag{3.4.20}$$

The precise branch can be fixed by requiring $\theta_P \in [\pi/2, \pi]$ for $s \in [0, 4]$.

Unfortunately the equations in (3.4.19) are still somewhat difficult to solve analytically and so we will proceed numerically. In agreement with the general discussion earlier in this section, but in marked contrast with the flat-space equations, we managed to find solutions to the AdS Landau equations everywhere we looked in the complex s plane.[19] For each value we computed the on-shell action and checked the sign of $\mathrm{Re}(\tilde{f}_t)$. The region where $\mathrm{Re}(\tilde{f}_t) > 0$ is the problematic region because the Landau diagram dominates over the correct saddle point. In figure 3.14 we show the result for $\mu/m = 0.501, 0.52, 0.6, 0.706 (\approx \sqrt{2}/2)$ in detail on the left. We again uncover a blob-like region, entirely contained in the region $|s - 4m^2| < 4m^2$, where the flat-space limit gives a divergent answer and the conjectures of section 3.2 do not hold. It is satisfying to see that the anomalous threshold is correctly reproduced: on the right we show that for general μ there is a perfect agreement between the flat-space and AdS Landau diagram thresholds.

3.5 Mellin space

In this section we will compare our conjectures with the flat-space prescription of [13] that was based on Mellin space [43, 72]. Recall that the Mellin space expression for a Witten diagram with n points $G(P_{ij})$ is

$$G(P_{ij}) = \int [d\gamma_{ij}] M(\gamma_{ij}) \prod_{1 \leq i < j \leq n} \Gamma(\gamma_{ij}) P_{ij}^{-\gamma_{ij}} \tag{3.5.1}$$

---

[19]The actual algorithm was fairly delicate. We used `FindRoot` in `Mathematica` to solve (3.4.19) for different values of s. Unfortunately this method would often fail without a nearly perfect initial guess of the values $\{\rho_X, \rho_Z, \theta_X\}$. We therefore proceeded iteratively, starting from an 'easy' point like $s = 4$ and then searching radially outward in small steps. We adjusted the step size dynamically, reducing it if no solution could be found. Additional radial searches were applied to check for non-convexities in the domain. Additional care needs to be taken because of the branch cuts in the square roots in the saddle point equations.
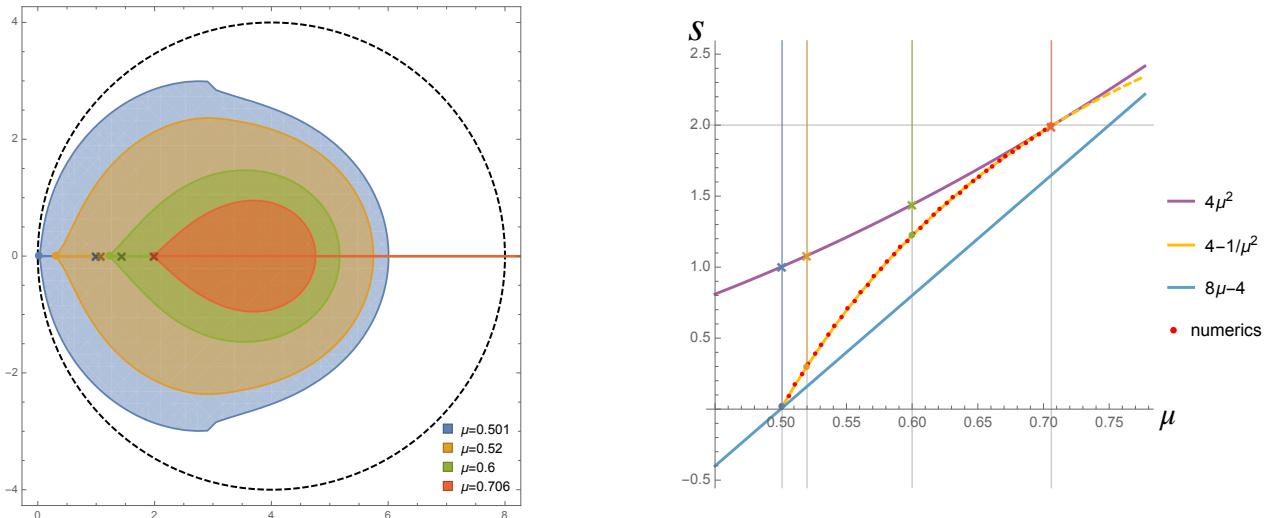
Figure 3.14. Left: Regions in the complex s plane (shaded) where the AdS Landau diagram dominates over the flat-space saddle point. We have set $m = 1$. The dots, lines and crosses are flat-space data: they are respectively the start of the anomalous threshold at $4m^2 - m^4/\mu^2$, the branch cuts emanating from it, and the physical threshold $4\mu^2$ which is a little further along the cut. (The anomalous and physical threshold coincide when $\mu/m = \sqrt{2}/2$.) The shaded regions are the 'bad' regions obtained numerically. Note that they always lie within the disk given by $|s - 4m^2| < 4m^2$ whose boundary is the black dashed circle. Right: the red dots indicate, for a given $\mu \in \left(1/2, 1/\sqrt{2}\right)$, the smallest real s for which the AdS Landau diagram dominates. They are in perfect agreement with the yellow curve which is the flat-space anomalous threshold. The physical threshold is indicated by the purple curve. The blue curve will be useful later for discussion in section 3.5. The vertical lines correspond to the branch cuts for different μ as in the left figure.

where

$$P_{ij} := -2P_i \cdot P_j \tag{3.5.2}$$

and the Mellin space (integration) variables γ_{ij} satisfy

$$\sum_{j \neq i}^{n} \gamma_{ij} = \Delta_i, \qquad \gamma_{ij} = \gamma_{ji}. \tag{3.5.3}$$

The integration measure $[d\gamma]$ is shorthand for a contour integral over the $n(n-3)/2$ independent Mellin variables and includes a factor of $1/2\pi i$ for each variable. The integration contour is of Mellin-Barnes type: it runs from $-i\infty$ to $+i\infty$ and separates the poles in the Gamma functions and the Mellin amplitude in the usual way. The Witten diagram is then encoded in the meromorphic *Mellin amplitude* $M(\gamma_{ij})$. For example, for an n-point contact Witten diagram the Mellin amplitude

is just a constant:

$$\text{contact diagram:} \qquad M(\gamma_{ij}) = \mathcal{N}/R^{n(d-1)/2-d-1} \tag{3.5.4}$$

with the canonical normalization constant

$$\mathcal{N} = \frac{1}{2}\pi^h \Gamma\left(\frac{\sum_i \Delta_i - d}{2}\right) \prod_{i=1}^n \frac{\mathcal{C}_{\Delta_i}}{\Gamma(\Delta_i)}.$$

Below we will investigate what happens to the Mellin representation in the flat-space limit in order to see what our conjecture (3.2.17) becomes for Mellin-representable functions.[20] This will also allow us to tie our conjectures to one of the two conjectures in [13], which we recall claimed that the scattering amplitude can be obtained directly in terms of the Mellin amplitude via:

$$(m_1)^{n(d-1)/2-d-1}\mathcal{T}(k_1 \ldots k_n) = \lim_{\Delta_i \to \infty} \frac{(\Delta_1)^{n(d-1)/2-d-1}}{\mathcal{N}} M\left(\gamma_{ij} = \frac{\Delta_i \Delta_j}{\sum_k \Delta_k}\left(1 + \frac{k_i \cdot k_j}{m_i m_j}\right)\right), \tag{3.5.5}$$

Notice that all momenta in this equation are again taken to be ingoing (so $k^0 < 0$ for momenta corresponding to 'out' states). As a zeroth order check, the prescription (3.5.5) clearly works for the contact diagram given in (3.5.4). Below we will essentially recover this conjecture, but in the process we will also be able to explain the appearance of the momentum-conserving delta function and find several subtleties that will explain the anomalous behaviour discussed in sections 3.3 and 3.4.

3.5.1 The saddle point

In the large R, Δ limit it is natural to rescale $\gamma_{ij} = R\sigma_{ij}$ with σ_{ij} fixed. We then find that

$$G(P_{ij}) \overset{R \to \infty}{\longrightarrow} R^{n(n-3)/2} e^{\sum_i \Delta_i \log(R)/2} \int [d\sigma_{ij}] M(R\sigma_{ij}) \exp\left(R F(\sigma_{ij}; P_{ij})\right) \tag{3.5.6}$$

with

$$F(\sigma_{ij}; P_{kl}) := \sum_{1 \leq i < j \leq n} \left(\sigma_{ij}\log(\sigma_{ij}) - \sigma_{ij} - \sigma_{ij}\log(P_{ij})\right) \tag{3.5.7}$$

If the Mellin amplitude does not scale exponentially with R then it is natural to assume that the integral can be approximated using a saddle point point analysis. Since the σ_{ij} variables obey linear constraints the saddle point equations are actually

---

[20]Although the Mellin space representation works very well for Witten diagrams [79, 80], it is more general and according to recent work [55] can also be used for certain non-perturbative CFT correlation functions. It would be extremely interesting to further explore the applicability of Mellin space because of the immediate implication on our conjectures as outlined below.

a little bit involved because one needs to pull back the partial derivatives $\partial F/\partial\sigma_{ij}$
to the constraint surface. When the dust settles one finds that

$$0 = \frac{\partial F}{\partial\sigma_{ij}} + \frac{2}{(n-1)(n-2)}\sum_{1\le k<l\le n}\frac{\partial F}{\partial\sigma_{kl}} - \frac{1}{n-2}\left(\sum_{k\neq i}\frac{\partial F}{\partial\sigma_{ik}} + \sum_{k\neq j}\frac{\partial F}{\partial\sigma_{kj}}\right) \quad (3.5.8)$$

A simple check of these equations is that they are trivially obeyed for $n = 3$, in
agreement with the fact that there are no independent integration variables left in the
original Mellin integral. Notice that these saddle point equations have to be solved
simultaneously with the constraints $\sum_{j\neq i}\sigma_{ij} = \Delta_i/R$. For the given $F(\sigma_{ij}; P_{kl})$ we
find that

$$\frac{\partial F}{\partial\sigma_{ij}} = \log(\sigma_{ij}) - \log(P_{ij}) \quad (3.5.9)$$

The case $n = 4$ is illustrative. We find that

$$\frac{\partial F}{\partial\sigma_{12}} + \frac{\partial F}{\partial\sigma_{34}} = \frac{\partial F}{\partial\sigma_{13}} + \frac{\partial F}{\partial\sigma_{24}} = \frac{\partial F}{\partial\sigma_{14}} + \frac{\partial F}{\partial\sigma_{23}} \quad (3.5.10)$$

If all the σ_{ij} and P_{ij} are real and positive then this gives:

$$\frac{\sigma_{12}\sigma_{34}}{\sigma_{13}\sigma_{24}} = \frac{P_{12}P_{34}}{P_{13}P_{24}} \qquad \frac{\sigma_{14}\sigma_{23}}{\sigma_{13}\sigma_{24}} = \frac{P_{14}P_{23}}{P_{13}P_{24}} \quad (3.5.11)$$

so the cross-ratios in the Mellin variables should equal the cross-ratios in position
space! Similar-looking expressions arise for $n > 4$.

Instead of solving these equations in full generality, let us consider the obvious
attempt for the solution σ_{ij}^* which is

$$\sigma_{ij}^* = \frac{\Delta_i\Delta_j}{2R\sum_k\Delta_k}P_{ij} = \frac{\Delta_i\Delta_j}{R\sum_k\Delta_k}\left(1 + \frac{k_i\cdot\eta\cdot k_j}{m_im_j}\right) \quad (3.5.12)$$

which are just the values for the Mellin space prescription (3.5.5). This attempt
solves the saddle point equations but the constraint equations now read:

$$\sum_{j\neq i}k_i\cdot\eta\cdot k_j = m_i^2 \quad (3.5.13)$$

up to unimportant subleading terms in $1/R$. But this is now a constraint on the k_i
(so on the P_i) which is solved whenever

$$\sum_j k_j^\mu = 0 \quad (3.5.14)$$

so precisely when we position the boundary operators on top of the support of the
momentum-conserving delta function. Positioning the operators in this configuration

is therefore part of the amplitude conjecture as discussed below equation (3.2.20). Since the Mellin amplitude $M(R\sigma_{ij})$ did not affect the location of the saddle point it is just an overall factor, and we can efficiently write the value at the saddle point as:

$$G(P_{ij}) \overset{\mathrm{R}\to\infty}{\longrightarrow} G_c(P_{ij}) R^{n(d-1)/2-d-1} M(R\sigma_{ij}^*)/\mathcal{N} \tag{3.5.15}$$

where $G_c(P_{ij})$ is the contact diagram in the same large R limit. It then immediately follows that our amplitude conjecture reduces precisely to the Mellin space prescription conjecture (3.5.5) as long as we can trust the saddle point approximation.

As for the contact diagram itself, we can reproduce all the computations of subsection 3.3.2 in Mellin space. For example, for $n = 4$ and all equal $\Delta_i = \Delta$ we can solve the Mellin saddle point equations to find:

$$\sigma_{12}^* = \sigma_{34}^* = \frac{\Delta\sqrt{P_{12}P_{34}}/R}{\sqrt{P_{12}P_{34}} + \sqrt{P_{13}P_{24}} + \sqrt{P_{14}P_{23}}} \tag{3.5.16}$$

and the obvious permutations. With some work, the saddle point approximation can then be shown to yield

$$G_c(P_{ij}) \overset{\mathrm{R}\to\infty}{\longrightarrow} \frac{2\pi^2 e^{2\Delta\log(\Delta)-2\Delta}}{\Delta^2} \frac{\left(\sqrt{P_{12}P_{34}} + \sqrt{P_{13}P_{24}} + \sqrt{P_{14}P_{23}}\right)^{-2\Delta+3/2}}{(P_{12}P_{13}P_{14}P_{23}P_{24}P_{34})^{1/4}} M_c(R\sigma_{ij}^*) \tag{3.5.17}$$

which reduces to precisely the same expression as equation (3.3.32) and so the position space and Mellin space analyses of this diagram are in complete agreement.

3.5.2 The steepest descent contour

In our previous analysis we determined that the Mellin space prescription (3.5.5) follows from our conjectures if we use a saddle point approximation for the Mellin integration variables. What remains to be checked is where the saddle point analysis can be trusted. In section 3.3 we found issues with the position-space analysis because the steepest descent contour for a bulk-bulk propagator may not pass inbetween the poles at $c = \pm\Delta$. As we discuss below, the same can happen in Mellin space where the steepest descent contour for the Mellin variables may lie on the wrong side of poles in the Mellin amplitude itself. We will see that the additional contribution from these poles is the Mellin space analogue of the AdS Landau diagram contributions discussed in section 3.4.

First consider the poles in the Gamma functions that are part of the definition of the Mellin amplitude given in equation (3.5.1). In our analysis these disappeared when we used the Stirling approximation, so really we should verify if none of the σ_{ij} is real and negative so this approximation is trustworthy. In terms of the Mandelstam

invariants $s_{ij} := -(k_i + k_j)^2$ we find that

$$\sigma_{ij}^* = \frac{1}{2\sum_k m_k}((m_i + m_j)^2 - s_{ij}) \tag{3.5.18}$$

We see σ_{ij}^* becomes real and negative precisely when the corresponding Mandelstam invariant lies above the two-particle threshold. We can therefore use the Mellin saddle point as long as we are on the principal sheet for all the Mandelstam invariants and stay at least an infinitesimal amount away from the physical values.[21]

To illustrate this phenomenon we consider a four-point function of identical operators, see also figure 3.15. After resolving the constraints on the Mellin variables we can write that

$$G(P_{ij}) = (P_{13}P_{24})^{-\Delta} \int \frac{d\gamma_{12}d\gamma_{14}}{(2\pi i)^2} M(\gamma_{12}, \gamma_{14})\Gamma^2(\gamma_{12})\Gamma^2(\gamma_{14})\Gamma^2(\Delta - \gamma_{12} - \gamma_{14})u^{-\gamma_{12}}v^{-\gamma_{14}} \tag{3.5.19}$$

The Gamma functions provide exponential damping for large imaginary values of their arguments, but this can be offset by extra phases introduced by the rotation of u and v in the complex plane. Starting from real and positive values of these cross ratios, we can rotate them by at most 2π before the exponential damping is overcome and the Mellin representation becomes invalid. In more detail we can say that the Mellin representation works for $\sqrt{u}$, $\sqrt{v}$ and $\sqrt{u/v}$ away from the negative real axis. In terms of the Mandelstam invariants this means that

$$-\pi < \arg\left(\frac{s - 4m^2}{\tilde{u} - 4m^2}\right) < \pi, \qquad -\pi < \arg\left(\frac{t - 4m^2}{\tilde{u} - 4m^2}\right) < \pi, \qquad -\pi < \arg\left(\frac{s - 4m^2}{t - 4m^2}\right) < \pi. \tag{3.5.20}$$

We see that for physical values of the Mandelstam variables (in either of the three channels) we are just at the boundary of the range of validity of the Mellin space representation and we need to use a small $i\epsilon$ prescription.[22]

Figure 3.15 shows the steepest descent contour in the σ_{12} plane for values of Mandelstam s approaching the physical threshold. We remark that in order to construct this figure we already performed the γ_{14} integral, after which the location of the saddle point and the steepest descent contour for large R depend only on Mandelstam s. More precisely, if we do the γ_{14} integral by saddle point approximation

---

[21]This analysis also highlights a potentially important difference between the Mellin space prescription and our amplitude conjecture: the former only works on the principal sheet but the latter has a chance of giving the right answer also on the other sheets that can be reached by passing through the multi-particle cuts. It would be interesting to explore this further.

[22]In practice we can probably send ϵ to zero as R goes to infinity. We have not worked out this scaling in detail.

(a) $s = 6.2 + 0.3i$ (b) $s = 6.2 + 0.05i$
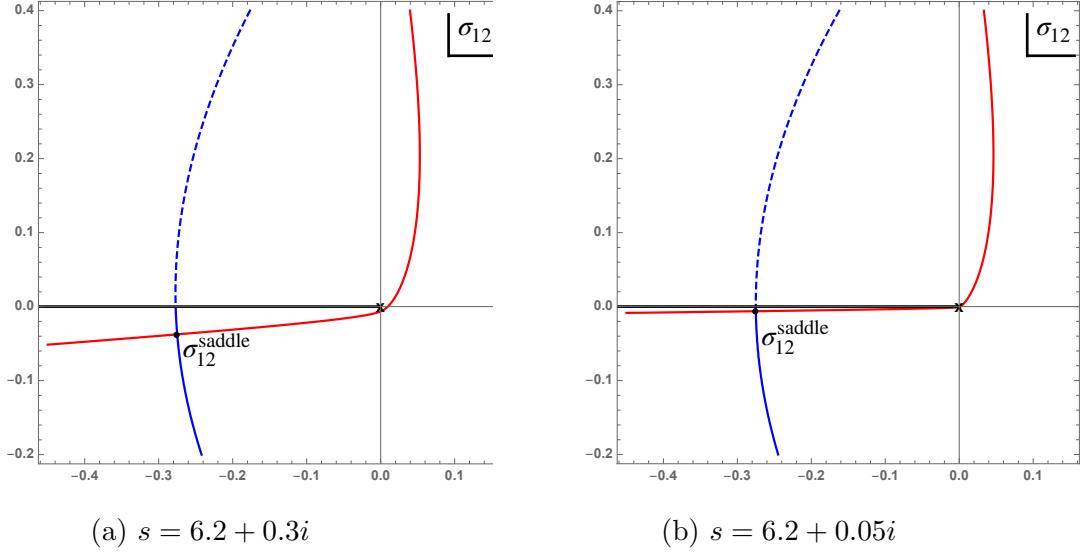
Figure 3.15. Steepest descent (red curve) and ascent (blue curve) contours of σ_{12} integral for $s = 6.2 + 0.3i$ (left) or $s = 6.2 + 0.05i$ (right). The black dot is the saddle point, and the cross indicates the starting poles of the semi-infinite sequences of poles in $\Gamma^2(R\sigma_{12})$. The other poles are represented by the black solid line. As s approaches the physical region, the steepest descent contour gets close to the first Γ-function pole, but does not cross it.

then

$$
G(P_{ij})|_{\text{cons}} \xrightarrow{\text{R}\to\infty} \int \frac{d\sigma_{12}}{2\pi i} (\ldots) M(R\sigma_{12}, R\sigma_{14}^*)
$$
$$
\times \exp\left(2R\left(\sigma_{12}\log(\sigma_{12}) + (m - \sigma_{12})\log(m - \sigma_{12}) + \sigma_{12}\log\left(\frac{s + 4m^2}{s - 4m^2} \right) \right) \right)
$$
$$(3.5.21)$$

where we have also made the substitution $\gamma_{12} = R\sigma_{12}$ and expressed the cross ratios in terms of the Mandelstam invariants. In deriving this expression we assumed that the P_i were chosen to lie on the support of the momentum-conserving delta function. The ellipsis refer to subleading terms in $1/R$ which do not affect the location of the steepest descent contour in figure 3.15 (but which are essential for recovering the delta function as described above).

A second potential issue is due to the existence of poles in the Mellin amplitude itself. These are present for non-contact Witten diagrams in AdS and therefore we need to understand how they affect the saddle point and the steepest descent contour analysis. Unfortunately at present we lack the technology to analyse the most general Witten diagram in the most general kinematical setup. We will therefore focus on the scalar exchange diagram as a case study.

3.5.3 The exchange diagram revisited

Let us again consider the scalar exchange diagram, already discussed in section 3.3.3, involving four external operators of dimension Δ with an exchange of a scalar operator with dimension Δ_b. The corresponding Mellin amplitude is [43]:

$$\mathcal{N}^{-1} M(\gamma_{12}) = -R^{5-d} \sum_{k=0}^{\infty} \frac{R_k}{2\Delta - 2\gamma_{12} - \Delta_b - 2k}, \qquad (3.5.22)$$

with

$$R_k = \frac{\Gamma(\frac{2\Delta + \Delta_b - d}{2})^2}{2\Gamma(\frac{4\Delta - d}{2})} \frac{(1 + \frac{\Delta_b - 2\Delta}{2})_k^2}{k! \Gamma(\Delta_b - \frac{d}{2} + 1 + k)}. \qquad (3.5.23)$$

For the flat-space limit we recall the analysis in [13]: set $k = R\kappa$ to find that, at large R,

$$R_k \overset{R \to \infty}{\longrightarrow} \frac{1}{4mR^2} \sqrt{\frac{64Rm^3}{\pi(4m^2 - m_b^2)^2}} \exp\left(-\frac{64Rm^3}{(4m^2 - m_b^2)^2}\left(\kappa - (2m - m_b)^2/8m\right)^2 + \dots\right) \qquad (3.5.24)$$

The sum over k therefore localizes at $\kappa^* = (2m - m_b)^2/8m$ and the remaining Gaussian sum (over k, not κ) gives a factor $(4mR)^{-1}$ so we find that

$$R^{d-5} \mathcal{N}^{-1} M(R\sigma_{12}^*) \overset{R \to \infty}{\longrightarrow} -\frac{1}{4mR^2(2m - 2\sigma_{12}^* - m_b - 2\kappa^*)} = -\frac{1}{R^2} \frac{1}{s - m_b^2} \qquad (3.5.25)$$

as expected from the flat-space formula in Mellin space [13].

Now we can analyse the steepest descent contour. Since the Mellin amplitude for the exchange diagram only depends on γ_{12}, we can safely do the γ_{14} integral by a saddle point approximation and start our analysis from (3.5.21), the important part of which is:

$$G(P_{ij})|_{\text{cons}} \overset{R \to \infty}{\longrightarrow} \int \frac{d\sigma_{12}}{2\pi i} (\dots) M(R\sigma_{12}, R\sigma_{14}^*) \exp\left(R\phi\left(m, \frac{4m^2 + s}{4m^2 - s}, \sigma_{12}\right)\right) \qquad (3.5.26)$$

$$\phi(\alpha, \beta, \sigma) := 2\sigma \log(\sigma) + 2(\alpha - \sigma) \log(\alpha - \sigma) + 2\sigma \log(\beta)$$

We will once more assume that we are on the support of the momentum-conserving delta function. The main idea is illustrated in figure 3.16, where deforming the original integration contour to the steepest descent contour may yield a number of contributions from the Mellin poles. Of course, if Mellin poles get picked up then we still have to check whether their contribution is leading or subleading at large R. So we naturally arrive at three regions: in region I no Mellin poles are picked up, in region II Mellin poles are picked up but their contribution is subleading, and finally in region III Mellin poles are picked up and leading. Only in region III does the flat

(a) $s = 2.2$ (b) $s = 4.2 + 2i$
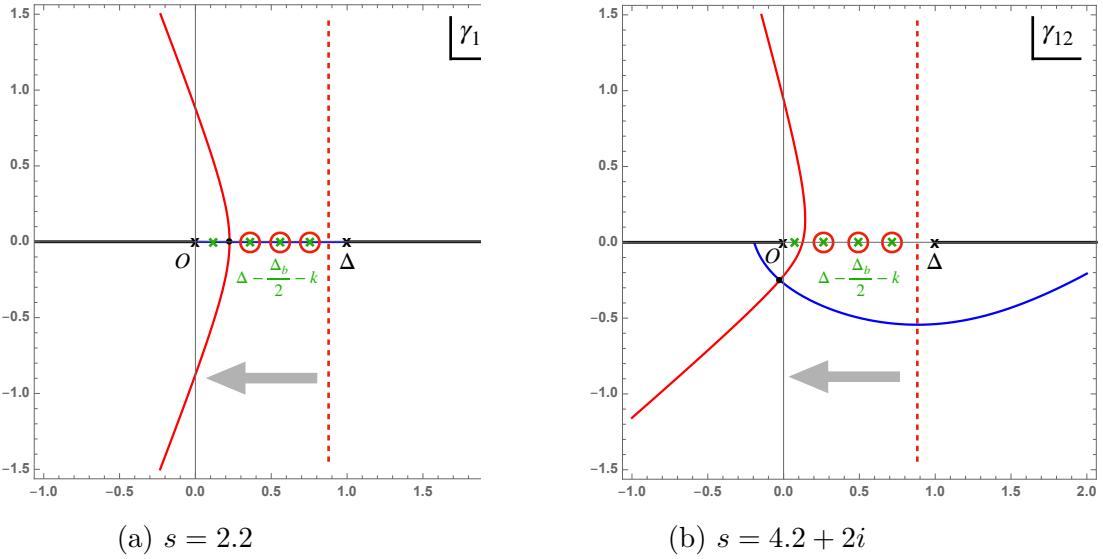
Figure 3.16. Steepest descent (red curve) and ascent (blue curve) contours of scalar exchange diagram with $m = 1$, $s = 2.2$ (left) or $s = 4.2 + 2i$ (right). The black dot is the saddle point. The red dashed line indicates the original integral contour. The green crosses are poles of the Mellin amplitude and those with a red circle are picked up during contour deformation. The black crosses are the starting poles of Γ-functions and the rest are represented by black solid lines.

space limit not work.

Finding these three regions is a technical exercise that involves finding the stationary phase contour in (3.5.26) and then estimating the contribution of any poles that get picked up in regions II and III. The details are left to appendix 3.B and the result is sketched in figure 3.17. This figure should of course be compared with figure 3.11 in section 3.3. Clearly the main results in each figure, namely the region III 'blobs' where the flat-space limit diverges, are exactly the same. The analyses were also remarkably similar: in both cases there were 'anomalous' contributions from either the pole at $c = \Delta_b$ or from the poles in the Mellin amplitude. Nevertheless the regions of type II are different: sometimes Mellin poles get picked up whereas the pole at $c = \Delta_b$ does not. This is not a contradiction: outside the blobs these contributions vanish anyway, so the discrepancy just shows that not all zeroes are created equally.

3.5.4 A bound on anomalous thresholds?

Compared to scattering amplitudes, conformal correlation functions have an extra feature that we have not exploited so far: a conformal block decomposition. Since a conformal block for an operator of dimension Δ_b and spin ℓ corresponds to a semi-infinite sequences of pole in the Mellin amplitude starting at $\Delta_b - \ell$, we are in the unique position that we know the singularities in the Mellin amplitudes if we know the spectrum of the theory (and assume that the correlation function can be
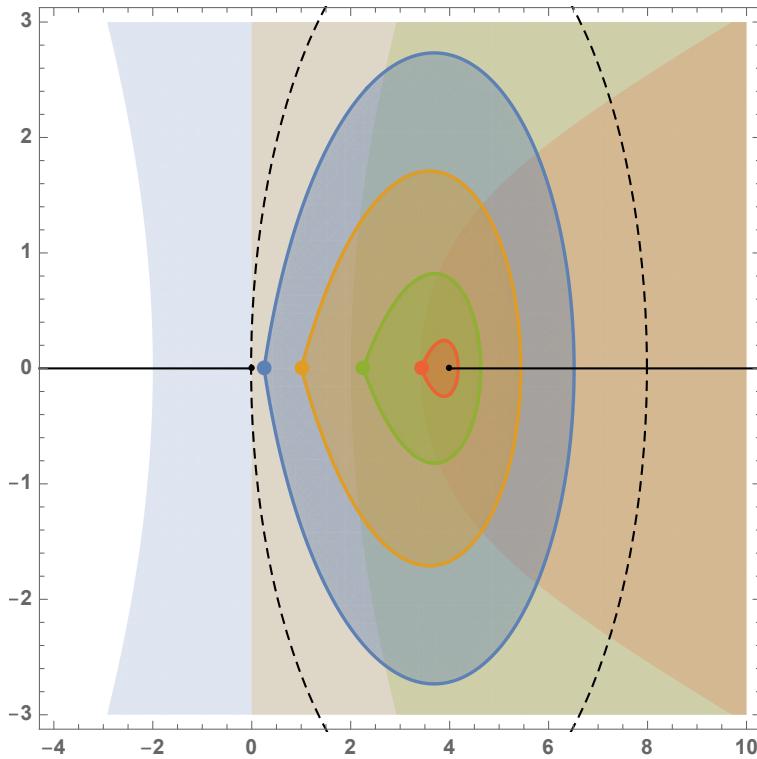
Figure 3.17. Light shading: regions in the complex s plane where we pick up poles in the
Mellin amplitude. Dark shading: regions where these poles dominate and our flat-space
limit diverges. We have set $m = 1$ and the blue, orange, green and red domains respectively
correspond to $m_b = 0.5, 1, 1.5, 1.85$. We have also highlighted the pole at $s = m_b^2$ for each
colour as well as the cut at $s = 4$. Although this is not entirely obvious from the plot, the
blue region extends rightward to include the orange, green and red regions and similarly
for the other colours.

represented as a Mellin amplitude). In other words, unlike scattering amplitudes
Mellin amplitudes cannot have anomalous thresholds like the one discussed for the
triangle diagram: if the first physical state, so the first non-trivial conformal block,
corresponds to an operator with twist τ_b then the Mellin amplitude should have
poles only for $\gamma_{12} \leq \Delta - \tau_b/2$. As examples we note that for the exchange diagram
$\tau_b = m_b R$ whereas for the triangle diagram discussed in section 3.4.2 $\tau_b = 2\mu R$ with
μ the mass of the internal particle.

In the flat-space limit we are supposed to evaluate the Mellin amplitude at

$$\gamma_{12} = \frac{\Delta}{8m^2}(4m^2 - s) \tag{3.5.27}$$

and therefore the Mellin poles can only interfere with the flat-space limit if

$$s > 4m(\tau_b/R - m) \tag{3.5.28}$$

on the real axis. For complex s the Mellin conjecture (3.5.5) would predict that there are no other singularities in the complex s plane as long as (3.5.20) is obeyed; for our amplitude conjecture we in addition need to restrict ourselves to s in region I so no Mellin poles are picked up. (This region is easily found using the results in appendix 3.B.) Either way, we see that the absence of anomalous thresholds in the Mellin amplitude leads to a region in the Mandelstam plane where Landau singularities should never appear, no matter how complicated the diagram.

Could the inequality be a universal threshold for Landau singularities? As a zeroth order check we have plotted the inequality (3.5.28) on the right in figure 3.14 and indeed find that it is obeyed by the anomalous triangle threshold. Of course, to obtain a general result we need to demand that equation (3.5.28) holds also for t and u with τ_b replaced with the first physical operator in the corresponding conformal block channel, and there may be additional subtleties if the Mellin amplitude depends non-trivially on both the Mandelstam variables. We should also note that this putative bound hinges on the validity of either the Mellin or the amplitude conjecture, but if it holds then it is a result that applies purely to flat-space scattering amplitudes. It would be interesting to investigate this further, either with QFT in AdS methods or perhaps even without reference to AdS.

3.6 S-matrices from conformal block expansions

Up to now we have motivated and examined our conjecture that CFT correlators become S-matrices in the flat space limit from a perturbative standpoint, examining specific diagrams for weakly coupled QFTs in AdS space. The goal of this section is to offer a complementary perspective by providing a non-perturbative argument for the validity of our central claim, in the case of 2-to-2 scattering. In that case we can explicitly use the OPE to express amplitudes in terms of the CFT data, and this will allow us to show that CFT correlators do indeed, under certain assumptions, become objects which obey the expected unitarity conditions for scattering amplitudes.

For simplicity we will consider identical scalar particles of mass m and we will mostly focus on physical kinematics, i.e. $s > 4m^2$ and real scattering angle. We will be able to see explicitly under which circumstances our conjectures have a chance of being valid, and under which it certainly fails.

3.6.1 Preliminaries

For the purposes of this section, we set:

$$\langle \underline{\tilde{k}}_3, \underline{\tilde{k}}_4 | S | \underline{k}_1, \underline{k}_2 \rangle = i(2\pi)^{d+1} \delta^{(d+1)}(k_1 + k_2 + k_3 + k_4) \mathcal{S}(\tilde{k}_3, \tilde{k}_4; k_1, k_2) \qquad (3.6.1)$$

Note that $\mathcal{S}(k_i)$ contains both connected and disconnected contributions, which may seem a bit unusual. In terms of $\mathcal{S}(k_i)$ our claim is:

$$\mathcal{S}(\tilde{k}_3, \tilde{k}_4; k_1, k_2) = \lim_{R \to \infty} \frac{\langle \mathcal{O}(\tilde{n}_3)\mathcal{O}(\tilde{n}_4)\mathcal{O}(n_1)\mathcal{O}(n_2)\rangle}{G_c(\tilde{n}_3, \tilde{n}_4, n_1, n_2)}\bigg|_{\text{S-matrix, cons}} \quad (3.6.2)$$

where $G_c(x_1, \ldots, x_4)$ is the contact diagram in AdS. Implicit in the equation is that $\Delta \to mR$ with the physical mass m fixed, which henceforth we set to unity. We can think of the above formula as something that can be done for any family of CFT correlators that depends on the parameter R such that the scaling dimensions grow with R. Below we will show that under certain assumptions the resulting $\mathcal{S}(k_i)$ will be finite and obey the expected unitarity conditions for an elastic amplitude.

By conformal invariance we can of course write:

$$\langle \mathcal{O}(x_1)\mathcal{O}(x_2)\mathcal{O}(x_3)\mathcal{O}(x_4)\rangle = \frac{\mathcal{G}_{\Delta_{\mathcal{O}}}(z, \bar{z})}{x_{13}^{2\Delta_{\mathcal{O}}}x_{24}^{2\Delta_{\mathcal{O}}}}, \qquad G_c(x_1, x_2, x_3, x_4) = \frac{\mathcal{D}_{\Delta_{\mathcal{O}}}(z, \bar{z})}{x_{13}^{2\Delta_{\mathcal{O}}}x_{24}^{2\Delta_{\mathcal{O}}}} \quad (3.6.3)$$

and with the conformal block decomposition:

$$\mathcal{G}_{\Delta_{\mathcal{O}}}(z, \bar{z}) = \sum_{\Delta, \ell} a_{\Delta, \ell} \frac{G_{\Delta, \ell}(z, \bar{z})}{(z\bar{z})^{\Delta_{\mathcal{O}}}} \quad (3.6.4)$$

with $a_{\Delta, \ell} = \lambda_{\mathcal{O}_{\Delta, \ell}}^2$ the squared OPE coefficient, $\phi \times \phi \sim \sum_{\Delta} \lambda_{\mathcal{O}_{\Delta, \ell}}\mathcal{O}_{\Delta, \ell}$.

As reviewed in section 3.2, the conformal cross ratios u and v are often parametrized in terms of the Dolan-Osborn variables z and $\bar{z}$ or in terms of the radial coordinates ρ and $\bar{\rho}$. In the following we will work with r and η which are related to the ρ and $\bar{\rho}$ variables via:

$$r(z, \bar{z}) = \sqrt{\rho}\sqrt{\bar{\rho}}, \qquad \eta = \frac{1}{2}\left(\sqrt{\frac{\rho}{\bar{\rho}}} + \sqrt{\frac{\bar{\rho}}{\rho}}\right). \quad (3.6.5)$$

Equation (3.2.30) is easily adapted to find the map between (r, η) and the Mandelstam variable s and the scattering angle[23] θ:

$$s = 4(1 - z_{\text{eff}}), \qquad \eta = -\cos(\theta), \quad (3.6.6)$$

where the introduction of

$$z_{\text{eff}} := \frac{4r}{(1 + r)^2} \quad (3.6.7)$$

will be useful to simplify the notation below. The technical advantage of working with r, η is that we may reach the physical kinematics scattering region, which is $s - i\epsilon > 4$ and real θ, from the Euclidean section without worrying about branch cuts. Indeed, if we start from the Euclidean region where $r \geq 0$ and $\eta \in [-1, 1]$

---

[23]Recall that Mandelstam $t = -\frac{1}{2}(s - 4)(1 - \cos(\theta))$.

then we can reach the physical s-channel scattering region by taking r negative with a small negative imaginary part. At the same time η is taken to $-\eta$ while always remaining real.

A particular family of correlators that will be important for us is that of generalized free fields, which describe free massive particles propagating in AdS space. For this theory the correlator of the elementary fields takes the form:

$$
\begin{aligned}
\langle \phi(x_1)\phi(x_2)\phi(x_3)\phi(x_4)\rangle &= \frac{1}{x_{12}^{2\Delta_{\mathcal{O}}}x_{34}^{2\Delta_{\mathcal{O}}}} + \frac{1}{x_{13}^{2\Delta_{\mathcal{O}}}x_{24}^{2\Delta_{\mathcal{O}}}} + \frac{1}{x_{14}^{2\Delta_{\mathcal{O}}}x_{23}^{2\Delta_{\mathcal{O}}}} \\
&= \frac{1}{x_{13}^{2\Delta_{\mathcal{O}}}x_{24}^{2\Delta_{\mathcal{O}}}} \left(\frac{1}{(z\bar{z})^{\Delta_{\mathcal{O}}}} + \sum_{\Delta,\ell} a_{n,\ell} \frac{G_{\Delta_{n,\ell},\ell}(z,\bar{z})}{(z\bar{z})^{\Delta_{\mathcal{O}}}} \right) .
\end{aligned}
\tag{3.6.8}
$$

where $\Delta_{n,\ell} = 2\Delta_{\mathcal{O}} + 2n + \ell$ corresponds to the scaling dimension of double twist operators of the form $\phi\partial^\ell\Box^n\phi$, and the OPE coefficients are given by:

$$
a_{n,\ell} = \frac{(d-2)_\ell}{(d/2-1)_\ell} \frac{2\left[(\Delta_{\mathcal{O}} - d/2 + 1)_n(\Delta_{\mathcal{O}})_{\ell+n}\right]^2}{\ell! n! (d/2+\ell)_n (n + 2\Delta_{\mathcal{O}} - d + 1)_n(\ell + 2n + 2\Delta_{\mathcal{O}} - 1)_\ell(\ell + n + 2\Delta_{\mathcal{O}} - d/2)_n}.
\tag{3.6.9}
$$

Below it will be useful to define an OPE density which is defined for continuous values of Δ:

$$
a_{\Delta,\ell}^{\mathrm{cont}} \equiv a_{n,\ell}\Big|_{n=\frac{\Delta - 2\Delta_{\mathcal{O}} - \ell}{2}} .
\tag{3.6.10}
$$

Note that in the flat-space limit the generalized free correlator should reduce to trivial scattering. For the last two terms in equation (3.6.8) this is indeed the case, since they are just products of two-point functions between one 'in' and one 'out' particle and the analysis of the two-point functions in section (3.3.1) is directly applicable. The first term corresponds to a Witten diagram where the two 'in' particles and the two 'out' particles are contracted. The corresponding Feynman diagram is certainly not part of a scattering amplitude, and we will analyse what remains of this contribution below.

3.6.2 Conformal block expansion at large $\Delta_{\mathcal{O}}$

After these preliminary remarks, we begin by examining the flat space limit. In the limit of large scaling dimensions Δ the conformal block reduces to [81]:

$$
G_{\Delta,\ell} \underset{\Delta\to\infty}{\sim} N_G \frac{r^\Delta}{(1-r^2)^\nu} \frac{C_\ell^{(\nu)}(\eta)}{\sqrt{(1+r^2)^2 - 4r^2\eta^2}} , \qquad N_G = \frac{\ell!}{(2\nu)_\ell} 4^\Delta .
\tag{3.6.11}
$$

with $\nu = (d-2)/2$. The second ingredient in our formula for $\mathcal{S}(k_i)$ is the contact term. In section 3.3.2 we determined that at large $\Delta_{\mathcal{O}}$ and in Euclidean kinematics

we have:

$$\mathcal{D}_{\Delta_{\mathcal{O}}}(r,\eta) = \frac{1}{N_D} \left(\frac{1 + r^2 + 2r\eta}{(1+r)^2} \right)^{2\Delta_{\mathcal{O}}} \frac{(1+r)^3}{\sqrt{r(1+r^2)^2 - 4r^3\eta^2}} \,. \tag{3.6.12}$$

where[24]

$$N_D = 2^{\frac{7+d}{2}} \Delta_{\mathcal{O}}^{5\frac{d-1}{2}} \pi^{\frac{d-1}{2}} \,. \tag{3.6.13}$$

To proceed we need to make some simplifying assumptions consistent with the
existence of a dual QFT description in flat space in the large radius limit. Let us
assume that in the particular family of correlators under consideration, the spectrum
of states consists of the identity, a finite set of scalar "bound states" with $1 \ll \Delta < 2\Delta_{\mathcal{O}}$ and infinite towers of states with spins $\ell \geq 0$ and with $\Delta \geq 2\Delta_{\mathcal{O}} + \ell$. The
latter will become the multiparticle continuum in the large R limit. Note that these
assumptions are satisfied for instance for the generalized free field considered above.
Physically we are stating that a hypothetical holographic flat-space QFT description
should contain only massive states, and that we are examining the scattering of the
lightest particle (otherwise multiparticle states would appear below $2\Delta_{\mathcal{O}}$). There
are further assumptions that must be made on the OPE coefficients, as we shall see
shortly.

We can now use the expressions above to write:

$$\lim_{\Delta_{\mathcal{O}} \to \infty} \frac{\mathcal{G}_{\Delta_{\mathcal{O}}}(r,\eta)}{\mathcal{D}_{\Delta_{\mathcal{O}}}(r,\eta)} = \lim_{\Delta_{\mathcal{O}} \to \infty} \left(\frac{\sqrt{r}}{(1+r)^3(1-r^2)^\nu} \right)$$

$$\left[I(r,\eta) + \sum_{0 < \Delta_b < 2\Delta_{\mathcal{O}}} \mathcal{N}_{\Delta_b}^{\text{bound}} \left(\frac{a_{\Delta_b,0}}{a_{\Delta_b}^{\text{bound}}} \right) \frac{r^{\Delta_b}}{z_{\text{eff}}^{2\Delta_{\mathcal{O}}}} + \sum_{\substack{\Delta > 2\Delta_{\mathcal{O}} + \ell \\ \ell = 0,2,\ldots}} \mathcal{N}_{\Delta}^{\text{cont}} \left(\frac{a_{\Delta,\ell}}{a_{\Delta,\ell}^{\text{cont}}} \right) \frac{r^{\Delta}}{z_{\text{eff}}^{2\Delta_{\mathcal{O}}}} C_\ell^{(\nu)}(\eta) \right]$$
$$\tag{3.6.14}$$

where $I(r,\eta)$ is the identity block contribution,

$$I(r,\eta) \equiv N_D \frac{\sqrt{(1+r^2)^2 - 4r^2\eta^2}}{z_{\text{eff}}^{2\Delta_{\mathcal{O}}}} (1-r^2)^\nu \tag{3.6.15}$$

and we have defined the parameters

$$\mathcal{N}_{\Delta}^{\text{cont}} = N_G \, N_D \, a_{\Delta,\ell}^{\text{cont}} \,, \qquad \mathcal{N}_{\Delta_b}^{\text{bound}} = N_G \, N_D \, a_{\Delta_b}^{\text{bound}} \,. \tag{3.6.16}$$

We will give $a_{\Delta}^{\text{bound}}$ below.

Our expression contains three kinds of contributions: the identity, "bound states"

---

[24]In this section we work with unit normalized operators which means that this normalization
factor is a little different from equation (3.3.32).

and the "continuum", i.e. states above the twist gap $\tau > 2\Delta_{\mathcal{O}}$. We will examine below each contribution in turn, but the logic is as follows. The third contribution is the most interesting one. We will see that for physical kinematics i.e. $s > 4m^2$ and under certain assumptions on the OPE coefficients it is finite and becomes the partial wave decomposition of the S-matrix, with an expression for the spin-ℓ phase shifts in terms of the CFT data. But before we see this we must take care of the first two contributions, which will turn out to be either zero or divergent depending on the choice of kinematical region.

Identity and bound states

We begin with the contribution of the identity. As stated above, from an S-matrix perspective it corresponds to an unphysical diagram that connects the particles in the 'in' states and the particles in the 'out' states with nothing propagating in between. It might therefore be reasonable to subtract it by hand. Alternatively, we see that in the large $\Delta_{\mathcal{O}}$ limit the factor $z_{\text{eff}}^{-2\Delta_{\mathcal{O}}}$ dominates and as long as

$$|z_{\text{eff}}| > 1 \Leftrightarrow |s - 4| > 4 , \tag{3.6.17}$$

the unwanted contribution vanishes automatically. In particular for physical kinematics this requires $s > 8$. On the other hand, the factor diverges as long as $|z_{\text{eff}}| < 1$.

Now for the bound states. In this case we need to know something about the behaviour of their OPE coefficients in the large $\Delta_{\mathcal{O}}$ limit. We will assume that for each such state we have

$$g_{\Delta_b}^2 \equiv \lim_{R \to \infty} \frac{a_{\Delta_b,0}}{a_{\Delta_b}^{\text{bound}}} < \infty \qquad (\Delta_b < 2\Delta_{\mathcal{O}}) \tag{3.6.18}$$

where:

$$a_{\Delta_b}^{\text{bound}} := \frac{\pi^d \Gamma\left(\frac{2\Delta_{\mathcal{O}}+\Delta_b-d}{2}\right)^2}{4\Delta_{\mathcal{O}}^{d-5}} \frac{\mathcal{C}_{\Delta_{\mathcal{O}}}^2 \mathcal{C}_{\Delta_b} \Gamma\left(\frac{\Delta_b}{2}\right)^4 \Gamma\left(\frac{2\Delta_{\mathcal{O}}-\Delta_b}{2}\right)^2}{\Gamma(\Delta_{\mathcal{O}})^4 \Gamma(\Delta_b)^2} \tag{3.6.19}$$

We have defined g_Δ^2 in this way since it becomes a physical coupling in the flat-space limit for a QFT in AdS space, as discussed in [13]. There is also some evidence for the validity of this bound from the numerical conformal bootstrap [13, 46] and a proof [82] for the special case $d = 1$.

Going to physical kinematics means we take $r < 0$, $z_{\text{eff}} < 0$ and changing the sign of η. With the appropriate $i\epsilon$ insertions this yields:

$$\frac{r^{\Delta_b}}{z_{\text{eff}}^{2\Delta_{\mathcal{O}}}} \to \frac{(-r)^{\Delta_b}}{(-z_{\text{eff}})^{2\Delta_{\mathcal{O}}}} e^{-i\pi(\Delta-2\Delta_{\mathcal{O}})} , \qquad \eta \to -\eta . \tag{3.6.20}$$

Note that the change in sign of η is immaterial in our case, because all states ap-

pearing in the OPE must have even spin and so η always appears squared.

In the flat space limit we set $s_b \equiv \Delta_b^2/\Delta_{\mathcal{O}}^2$ and find

$$\mathcal{N}_{\Delta_b}^{\text{bound}} \left(\frac{a_{\Delta_b,0}}{a_{\Delta_b}^{\text{bound}}} \right) \frac{(-r)^{\Delta_b}}{(-z_{\text{eff}})^{2\Delta_{\mathcal{O}}}} \underset{\Delta_{\mathcal{O}} \to \infty}{\sim} \Delta_{\mathcal{O}}^{2d-\frac{3}{2}} g_{\Delta_b}^2 \, R(s,s_b) \times E(s,s_b)^{\Delta_{\mathcal{O}}} \tag{3.6.21}$$

where $R(s,s_b)$ is independent of $\Delta_{\mathcal{O}}$ and

$$E(s,s_b) := \left(\frac{4-s_b}{s-4} \right)^2 \left[\frac{(\sqrt{s}-2)(2+\sqrt{s_b})}{(\sqrt{s}+2)(2-\sqrt{s_b})} \right]^{\sqrt{s_b}} \tag{3.6.22}$$

The exponential factor implies that the contribution of the bound states is either zero or infinite. In fact, the expression for a single 'bound state' conformal block is exactly the same as the contribution of the pole at $c = \Delta_b$ in the exchange diagram discussion of section 3.3.3, as follows from the discussion in appendix 3.D. (If it diverges then it also agrees with the contribution from the Mellin poles discussed in section 3.5.3.) Therefore, as can also be gleaned from the expression (3.6.22) itself, the region where the contribution from a bound state diverges is the same as already shown in figures 3.11 and 3.17. The worst case scenario corresponds to $s_b = 0$, i.e. massless bound states, for which $|E(s,s_b)| < 1$ if $|s-4| > 4$, i.e. the same result as for the identity. As we increase s_b divergences are avoided in an increasingly wider region.

3.6.3 The phase shift formula

Now let us look at those states which lie above the twist gap $\tau > 2\Delta_{\mathcal{O}}$. We would like to commute the large $\Delta_{\mathcal{O}}$ limit with the sum over blocks. For general kinematics we cannot do this: each term in the sum will diverge. This does not necessarily mean that our formula for $\mathcal{S}(k_i)$ is wrong, but merely that we cannot commute the OPE and flat space limits. However, let us again restrict to physical kinematics. As explained above, after continuation we get the sum

$$i \left(\frac{\sqrt{-r}}{(1+r)^3(1-r^2)^\nu} \right) \sum_{\substack{\Delta > 2\Delta_{\mathcal{O}}+\ell \\ \ell=0,2,\dots}} \mathcal{N}_\Delta^{\text{cont}} \left(\frac{a_{\Delta,\ell}}{a_{\Delta,\ell}^{\text{cont}}} \right) \frac{(-r)^\Delta}{(-z_{\text{eff}})^{2\Delta_{\mathcal{O}}}} e^{-i\pi(\Delta-2\Delta_{\mathcal{O}})} C_\ell^{(\nu)}(\eta) \tag{3.6.23}$$

Notice that here it is important that we perform the continuation, and in particular take r to be arbitrarily close to the negative real axis, *before* taking the large radius limit.

The S-matrix is usually expressed in terms of polynomials related to Gegenbauer polynomials in the following way:

$$P_\ell^{(d)}(\eta) := p_{d,\ell} \, C_\ell^{(\nu)}(\eta), \qquad p_{d,\ell} = (d-2+2\ell)2^{2d-3}\pi^\nu \, \Gamma(\nu)]. \tag{3.6.24}$$

We now notice that

$$\left(\frac{\sqrt{-r}}{(1+r)^3(1-r^2)^\nu}\right)\frac{1}{p_{d,\ell}}\mathcal{N}_\Delta\frac{(-r)^\Delta}{(-z_{\text{eff}})^{2\Delta_\mathcal{O}}}\underset{R\to\infty}{\sim}\frac{4\sqrt{s}}{(s-4)^\nu}\left(\frac{e^{-\frac{(\Delta-2\Delta_\mathcal{O}\sqrt{1-z_{\text{eff}}})^2}{2\Delta_\mathcal{O}(-z_{\text{eff}})}}}{\sqrt{2\pi\Delta_\mathcal{O}(-z_{\text{eff}})}}\right),\qquad \Delta>2\Delta_\mathcal{O}$$
(3.6.25)

We see that for real and negative z_{eff} this is bounded and exponentially suppressed except in a region centred at

$$\left(\frac{\Delta}{2\Delta_\mathcal{O}}\right)^2\sim 1-z_{\text{eff}}=\frac{s}{4}$$
(3.6.26)

and with half-width of order $\sqrt{2\Delta_\mathcal{O}(-z_{\text{eff}})}$. Hence, the sum over states effectively receives only contributions from that region as long as the OPE ratios which appear in (3.6.23) are suitably bounded.

Let us now restrict ourselves to a kinematic region where both identity and bound states do not contribute. Putting all the ingredients together we find

$$\mathcal{S}(k_i)=\frac{2i\sqrt{s}}{(s-4)^\nu}\sum_{\ell=0,2,\ldots}e^{2i\delta_\ell(s)}P_\ell^{(d)}(\eta)$$

$$e^{2i\delta_\ell(s)}:=\lim_{\Delta_\mathcal{O}\to\infty}\sum_{\Delta>2\Delta_\mathcal{O}+\ell}2\left(\frac{a_{\Delta,\ell}}{a_{\Delta,\ell}^{\text{cont}}}\right)e^{-i\pi(\Delta-2\Delta_\mathcal{O})}\left(\frac{e^{-\frac{(\Delta-2\Delta_\mathcal{O}\sqrt{1-z_{\text{eff}}})^2}{2\Delta_\mathcal{O}(-z_{\text{eff}})}}}{\sqrt{2\pi\Delta_\mathcal{O}(-z_{\text{eff}})}}\right)$$
(3.6.27)

This is the main result of this section. It tells us that in the physical region the conformal block expansion computes an object which at least kinematically takes the same form as the partial wave decomposition of an S-matrix, with spin-ℓ phase shifts computable in terms of the CFT data. Note that the derivation of this formula required restricting ourselves to the region $s>8$. However, this is a shortcoming of our original conjecture relating the S-matrix to the correlator, and not of the formulae above which are expected to be valid for the full range of physical kinematics. For instance, for the GFF correlator our formula gives:

$$e^{2i\delta_\ell(s)}=\lim_{\Delta_\mathcal{O}\to\infty}\sum_{n=0}^\infty 2\left(\frac{e^{-\frac{(\Delta_{n,\ell}-2\Delta_\mathcal{O}\sqrt{1-z_{\text{eff}}})^2}{2\Delta_\mathcal{O}(-z_{\text{eff}})}}}{\sqrt{2\pi\Delta_\mathcal{O}(-z_{\text{eff}})}}\right)=1\,.$$
(3.6.28)

as it should be, independently of the range of s.

Arguably one of the most important properties of the S-matrix is that it should satisfy unitarity, which in the current context states that:

$$|e^{2i\delta_l(s)}|\leq 1\,.$$
(3.6.29)

This is not automatic from our formula, and to show it will require us to make one
last but crucial assumption:

$$\lim_{\Delta_{\mathcal{O}} \to \infty} \sum_{|\Delta - E\Delta_{\mathcal{O}}| < \Delta_{\mathcal{O}}^{\alpha}} \left(\frac{a_{\Delta,\ell}}{a_{\Delta,\ell}^{\mathrm{cont}}} \right) = \Delta_{\mathcal{O}}^{\alpha}, \qquad \text{with } E > 2 \text{ fixed, and for some } \alpha \in [0, \tfrac{1}{2}) \,.$$

(3.6.30)

Physically we are demanding that in the flat space limit, the average OPE density
per unit size bin in scaling dimension space matches that of a generalized free field.
Note that the requirement of $\alpha < 1/2$ is such that the averaging must be apparent on
a scale which is smaller than the scale of variation of the Gaussian, namely $O(\sqrt{\Delta_{\mathcal{O}}})$.
We can think of this assumption as a natural condition for a family of CFTs to have
a well-defined flat-space limit. It would be interesting to explore whether this is
really an assumption or if it can be proved as a general property of CFT correlators.
Using this assumption it is not hard to show that firstly the sum over states indeed
localizes in a region around $\Delta \sim \sqrt{s}\Delta_{\mathcal{O}}$ of width $\sim \sqrt{\Delta_{\mathcal{O}}}$ and secondly that the
all-important unitarity condition on the S-matrix actually holds.

The attentive reader may have noticed that in fact, for both these statements to
be true it would actually be sufficient that the equal sign in (3.6.30) was demoted
to a less-than sign. She may have also noticed that a similarly looking formula for
the phase shift was given already in [13]. These two observations are in fact related:
equality is needed in order for our formula to match the one given in [13], as we
show in detail in appendix 3.E. A second argument for the equality sign to hold in
equation (3.6.30) is that it leads to a nice relation between the imaginary part of the
connected amplitude and the double discontinuity of the CFT correlator as defined
in [1], as we now discuss.

Consider the connected part of the S-matrix, which arises by subtracting the full
GFF solution from the correlator,

$$\mathcal{T}(s, \eta) = \frac{2\sqrt{s}}{(s-4)^{\nu}} \sum_{\ell=0,2,\ldots} i(e^{2i\delta_{\ell}(s)} - 1) P_{\ell}^{(d)}(\eta)$$

(3.6.31)

Thanks to our assumption (3.6.30) we may write

$$e^{2i\delta_{\ell}(s)} - 1 = \lim_{\Delta_{\mathcal{O}} \to \infty} \sum_{\Delta > 2\Delta_{\mathcal{O}} + \ell} 2 \left(\frac{a_{\Delta,\ell}}{a_{\Delta,\ell}^{\mathrm{cont}}} \right) (e^{-i\pi(\Delta - 2\Delta_{\mathcal{O}})} - 1) \left(\frac{e^{-\frac{(\Delta - 2\Delta_{\mathcal{O}}\sqrt{1-z_{\mathrm{eff}}})^2}{2\Delta_{\mathcal{O}}(-z_{\mathrm{eff}})}}}{\sqrt{2\pi\Delta_{\mathcal{O}}(-z_{\mathrm{eff}})}} \right)$$

(3.6.32)

where the equality sign in that equation was crucial to move the subtracted '1' inside

the sum. This now means that the imaginary part of the amplitude will involve

$$1 - \operatorname{Re} e^{2i\delta_\ell(s)} = \lim_{\Delta_\mathcal{O} \to \infty} \sum_{\Delta > 2\Delta_\mathcal{O} + \ell} 2 \left(\frac{a_{\Delta,\ell}}{a_{\Delta,\ell}^{\text{cont}}}\right) \sin\left[\frac{\pi(\Delta - 2\Delta_\mathcal{O})}{2}\right]^2 \left(\frac{e^{-\frac{(\Delta - 2\Delta_\mathcal{O}\sqrt{1-z_{\text{eff}}})^2}{2\Delta_\mathcal{O}(-z_{\text{eff}})}}}{\sqrt{2\pi\Delta_\mathcal{O}(-z_{\text{eff}})}}\right).$$

(3.6.33)

and hence

$$\operatorname{Im} \mathcal{T}(s, \eta) = \lim_{\Delta_\mathcal{O} \to \infty} \frac{\mathrm{dDisc}\, \mathcal{G}(r, \eta)}{\mathcal{D}(r, \eta)}.$$

(3.6.34)

where we may define here

$$\mathrm{dDisc}\, \mathcal{G}(r, \eta) = \lim_{\epsilon \to 0^+} \frac{1}{4} \left[2\, \mathcal{G}(-r, -\eta) - \mathcal{G}(r + i\epsilon, \eta) - \mathcal{G}(r - i\epsilon, \eta)\right], \quad r < 0.$$

(3.6.35)

This relation is the precise sense that the double discontinuity of a correlator captures the imaginary part of a scattering amplitude. Notice that we have derived the above equation for physical kinematics, since there we could use the conformal block decomposition, but for the Lorentzian inversion formula of [1] or the dispersion relation of [83] the double discontinuity is integrated over a region in cross ratio space that does not reduce to a physical kinematics in the flat-space limit. The precise flat-space limit of these equations will be discussed in future work.

3.7 Conclusions

In this chapter we presented two related conjectures concerning the flat-space limit of the correlators on the conformal boundary for a gapped QFT in AdS. For a given Witten diagram we have seen that all the propagators and vertices reduce to their flat-space counterparts, and our S-matrix conjecture is the natural one that 'erases the circle' and reduces it to a Feynman diagram contributing to an S-matrix element in the flat-space limit. In contrast with many other conjectures, the flat-space limit can be taken directly in position space and no integral transform is necessary. On the other hand, for certain choices of the external momenta the interactions may be spread out over distances comparable to the AdS scale and therefore the conjectures do not always work.

Earlier recipes for extracting amplitudes from correlators include one based on Mellin space and a phase shift formula, both presented in [13]. In regions where our conjectures work we can recover these recipes, as we showed in detail in section 3.5 and 3.6, but we view our conjectures as more general: they also work for functions that are not representable in Mellin space (with disconnected correlators being the easiest example) and they are not restricted to elastic scattering like the phase shift formula. An important qualification is that, within the domain given in equation (3.5.20), the Mellin-space prescription seems to work for any correlator that can

be written in Mellin space and does not suffer from the same divergences as our conjectures.

In section 3.3 we discussed how the conjectures work for simple Witten diagrams but fail for some values of the Mandelstam s for the exchange diagram. This led us to introduce the general notion of Landau diagrams in AdS in section 3.4. As in flat space, they correspond to classical particles propagating over long distances and interacting in a momentum-conserving fashion; unlike in flat space, the momentum conservation equations can always be solved and an AdS Landau diagram exists for all values of the external momenta. They can however only be important if the real part of the corresponding on-shell 'action' is positive, which indicates a failure of the conjectures because the flat-space limit of the correlator diverges.

The most important open question concerns the range of external momenta where the limit used in our conjectures is actually finite, and the assumptions needed to show this. Notice that in all the examples we considered a divergence in the flat-space limit only occurred within a subregion of

$$|s - 4m^2| \leq 4m^2\,, \tag{3.7.1}$$

and similarly for t and u. This is in good agreement with the physical picture given in section 3.2.4: close operator insertions in the Euclidean cap generate less energetic particles, and the Euclidean geodesic connecting them dominates over the Lorentzian one. Furthermore, for functions that can be represented in Mellin space we have also seen that singularities are also unlikely to arise if s is real and

$$s < 4m(\mu - m) \tag{3.7.2}$$

and again similarly for t and u, and with μ the energy of the first state in the corresponding channel. Could these inequalities hold more generally? Are there more refined inequalities to be found? We can try to answer these questions either at a perturbative or at a non-perturbative level.

Perturbatively there are important open questions concerning the structure of the most general AdS Landau diagram and the region where it diverges. We also need to better understand the AdS version of the well-known intricacies of flat-space Landau diagrams as described for example in [77] and references therein. For example, we can extend the numerical investigation of the triangle diagram in section 3.4.2 to include the box and the acnode diagrams which are known to have a richer set of anomalous thresholds. Similarly we should investigate singularities on other Riemann sheets, which generally have complex displacement parameters α, as well as understand the AdS analogue of 'second type' singularities that correspond to pinch configurations with infinite momenta. Furthermore, recall that flat-space Landau diagrams can only be drawn for specific configurations of the external momenta whereas AdS Landau

diagrams can always be drawn, as discussed in section 3.4. Correspondingly, the flat-space Landau diagrams capture the threshold where (anomalous) singularities can appear but do not capture the branch cut that is often attached to such thresholds. It would be interesting to see if the AdS Landau diagrams can do better and whether branch cuts in the flat-space amplitude can always be taken to lie in the 'blobs' where the AdS Landau diagrams diverge.

In this chapter we have not yet made enough use of the conformal block decomposition of conformal correlation functions. As is by now well-known, this property implies all sorts of wonderful boundedness and analyticity properties of the correlation functions themselves. Can we use them to infer boundedness[25] (unitarity) and analyticity of the flat-space scattering amplitudes? Abstractly, consider a one-parameter family of consistent conformal correlation functions and make a few natural assumptions concerning its spectrum as the parameter $R \to \infty$. When does such a family limit to a consistent S-matrix? And supposing that it does, what are the analyticity properties of the resulting scattering amplitudes? To answer these questions it is essential to obtain a better handle on the possible behaviour of correlation functions and their OPE coefficients in the flat-space limit. The analysis in section 3.6 provided a first step in this direction. In particular we showed that, for a four-point function of identical operators the unitarity condition can be rather precisely tied to the OPE coefficient density. On the other hand, additional tools are necessary to conclude anything about the analyticity of the resulting amplitude.

We should note that in all of the above the divergences in the flat-space limit were considered a 'given' and that we only attempted to avoid them by choosing the external momenta appropriately. However one could also try to *subtract* all the AdS Landau diagrams by hand so the flat-space limit is everywhere finite, thereby improving the region of validity of our original conjectures. A possible way to do this is suggested by our computation in section 3.6: from the conformal block perspective one could naturally subtract crossing-symmetric sums of AdS exchange diagrams for every block below the two-particle threshold, the effect of which can then be reinstated by adding simple poles to the resulting S-matrix after taking the flat-space limit. It would be interesting to find out whether this procedure can also be done if the number of blocks below threshold becomes unbounded as $R \to \infty$, which should be the case if we do not scatter the lightest particle in the theory.

Finally it would be interesting to generalize our formalism to scattering amplitudes of massless particles, including photons and gravitons. One important point which is not fully understood is how infrared divergences in such theories arise when taking the flat-space limit. Landau diagrams in AdS introduced in this chapter might

---

[25]There are many interesting and well-known consequences of analyticity and unitarity including elastic unitarity as was recently explored in [37]. For all of these it would be very interesting to find their AdS ancestors. As an example we can mention the high-energy behaviour, which was done in [84, 85].

provide a useful tool for addressing this question. Another related question is to develop a detailed understanding of the soft theorem in flat space [86–88] (see also recent discussions in [89] on the soft theorem and the flat-space limit of AdS/CFT). We hope our position-space approach will prove useful for this purpose since it would allow us to directly analyse the flat-space limit of the Ward identity of the boundary correlators. Of course the ultimate goal would be to understand quantum gravity in flat space by taking the flat-space limit of AdS/CFT, but also on this front we still have a long journey ahead of us.

3.A   Analytic continuation in cross ratio space

It is worthwhile to see what the analytic continuation to the S-matrix configuration becomes in terms of the familiar cross-ratios (u, v) and $(z, \bar{z})$ for four-point conformal correlation functions. In spherical boundary coordinates they are

$$
\begin{aligned}
u &= z\bar{z} = \frac{(1 - \hat{n}_1 \cdot \hat{n}_2)(1 - \hat{n}_3 \cdot \hat{n}_4)}{(1 - \hat{n}_1 \cdot \hat{n}_3)(1 - \hat{n}_2 \cdot \hat{n}_4)}, \\
v &= (1 - z)(1 - \bar{z}) = \frac{(1 - \hat{n}_1 \cdot \hat{n}_4)(1 - \hat{n}_2 \cdot \hat{n}_3)}{(1 - \hat{n}_1 \cdot \hat{n}_3)(1 - \hat{n}_2 \cdot \hat{n}_4)}.
\end{aligned}
\tag{3.A.1}
$$

For the analytic continuation to the S-matrix configuration it will be necessary to view two cross ratios as independent complex variables.

We will consider the analytic continuation to a scattering amplitude where particles 1 and 2 are incoming and particles 3 and 4 are outgoing. Therefore, upon substitution of

$$
(n^0, \underline{n}) = -(k^0, -i\underline{k})/m,
\tag{3.A.2}
$$

we will take k_1^0 and k_2^0 positive and k_3^0 and k_4^0 negative. We will assume that we are on the support of the momentum conserving delta function $\sum_i k_i^\mu = 0$, where the remaining kinematical Lorentz-invariant degrees of freedom are captured in terms of the Mandelstam invariants[26]

$$
s = -(k_1 + k_2)^2, \qquad t = -(k_1 + k_4)^2, \qquad \tilde{u} = -(k_1 + k_3)^2 = \sum_i m_i^2 - s - t
\tag{3.A.3}
$$

In terms of which we find that

$$
u = \frac{(s - (m_1 + m_2)^2)(s - (m_3 + m_4)^2)}{(\tilde{u} - (m_1 + m_3)^2)(\tilde{u} - (m_2 + m_4)^2)}, \qquad v = \frac{(t - (m_2 + m_3)^2)(t - (m_1 + m_4)^2)}{(\tilde{u} - (m_1 + m_3)^2)(\tilde{u} - (m_2 + m_4)^2)}
\tag{3.A.4}
$$

---

[26]Notice that the Mandelstam t variable is defined following CFT conventions where the 't-channel' is traditionally the one where operators 1 and 4 are fused together.

(a) Analytic continuation of u and v (b) Analytic continuation of z and $\bar{z}$
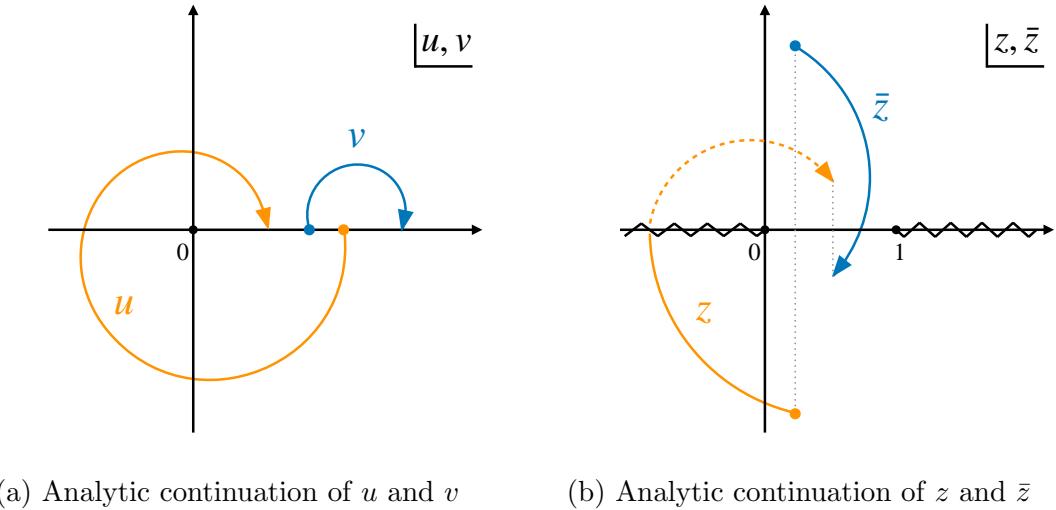
Figure 3.18. Analytic continuation to s-physical S-matrix configuration. Left: u takes a full clockwise turn around 0 while v does not. Right: the orange dashed curve indicates that z moves on the second Riemann sheet. Black dotted lines indicate that z and $\bar{z}$ are complex conjugate of each other at the starting point (corresponding to a Euclidean configuration) and the end point (corresponding to an S-matrix configuration).

We can now analytically continue from the Euclidean region, where the Mandelstam invariants s, t and $\tilde{u}$ are all real and positive, to the physical S-matrix region for the $12 \rightarrow 34$ process, where $s \geq \max\left((m_1 + m_2)^2, (m_3 + m_4)^2\right) + i\epsilon$ and t and $\tilde{u}$ such that the scattering angle is real. The corresponding continuation in the cross-ratios u and v is shown in figure 3.18a. We see that u makes a clockwise turn around the origin and v remains real. The corresponding continuation in terms of the z and $\bar{z}$ variables is shown in figure 3.18b: we start from a Euclidean configuration with $\bar{z} = z^*$, take one variable (which we take to be z) in a clockwise fashion through the branch cut on the negative real axis, and end on an 'S-matrix' configuration where again $\bar{z} = z^*$ but on another sheet.

In the equal mass case we can write that

$$\sqrt{u} = \frac{s - 4m^2}{\tilde{u} - 4m^2}, \qquad \sqrt{v} = \frac{t - 4m^2}{\tilde{u} - 4m^2} \tag{3.A.5}$$

In this formulation the Euclidean configuration corresponds to the principal branch of the square roots. We find that restricting to physical Lorentzian momenta implies that $\sqrt{u} \leq 0$ and $\sqrt{v} \geq 0$. In terms of the scattering angle θ, defined as

$$t = \frac{1}{2}(4m^2 - s)(1 - \cos(\theta)), \qquad \tilde{u} = \frac{1}{2}(4m^2 - s)(1 + \cos(\theta)) \tag{3.A.6}$$

we find a particularly simple form in the ρ variables, namely

$$\rho = \frac{\sqrt{s} - 2m}{\sqrt{s} + 2m} e^{i(\theta - 2\pi)}, \qquad \bar{\rho} = \frac{\sqrt{s} - 2m}{\sqrt{s} + 2m} e^{-i\theta} \tag{3.A.7}$$

So the physical parameters s and θ simply correspond to the modulus and argument of the ρ variables. Notice that it is again understood that ρ, like z above, is evaluated on the second sheet obtained by circling around zero in a clockwise fashion in order to ensure that $\sqrt{u} \leq 0$.
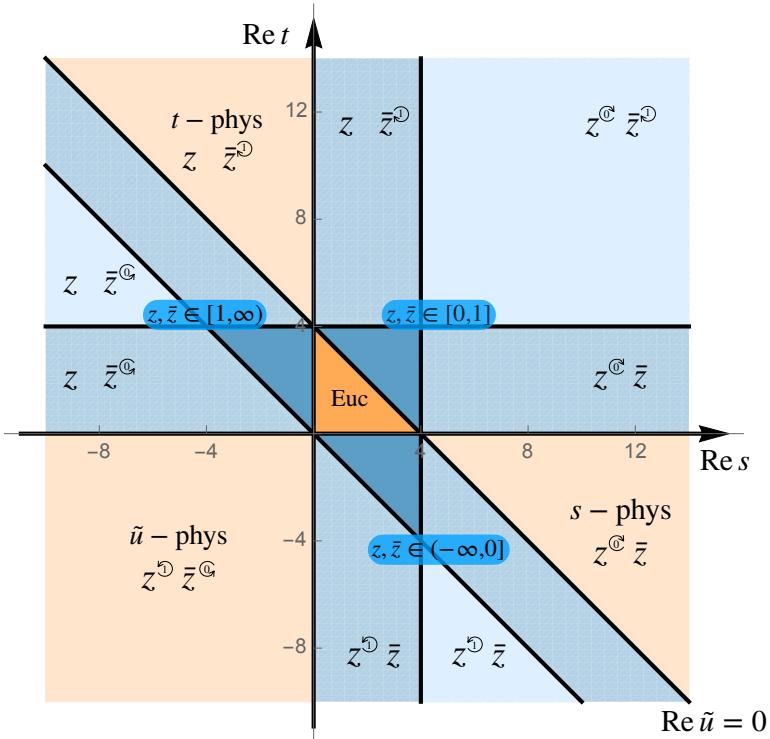
Figure 3.19. Analytic continuation of cross ratios on the real $s - t$ plane. The orange triangle is the Euclidean region and where all analytic continuations start from. The larger triangle (including the Euclidean region) is the region where u and v stay in their principal branch. It is also the so-called Mandelstam triangle where all Mandelstam variables are below their two-particle threshold. The lighter orange regions correspond to $s/t/\tilde{u}$-physical region, respectively. All the blue regions are Lorentzian regions where z and $\bar{z}$ are real and independent, and lie within the indicated intervals. The round arrows (notice the different directions) indicate how the cross ratios $z, \bar{z}$ should be analytically continued through the $(-\infty, 0]$ or $[1, \infty)$ branch cut in the complex plane. In unlabelled regions $z, \bar{z}$ stay in the principal branch.

So far we have focused on s-channel physics, with operators 1 and 2 moved to an 'in' configuration and particles 3 and 4 to an 'out' configuration. Of course we could have continued the positions differently in order to reach the physical regions of the

t and the u channel which would involve different analytic continuations of the cross ratios. We can also consider the 'Euclidean' configuration where all Mandelstam invariants lie between 0 and $4m^2$ – in this configuration $\sqrt{u}$ and $\sqrt{v}$ are both real and positive, and the ρ variable does not need to be analytically continued around zero. Figure 3.19 shows the various continuations that are necessary to reach these regions.[27] For each of the physical regions the indicated continuation lands us above the cut in the corresponding Mandelstam variable.

3.A.1 Different kinematic limits

To gain a bit more insight we will now explore various kinematic limits and relate each of them between Mandelstam invariants s, t and cross ratios z, $\bar{z}$. The limits under consideration are a double lightcone limit and five $s \to \infty$ limits:

$$
\left\{
\begin{array}{l}
\text{double lightcone limit: } z \to 0, \ \bar{z} \to 1 \\[4pt]
s \to \infty :
\left\{
\begin{array}{l}
\theta \text{ fixed}
\left\{
\begin{array}{l}
\cos(\theta) > 1 \\
0 < \cos(\theta) < 1 \,(\text{bulk-point limit})
\end{array}
\right. \\[10pt]
\begin{array}{c} t \text{ fixed} \\ {\scriptstyle (\text{Regge limit})} \end{array}
\left\{
\begin{array}{l}
t > 0 \\
t = 0 \,(\text{forward limit}) \\
t < 0
\end{array}
\right.
\end{array}
\right.
\end{array}
\right.
\tag{3.A.8}
$$

where we recall that

$$
t = \frac{1}{2}(4m^2 - s)(1 - \cos(\theta)).
\tag{3.A.9}
$$

In the Mandelstam s and t plane these different limits are shown in figure 3.20 and in the complex z and $\bar{z}$ plane they are shown in figure 3.21. Note that the starting point for each limit always lies inside the Euclidean region and the endpoints of the limits are always outside. The $i\epsilon$ prescription we adopted for these continuations is as follows: if the endpoint of s/t is greater than 4, then keep $\text{Im}\,(s/t)$ *non-negative*; if the endpoint of s/t is smaller than 0, then keep $\text{Im}\,(s/t)$ *non-positive*; otherwise the continuation can be arbitrary.

Let us offer a few comments on these limits. First of all, we find that the double lightcone limit where $z \to 0$ and $\bar{z} \to 1$ corresponds to $s \to 4m^2$ and $t \to 4m^2$. (We are not too concerned about the precise order in which these limits are taken here.) At this point the two lightcones in the position space correlation function intersect,

---

[27]Note that the continuations of $z, \bar{z}$ are somewhat arbitrary because those of Mandelstam variables only depend on products of $z, \bar{z}$ (for example see (3.2.30)). In addition, the symmetry $z \leftrightarrow \bar{z}$ adds even more arbitrariness. In particular, to reach a given point on $s - t$ plane, a phase rotation in $z(\bar{z})$ can be traded with one in $\bar{z}(z)$ provided the phases are the same. Therefore, depending on different conventions the reader may find different continuation prescriptions for $z, \bar{z}$, but the one for u, v should have no ambiguity.
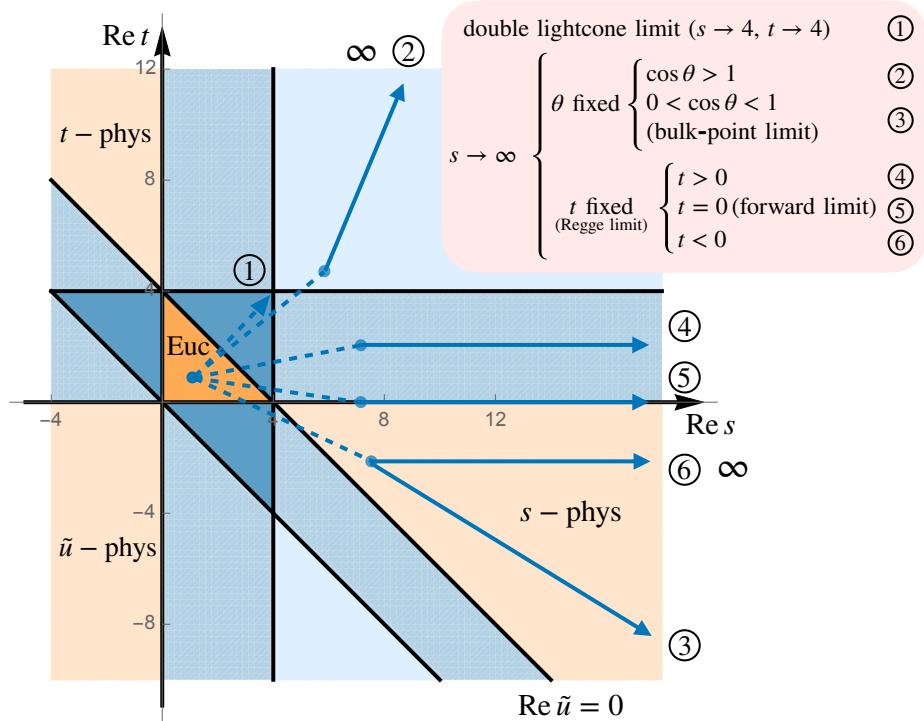
Figure 3.20. Different kinematic limits in real $s-t$ plane. The dark blue dashed lines indicate analytic continuation of s, t into their complex planes, respectively. Details of analytic continuation are explained in the text. The dark blue arrows lie on the real $s-t$ plane. The orange triangle is the Euclidean region, and within it lies the starting point of all limits and their corresponding analytic continuation.

and similarly the s-channel and t-channel cuts intersect in the amplitude. In both cases the region *beyond* this point is a bit mysterious. For example, as shown in figure 3.21, limit ② requires an analytic continuation of z around 0 and $\bar{z}$ around 1, and so we are beyond the radius of convergence of any conformal block decomposition. It would be interesting to see if some theory can be developed in order to better understand this region.

Secondly let us consider the fixed angle high-energy limit ③. In cross ratio space this corresponds to the familiar bulk point limit. This is known to be the region in cross ratio space where the flat-space scattering amplitude can be obtained from the conformal correlation function in the case of *massless* external particles, which is of course important in the context of AdS/CFT. In our case we recover this limit at high energies where in some approximate sense the masses of the external particles no longer matter. We have however not checked in detail that the bulk point limit prescription is exactly reproduced here.

Lastly there are the various Regge limits[28] ④, ⑤ and ⑥ which correspond to

---

[28]Note that here we discuss the Regge limits in the s-channel, as opposed to t-channel one in
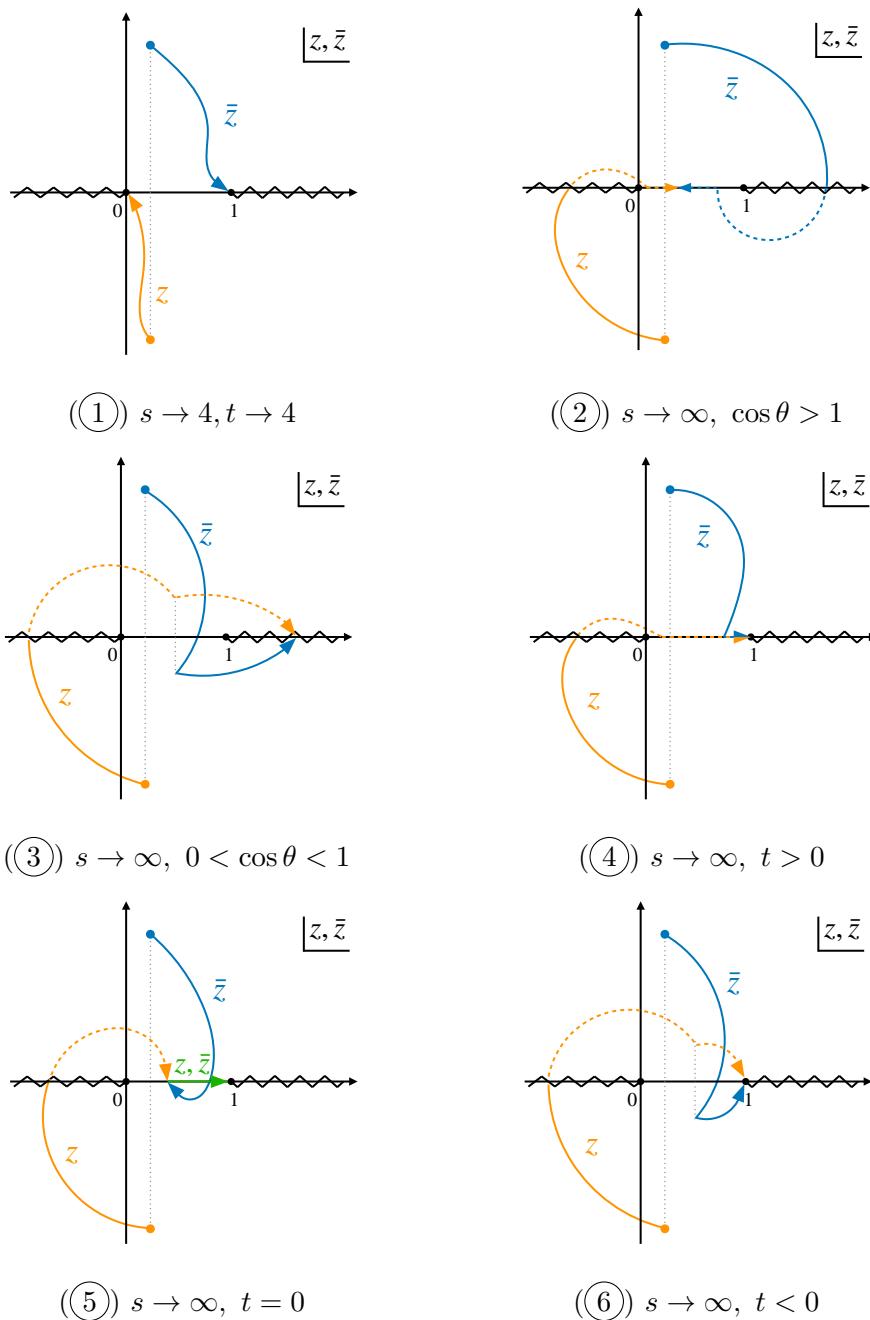
Figure 3.21. Different kinematic limits in z, $\bar{z}$. The dashed curves indicate that the cross ratios are in the second sheet. The grey dotted lines indicate that z and $\bar{z}$ are complex conjugate of each other.

---

section 3.2.5. The two limits are simply related by $s \leftrightarrow t, u \leftrightarrow v$.

large s and fixed t. In plot $\textcircled{4}$, z and $\bar{z}$ approach 1 in a way such that

$$\frac{1-z}{1-\bar{z}} \overset{s\to\infty}{=\!=} \left(\frac{\sqrt{t}+2}{\sqrt{t}-2}\right)^2. \tag{3.A.10}$$

In plot $\textcircled{5}$, $z = \bar{z}$ when approaching 1, whereas in plot $\textcircled{6}$, z and $\bar{z}$ are complex conjugate of each other up to a phase $e^{2\pi i}$.

As discussed in the main text, these limits exactly correspond to the Regge limit of conformal correlation functions. In this case only the z variable is continued around 0 and so we are at the boundary of the radius of convergence of the s channel conformal block decomposition.

3.B Steepest descent contours for the exchange diagram in Mellin space

In this appendix we analyse the location of the steepest descent contour for the exchange diagram in Mellin space and determine the contribution of any Mellin poles that are picked up in deforming the original integration contour to the steepest descent contour.

First we have to decide which poles are picked up. This is determined by the crossing point of the steepest descent contour with the real axis. With the integrand as in (3.5.26) the saddle point is located at

$$\sigma_{12}^* = \frac{4m^2 - s}{8m} \tag{3.B.1}$$

and at this point

$$\phi\left(m, \frac{4m^2 + s}{4m^2 - s}, \sigma_{12}^*\right) = -2m \log\left(\frac{8m}{4m^2 + s}\right) \tag{3.B.2}$$

so we see that

$$\text{Im}\left[\phi\left(m, \frac{4m^2 + s}{4m^2 - s}, \sigma_{12}^*\right)\right] = 2m \arg\left(4m^2 + s\right) \tag{3.B.3}$$

so the real σ_{12} axis is crossed at

$$\bar{\sigma}_{12}(s) := \frac{m \arg[4m^2 + s]}{\arg[4m^2 + s] - \arg[4m^2 - s]} \tag{3.B.4}$$

where we used that the steepest descent contour crossed the real axis for $0 < \sigma_{12} < m$ as explained above. (As a consistency check we recover σ_{12}^* from $\bar{\sigma}_{12}(s)$ for s real and

Euclidean via a limiting procedure.) We pick up Mellin poles if:

$$\bar{\sigma}_{12}(s) < m - m_b/2\,. \tag{3.B.5}$$

This gives rise to a region in the complex s plane that is shown as the lightly shaded region in figure 3.17. Notice that it in particular includes the entire physical line $s > 4m^2$ and the pole at $s = m_b^2$. A little further experimentation shows that we do not pick up any Mellin poles for $\text{Re}(s) < 0$ as long as $m_b > m$, and also that for fixed $\text{Re}(s) > 0$ the function $\bar{\sigma}_{12}(s)$ is increasing with $|\text{Im}(s)|$, so if we do not pick up poles for a given s with $\text{Re}(s) > 0$ then we will also not pick up poles for any s with greater imaginary part. Altogether this means that the region where we pick up poles is within the region defined by $\text{Re}(s) > 4m(m_b - m)$ for $m_b > m$.

The picked up Mellin poles give rise to a sum which we should compare to the order of magnitude of the Mellin saddle point at σ_{12}^*. In equations, we can say that we are safe if

$$\sum_{k=0}^{\bar{k}(s)} R_k \exp\left(R\,\phi\left(m, \frac{4m^2 + s}{4m^2 - s}, m - m_b/2 - k/R\right) - R\,\phi\left(m, \frac{4m^2 + s}{4m^2 - s}, \sigma_{12}^*\right)\right) \xrightarrow{R\to\infty} 0 \tag{3.B.6}$$

with $\bar{k}(s) = R(m - m_b/2 - \bar{\sigma}_{12}(s))$. We will henceforth assume $\bar{k}(s) > 0$ otherwise there is nothing to estimate. To analyse the k sum we will ignore the phase factor and instead investigate the slightly larger expression

$$\sum_{k=0}^{\bar{k}(s)} R_k \exp\left(R\,\phi\left(m, \frac{|4m^2 + s|}{|4m^2 - s|}, m - m_b/2 - k/R\right) - R\,\phi\left(m, \frac{4m^2 + s}{4m^2 - s}, \sigma_{12}^*\right)\right) \xrightarrow{R\to\infty} 0\,. \tag{3.B.7}$$

We now substitute the large R expression for the R_k and can attempt to find a saddle point approximation for the sum. Notice that the location of the saddle point has changed compared to the discussion around equation (3.5.24) because of the extra k-dependent factor. We find two stationary points at

$$k_\pm^*(s)/R = \frac{m_b}{8}\left(-4 \pm \frac{|4m^2 + s|}{m\sqrt{\text{Re}(s)}}\right) \tag{3.B.8}$$

If $\text{Re}(s) > 0$ then exactly one of the saddle points is real and positive. The value of the summand at the saddle point is

$$\exp\left(R\,(2m + m_b)\left(\log(2m + m_b) - \frac{1}{2}\log\left(|4m^2 + s| + 4m\sqrt{\text{Re}(s)}\right)\right)\right.$$
$$\left. + R\,(2m - m_b)\left(\log(2m - m_b) - \frac{1}{2}\log\left(|4m^2 + s| - 4m\sqrt{\text{Re}(s)}\right)\right)\right) \tag{3.B.9}$$

up to an unimportant prefactor.

We can now distinguish several possibilities:

- If $0 < \bar{k}(s)$ but $\text{Re}(s) < 0$ then the stationary points in the sum are complex. We checked numerically that the summand is monotonically increasing and so it is bounded from above by its value at $\bar{k}(s)$. This can only happen when $m_b < m$.

- If $\text{Re}(s) > 0$ and $0 < k_+^*(s) < \bar{k}(s)$ then the saddle point approximation should work well for the sum.

- If $\text{Re}(s) > 0$ and $0 < \bar{k}(s) < k_+^*(s)$ then we can again take the value at $\bar{k}(s)$ as an upper bound for the sum.

Each of these cases corresponds to a domain in the complex s plane (which all lie within region I as defined around figure 3.17 because we assume $\bar{k}(s) > 0$). We have numerically checked that the summand in (3.B.7) in the first and third possibility always goes to zero in the large R limit, so the problematic region is the subregion of the second possibility where (3.B.9) does not vanish at large R. This is now easily plotted numerically, leading to the domains shaded in figure 3.17.

3.C   Verification of momentum conserving delta function

In this appendix we show that in the flat-space limit, the normalized, analytically continued four-point contact diagram $G_c(P_i)$ equals the momentum conserving delta function,

$$Z^2 G_c(P_i)|_{\text{S-matrix}} \xrightarrow{R \to \infty} i(2\pi)^{d+1} \delta^{(d+1)}(k_1 + k_2 + k_3 + k_4), \qquad (3.C.1)$$

where the normalization factor is defined in (3.2.8):

$$Z = \frac{2^{2\Delta} R^{d-1}}{\mathcal{C}_\Delta^2}. \qquad (3.C.2)$$

Our starting point is (3.3.32), which is reproduced here:

$$G_c(P_i) \xrightarrow{R \to \infty} R^{-d+3} 2^{2\Delta - d/2 - 6} \pi^{-3d/2 + 1/2} \Delta^{3d/2 - 9/2} \frac{\left(\sqrt{P_{12}P_{34}} + \sqrt{P_{13}P_{24}} + \sqrt{P_{14}P_{23}}\right)^{-2\Delta + 3/2}}{(P_{12}P_{13}P_{14}P_{23}P_{24}P_{34})^{1/4}}. \qquad (3.C.3)$$

In Euclidean signature the P_{ij} are all real and positive and so the amplitude in the large Δ limit gets support only around $P_{ij} = 0$. This changes if we analytically continue to the S-matrix configuration (3.2.18) as our conjecture dictates. Consider again the case where particles 1 and 2 are the 'in' particles and 3 and 4 the 'out'

particles. We are then instructed to take P_{12} and P_{34} negative with a small negative imaginary part. We may write:

$$G_c(P_{ij})|_{\text{S-matrix}} \overset{\text{R}\to\infty}{\longrightarrow} iR^{-d+3}2^{2\Delta-d/2-6}\pi^{-3d/2+1/2}\Delta^{3d/2-9/2} \frac{(f(P_{ij}))^{-2\Delta+3/2}}{(P_{12}P_{13}P_{14}P_{23}P_{24}P_{34})^{1/4}}\bigg|_{\text{S-matrix}} \tag{3.C.4}$$

where we have introduced

$$f(P_{ij}) := -\sqrt{P_{12}P_{34}} + \sqrt{P_{13}P_{24}} + \sqrt{P_{14}P_{23}}. \tag{3.C.5}$$

Our first benefit is the factor of i, which matches (3.2.19). Taking into account the wave function factors $\sqrt{Z}$ we realize that the large Δ limit of the normalized contact diagram should, after substitution of $P_{ij} = 2(1+m^{-2}k_i \cdot \eta \cdot k_j)$, become equal to the momentum conserving delta function:

$$\lim_{R\to\infty} iZ^2 R^{-d+3}2^{2\Delta-d/2-6}\pi^{-3d/2+1/2}\Delta^{3d/2-9/2}\frac{(f(P_{ij}))^{-2\Delta+3/2}}{(P_{12}P_{13}P_{14}P_{23}P_{24}P_{34})^{1/4}}$$
$$\overset{?}{=} i(2\pi)^{d+1}\delta^{(d+1)}(k_1 + k_2 + k_3 + k_4) \tag{3.C.6}$$

A complication in the verification of this claim is that both sides are meant to be understood as functions of *on-shell* momenta, so the independent variables on either side are really the spatial components $\underline{k}_i$ of the four momenta.

Our first claim is that the contact diagram is maximized on the support of the delta function. At large Δ it is the function $f(P_{ij})$ that provides exponential damping and it is maximized whenever

$$\frac{\partial \log(f(P_{ij}))}{\partial \underline{k}_3^i} = \frac{\partial \log(f(P_{ij}))}{\partial \underline{k}_4^i} = 0 \tag{3.C.7}$$

which is solved on the momentum conserving configuration. More generally the form of $f(P_{ij})$ leads us to believe that there should be a Minkowskian version of Ptolemy's inequality that rigorously proves the maximization of $f(P_{ij})$ uniquely and exactly when momentum conservation is obeyed, but we have not tried to obtain it. At the saddle point we easily find that

$$f(P_{ij})|_{\text{saddle point}} = 8, \tag{3.C.8}$$

independently of the values of the momenta themselves.

Next we need to check the volume of the bump centred at the momentum conserving configuration, so whether the integrations over both sides of (3.3.33) agree.

To integrate, we parametrize P_i, or equivalently k_i^μ, using rapidity and spherical coordinates:

$$P_i = (1, \mp \cosh(\theta_i), i \sinh(\theta_i)\hat{n}_i^{(d)}) \qquad -/+ : \text{in/out-going}$$
$$k_i^\mu = (\pm m \cosh(\theta_i), m \sinh(\theta_i)\hat{n}_i^{(d)}) \qquad +/- : \text{in/out-going} \qquad (3.\text{C}.9)$$
$$\hat{n}_i^{(d)} = (\cos(\phi_{i,1}), \sin(\phi_{i,1})\,\hat{n}_i^{(d-1)})$$

Integrating over the right-hand side of (3.3.33) gives

$$\int d|\underline{k}_3||\underline{k}_3|^{d-1} d^d\underline{k}_4 \left[i(2\pi)^{d+1}\delta^{(d+1)}(k_1 + k_2 + k_3 + k_4) \right]$$
$$= i(2\pi)^{d+1}\left(\frac{E_{CM}^2}{4} - m^2\right)^{d/2-1}\frac{E_{CM}}{4} \qquad (3.\text{C}.10)$$
$$= i(2\pi)^{d+1}\frac{m^{d-1}}{2}\cosh(\theta_1)\sinh^{d-2}(\theta_1).$$

This function of θ_1 needs to be matched on the left-hand side. To perform the integrals we again resort to the saddle point approximation. Going to the centre of mass frame of ingoing particles 1 and 2, the momentum-conserving saddle point now reads

$$\theta_3^* = \theta_4^* = \theta_1, \qquad \hat{n}_4^{(d)*} = -\hat{n}_3^{(d)}. \qquad (3.\text{C}.11)$$

We also need to calculate the determinant of the matrix of second-order derivatives of $\log(f(P_{ij}))$. Let us denote this as Det_d for the d-dimensional case. It turns out that using our coordinates the determinant at the saddle point can be easily calculated for any dimension. To be precise, we set the ordering of the coordinates as

$$\{\theta_3, \theta_4, \phi_{4,1}, \ldots, \phi_{4,d-1}\} \qquad (3.\text{C}.12)$$

and then the result reads

$$\left.\frac{\text{Det}_d}{\text{Det}_2}\right|_{\text{saddle point}} = \left(\frac{\sinh^2(\theta_1)}{8}\right)^{d-2}\sin^{2d-4}(\phi_{3,1})\sin^{2d-6}(\phi_{3,2})\ldots\sin^2(\phi_{3,d-2}) \qquad (3.\text{C}.13)$$

where Det_2 satisfies

$$\left.\sqrt{\frac{1}{\text{Det}_2}}\frac{(f(P_{ij}))^{3/2}}{(P_{12}P_{13}P_{14}P_{23}P_{24}P_{34})^{1/4}}\right|_{\text{saddle point}} = \frac{32}{\cosh(\theta_1)\sinh^2(\theta_1)}. \qquad (3.\text{C}.14)$$

The simplicity of this calculation follows from the fact that additional matrix elements in higher dimensional cases compared to the two-dimensional case are all

zeros except for the diagonal terms. To check this, we need to calculate

$$
\begin{aligned}
&\frac{\partial^2 \log(f(P_{ij}))}{\partial \theta_k \partial \phi_{4,l}}, && k = 3, 4, \quad 2 \le l \le d-1 \\
&\frac{\partial^2 \log(f(P_{ij}))}{\partial \phi_{4,l} \partial \phi_{4,m}}, && 1 \le l \le m \le d-1
\end{aligned}
\tag{3.C.15}
$$

A useful observation is that when $l \ge 2$, $\partial f(P_{ij})/\partial \phi_{4,l}$ is only proportional to $\partial P_{34}/\partial \phi_{4,l}$ and it vanishes at the saddle point. Explicitly, we have

$$
P_{34} = 2(1 - \cosh(\theta_3)\cosh(\theta_4) + \sinh(\theta_3)\sinh(\theta_4)\hat{n}_3 \cdot \hat{n}_4)
\tag{3.C.16}
$$

$$
\frac{\partial P_{34}}{\partial \phi_{4,l}}\bigg|_{\text{saddle point}} = 2\sinh(\theta_3)\sinh(\theta_4)\frac{\partial\left(\hat{n}_3^{(d)} \cdot \hat{n}_4^{(d)}\right)}{\partial \phi_{4,l}}\bigg|_{\text{saddle point}} = 0
\tag{3.C.17}
$$

where the last equal sign is because at the saddle point $\partial \hat{n}_3^{(d)}/\partial \phi_{4,l}$ is orthogonal to $\hat{n}_4^{(d)}$ and vice versa. It follows similarly that all the second-order partial derivatives in (3.C.15) are zero due to orthogonality, except for one term, which is

$$
\frac{\partial^2 f(P_{34})}{\partial \phi_{4,l}^2}\bigg|_{\text{saddle point}} = 2\sinh^2(\theta_1)\sin(\phi_{3,1})^2 \ldots \sin(\phi_{3,l-1})^2 .
\tag{3.C.18}
$$

Altogether we find that the integral over the left-hand side becomes[29]

$$
\begin{aligned}
\int d|\underline{k}_3| &|\underline{k}_3|^{d-1} d^d \underline{k}_4 \left[iZ^2 R^{-d+3} 2^{2\Delta - d/2 - 6} \pi^{-3d/2+1/2} \Delta^{3d/2-9/2} \frac{(f(P_{ij}))^{-2\Delta+3/2}}{(P_{12}P_{13}P_{14}P_{23}P_{24}P_{34})^{1/4}} \right] \\
&\simeq iZ^2 R^{-d+3} 2^{2\Delta-d/2-6} \pi^{-3d/2+1/2} \Delta^{3d/2-9/2} (m\cosh(\theta_1))^2 (m\sinh(\theta_1))^{2d-2} \\
&\quad \times \left(\frac{\pi}{\Delta}\right)^{(d+1)/2} \left(\frac{\sinh^2(\theta_1)}{8}\right)^{-(d-2)/2} \frac{8^{-2\Delta+5/3}}{\cosh(\theta_1)\sinh^2(\theta_1)} \\
&\overset{R\to\infty}{=} i(2\pi)^{d+1} \frac{m^{d-1}}{2} \cosh(\theta_1) \sinh^{d-2}(\theta_1)
\end{aligned}
\tag{3.C.19}
$$

which exactly agrees with (3.C.10). We have therefore shown that our S-matrix conjecture is also correct for the four-point contact Witten diagram of identical operators in any spacetime dimension.

---

[29]The product of sine functions in (3.C.13) precisely cancels against the spherical integration measure of $\hat{n}_4^{(d)}$.

3.D Saddle-point analysis of the exchange diagram

In this appendix, we explain details of the saddle-point computation of the exchange diagram discussed in subsection 3.3.3. For this purpose, we first integrate out X, Y and Q in (3.3.35) to get

$$G_e(P_i) = \frac{R^{-d+5}}{32\pi^h (P_{12})^\Delta (P_{34})^\Delta} \int_{-i\infty}^{i\infty} \frac{dc}{2\pi i} \frac{1}{c^2 - (\Delta_b - h)^2} \left(\frac{\Gamma\left(\Delta - \frac{h}{2} + \frac{c}{2}\right) \Gamma\left(\Delta - \frac{h}{2} - \frac{c}{2}\right)}{2\pi^h (\Gamma(\Delta - h + 1))^2} \right)^2$$

$$\times \left[\mathsf{k}_c G_{h+c,0}(\rho, \bar\rho) + \mathsf{k}_{-c} G_{h-c,0}(\rho, \bar\rho) \right] , \qquad (3.D.1)$$

where $G_{\Delta,l}$ is the conformal block and k_a is defined by

$$\mathsf{k}_a := \frac{\left(\Gamma(\frac{h}{2} + \frac{a}{2}) \right)^4}{\Gamma(h+c)\Gamma(c)} . \qquad (3.D.2)$$

In the flat-space limit $(\Delta \sim c \gg 1)$, (3.D.1) can be approximated by

$$G_e(P_i) \sim \frac{R^{-d+5}}{32\pi^h (P_{12})^\Delta (P_{34})^\Delta} \int_{-i\infty}^{i\infty} \frac{dc}{2\pi i} \frac{\mathcal{N}}{c^2 - \Delta_b^2} \left(c^{h-1} e^{g(c)} + (-c)^{h-1} e^{g(-c)} \right) , \quad (3.D.3)$$

with

$$\mathcal{N} = \frac{2\pi^{1-2h} \Delta^{4h-2} (\rho\bar\rho)^{h/2}}{\sqrt{(1-\rho^2)(1-\bar\rho^2)} (\Delta^2 - \frac{c^2}{4})^{h+1} (1 - \rho\bar\rho)^{h-1}} ,$$

$$g(x) = -4\Delta \log(\Delta) + 2(\Delta + \tfrac{x}{2}) \log(\Delta + \tfrac{x}{2}) + 2(\Delta - \tfrac{x}{2}) \log(\Delta - \tfrac{x}{2}) + \frac{x}{2} \log \rho\bar\rho ,$$
$$(3.D.4)$$

where ρ and $\bar\rho$ are the radial coordinates. We can then perform the saddle-point analysis for the c-integral. The two exponential factors $e^{g(c)}$ and $e^{g(-c)}$ give two different saddle points but their contributions turn out to be identical. Including the one-loop fluctuations around the saddle-point we get the result quoted in the main text

$$G_c(P_i) \sim G_c(P_i)|_{R\to\infty} \times \frac{R^2}{\Delta_b^2 - c^2} . \qquad (3.D.5)$$

On the other hand, the contributions from the poles can be determined by evaluating $e^{g(c)}$ and $e^{g(-c)}$ at the positions of the poles $c = \pm\Delta_b$. For the $c = \Delta_b$ pole, $e^{g(-c)}$ can be neglected and the dominant contribution at large R is given by a product of $e^{g(\Delta_b)}$ and $(P_{12}P_{34})^\Delta$. This leads to the formula (3.3.55) in the main text.

3.E Comparison with the phase shift formula

In reference [13], following a different derivation, a formula for the spin-ℓ phase shifts was proposed for the scattering of two identical particles which in our notation can

be written as

$$
e^{2i\delta_\ell(s)} = \lim_{\Delta_\mathcal{O}\to\infty} N_\ell(s)^{-1} \sum_{|\Delta-\sqrt{s}\Delta_\mathcal{O}|<\Delta_\mathcal{O}{}^\alpha} w(\Delta)^2 a_{\Delta,\ell} e^{i\pi(\Delta-2\Delta_\mathcal{O})} \,,
$$
$$
N_\ell(s) = \sum_{|\Delta-\sqrt{s}\Delta_\mathcal{O}|<\Delta_\mathcal{O}{}^\alpha} w(\Delta)^2 a_{\Delta,\ell} \,,
\tag{3.E.1}
$$

where the constraint on $\alpha > 0$ was not examined very carefully, other than it should be smaller than one. The explicit form of the weight $w(\Delta)$ will not be required here. It is sufficient to say that its dependence on Δ is such that $w(\Delta)^2 a_{\Delta,\ell}^{\mathrm{cont}}$ does not vary exponentially with Δ in the limit of large $\Delta_\mathcal{O}$. This implies that for the GFF theory we have

$$
N_\ell^{\mathrm{gff}}(s) \underset{\Delta_\mathcal{O}\to\infty}{=} \Delta_\mathcal{O}{}^\alpha \left[w(\Delta)^2 a_{\Delta,\ell}^{\mathrm{cont}} \right]\Big|_{\Delta=\sqrt{s}\Delta_\mathcal{O}}
\tag{3.E.2}
$$

Let us now assume that $N_\ell(s)$ is universal for CFTs which describe QFTs in AdS, and in particular equal to the GFF result above. This assumption was originally made in [13] in order to match the above phase shift formula with the prescription for the S-matrix based on the Mellin amplitude in that same reference, which is our equation (3.5.5). We now point out that using the result above this is nothing but the condition

$$
\sum_{|\Delta-\sqrt{s}\Delta_\mathcal{O}|<\Delta_\mathcal{O}{}^\alpha} \left(\frac{a_{\Delta,\ell}}{a_{\Delta,\ell}^{\mathrm{cont}}} \right) = \Delta_\mathcal{O}{}^\alpha
\tag{3.E.3}
$$

i.e. the same as our assumption (3.6.30). This also leads to

$$
e^{2i\delta_\ell(s)} = \lim_{\Delta_\mathcal{O}\to\infty} \Delta_\mathcal{O}{}^{-\alpha} \sum_{|\Delta-\sqrt{s}\Delta_\mathcal{O}|<\Delta_\mathcal{O}{}^\alpha} \left(\frac{a_{\Delta,\ell}}{a_{\Delta,\ell}^{\mathrm{cont}}} \right) e^{i\pi(\Delta-2\Delta_\mathcal{O})} \,.
\tag{3.E.4}
$$

Comparing this to our own expression (3.6.27) we see that they differ only in the way the averaging in the sum over states is being done: with a Gaussian in our case and with a rectangular "window" in the above. Both averaging kernels tend to delta functions in the large $\Delta_\mathcal{O}$ limit. As long as both limits exist they must describe the same limiting function. The main difference is that the Gaussian prescribes that the sum over states must be done over a precise region of width $O(\sqrt{\Delta})$, whereas the exact width of the averaging window was not as precisely determined in the above.

Chapter 4

Line and Surface Defects for the Free Scalar Field

4.1 Introduction and summary

Extended operators, also called *defects*, are useful objects in quantum field theories because they can probe non-local phenomena that are inaccessible to local operators. For a given field theory there are often infinitely many different defects and universal results are hard to come by. However, this situation improves if we focus on long distances where we recover the *conformal defects* which correspond to the (forced) symmetry breaking pattern

$$\mathfrak{so}(d+1,1) \quad \longrightarrow \quad \mathfrak{so}(p+1,1) \times \mathfrak{so}(d-p). \tag{4.1.1}$$

The rationale for this pattern is as follows. First, if we assume locality and reflection positivity then a d-dimensional infrared theory generally has $\mathfrak{so}(d+1,1)$ conformal invariance. If we now put the p-dimensional defect on an $\mathbb{R}^p$ subspace of $\mathbb{R}^d$ then we can assume that it preserves: (a) a p-dimensional Poincaré symmetry, (b) rotations in the transverse $d-p$ dimensions, and (c) an overall dilatation symmetry in the infrared. There are exceptions to (a) and (b), see for example [90] for the kinematics of defects charged under transverse rotations, but we will not consider this here. As for (c), a simple computation involving the bulk stress tensor shows that this scale invariance is enhanced to $\mathfrak{so}(p+1,1)$, so p-dimensional conformal invariance, if the defect does not contain a specific 'virial current' of dimension $p-1$, see for example [91]. In this precise sense the pattern in (4.1.1) is considered to be the generic situation at long distances.

In the following we will follow standard notation and introduce

$$q = d - p \tag{4.1.2}$$

as the co-dimension of the p-dimensional defect. In this work we will consider $q > 1$ and, since $p > 0$, $d > 2$ as well. The case $q = 1$ is analysed in [92].[1]

For the physics of the defect both sides of (4.1.1) are important. Away from the defect the $\mathfrak{so}(d+1,1)$ symmetry algebra acts on the local bulk operators and implies the existence of a convergent *bulk operator product expansion*. On the defect the local operators are organized in representations of $\mathfrak{so}(p+1,1) \times \mathfrak{so}(q)$, with the first factor acting as the usual conformal algebra in p dimensions and the latter as a usual global symmetry – although neither of these symmetries is generated by a local current on the defect. Furthermore, these defect local operators have their own convergent *defect operator product expansion*. The connection with the bulk operators is provided by the *bulk-defect operator expansion* which states that a local bulk operator in the vicinity of the defect can be written as a sum over defect operators. For example, for a scalar operator and a co-dimension two defect we can write:

$$\phi(\vec{x}, z, \bar{z}) = \sum_k \left(\frac{b_\phi^k \, \bar{z}^{s_k}}{|z|^{\Delta_\phi - \widehat{\Delta}_k + s_k}} \mathfrak{C}_{\widehat{\Delta}_k}[|z|, \vec{\nabla}^2] \widehat{\mathcal{O}}_{s_k}(\vec{x}) + \text{c.c.} \right) \qquad (4.1.3)$$

where we split the d-dimensional Euclidean coordinates as $x^\mu = (\vec{x}, \text{Re}(z), \text{Im}(z))$ with the latter two coordinates taken to be orthogonal to the defect. The index k labels the different primary defect operators $\widehat{\mathcal{O}}_{s_k}$, which in this case are all scalars and therefore labelled by their scaling dimensions $\widehat{\Delta}_k$ and $SO(2)$ spin s_k. The contribution of their descendants is taken into account by the (explicitly known [94]) differential operator $\mathfrak{C}_{\widehat{\Delta}_k}[|z|, \vec{\nabla}^2]$. The expansion also furnishes the bulk-defect operator expansion coefficients b_ϕ^k.

For co-dimension two defects the following comment is in order. In equation (4.1.3) the spins s are integers if the bulk fields are to be single-valued around the defect. This is however not necessary. If the bulk theory has a global symmetry G then one might alternatively require that

$$\phi(\vec{x}, e^{2\pi i} z, e^{-2\pi i} \bar{z}) = \phi^g(\vec{x}, z), \text{ for } g \in G. \qquad (4.1.4)$$

For non-trivial g such defects are called *monodromy defects*. One may think of them as the boundaries of the co-dimension one defects that implement g. We will only consider $G = \mathbb{Z}_2$ and then there is a single type of monodromy defect corresponding to the non-trivial element of G. In the presence of such a defect the odd bulk operators have a bulk-defect expansion of the form given in equation (4.1.3) with half-integer s. For more general G, like the case studied in [95], the expansion would need further modifications.

The philosophy of the *defect bootstrap* is to explore the consistency conditions that follow from the associativity of the three operator expansions given above. In

---

[1]See also [93] for recent work on free scalars that interact through a boundary.

recent years there has been significant progress on this programme [96–106]. Just
as in the ordinary (bulk) conformal bootstrap, it is essential to know the relevant
conformal blocks which group the contributions of an entire conformal representation.
Pioneering work in this direction was done by [107, 108] in the case of co-dimension
1, whereas [94, 97, 109–113] contains results for higher co-dimensions.

Ideally the defect bootstrap would lead to a classification of all the possible
defects for a given bulk CFT. In the future it might for example be possible to
show that the monodromy defect is the only non-trivial line defect in the three-
dimensional Ising model, or that the known co-dimension two and four defects are
the only conformal defects in the six-dimensional $(2,0)$ theories. In this chapter we
consider a more modest problem: that of the classification of defects in the theory
of a single real free scalar. Our most important conclusion is that there is very
little scope for non-trivial conformal defects of co-dimension two and higher in such
theories. We consider this somewhat surprising: for example, we do not expect this
conclusion to hold for co-dimension one (boundaries). Indeed, for $d > 2$ several non-
trivial boundary conditions appear possible [92, 114–118] and for $d = 2$ there exists
a family of conformal boundary conditions for a free (compact) scalar [119]. Also,
non-trivial defects do exist in other cases where the bulk is free, like the non-trivial
co-dimension two monodromy defects for a free hypermultiplet in 4d with $\mathcal{N} = 2$
[120, 121] (see also [122, 123] for not necessarily conformal defects in this theory)
and the co-dimension four surface operators in the Abelian $(2,0)$ theory [124–130].
Another example are the infinity of possible boundary conditions in a free four-
dimensional Maxwell theory [131], see also [132–134], which of course also features
conformal Wilson and 't Hooft lines.

4.1.1 Summary

Although this work contains some more general results, our main outcome is that
most defects in the free scalar theory are 'trivial' in the sense that there is no room for
any interesting dynamics on the defect: up to potentially an undetermined one-point
function (for $q = p + 2$ only), all the n-point correlation functions of the bulk field
ϕ are completely fixed.[2] More precisely, we will show that, in a reflection positive
setup (also see Table 4.1):

- monodromy defects with $q = 2$ can be non-trivial only if $d \geq 4$;

- non-monodromy defects can be non-trivial only if $q = 3$ and if $d \geq 5$.

---

[2]More precisely, the connected two-point function of ϕ is simply the unique Klein-Gordon prop-
agator with boundary conditions on the defect defined as below, and the connected higher-point
functions of ϕ are all zero. This definition relies on the Gaussian properties of the bulk scalar
field theory, which are not spoiled by a trivial defect. In the literature the word 'trivial defect'
is often used to mean 'no defect'. This definition of 'trivial' agrees with ours only in the case of
non-monodromy defects without one-point functions.

Our reasoning proceeds as follows.

First, in section 4.2 we show that the equation of motion for two-point functions strongly constrains the bulk-defect operator expansion of the bulk field ϕ. We will discuss how, in all cases except the ones given above, this expansion is *completely fixed*. For example, for co-dimension two it must take the form

$$\phi(\vec{x}, z, \bar{z}) = \sum_s \left(b_\phi^{+,s} \, \bar{z}^s \mathfrak{C}_{\Delta_\phi + s}[|z|, \vec{\nabla}^2] \psi_s^{(+)}(\vec{x}) + \text{c.c.} \right) , \qquad (4.1.5)$$

for some operators $\psi_s^{(+)}$ with dimensions $\widehat{\Delta}_s^{(+)} = \Delta_\phi + s$ and transverse spins $s \geq 0$ constrained to be either half-integer or integer depending on the monodromy type of the defect. The coefficients $b_\phi^{+,s}$ are given below.

An expansion like equation (4.1.3) completely fixes the two-point function of the bulk field ϕ, but more work is required to also constrain the higher-point functions: we have to learn about the defect OPE of the operators $\psi_s^{(+)}$ themselves. This we do in sections 4.3 and 4.4, where we will demonstrate that the operators $\psi_s^{(+)}$ are generalized free fields and their n-point functions are given by a sum over Wick contractions. In more detail, in section 4.3 we analyse the singularities in the three-point function of one free bulk and two defect operators. Requiring the absence of unphysical singularities implies that the defect OPE of two $\psi_s^{(+)}$ operators can only contain non-trivial operators of the 'double twist' type. This analysis however cannot fix the OPE coefficients nor the multi-OPEs of the $\psi_s^{(+)}$ operators. To finish the proof we therefore need one more ingredient and this is provided in section 4.4: we can use a dispersion relation in the complex time plane for the n-point functions of the $\psi_s^{(+)}$ operators. Since the discontinuities in this dispersion relation are trivial the n-point functions must be trivial as well, and so our claim of the triviality of the n-point functions of the bulk field ϕ also follows.

In section 4.5 we will specialize to the case of line defects. Although the derivation is *grosso modo* the same, some subtleties arise because the analyticity properties of conformal correlation functions on a line are different. However if we assume parity on the defect then our conclusions remain the same. This in particular rules out a non-trivial parity-preserving monodromy defect for a real scalar in $d = 3$, in sharp contrast with the non-trivial supersymmetric monodromy defects in $d = 4$.

Section 4.6 is devoted to perturbative tests of our results. We consider examples in conformal perturbation theory that could lead to a non-trivial defect for the free scalar theory and therefore a counterexample to our main claim. As expected these attempts fail, but they do so in a rather interesting manner.

Some applications of our results will be discussed in section 4.7.

4.2 The two-point function of the free scalar

In this section we will analyse the spectrum of operators appearing in the bulk-defect operator expansion (4.1.3) for a free scalar field ϕ. To do so it suffices to look at two-point functions involving one bulk field ϕ and a defect operator $\widehat{\mathcal{O}}$. By imposing the equation of motion $\Box\phi = 0$ (away from contact points), we will find that the spectrum in the bulk-defect operator expansion is highly constrained. We will then consider the two-point function of ϕ to fix almost all the coefficients. In the main text we will focus on $q = 2$ for simplicity of notation. The case with $q > 2$ is discussed in appendix 4.A.

This section is mostly a review of results that have already appeared in the literature. The defect blocks for the scalar two-point function in the presence of the twist defect were first presented in [97]. For generic p, q defects, the blocks for the scalar two-point functions were computed in [94] (see also [110, 112]). The constraints imposed by the bulk equation of motion and by unitarity on the bulk-defect expansion of a free scalar were first discussed in [135] (see also [97]) for the case of the twist defect. This analysis was extended to generic p and q in Appendix B of [94], and the equation "$s \leq (4-q)/2$" of that reference is a less refined version of the information presented in the two tables below. For $q = 1$, the blocks for the scalar two-point function were obtained in [107] while the spectrum of boundary modes of the free scalar was discussed in [96, 98, 136, 137].

4.2.1 General form of the two-point functions

In this section we consider the two-point function of a general scalar bulk primary ϕ and a defect primary operator $\widehat{\mathcal{O}}$. For a defect operator with transverse spin s and scaling dimension $\widehat{\Delta}_{\widehat{\mathcal{O}}}$ one finds that[3]

$$\langle \phi(\vec{x}, z, \bar{z})\widehat{\mathcal{O}}_{-s}(0)\rangle = \frac{b_\phi^{\widehat{\mathcal{O}}}\, \bar{z}^s}{|z|^{\Delta_\phi - \widehat{\Delta}_{\widehat{\mathcal{O}}} + s}(|z|^2 + |\vec{x}|^2)^{\widehat{\Delta}_{\widehat{\mathcal{O}}}}}. \tag{4.2.1}$$

where we used the same conventions for parallel and transverse coordinates as listed in the introduction. Recall that in CFTs without defects the functional form of three-point functions efficiently encapsulates the contribution of descendants in the bulk OPE. In the defect setup the two-point function in equation (4.2.1) similarly encodes the contribution of descendants in the bulk-defect operator expansion. This is analysed in appendix 4.A; the corresponding infinite-order differential operator is given in equation (4.A.4).

---

[3]See [94, 97, 109–113] for recent work on kinematical constraints for defect CFTs and also [96, 107, 108] for previous studies in the co-dimension one case.

Next we consider the two-point functions of two general bulk scalar operators ϕ,

$$\langle \phi(\vec{x}_1, z_1, \bar{z}_1) \phi(\vec{x}_2, z_2, \bar{z}_2) \rangle. \tag{4.2.2}$$

This correlation function depends non-trivially on two cross-ratios, which we can take to be:

$$\chi \equiv \frac{|\vec{x}_{12}|^2 + |z_1|^2 + |z_2|^2}{|z_1||z_2|}, \quad \varphi = \arg\left(\frac{z_1}{z_2}\right). \tag{4.2.3}$$

In the following we will need the *defect channel decomposition* of this two-point function which is obtained by plugging in the bulk-defect operator expansion twice. This leads to two infinite-order differential operators of the form given in equation (4.A.4) acting on the two-point function of a defect primary. In appendix 4.C we resum these contributions from the defect descendants and obtain the *defect channel decomposition*:

$$\langle \phi(\vec{x}_1, z_1, \bar{z}_1) \phi(\vec{x}_2, z_2, \bar{z}_2) \rangle = \frac{1}{(|z_1||z_2|)^{\Delta_\phi}} \sum_s \sum_{\widehat{\mathcal{O}}} |b_\phi^{\widehat{\mathcal{O}}}|^2 \, e^{-i\,s\,\varphi} \mathcal{F}_{\widehat{\Delta}_{\widehat{\mathcal{O}}}}(\chi). \tag{4.2.4}$$

where we introduced the *defect conformal blocks* as:

$$\mathcal{F}_{\widehat{\Delta}_{\widehat{\mathcal{O}}}}(\chi) = \chi^{-\widehat{\Delta}_{\widehat{\mathcal{O}}}} {}_2F_1\left(\frac{\widehat{\Delta}_{\widehat{\mathcal{O}}}}{2}, \frac{\widehat{\Delta}_{\widehat{\mathcal{O}}}+1}{2}; \widehat{\Delta}_{\widehat{\mathcal{O}}} + 1 - \frac{p}{2}; \frac{4}{\chi^2}\right). \tag{4.2.5}$$

We remark that these functions can also be computed by solving certain Casimir equations with appropriate boundary conditions [94, 97, 110, 112]. One could also consider a *bulk channel decomposition* of the same two-point function in terms of a sum over bulk one-point functions. We will not need this decomposition in our analysis.

4.2.2 Two-point functions of the free scalar

We now specialise to the case where ϕ is a free bulk scalar of canonical dimension $\Delta_\phi = \frac{d}{2} - 1$ and therefore obeys $\Box \phi = 0$ away from contact points.

For the bulk-defect two-point function given in (4.2.1) the action of the Laplacian gives

$$0 = \langle \Box \phi(\vec{x}, z, \bar{z}) \widehat{\mathcal{O}}_{-s}(0) \rangle \sim (\widehat{\Delta}_{\widehat{\mathcal{O}}} - \Delta_\phi + |s|)(\widehat{\Delta}_{\widehat{\mathcal{O}}} - \Delta_\phi - |s|) \frac{b_\phi^{\widehat{\mathcal{O}}} \, \bar{z}^s}{|z|^{2+\Delta_\phi - \widehat{\Delta}_{\widehat{\mathcal{O}}} + s}(|z|^2 + |\vec{x}|^2)^{\widehat{\Delta}_{\widehat{\mathcal{O}}}}}. \tag{4.2.6}$$

Therefore, the only defect primaries allowed to appear in the bulk-to-defect OPE of a free scalar belong to one of the two families that we denote as $\psi_s^{(\mathfrak{p})}$ with $\mathfrak{p} = \pm$,

with dimensions $\widehat{\Delta}_s^{(\mathfrak{p})}$ given by:[4]

$$\psi_s^{(\pm)} \quad \widehat{\Delta}_s^{(\pm)} = \Delta_\phi \pm |s|. \tag{4.2.7}$$

We recall that we have set $q = 2$ and then have the spins $s \in \mathbb{Z}$ or $\mathbb{Z} + \frac{1}{2}$, depending on the choice for the $\mathbb{Z}_2$ monodromy, and $[\psi_s^{(\pm)}]^\dagger = \psi_{-s}^{(\pm)}$. As we explain in more detail in appendix 4.B, for $s = 0$ the two families merge and there is no degeneracy.

In reflection positive setups the spectrum is further constrained. The scaling dimensions $\widehat{\Delta}$ of any operator $\widehat{\mathcal{O}}$ on a p-dimensional defect need to obey the standard unitarity condition

$$\begin{aligned}
\widehat{\Delta} &\geq \frac{p}{2} - 1 \text{ or } \widehat{\Delta} = 0, && \text{if} \quad p > 2, \\
\widehat{\Delta} &\geq 0, && \text{if} \quad p \leq 2. \tag{4.2.8}
\end{aligned}$$

If the inequality for $p > 2$ is saturated then the operator is necessarily a free field and its correlators must obey $\Box\widehat{\mathcal{O}} = 0$. If $\widehat{\Delta} = 0$ for any p then the operator is position-independent, $\partial\widehat{\mathcal{O}} = 0$. We will also assume cluster decomposition and then, by moving the position-independent operator far away, $\langle\widehat{\mathcal{O}}\ldots\rangle = \langle\widehat{\mathcal{O}}\rangle\langle\ldots\rangle$. The operator $\widehat{\mathcal{O}}$ therefore behaves as a multiple of the identity operator and in particular cannot be charged under transverse rotations.

For our operators $\psi_s^{(\pm)}$ these conditions happen to rule out almost all of the $\psi_s^{(-)}$ since their dimensions are $\frac{p}{2} - s$. In more detail, we first of all observe that the $\psi_s^{(-)}$ modes with $s > 1$ all sit below the unitarity bounds. For non-monodromy defects this leaves the $s = 1$ case but it also happens to always be disallowed: it would be below the unitarity bound for $p = 1$, a charged dimension zero operator for $p = 2$, and a free field for $p > 2$ for which the bulk-defect two-point function does not obey its equation of motion. For monodromy defects the condition $s \leq 1$ leaves the $\psi_{\pm\frac{1}{2}}^{(-)}$ operators and these are allowed for all $p > 1$ but not for $p = 1$ because then they would again correspond to a dimension zero operator.

The analysis of the previous paragraph is summarized in the $q = 2$ column of table 4.1. The other columns are obtained by repeating the analysis for higher co-dimensions, the detailed computations for which can be found in appendix 4.A. We note that the aforementioned $s = 0$ degeneracy is lifted if $q > 2$ and in that case the $\psi_0^{(-)}$ mode can become a defect identity operator precisely when $q = p + 2$, and also that free defect fields can never appear because the bulk-defect two-point function never obeys the Laplace equation. Below we will demonstrate that defects are necessarily trivial if none of the non-identity $\psi_s^{(-)}$ operators appears, and this leads directly to the main claim given in the introduction: interesting monodromy

---

[4]Note that $\widehat{\Delta}_s^{(+)} + \widehat{\Delta}_s^{(-)} = 2\Delta_\phi = d - 2 = p$ and in this sense the operators $\psi_s^{(+)}$ and $\psi_s^{(-)}$ on the p-dimensional defect are like a shadow pair.

defects can exists only for $p \geq 2$ and interesting non-monodromy defects only for $q = 3$ and $p \geq 2$.

$\mathbf{s \in \mathbb{Z} + \frac{1}{2}}$	$\mathbf{q = 2}$
$\mathbf{p = 1}$	$\psi_s^{(+)}$
$\mathbf{p \geq 2}$	$\psi_s^{(+)}$ and $\psi_{\pm 1/2}^{(-)}$

$\mathbf{s \in \mathbb{Z}}$	$\mathbf{q = 2}$	$\mathbf{q = 3}$	$\mathbf{q = 4}$	$\mathbf{q = 5}$	$\mathbf{q = 6}$
$\mathbf{p = 1}$		$\psi_s^{(+)}$ and $\mathbf{1}$	$\psi_s^{(+)}$		
$\mathbf{p = 2}$	$\psi_s^{(+)}$		$\psi_s^{(+)}$ and $\mathbf{1}$	$\psi_s^{(+)}$	
$\mathbf{p = 3}$		$\psi_s^{(+)}$ and $\psi_0^{(-)}$	$\psi_s^{(+)}$	$\psi_s^{(+)}$ and $\mathbf{1}$	$\psi_s^{(+)}$
$\mathbf{p = 4}$				$\psi_s^{(+)}$	$\psi_s^{(+)}$ and $\mathbf{1}$

Table 4.1. Table of unitary defect spectrum in the free theory: for monodromy defects with $q = 2$ and half-integer s on the top, and for general non-monodromy defects on the bottom. The pattern in the bottom table continues outside the shown range of p and q. For $q > 2$ the listed operators transform as symmetric traceless $SO(q)$ tensors and then s corresponds to its rank.

Before concluding this section, let us comment on the bulk-defect coefficients for the operators $\psi_s^{(\pm)}$. As discussed in [97] and reviewed in appendix 4.B, in order to reproduce the contact term in the Klein-Gordon equation,

$$\langle \Box \phi(x)\, \phi(x') \rangle = -\frac{4\pi^{\frac{p}{2}+1}}{\Gamma\left(\frac{p}{2}\right)}\, \delta^{p+2}(x - x'), \qquad (4.2.9)$$

the coefficients of the $\psi_s^{(+)}$ are necessarily fixed to be

$$|b_\phi^{+,s}|^2 + (p-1)|b_\phi^{-,s}|^2 = \frac{(\Delta_\phi)_{|s|}}{|s|!}. \qquad (4.2.10)$$

Note that any phases in $b_\phi^{\pm,s}$ can be absorbed in a phase of the corresponding operators $\psi_s^{(\pm)}$, and therefore we can take the bulk operator expansion coefficients to be real and positive. It follows that any freedom in the bulk-defect expansion coefficients is solely due to the appearance of the '$-$' modes, with only one real parameter introduced for every such mode. Without these modes the two-point function is completely fixed.[5]

---

[5]The appearance of the '$-$' mode in the free theory was not considered in [97]. Note that this mode plays an important role in the free hypermultiplet example of [121]. Furthermore, as a small

4.3 Constraining defect interactions

The goal of this section is to derive constraints on the defect spectrum from analyt-
icity requirements on correlation functions in the presence of defects. The bulk of
this section concerns $q = 2$ defects, but our argument can be extended to higher q
with only small changes; the relevant formulae for generic q are collected in appendix
4.C. Whenever necessary, we comment about results and differences with respect to
the higher co-dimension case. The main characters will be the three-point functions
involving the free scalar ϕ and one or two defect operators $\widehat{\mathcal{O}}$ and $\widehat{\mathcal{O}}'$:

$$\langle \phi(x)\widehat{\mathcal{O}}(\vec{x}')\widehat{\mathcal{O}}'(\vec{x}'')\rangle, \quad \langle \phi(x_1)\phi(x_2)\widehat{\mathcal{O}}(\vec{x}'')\rangle. \tag{4.3.1}$$

We will show that the bulk-defect operator expansion of these correlators features
unphysical singularities, which can be removed only if very special conditions are
met.

Even though our analysis can be carried over to any unitary representation of the
parallel Lorentz group, we will restrict ourselves to symmetric and traceless tensors
of $SO(p)$. We will contract the Lorentz indices with "parallel" polarization vectors
θ^a, $(a = 1, \ldots, p)$ on the defect and work with polynomials in θ, see for example [139]
for details. Concretely, for any symmetric and traceless $SO(p)$ tensor of spin j we
define

$$\widehat{\mathcal{O}}_s^{(j)}(\theta, \vec{x}) \equiv \theta^{a_1} \ldots \theta^{a_j} \widehat{\mathcal{O}}_s^{a_1 \ldots a_j}(\vec{x}), \quad \theta \bullet \theta = 0, \tag{4.3.2}$$

where $\bullet$ represents the $SO(p)$-invariant scalar product.

4.3.1 Bulk-defect-defect three-point functions

Let us consider first the three-point function of one bulk operator ϕ and two defect
primaries. For simplicity we take one of them, denoted $\widehat{\mathcal{O}}$, to be an $SO(p)$ scalar,
and the second one, denoted $\widehat{T}$, to be a symmetric and traceless tensor of parallel
spin j. Without loss of generality we can place the third operator at infinity and so
we investigate:

$$\langle \phi(\vec{x}_1, z, \bar{z})\widehat{\mathcal{O}}_{s_1}(\vec{x}_2)\widehat{T}_{s_2}^{(j)}(\theta, \infty)\rangle. \tag{4.3.3}$$

This correlator is completely determined, via the bulk-defect operator expansion,
by the defect three-point functions between $\widehat{T}, \widehat{\mathcal{O}}$ and the defect modes of the free

---

generalization of our result we note that a very similar analysis applies to conical metric singularities.
In that case the only difference is that the transverse spins s do not have to be half-integers. Such
singularities are relevant for the computation of Renyi entropies, see for example appendix C of [138]
for a computation in the free scalar theory. It would be interesting to understand the appearance of
the '−' modes in more detail in this context. We thank Lorenzo Bianchi, Chris Herzog and Marco
Meineri for raising this point with us.

scalar $\psi_s^{(\mathfrak{p})}$ introduced above. These are, in turn, constrained by the defect conformal symmetry to be

$$\langle \psi_s^{(\mathfrak{p})}(\vec{x}_1) \widehat{\mathcal{O}}_{s_1}(\vec{x}_2) \widehat{T}_{s_2}^{(j)}(\theta, \infty) \rangle = \frac{\hat{f}_{s\widehat{\mathcal{O}}\widehat{T}}^{(\mathfrak{p})}}{|\vec{x}_{12}|^{\widehat{\Delta}_s^{\mathfrak{p}} + \widehat{\Delta}_{\widehat{\mathcal{O}}} - \widehat{\Delta}_{\widehat{T}}}} P_{\parallel}^{(j)}(\hat{x}_{12}, \theta). \tag{4.3.4}$$

where we should require that

$$s_1 + s_2 + s = 0. \tag{4.3.5}$$

Note that the dependence on the $SO(p)$ spin is captured by a unique polynomial, homogeneous of degree j in the parallel polarization vector [139]

$$P_{\parallel}^{(j)}(\hat{x}_{12}, \theta) \equiv (-\hat{x}_{12} \bullet \theta)^j, \quad \hat{x}^a \equiv \frac{x^a}{|\vec{x}|}. \tag{4.3.6}$$

By Bose symmetry the three-point function above cannot depend on the operator ordering[6] and therefore

$$\hat{f}_{\widehat{\mathcal{O}}\psi\widehat{T}} = (-1)^j \hat{f}_{\psi\widehat{\mathcal{O}}\widehat{T}}. \tag{4.3.7}$$

This implies in particular that only even j are allowed if the first two operators are identical. The complete expression for (4.3.3) can be obtained by plugging the bulk-to-defect OPE and resumming the contributions from descendants. After some algebra, which we relegate to appendix 4.C, the result of this procedure is the *defect channel expansion* of equation (4.3.3). This expansion takes the form

$$\langle \phi(\vec{x}_1, |z|e^{i\varphi}) \widehat{\mathcal{O}}_{s_1}(\vec{x}_2) \widehat{T}_{s_2}^{(j)}(\theta, \infty) \rangle = \frac{P_{\parallel}^{(j)}(\hat{x}_{12}, \theta)}{|z|^{\Delta_\phi + \widehat{\Delta}_{\widehat{\mathcal{O}}} - \widehat{\Delta}_{\widehat{T}}}} \sum_{\mathfrak{p} \in \{+, -\}} b_\phi^{(\mathfrak{p}, s)} \hat{f}_{s\widehat{\mathcal{O}}\widehat{T}}^{(\mathfrak{p})} e^{-is\varphi} \mathcal{F}_{\mathfrak{p}, s}^{\widehat{\mathcal{O}}\widehat{T}}(\hat{\chi}),$$

$$s = -s_1 - s_2. \tag{4.3.8}$$

The defect blocks in this expression are simple Hypergeometric functions of the cross-ratio[7]

$$\hat{\chi} = \frac{|\vec{x}_{12}|^2}{|z|^2}. \tag{4.3.9}$$

---

[6]For line defects the three-point functions generically depend on the ordering of the operators on the line. This will be discussed in section 4.5.1.

[7]Since the defect three-point functions (4.3.4) do not depend on the transverse angle, the dependence on φ in (4.3.8) enters only via the prefactor $e^{is\varphi}$ in the bulk-to-defect OPE. It follows that the defect blocks will only depend on $|\vec{x}_{12}|$ and $|z|$, so (4.3.9) must be the appropriate cross-ratio.

and in appendix 4.C we show they are given by[8]

$$\mathcal{F}_{\mathfrak{p},s}^{\widehat{\mathcal{O}}\widehat{T}}(\hat{\chi}) = \hat{\chi}^{\kappa_{\mathfrak{p}\widehat{\mathcal{O}}\widehat{T}}+\frac{j}{2}} \, {}_2F_1\left(1 - \frac{p}{2} - j - \kappa_{\mathfrak{p}\widehat{\mathcal{O}}\widehat{T}}, -\kappa_{\mathfrak{p}\widehat{\mathcal{O}}\widehat{T}}, 1 - \frac{p}{2} + \widehat{\Delta}_s^{(\mathfrak{p})}; -\frac{1}{\hat{\chi}}\right), \quad (4.3.10)$$

where we introduced

$$\kappa_{\mathfrak{p}\widehat{\mathcal{O}}\widehat{T}} = -\frac{1}{2}(\widehat{\Delta}_s^{(\mathfrak{p})} + \widehat{\Delta}_{\widehat{\mathcal{O}}} - \widehat{\Delta}_{\widehat{T}} + j). \quad (4.3.11)$$

Notice that the sum on the r.h.s. of (4.3.8) contains at most two terms. For $q > 2$ the prefactors in equation (4.3.8) change a bit but the functional form of the blocks given in equation (4.3.10) happens to remain the same, with the index s now denoting the rank of an $SO(q)$ symmetric and traceless tensor. We refer the reader to appendix 4.C for details.

4.3.2 Constraints from analyticity

In equation (4.3.8) the $\hat{\chi} \to \infty$ limit corresponds to the bulk-defect operator expansion. If we take the opposite limit $\hat{\chi} \to 0$ we are sending $\vec{x}_{12} \to 0$ and for finite transverse separation the correlator should be analytic at $\vec{x}_1 = \vec{x}_2$. However a generic term in (4.3.8) is not analytic since:[9]

$$P_{\parallel}^{(j)}(\hat{x}_{12}, \theta)\mathcal{F}_{\mathfrak{p},s}^{\widehat{\mathcal{O}}\widehat{T}}(\hat{\chi}) \underset{\hat{\chi}\to 0}{\sim} \frac{(-x_{12}\bullet\theta)^j}{|z|^j}\hat{\chi}^{1-j-\frac{p}{2}}\frac{\Gamma\left(j + \frac{p}{2} - 1\right)\Gamma\left(1 - \frac{p}{2} + \widehat{\Delta}_s^{(\mathfrak{p})}\right)}{\Gamma(-\kappa_{\mathfrak{p}\widehat{\mathcal{O}}\widehat{T}})\Gamma(j + \widehat{\Delta}_s^{(\mathfrak{p})} + \kappa_{\mathfrak{p}\widehat{\mathcal{O}}\widehat{T}})} + \dots. \quad (4.3.12)$$

Such unphysical singularities must cancel out from the r.h.s. of (4.3.8). This can happen either because of a relation among the OPE coefficients $\hat{f}$ or because the quantum numbers are such that (4.3.12) does not hold and the block is actually regular. For all p and q we find that either of the following possible scenarios must be realized.

1. In the first scenario the quantum numbers are such that the 'generic' relation (4.3.12) is valid. Let us first suppose that both the "+" and "−" mode are present, then the cancellation of the unphysical singularities can be enforced

---

[8]The notation employed in eq. (4.3.10) is a bit loose, since the defect blocks depend on the quantum numbers of the operators $\widehat{T}$ and $\widehat{\mathcal{O}}$ and not on the operators themselves. May the reader forgive this licentious choice.

[9]When $p = 2$ and $j = 0$ the singularity is actually logarithmic in $\hat{\chi}$ but the coefficient is essentially the same. For $p = 1$ the non-analyticity of (4.3.12) is due to odd powers of $\sqrt{\chi} \sim |\vec{x}_{12}|$. More details on the continuation to $p = 1$ are given in section 4.5.1.

by the following relation between the OPE coefficients:[10]

$$
\hat{f}^{(-)}_{s\widehat{\mathcal{O}}\widehat{T}} = -\frac{b^{(+,s)}_{\phi}}{b^{(-,s)}_{\phi}} \frac{\Gamma\left(1 - \frac{p}{2} + \widehat{\Delta}^{(+)}_s\right) \Gamma\left(\frac{j+p-\widehat{\Delta}^{(+)}_s+\widehat{\Delta}_{\widehat{\mathcal{O}}}-\widehat{\Delta}_{\widehat{T}}}{2}\right) \Gamma\left(\frac{j+p-\widehat{\Delta}^{(+)}_s-\widehat{\Delta}_{\widehat{\mathcal{O}}}+\widehat{\Delta}_{\widehat{T}}}{2}\right)}{\Gamma\left(1 + \frac{p}{2} - \widehat{\Delta}^{(+)}_s\right) \Gamma\left(\frac{j+\widehat{\Delta}^{(+)}_s+\widehat{\Delta}_{\widehat{\mathcal{O}}}-\widehat{\Delta}_{\widehat{T}}}{2}\right) \Gamma\left(\frac{j+\widehat{\Delta}^{(+)}_s-\widehat{\Delta}_{\widehat{\mathcal{O}}}+\widehat{\Delta}_{\widehat{T}}}{2}\right)} \hat{f}^{(+)}_{s\widehat{\mathcal{O}}\widehat{T}},
$$

(4.3.13)

where we used the shadow relation $\widehat{\Delta}^{(+)}_s + \widehat{\Delta}^{(-)}_s = p$. On the other hand, if the "−" mode is absent (or equal to the identity operator for which there is no $\chi \to 0$ singularity), then the coefficient of the corresponding "+" mode must be zero.

2. In the second scenario the scaling dimensions align such that (4.3.12) is not valid. This can happen if

   - $\kappa_{\mathfrak{p}\widehat{\mathcal{O}}\widehat{T}} = n$ with $n \in \mathbb{N}$. In other words,

$$
\widehat{\Delta}_{\widehat{T}} = \widehat{\Delta}^{(\mathfrak{p})}_s + \widehat{\Delta}_{\widehat{\mathcal{O}}} + j + 2n, \quad n \in \mathbb{N} \tag{4.3.14}
$$

   so the dimension of $\widehat{T}$ equals that of a "double twist" combination of $\widehat{\mathcal{O}}$ and $\psi^{(\mathfrak{p})}_s$.

   - $j + \kappa_{\mathfrak{p}\widehat{\mathcal{O}}\widehat{T}} + \widehat{\Delta}^{(\mathfrak{p})}_s = -n$ with $n \in \mathbb{N}$. In other words,

$$
\widehat{\Delta}_{\widehat{\mathcal{O}}} = \widehat{\Delta}^{(\mathfrak{p})}_s + \widehat{\Delta}_{\widehat{T}} + j + 2n, \quad n \in \mathbb{N} \tag{4.3.15}
$$

   so the dimension of $\widehat{\mathcal{O}}$ equals that of a "double twist" combination of $\widehat{T}$ and $\psi^{(\mathfrak{p})}_s$.

As shown in table 4.1, the "−" family does not occur in a large class of defects and then the second scenario is the only one that can give non-zero three-point functions. This is the case we will focus on below. It is however interesting to point out that even in the other cases the non-triviality of the correlators is entirely due to the appearance of the single "−" mode compatible with unitarity listed in table 4.1. Including this mode leads to an interesting variation of the usual bootstrap problem because of the "shadow" relations (4.3.13) between OPE coefficients. A first numerical analysis of this type of problem already appeared in the context of the long-range Ising model [142] and in [92] similar equations were analysed in the context of boundary conditions for free scalar fields.

---

[10]These special relations, which re-emphasize that one should think of the $\psi^{(\pm)}_s$ as shadow pairs, have appeared already in the context of the long-range Ising model [91, 140–142]. This is not surprising, since the latter has a description in terms of a conformal defect of non-integer co-dimension q.

4.3.3 Reconstructing the bulk

We will now go one step beyond the analysis in the previous subsection and consider
three-point functions of the type:

$$\langle \phi(x_1)\phi(x_2)\widehat{T}_s^{(j)}(\theta,\infty)\rangle. \tag{4.3.16}$$

Note that the only allowed Lorentz representation for $\widehat{T}$ are symmetric traceless
tensors. In a 'defect channel' these three-point functions become a sum over the sort
of three-point functions that we just considered. Importantly, this sum should be
able to reproduce the 'bulk channel' OPE which corresponds to bringing the two ϕ
operators together. We will see that this is indeed the case.[11]

The defect-channel expansion

Our first goal will be to compute the defect channel blocks for the three-point function
(4.3.16). Our starting point is equation (4.3.4) specialized to the case where $\widehat{\mathcal{O}}$ is
one of the $\psi_s^{(\mathfrak{p})}$, which is:

$$\langle \psi_{s_1}^{(\mathfrak{p}_1)}(\vec{x}_1)\psi_{s_2}^{(\mathfrak{p}_2)}(\vec{x}_2)\widehat{T}_s^{(j)}(\theta,\infty)\rangle = \frac{\hat{f}_{s_1 s_2 \widehat{T}}^{(\mathfrak{p}_1,\mathfrak{p}_2)}}{|\vec{x}_{12}|^{\widehat{\Delta}_{s_1}+\widehat{\Delta}_{s_2}-\widehat{\Delta}_{\widehat{T}}}} P_{\parallel}^{(j)}(\hat{x}_{12},\theta)\,\delta_{s_1+s_2+s,0}. \tag{4.3.17}$$

The correlator (4.3.16) can be obtained by acting twice with the bulk-to-defect OPE
on the three-point functions (4.3.17) and resumming the contributions from descend-
ants. As we show in appendix 4.C the result of this computation takes a simple form
when we specialize to the kinematical configuration where the two bulk operators lie
at the same transverse distance from the defect

$$z_1 = |z|e^{i\varphi}, \quad z_2 = |z|. \tag{4.3.18}$$

In this configuration, the full three-point function takes the following form

$$\langle \phi(\vec{x}_1,|z|e^{i\varphi})\phi(\vec{x}_2,|z|)\widehat{T}_s^{(j)}(\theta,\infty)\rangle =$$
$$\frac{P_{\parallel}^{(j)}(\hat{x}_{12},\theta)}{|z|^{2\Delta_\phi-\widehat{\Delta}_{\widehat{T}}}} \sum_{\mathfrak{p}_i\in\{+,-\}} \sum_{s_1} b_\phi^{(\mathfrak{p}_1,s_1)} b_\phi^{(\mathfrak{p}_2,s_2)} \hat{f}_{s_1 s_2 \widehat{T}}^{(\mathfrak{p}_1,\mathfrak{p}_2)} \, e^{-is_1\varphi}\mathcal{F}_{(\mathfrak{p}_1,s_1),(\mathfrak{p}_2,s_2)}^{\widehat{T}}(\hat{\chi})\delta_{s_1+s_2+s,0}\,.$$
$$\tag{4.3.19}$$

---

[11]One might try to go even further and also analyse the three-point function of the bulk field,
$\langle\phi\phi\phi\rangle$, in the presence of the defect. We found that this correlation function does not lead to
additional constraints. Note that it automatically vanishes for a monodromy defect.

The defect blocks in the expression above are computed in appendix 4.C and read

$$\mathcal{F}^{\widehat{T}}_{(\mathfrak{p}_1,s_1),(\mathfrak{p}_2,s_2)}(\hat{\chi}) = \hat{\chi}^{\kappa_{\mathfrak{p}_1,\mathfrak{p}_2}+\frac{j}{2}}$$
$${}_4F_3\left(\overline{\Delta}_{12}-\hat{h}-\frac{1}{2}, \overline{\Delta}_{12}-\hat{h}, -\kappa_{\mathfrak{p}_1\mathfrak{p}_2}, -\kappa_{\mathfrak{p}_1\mathfrak{p}_2}-j-\hat{h}; \widehat{\Delta}^{(\mathfrak{p}_1)}_{s_1}-\hat{h}, \widehat{\Delta}^{(\mathfrak{p}_2)}_{s_2}-\hat{h}, 2\overline{\Delta}_{12}-2\hat{h}-1; -\frac{4}{\hat{\chi}}\right),$$
$$\overline{\Delta}_{12} \equiv \frac{1}{2}(\widehat{\Delta}^{(\mathfrak{p}_1)}_{s_1}+\widehat{\Delta}^{(\mathfrak{p}_2)}_{s_2}), \quad \kappa_{\mathfrak{p}_1\mathfrak{p}_2} \equiv -\frac{1}{2}(\widehat{\Delta}^{(\mathfrak{p}_1)}_{s_1}+\widehat{\Delta}^{(\mathfrak{p}_2)}_{s_2}-\widehat{\Delta}_{\widehat{T}}+j), \quad \hat{h} \equiv \frac{p}{2}-1,$$

$$(4.3.20)$$

where $\hat{\chi}$ is the cross-ratio defined in (4.3.9). Again we should emphasize that the result (4.3.20) holds for all q, as we show in appendix 4.C.

Consistency with the bulk OPE

Our next goal will be to deduce under which conditions the 'defect channel' expansion (4.3.19) is consistent with the 'bulk channel' OPE. In order to facilitate this analysis, we integrate both sides of (4.3.19) against $e^{is'\varphi}$ to obtain

$$\frac{1}{2\pi}\int_0^{2\pi}\mathrm{d}\varphi\ e^{is'\varphi}\langle\phi(\vec{x}_1,|z|e^{i\varphi})\phi(\vec{x}_2,|z|)\widehat{T}^{(j)}_s(\theta,\infty)\rangle$$
$$=\frac{P^{(j)}_\parallel(\hat{x}_{12},\theta)}{|z|^{2\Delta_\phi-\widehat{\Delta}_{\widehat{T}}}}\sum_{\mathfrak{p}\in\{+,-\}}b^{(\mathfrak{p}_1,s')}_\phi b^{(\mathfrak{p}_2,s_2)}_\phi \hat{f}^{(\mathfrak{p}_1,\mathfrak{p}_2)}_{s',s_2\widehat{T}}\ \mathcal{F}^{\widehat{T}}_{(\mathfrak{p}_1,s'),(\mathfrak{p}_2,s_2)}(\hat{\chi})\ \delta_{s'+s_2+s,0}. \qquad (4.3.21)$$

In contrast with equation (4.3.19), the sum on the r.h.s. of the above expression contains at most three terms. In the higher co-dimension case we can analogously integrate the three-point function against the appropriate spherical harmonics, to isolate each $SO(q)$ irrep. We will now proceed similarly to what we have done in Section 4.3.2. On the one hand, the bulk self-OPE of the free scalar requires analyticity at $\vec{x}_1 = \vec{x}_2$ for both the original as well as the integrated correlator (4.3.21). (Note that the identity operator in the $\phi \times \phi$ OPE does not contribute.) On the other hand, for generic values of its parameters the r.h.s. of (4.3.21) becomes singular in this limit. For generic values of p and j the most singular term is given by:

$$P^{(j)}_\parallel(\hat{x}_{12},\theta)\mathcal{F}^{\widehat{T}}_{(\mathfrak{p}_1,s_1),(\mathfrak{p}_2,s_2)}(\hat{\chi}) \underset{\hat{\chi}\to 0}{\sim} \frac{(-x_{12}\bullet\theta)^j}{|z|^j}\hat{\chi}^{1-j-\frac{p}{2}}$$
$$\times \frac{\Gamma(\widehat{\Delta}^{(\mathfrak{p}_1)}_{s_1}-\hat{h})\Gamma(\widehat{\Delta}^{(\mathfrak{p}_2)}_{s_2}-\hat{h})\Gamma(\hat{h}+j)\Gamma(j+\widehat{\Delta}_{\widehat{T}}-1)}{\Gamma(-\kappa_{\mathfrak{p}_1\mathfrak{p}_2})\Gamma(j+\widehat{\Delta}^{(\mathfrak{p}_1)}_{s_1}+\kappa_{\mathfrak{p}_1\mathfrak{p}_2})\Gamma(j+\widehat{\Delta}^{(\mathfrak{p}_2)}_{s_2}+\kappa_{\mathfrak{p}_1\mathfrak{p}_2})\Gamma\left(\frac{\widehat{\Delta}^{(\mathfrak{p}_1)}_{s_1}+\widehat{\Delta}^{(\mathfrak{p}_2)}_{s_2}+\widehat{\Delta}_{\widehat{T}}+j-p}{2}\right)} + \dots.$$

$$(4.3.22)$$

but there are also powers of $\hat{\chi}^{\frac{1}{2}(1-j-p+\widehat{\Delta}_{\widehat{T}})}$ and $\hat{\chi}^{\frac{1}{2}(2-j-p+\widehat{\Delta}_{\widehat{T}})}$ with equally involved coefficients.

As in the previous subsection, we can find constraints by demanding that such singularities are absent in the full correlator. If both the '−' and the '+' modes are present then there is an interesting spectrum of constraints to be found on both OPE coefficients and scaling dimensions of $\widehat{T}$ that we will not fully report here. Instead, we focus on the case where only the '+' modes are present which is important for the rest of the chapter. In that case three-point functions can only be non-zero if the second scenario of section 4.3.2 is realized. Furthermore, we should take $\widehat{\mathcal{O}}$ to also be a defect mode of ϕ, so $\widehat{\mathcal{O}} = \psi_{s'}^{(+)}$, and after projecting on a given s' as above we get to apply the 'double twist' conditions on $\widehat{\Delta}_{\widehat{T}}$ of that scenario twice. Only the first of the two possibilities listed in that subsection then gives a dimension $\widehat{\Delta}_{\widehat{T}}$ that is above the unitarity bound, and we conclude that:

$$\widehat{\Delta}_{\widehat{T}} = \widehat{\Delta}_{s_1}^{(\mathfrak{p}_1)} + \widehat{\Delta}_{s_2}^{(\mathfrak{p}_2)} + j + 2n, \quad n \in \mathbb{N}. \tag{4.3.23}$$

In short, in the absence of the '−' modes the OPE of the $\psi_s^{(+)}$ operators contains only 'double twist' operators! Armed with this condition we see that there is no further constraint to be gained from equation (4.3.22), since the coefficient of the singular term now vanishes and the $\langle\phi\phi\widehat{T}\rangle$ correlator is analytic at $\vec{x}_1 = \vec{x}_2$.

4.4 Triviality of defects of dimension 2 and higher

We have established that for many defects the bulk-defect operator expansion of a free scalar field is constrained to only contain operators that we called $\psi_s^{(+)}$, with fixed coefficients. We have also shown that the non-trivial operators in the OPE of the $\psi_s^{(+)}$ must be of a 'double twist' type. In this section we will show that the latter statement implies that all the correlation functions of the $\psi_s^{(+)}$ operators must be those of a generalized free theory. From this the triviality of the n-point functions of ϕ follows immediately.[12]

We will consider here the case $p \geq 2$. The line with $p = 1$ will be discussed in the next section. To apply the theorem below to our analysis of defects with $q > 2$ one should in principle group the operators in representations of the non-Abelian transverse rotation algebra. It is however easy to see that this just produces some extra factors that do not change the gist of the argument.

The result 'GFF spectrum implies GFF n-point functions' might be interesting on its own; for $n = 4$ it can be rephrased as the statement that a trivial double

---

[12]To be precise, when $q = p + 2$ the identity operator can also appear in the bulk-defect operator expansion of ϕ. Its coefficient is the only variable not fixed by our analysis.

discontinuity [1] in all channels implies that the correlation function itself is trivial.[13]

Theorem 1. *Consider a conformal theory in more than one dimension with a state-operator correspondence and a discrete spectrum such that cluster decomposition is obeyed. Suppose the theory has a set of scalar operators $\psi_s(x)$ whose OPEs take the form*

$$\psi_{s_1} \times \psi_{s_2} = \delta_{s_1,s_2}\mathbf{1} + \text{(operators with twist } \widehat{\Delta}_{s_1} + \widehat{\Delta}_{s_2} + 2k, \text{ with } k \in \mathbb{N}) \quad (4.4.1)$$

Then all the n-point correlation functions of $\psi_s(x)$ are those of generalized free fields.

The main ingredient in our proof will be a dispersion relation in the complex time plane[14] for which we will need the commutator $[\psi(x), \psi(y)]$. For spacelike separation we write the operator product expansion as[15]

$$\psi_{s_1}(x)\psi_{s_2}(0) = \frac{\delta_{s_1,s_2}}{(x^2)^{\widehat{\Delta}_{s_1}}}\mathbf{1} + \sum_k \lambda_{12}{}^k \frac{x^{\mu_1}\dots x^{\mu_{\ell_k}}}{(x^2)^{(\widehat{\Delta}_{s_1}+\widehat{\Delta}_{s_2}-\widehat{\Delta}_k+\ell_k)/2}}\mathcal{O}^k_{\mu_1\dots\mu_{\ell_k}}(0) \quad (4.4.2)$$

where in the sum over non-trivial operators k we do not distinguish between primaries and descendants. By assumption $\widehat{\Delta}_k - \ell_k = \widehat{\Delta}_{s_1} + \widehat{\Delta}_{s_2} + 2k$, and therefore every term in the sum only yields non-negative integer powers of x^2. Passing to the commutator therefore yields

$$[\psi_{s_1}(x), \psi_{s_2}(0)] = \text{disc}\left[\frac{\delta_{s_i,s_j}}{(x^2)^{\widehat{\Delta}_{s_i}}}\right]\mathbf{1}, \quad (4.4.3)$$

which is valid as an operator equation as long as the OPE converges. As usual, operator orderings in the commutator must be understood as the Euclidean time orderings and the discontinuity has support only when the operators are causally connected. We will not need the detailed expression of the discontinuity but it is straightforward to work out.[16]

Our proof will now proceed inductively. We will study the n-point function

$$\langle\psi_{s_1}(x_1)\psi_{s_2}(x_2)\psi_{s_3}(x_3)\dots\psi_{s_n}(x_n)\rangle \quad (4.4.4)$$

---

[13]For four-point functions of identical operators this theorem is a corollary of theorem 1 in [143]. In all other cases we believe this result is new.

[14]A discussion of the analytic structure of conformal correlation functions can found, for example, in [144]. Recent other work on dispersion relations for four-point functions includes [83, 145].

[15]The attentive reader will have noticed a small change of notation: in this section the operators ψ_s are taken to be Hermitian. They should be thought of as the real and imaginary part of the $\psi_s^{(+)}$ operators of the previous sections.

[16]For integer Δ the discontinuity is supported only at $x^2 = 0$, in agreement with Huygens' principle.
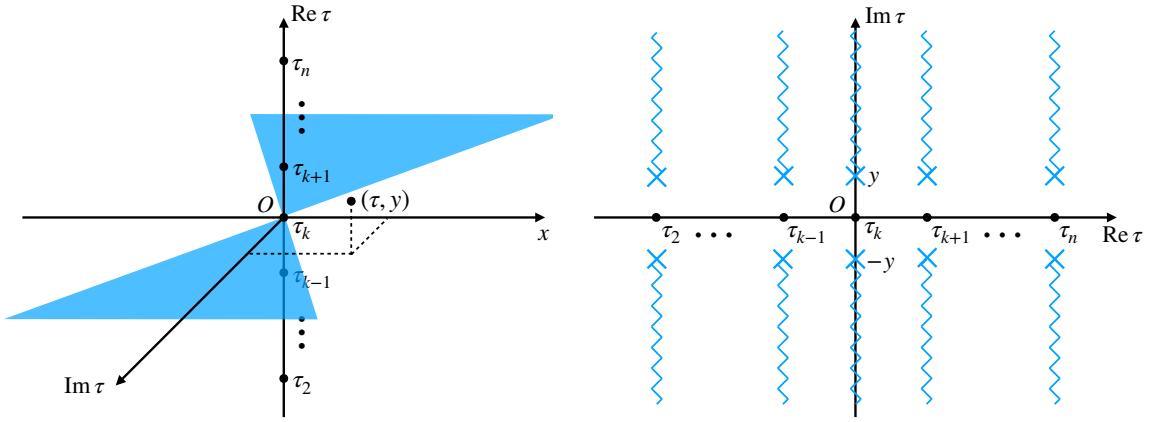
Figure 4.1. Left: Operators ψ_{s_k} ($k \geq 2$) are inserted along the Euclidean time ($\mathrm{Re}\,\tau$) axis. Lorentzian time is along the imaginary-τ axis. The lightcone of ψ_{s_k} is illustrated in blue triangles. ψ_{s_1} is off the line and its time component τ is complex in general. Right: Lightcone branch cuts on the complex-τ plane.

in the following specific kinematic configuration. We put all operators but the first one on a line:

$$x_k^\mu = (\tau_k, 0, 0, 0, \ldots), \qquad 2 \leq k \leq n, \tag{4.4.5}$$

ordered such that $\tau_k < \tau_{k+1}$, whereas for the first operator we choose:

$$x_1^\mu = (\tau, y, 0, 0, \ldots) \tag{4.4.6}$$

with $y > 0$ a social distancing parameter and τ an arbitrary *complex* time coordinate. In the τ plane the correlator is analytic except on the vertical lightcone cuts starting at $\tau = \tau_k \pm iy$ for $2 \leq k \leq n$ and running off to $\pm i\infty$ (see figure 4.1). The discontinuities across these cuts completely determine the correlator because it vanishes at large $|\tau|$ by cluster decomposition (see below for more details). This can be formalized as a dispersion relation:[17]

$$
\begin{aligned}
G_n(\tau) &= \oint \frac{d\tau'}{2\pi i} \frac{1}{\tau' - \tau} G_n(\tau') \\
&= \int_{-\infty}^{\infty} \frac{dt'}{2\pi} \Big(\frac{1}{\tau - \tau_2 - it'} \langle [\psi_{s_1}(\tau_2 + it, y), \psi_{s_2}(\tau_2)] \psi_{s_3}(\tau_3) \psi_{s_4}(\tau_4) \ldots \psi_{s_n}(\tau_n) \rangle \\
&\quad + \ldots \\
&\quad + \frac{1}{\tau - \tau_n - it'} \langle \psi_{s_2}(\tau_2) \psi_{s_3}(\tau_3) \ldots [\psi_{s_1}(\tau_n + it, y), \psi_{s_n}(\tau_n)] \rangle \Big),
\end{aligned}
\tag{4.4.7}
$$

---

[17]Single-variable and two-variable dispersion relations in CFT were recently studied in [145] and [83] respectively.

where we used that Euclidean time ordering determines the operator ordering.

Next we would like to substitute OPEs and conclude that only the identity contributes in each commutator as in equation (4.4.3). Before doing so we need to ensure that the OPE actually converges. Consider the contribution of the commutator between the first and the k'th operator in the dispersion relation. It will only have support if the operators become timelike separated, so if $|t'| > y$. OPE convergence for all values of t' can be shown by mapping the configuration into the more familiar z and $\bar{z}$ coordinates. These can be found by performing a Möbius transformation:

$$x \mapsto \frac{x - \tau_k}{x - \tau_{k-1}} \frac{\tau_{k+1} - \tau_{k-1}}{\tau_{k+1} - \tau_k} \tag{4.4.8}$$

which maps τ_k to the origin, τ_{k+1} to 1 and τ_{k-1} to infinity; the image of operator 1 then defines what we call z and $\bar{z}$. One finds:

$$z = \frac{\tau - \tau_k + iy}{\tau - \tau_{k-1} + iy} \frac{\tau_{k+1} - \tau_{k-1}}{\tau_{k+1} - \tau_k} \qquad \bar{z} = \frac{\tau - \tau_k - iy}{\tau - \tau_{k-1} - iy} \frac{\tau_{k+1} - \tau_{k-1}}{\tau_{k+1} - \tau_k} \tag{4.4.9}$$

The Möbius transformation maps the other operators somewhere on the real axis between 1 and ∞. As is familiar from studies of conformal four-point functions, the desired OPE converges for any z and $\bar{z}$ away from the real interval $[1, \infty)$, even if we take z and $\bar{z}$ complex and independent.[18] Fortunately the entire t' integration region stays in that region: substituting $\tau = \tau_k + it$ shows that the imaginary parts of z and $\bar{z}$ are never zero for $|t| > y$. Therefore, the OPE converges and we can substitute equation (4.4.3) in equation (4.4.7).

It is useful to analyse the large $|\tau|$ behaviour in the z and $\bar{z}$ variables. One finds that $z, \bar{z} \to (\tau_{k+1} - \tau_{k-1})/(\tau_{k+1} - \tau_k)$ which is a real number greater than one.[19] This being the image of infinity, we conclude that there is no operator inserted at this point and the correlator in the $z, \bar{z}$ coordinates does not blow up.[20] It follows that the original correlator must vanish due the Jacobian factor proportional to $(\tau + iy - \tau_{k-1})^{-\Delta}(\tau - iy - \tau_{k-1})^{-\Delta}$. This is the 'cluster decomposition' that we

---

[18]After doing a further transform to the configuration corresponding to the ρ coordinates of [67] we find the OPE yields an absolutely convergent expansion in powers of $\rho\bar{\rho} = e^{2\tau}$ with coefficients that are polynomials in $\sqrt{\rho/\bar{\rho}} + \sqrt{\bar{\rho}/\rho} = 2\cos(\theta)$ with τ and θ cylinder coordinates and $\tau < 0$. Adding an imaginary part to τ clearly does not affect the convergence. Adding an imaginary part to θ may seem more problematic, but since the twists of all the non-trivial operators are non-negative we can rewrite the expansion as an absolutely convergent series in ρ and $\bar{\rho}$. This series will then still converge when ρ and $\bar{\rho}$ are complex and independent, as long as they both have a modulus smaller than one.

[19]This is actually at the very limit of the domain where the OPE between operator 1 and operator k converges, which illustrates that OPE convergence is not at all guaranteed for a less judicious choice of the $n - 1$ operator insertions.

[20]In fact, the operators at τ_k, τ_{k+1}, τ_{k+2}, ... τ_n lie to the left of this point and the other ones to its right, with τ_{k-1} as stated at infinity. Fusing these two groups of operators together yields a natural OPE channel for this point which converges for large $|\tau|$ both in the Euclidean window and in between the cuts emanating from τ_k and τ_{k+1}.

alluded to above.

Now let us return to equation (4.4.7). Since each commutator is proportional to the identity operator, each of the $(n-1)$ terms in the dispersion relation factorizes into an $n-2$ point function times the discontinuity of the two-point function, and it is the latter that contains all the t' dependence. The t' integrals are therefore easily done and we find that

$$
\begin{aligned}
G_n(t_1) = & \frac{\delta_{s_1,s_2}}{(x_{12}^2)^{\widehat{\Delta}_{s_1}}} \langle \psi_{s_3}(\tau_3)\psi_{s_4}(\tau_4)\ldots\psi_{s_n}(\tau_n)\rangle \\
& + \frac{\delta_{s_1,s_3}}{(x_{13}^2)^{\widehat{\Delta}_{s_1}}} \langle \psi_{s_2}(\tau_2)\psi_{s_4}(\tau_4)\ldots\psi_{s_n}(\tau_n)\rangle \\
& + \ldots \\
& + \frac{\delta_{s_1,s_n}}{(x_{1n}^2)^{\widehat{\Delta}_{s_1}}} \langle \psi_{s_2}(\tau_2)\psi_{s_3}(\tau_3)\ldots\psi_{s_{n-1}}(\tau_{n-1})\rangle.
\end{aligned}
\tag{4.4.10}
$$

By the induction hypothesis all the $(n-2)$-point functions in the preceding expression are generalized free correlation functions, which when n is even are given by a sum over the $(n-3)!!$ possible complete Wick contractions. For the n-point function the above expression gives $(n-1) \times (n-3)!! = (n-1)!!$ terms, and indeed it is easy to verify that this is again just the sum of all possible Wick contractions. We can therefore do induction in steps of two, using the one- and two-point function as a starting point. This also means that the correlation functions vanish for odd n, in agreement with the more general result of the previous section.

To complete the proof we need to relax the restricted kinematics where all but one of the operators sit on a straight line. This is straightforward: our argument also goes through for descendants of ψ_s, so we are free to take any number of derivatives in any given direction acting on any of the n operators. The analyticity of the Euclidean correlation functions away from contact points then dictates that our correlation functions are also equal to those of the generalized free theory for more general choices of the insertion points.

4.5 Triviality of line defects

In this section we consider line defects with $p = 1$. The equivalent of the rotation group on the line is $O(1) \simeq \mathbb{Z}_2$ which is really just a parity symmetry.[21] An important assumption in what follows is that this symmetry is preserved. For definiteness we will take the bulk scalar to be parity even and leave the parity odd case as an exercise.

The main objective of this section is then to prove that there is no room for interacting line defects in our setup, either with or without a monodromy. To this end we will first discuss how the results of section 4.3 can be adapted to the special

---

[21]In the context of the 3d Ising model, this parity has been called S-parity of [97, 135].

case of $p = 1$. We then adapt the theorem of the previous section and again prove that the "double twist" spectrum of defect operators implies that their correlation functions must be those of a generalized free theory.

4.5.1 Analytic continuation to line defects

Let us first revisit the results of section 4.3. For the sake of simplicity we will again take $q = 2$, but also comment on the main differences with respect to the higher co-dimension case, where necessary. For line defects with parity the only allowed representations for the parallel spin j are the scalar with $j = 0$ and the pseudo-scalar with $j = 1$. The parity action is given by

$$x \to \mathcal{R}\, x = -x, \quad \widehat{\mathcal{O}}^{\mathcal{R}(j)}(\mathcal{R}x) = (-1)^j \widehat{\mathcal{O}}^{(j)}(x). \tag{4.5.1}$$

We also recall table 4.1, which states that only the $\psi_s^{(+)}$ modes are allowed in the bulk-to-defect OPE of the free scalar. So to prove the triviality of all line defects it suffices to prove that those modes are generalized free.

The kinematics of correlation functions in the presence of line defects can be obtained from their higher dimensional counterparts presented in section 4.3. The $O(1)$ spin dependence is captured by the polynomials (4.3.6) for $j = 0$ or $j = 1$. With this in mind, the *most general* three-point function between the defect modes $\psi_s^{(+)}$ and any other two defect operators reads

$$\langle \psi_s^{(+)}(x_1) \widehat{\mathcal{O}}_{s_1}^{(j_1)}(x_2) \widehat{T}_{s_2}^{(j_2)}(\infty) \rangle = \frac{\widehat{f}_{s\widehat{\mathcal{O}}\widehat{T}}^{(+)}}{|x_{12}|^{\widehat{\Delta}_s^{(+)} + \widehat{\Delta}_{\widehat{\mathcal{O}}} - \widehat{\Delta}_{\widehat{T}}}} (\text{sign } x_{12})^j \, \delta_{s+s_1+s_2,0}, \tag{4.5.2}$$

$$j \equiv j_1 + j_2 \mod 2.$$

Note that, because of the sign function above, the defect correlators may depend on the cyclic order of the operators on the line, which is preserved by the conformal algebra but reversed by the parity operation. The operator ordering along the line will play an important role later in this section, when we will be interested in n-point correlation functions of the ψ's.

We can now repeat the arguments of sections 4.3.1 and 4.3.2 to obtain constraints on the defect spectrum from the analyticity properties of correlators like

$$\langle \phi(x_1, z, \bar{z}) \widehat{\mathcal{O}}_{s_1}^{(j_1)}(x_2) \widehat{T}_{s_2}^{(j_2)}(\infty) \rangle. \tag{4.5.3}$$

The defect channel expansion of such correlators is again derived by acting with the bulk-defect operator expansion on the three-point functions (4.5.2) and resumming the descendants. It is easy to verify that the result is the natural continuation of

(4.3.8) to $p = 1$:

$$\langle \phi(x_1, |z|e^{i\varphi})\widehat{\mathcal{O}}^{(j_1)}_{s_1}(x_2)\widehat{T}^{(j_2)}_{s_2}(\infty)\rangle = \frac{(\text{sign } x_{12})^j}{|z|^{\Delta_\phi + \widehat{\Delta}_{\widehat{\mathcal{O}}} - \widehat{\Delta}_{\widehat{T}}}} b^{(+,s)}_\phi \hat{f}^{(+)}_{s\widehat{\mathcal{O}}\widehat{T}} \ e^{-is\varphi} \mathcal{F}^{\widehat{\mathcal{O}}\widehat{T}}_{+,s}(\hat{\chi}),$$

$$s = -s_1 - s_2, \tag{4.5.4}$$

where $j \equiv j_1 + j_2 \mod 2$ and with blocks given by (4.3.10). Compared to the result obtained earlier for generic $p > 1$ – see equation (4.3.8) – the r.h.s. of (4.5.4) contains only a single defect block.[22] Hence, from the analyticity argument of section 4.3.2, we immediately conclude that the defect three-point function (4.5.2) vanishes unless

$$\widehat{\Delta}_{\widehat{T}} = \widehat{\Delta}^{(+)}_s + \widehat{\Delta}_{\widehat{\mathcal{O}}} + j + 2n, \quad n \in \mathbb{N}, \quad j \equiv j_1 + j_2 \mod 2,$$

$$\text{or}$$

$$\widehat{\Delta}_{\widehat{\mathcal{O}}} = \widehat{\Delta}^{(+)}_s + \widehat{\Delta}_{\widehat{T}} + j + 2n, \quad n \in \mathbb{N}, \quad j \equiv j_1 + j_2 \mod 2. \tag{4.5.5}$$

In particular, when $\widehat{\mathcal{O}}$ is itself a defect mode of ϕ we find that the scaling dimension of $\widehat{T}^{(j)}_s$ must equal

$$\widehat{\Delta}_{\widehat{T}} = \widehat{\Delta}^{(+)}_{s_1} + \widehat{\Delta}^{(+)}_{s_2} + j + 2n, \quad n \in \mathbb{N}. \tag{4.5.6}$$

In conclusion, by repeating the analysis of section 4.3 for line defects, we have proven that the $\psi \times \psi$ OPE contains only operators with "double twist" spectrum. In the next section we will argue that the n-point functions of the ψ's on the line must again necessarily be those of a generalized free field.

4.5.2 Line defects and generalized free field theories

In this subsection we will discuss the one-dimensional version of theorem 1. We will again write equations for the co-dimension 2 case, but the generalization to higher co-dimensions is again straightforward.

Theorem 2. *Consider a conformal theory in one dimension with parity, a convergent operator product expansion and a discrete spectrum such that cluster decomposition is obeyed. Suppose the theory has scalar operators $\psi_s(x)$, with even parity, whose OPEs take the form*

$$\psi_{s_1} \times \psi_{s_2} = \delta_{s_1,s_2}\mathbf{1} + (\text{operators with twist } \Delta_{s_1} + \Delta_{s_2} + 2k, \text{ with } k \in \mathbb{N}, \text{ and spin } j \in \{0,1\})$$

$$\tag{4.5.7}$$

Then all the n-point correlation functions of the $\psi_s(x)$ are those of generalized free fields.

---

[22] In the case where $q = 3$ the identity operator is also allowed to appear which gives a disconnected contribution.

The main idea of this proof is similar to that of Theorem 1, that is, we use a dispersion relation and use the GFF spectrum to compute all the discontinuities. However, a subtlety arises in one-dimensional CFT because two correlation functions with different operator ordering modulo cyclic permutations are generically not related by an analytic continuation. For example, if we start with the correlator $\langle \psi_1(0)\psi_2(z)\psi_3(1)\psi_4(\infty) \rangle$ with $0 < z < 1$ and analytically continue it into the complex z plane then its value at negative real z generally does not agree with $\langle \psi_2(z)\psi_1(0)\psi_3(1)\psi_4(\infty) \rangle$. In our case we start with an n-point function with operators sequentially ordered,

$$\langle \psi_{s_1}(x_1)\psi_{s_2}(x_2)\ldots\psi_{s_n}(x_n) \rangle, \qquad x_1 < x_2 < \ldots < x_n, \tag{4.5.8}$$

and we would like to explore the complex x_1 plane. Suppose we continue x_1 via the upper half plane to a real value between x_2 and x_3. We can use the above OPE to see what happens. If we include the position dependence then it becomes

$$\psi_{s_1}(x_1)\psi_{s_2}(x_2) = \frac{\delta_{s_1,s_2}\mathbf{1}}{(x_2 - x_1)^{2\widehat{\Delta}_{s_1}}} + \sum_k \frac{\lambda_{12}{}^k}{(x_2 - x_1)^{\widehat{\Delta}_{s_1}+\widehat{\Delta}_{s_2}-\widehat{\Delta}_k}}\mathcal{O}^k(x_2), \qquad x_1 < x_2, \tag{4.5.9}$$

By the main assumption of the theorem the contribution of the non-trivial operators gives an analytic contribution in x_1 in the vicinity of x_2. For the identity operator, on the other hand, we generally obtain a cut and some more detail is needed. We will put the cut in the lower half of the x_1 plane, which we emphasize by writing

$$\psi_{s_1}(x_1)\psi_{s_2}(x_2) = \frac{\delta_{s_1,s_2}e^{i\pi\widehat{\Delta}_{s_1}}\mathbf{1}}{\left(e^{i\pi/2}(x_2 - x_1)\right)^{2\widehat{\Delta}_{s_1}}} + \sum_k \frac{\lambda_{12}{}^k}{(x_2 - x_1)^{\widehat{\Delta}_{s_1}+\widehat{\Delta}_{s_2}-\widehat{\Delta}_k}}\mathcal{O}^k(x_2) \tag{4.5.10}$$

and the fractional power is now understood to be evaluated on the principal branch. The analytic continuation via the upper half plane leads to the *analytically continued OPE* given by:

$$\psi_{s_1}(x_1)\psi_{s_2}(x_2) = \frac{\delta_{s_1,s_2}e^{i\pi\widehat{\Delta}_{s_1}}\mathbf{1}}{\left(e^{-i\pi/2}(x_1 - x_2)\right)^{2\widehat{\Delta}_{s_1}}} + \sum_k \frac{\lambda_{12}{}^k(-1)^{j_k}}{(x_1 - x_2)^{\widehat{\Delta}_{s_1}+\widehat{\Delta}_{s_2}-\widehat{\Delta}_k}}\mathcal{O}^k(x_2), \qquad x_2 < x_1, \tag{4.5.11}$$

Now we use the assumed parity symmetry. It dictates that

$$\lambda_{21}{}^k = (-1)^j\lambda_{12}{}^k, \tag{4.5.12}$$

and this allows us to claim that, up to the contribution of the identity operator, the
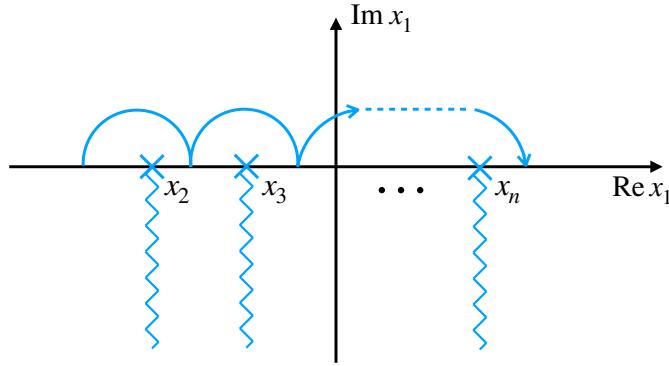
Figure 4.2. Analyticity structure of n-point correlation function is established by consecutively hopping around the $n - 1$ operators in the complex x_1 plane. The branch cuts are chosen to stretch along the negative imaginary direction.

analytically continued OPE is the same as the re-ordered OPE. In equations:

$$\psi_{s_1}(x_1)\psi_{s_2}(x_2) = \frac{\delta_{s_1, s_2}(e^{2i\pi\widehat{\Delta}_{s_1}} - 1)\mathbf{1}}{(x_1 - x_2)^{2\widehat{\Delta}_{s_1}}} + \psi_{s_2}(x_2)\psi_{s_1}(x_1), \qquad x_1 > x_2. \qquad (4.5.13)$$

This is a useful formula. Indeed, since our original correlation function had a $\langle \psi_1 \psi_2 \psi_3 \ldots \rangle$ ordering, it would normally be impossible to use an OPE to analyse what happens when x_1 approaches x_3 via analytic continuation. Equation (4.5.13) however shows us that, up to a factor proportional to the identity operator, this approach is actually determined by the OPE in the $\langle \psi_2 \psi_1 \psi_3 \ldots \rangle$ correlator. In terms of the dispersion relation, this indicates that no unwanted contribution arises because the extra factor has vanishing discontinuity along the lightcone branch cut of $\psi_{s_3}, \psi_{s_4}, \ldots, \psi_{s_n}$. Of course we can now keep hopping around the remaining $n - 2$ operators and discover the full analytic structure of the n-point function in the complex x_1 plane: with our choice of cuts, there are vertical branch cuts starting at $x_2, x_3, \ldots x_n$ and no other singularities (see figure 4.2). What is more, the discontinuity across those cuts is proportional to a two-point function times an $(n - 2)$-point function.[23] Since the correlation function also falls off[24] at large $|x_1|$ it is once more

---

[23]OPE convergence along the discontinuity is guaranteed by the same arguments as before.

[24]We claim that any correlation function $\langle \ldots \psi(x) \ldots \rangle$ in one dimension (that obeys cluster decomposition and without operator insertions at infinity) vanishes when sending $|x| \to \infty$ not along the real axis. To see this, first perform a conformal inversion such that the new variable $x' = -1/x$ goes to zero. We claim that this inverted correlator is finite and the original correlation function therefore vanishes as $|x|^{-2\Delta_\psi}$, which is the Jacobian factor from the inversion. To prove finiteness, suppose first that $\psi(x)$ was the leftmost or rightmost operator. Then finiteness is immediate: the point $x' = 0$ is a physical point with no operators touching. If $\psi(x)$ was not the leftmost or rightmost operator then we need to hop over the other operators to reach $x' = 0$. For the correlator at hand the discontinuity is known and does not lead to a further singularity, so finiteness of the inverted correlator follows. But the result is actually more general: just fuse the operators to the left and to the right of 0 to obtain a sum over three-point functions like $\langle \psi(x')\mathcal{O}(y_L)\mathcal{O}(y_R) \rangle$ with

completely determined by these discontinuities, and the same arguments as those in the previous section show that it equals the generalized free correlation function for all n.

4.6   Tests in conformal perturbation theory

In this section we present some tests of our claims in the context of co-dimension two defects. In all the examples we consider, the candidate conformal defect is obtained by coupling the free bulk scalar to the local operators of a lower-dimensional CFT_p living on the defect, and flowing to the IR. In the UV the interaction is taken to be

$$S_{\text{int}} = \sum_I g_I \int_{\mathbb{R}^p} \mathrm{d}^p x \, \widehat{\varphi}_I(\vec{x}), \tag{4.6.1}$$

where $\widehat{\varphi}_I$ are some scalar composites made of (derivatives of) the bulk fields as well as of local operators in the CFT_p. We then seek for IR fixed points of (4.6.1) which allow for non-trivial bulk-to-defect interactions. If all the operators $\widehat{\varphi}_I$'s have dimensions $\widehat{\Delta}_I = p - \delta_I$ with $0 < \delta_I \ll 1$, then the deformation (4.6.1) is slightly relevant and the RG flow can be studied perturbatively. At the first order in couplings g_I the beta functions read [146]

$$\beta_K = -\delta_K g_K + \frac{S_{p-1}}{2} \sum_{I,J} \widehat{f}_{IJK} \, g_I g_J + O(g^3). \tag{4.6.2}$$

In the equation above, S_{p-1} is the volume of the $(p-1)$-sphere and the numbers $\widehat{f}_{IJK}$, which are real in unitary theories, denote the three-point functions of the φ's computed at $g_I = 0$

$$\widehat{f}_{IJK} \equiv \langle \widehat{\varphi}_I(0) \widehat{\varphi}_J(1) \widehat{\varphi}_K(\infty) \rangle. \tag{4.6.3}$$

A simple example of this scenario is the case where $\varphi_I = \phi$, which is marginal when $q = p + 2$ and was also considered in [94]. In agreement with our main result, the only effect of this defect is to give a one-point function to ϕ that is proportional to g. Below we will present some other concrete realizations of the flow (4.6.1). For these examples, we will check explicitly (using conformal perturbation theory) that the CFT_p decouples from the bulk at the unitary IR fixed points, whenever the $\psi^{(-)}$ modes are not generated.

$y_L < 0$ and $y_R > 0$ the fusion points. The sum converges absolutely in a domain determined by the coordinate differences $|x_i' - y_{L/R}|$ and one can always find a path in the complex x' plane to reach $x' = 0$ without exiting this domain. The sum is therefore finite.

4.6.1 Coupling the trivial defect to lower-dimensional matter

We start by considering a slightly relevant deformation which couples the defect limit
of ϕ to some operator $\widehat{\mathcal{O}}$ of a given CFT_p. If $\widehat{\mathcal{O}}$ has dimension $\frac{p}{2} - \delta$, with $0 \leq \delta \ll 1$,
then a natural coupling is

$$S_{\mathrm{int}} = \int_{\mathbb{R}^p} \mathrm{d}^p x \ \left(g_1 \, \phi(\vec{x}, 0)\widehat{\mathcal{O}}(\vec{x}) + g_2 \, \phi^2(\vec{x}, 0) \right). \tag{4.6.4}$$

Note that the "single-trace" coupling controlled by g_1 generates the marginal op-
erator ϕ^2 at the leading order along the RG flow. The interaction (4.6.4) has the
form of (4.6.1) with $\widehat{\varphi}_1 \equiv \phi \, \widehat{\mathcal{O}}$ and $\widehat{\varphi}_2 \equiv \phi^2$. From the general result (4.6.2) it is
straightforward to obtain the beta functions at the first order:

$$\beta_1 = -\delta g_1 + \frac{S_{p-1}}{2} \widehat{f}_{211} \, g_1 g_2, \quad \beta_2 = \frac{S_{p-1}}{2} \left(\widehat{f}_{222} \, g_2^2 + \widehat{f}_{112} \, g_1^2 \right). \tag{4.6.5}$$

From the second equation above, it is clear that a unitary and non-trivial fixed point
of this deformation will exist only if $\widehat{f}_{222}$ and $\widehat{f}_{112}$ have opposite sign. On the other
hand, these numbers can be computed using Wick's theorem (since the bulk and the
defect are decoupled at $g_1 = g_2 = 0$), and as such they are product of two-point
functions. Since two-point functions, in turn, must be positive in unitary theories,
we conclude that the only possible fixed point at this order is the trivial one, and
the CFT_p is decoupled.

For a concrete realization of the "single-trace" deformation (4.6.4) we can con-
sider the Yukawa coupling of a 4d free scalar field to a 2d free fermion χ:

$$S_{\mathrm{int}} = \int_{\mathbb{R}^2} \mathrm{d}^2 x \ \left(g_1 \bar{\chi}\chi\phi + g_2\phi^2 + g_3(\bar{\chi}\chi)^2 \right). \tag{4.6.6}$$

Since the fermion has UV dimension $\widehat{\Delta}_\chi = \frac{p-1}{2} = \frac{1}{2}$, the Yukawa coupling is classically
marginal. As soon as we turn on g_1, the marginal couplings ϕ^2 and $(\bar{\chi}\chi)^2$ will be
generated at one-loop. From (4.6.2), the beta functions at the first order read

$$\beta_1 = \frac{S_{p-1}}{2} \widehat{f}_{131} \, g_1 g_3, \quad \beta_2 = \frac{S_{p-1}}{2} \left(\widehat{f}_{222} \, g_2^2 + \widehat{f}_{112} \, g_1^2 \right), \quad \beta_3 = \frac{S_{p-1}}{2} \left(\widehat{f}_{333} \, g_3^2 + \widehat{f}_{113} \, g_1^2 \right). \tag{4.6.7}$$

As in the previous example, the three-point function coefficients above, which can be
computed in free theory, are positive numbers. We conclude that the only possible
fixed point of (4.6.6) is the trivial one.

The story becomes more interesting if we dimensionally continue (4.6.6) below
dimension two while keeping the co-dimension fixed, i.e. work with $p = 2 - \delta$ and
$d = 4 - \delta$ ($0 \leq \delta \ll 1$). When doing so, the operator ϕ^2 remains marginal, while

g_1, g_3 become slightly relevant and therefore we find

$$\beta_1 = -\frac{g_1\delta}{2} + \frac{S_{p-1}}{2}\widehat{f}_{131}\, g_1 g_3, \quad \beta_2 = \frac{S_{p-1}}{2}\left(\widehat{f}_{222}\, g_2^2 + \widehat{f}_{112}\, g_1^2\right),$$
$$\beta_3 = -g_3\delta + \frac{S_{p-1}}{2}\left(\widehat{f}_{333}\, g_3^2 + \widehat{f}_{113}\, g_1^2\right). \tag{4.6.8}$$

Assuming unitarity, the first two equations set $g_1 = g_2 = 0$, while from the third we get $g_3 \sim \delta$. In other words, the deformation (4.6.6) flows towards a decoupled Gross–Neveu model.

4.6.2 A nearly marginal deformation in free theory

As another case of the general setup discussed at the beginning of this section, we can try the classically marginal deformation of the free theory

$$S_{\text{int}} = \frac{g}{2} \int_{\mathbb{R}^p} \mathrm{d}^p x\ \phi^2(x, 0). \tag{4.6.9}$$

Although scale invariance is preserved classically, this example turns out to break it in a subtle way quantum-mechanically. To establish this fact, it is sufficient to compute the exact bulk-to-defect correlator $\langle\phi(x)\phi(0)\rangle_g$. In order to simplify the task, we will work in p-dimensional momentum space and consider

$$\langle\phi(\vec{k}, |z_1|)\phi(-\vec{k}, 0)\rangle_g. \tag{4.6.10}$$

The tree-level contribution can be extracted from the propagator obtained in appendix 4.B and reads

$$G_{\phi\widehat{\phi}}(\vec{k}, |z_1|) \equiv \langle\phi(\vec{k}, |z_1|)\phi(-\vec{k}, 0)\rangle_{g=0} = \frac{C_\phi}{(2\pi)} K_0(|\vec{k}||z_1|). \tag{4.6.11}$$

The propagator between two $\phi(\vec{k}, 0)$'s on the defect, which can be obtained by taking the limit as $z_1 \to 0$ of the expression above, contains a $\log|z_1|$ divergence. Setting $|z_1| = \mu$ the leading term in this expansion is

$$G_{\widehat{\phi}\widehat{\phi}}(\vec{k}) \equiv \langle\phi(\vec{k}, 0)\phi(-\vec{k}, \mu)\rangle_{g=0} = -\frac{C_\phi}{(2\pi)}(\gamma + \log(|\vec{k}|\mu) - \log 2), \tag{4.6.12}$$

up to subleading terms as the scale μ is sent to zero. Because of this log, the propagator (4.6.12) depends on the scale. This dependence is only "small", since the μ-derivative of (4.6.12) maps exactly to a contact term in position space, and as such it can be understood as a "small" conformal anomaly [147, 148] and not something to worry about. On the other hand, order by order in perturbation theory, the corrections to the bulk-to-defect correlator are geometric and they can be exactly

resummed:

$$\langle\phi(\vec{k},|z_1|)\phi(-\vec{k},0)\rangle_g = G_{\phi\widehat{\phi}}(\vec{k},|z_1|)\sum_{n=0}^{\infty}\left(-g\,G_{\widehat{\phi}\widehat{\phi}}(\vec{k},\mu)\right)^n = \frac{G_{\phi\widehat{\phi}}(\vec{k},|z_1|)}{1+g\,G_{\widehat{\phi}\widehat{\phi}}(\vec{k},\mu)}.$$
(4.6.13)

In this final expression, the μ dependence is far from being a contact term in position space since

$$\mu\frac{\partial}{\partial\mu}\langle\phi(\vec{k},|z_1|)\phi(-\vec{k},0)\rangle_g = \frac{C_\phi}{(2\pi)}\frac{g\,G_{\phi\widehat{\phi}}(\vec{k},|z_1|)}{\left(1+g\,G_{\widehat{\phi}\widehat{\phi}}(\vec{k},\mu)\right)^2},$$
(4.6.14)

and, as such, it cannot be interpreted as a "small" conformal anomaly. The "small" conformal anomaly of (4.6.12) has exponentiated, leading to a "large" breaking of scale invariance and we conclude that the deformation (4.6.9) does not lead to a non-trivial conformal defect.

4.6.3 A monodromy defect in free theory

For our final example we couple a free scalar with non-trivial $\mathbb{Z}_2$ monodromy to a lower dimensional CFT_p equipped with an additional $SO(2)_I$ global symmetry. If the latter contains in its spectrum a operator $\widehat{\mathcal{O}}_s$ of dimension $\widehat{\Delta} = \frac{p-1}{2} - \delta$, charged under $SO(2)_I$ with spin $|s| = 1/2$, then we can consider an interaction that preserves the diagonal of $SO(2) \times SO(2)_I$:

$$S_{\mathrm{int}} = g\int \mathrm{d}^p x\ \psi_{\frac{1}{2}}^{(+)}\widehat{\mathcal{O}}_{-\frac{1}{2}} + \text{c.c.}$$
(4.6.15)

This coupling is consistent with unitarity if $p > 1$ and it is slightly relevant if $0 < \delta \ll 1$.

Since the three-point functions of $\psi_{1/2}^{(+)}$ vanish due to $SO(2)$ symmetry, the existence of an IR fixed point for the interaction (4.6.15) depends on certain complicated conditions that arise at the next-to-leading order in conformal perturbation theory.[25]

Assuming that there exists a non-trivial fixed point $g^2 \sim \delta$, one may wonder how this would fit in with our claims of the previous sections. The applicability of our theorem to defect setups hinges on the absence of the so-called $\psi^{(-)}$ modes in the bulk-defect operator expansion of the bulk field ϕ. For $p = 1$ these modes are excluded by cluster decomposition, but for $p > 1$ our theorem would still dictate that the dynamics of the CFT_p must decouple from the bulk if we could consistently set these modes to zero.

---

[25]At the next-to-leading order the existence of the fixed point depends on the sign of certain regularized integrals of the four-point function of the deformation, see e.g. [140, 149] and also [150] for the case of 1d CFTs.

As it happens, a deformation of the form (4.6.15) necessarily induces the appearance of the $\psi^{(-)}$ modes in the bulk-to-defect OPE of ϕ at order g. To establish this, it is sufficient to note that the bulk-to-defect two-point function between ϕ and $\widehat{\mathcal{O}}_{-1/2}$ is non-zero at order g:

$$\langle \phi(0,z,\bar{z})\widehat{\mathcal{O}}_{-s}(0)\rangle = - g \int \mathrm{d}^p w \, \frac{\bar{z}^s}{(|z|^2+|\vec{w}|^2)^{\Delta_\phi+s}} \frac{C_{\widehat{\mathcal{O}}\widehat{\mathcal{O}}}}{|\vec{w}|^{2\Delta_\phi-2s-2\delta}} + O(g^2)$$

$$= - g \, C_{\widehat{\mathcal{O}}\widehat{\mathcal{O}}} S_{p-1} \frac{\bar{z}^s}{|z|^p} \frac{\Gamma\left(\frac{p}{2}\right)\Gamma(s)}{2\Gamma\left(\frac{p}{2}+s\right)} + O(\delta^{\frac{3}{2}}), \quad s = 1/2. \qquad (4.6.16)$$

This result matches the expected form of a correlator between ϕ, and $\psi^{(-)}_{-1/2}$ – see equation (4.2.1) – with bulk-to-defect coefficients $b^{-,-1/2}_\phi \propto g$.

In conclusion, the deformation (4.6.15) could provide an example of a unitary, non-trivial conformal defect for $p > 1$. The way it is allowed to be non-trivial is consistent with our theorem.

4.7 Applications

For the single free scalar field ϕ the space of possible conformal defects is remarkably constrained, and in many cases the only allowed defects are trivial in the sense specified in the introduction. In all dimensions and co-dimensions the appearance of a $\psi^{(-)}$ mode in the bulk-to-defect expansion of ϕ is a necessary condition for a defect to not be trivial.

We should point out that our results also apply when the bulk theory has a decoupled real free scalar, since one can integrate out all the other bulk matter and conclude that the n-point functions of the scalar are trivial. This works in particular for some supersymmetric theories. For example, consider the surface defects in the Abelian $(2,0)$ theories in six dimensions that were recently discussed in [129]. If conformality is not spoiled by an anomaly as in the example discussed above, we would expect triviality of the scalar correlation functions. Another example are the aforementioned defects in the $\mathcal{N}=2$ four-dimensional free hypermultiplet. These appear to be labelled by a monodromy $\Phi \to e^{i\alpha}\Phi$ with Φ a complex scalar. We can immediately conclude that no defect can exist for $\alpha = 0$ and that for other values of α any non-triviality is allowed because of the single $\psi^{(-)}$ mode in the two-point function of the bulk scalar. This is in line with some recent explicit computations in [121]. In three dimensions our results also match with the supersymmetric literature: for example, the non-trivial defects in free $\mathcal{N}=4$ theories in [151] all appear to have a scale associated with them.

Defects and free scalar fields also naturally appear as the infrared description of vortices and Goldstone bosons in setup where a $U(1)$ global symmetry is spontaneously broken. In that case the size R of the vortex provides a natural scale. Our

results imply that interactions between the Goldstone degrees of freedom and the
vortex trivialize in the deep infrared when $R \to 0$. A good physical example of this
situation is the scattering of phonons off a vortex in superfluid helium. In this case a
microscopic model is available, and computations in for example [152] (but see also
references therein) confirm this view.

Let us finally point out an interesting possible extension of our results to con-
formal defects in (weakly) interacting theories. As explained in section 4.3 there are
always unphysical singularities when we apply the bulk-defect operator expansion
to three-point functions, and their cancellation will therefore imply a infinite and
non-trivial sum rule. It would be interesting to analyse these constraints further, for
example in an epsilon expansion or in a large N limit.

4.A   Details of the scalar bulk-to-defect OPE

In this appendix we give some details about the bulk-to-defect OPE of a scalar bulk
operator. We then specialize to the case where the bulk operator is a free field, and
we spell out the constraints imposed by the equations of motion on the spectrum of
its defect modes.

For the sake of completeness, we consider generic conformal defects of dimension
p and co-dimension q. In order to encode the $SO(p) \times SO(q)$ spin it is convenient to
contract the corresponding indices with "parallel" or "transverse" polarizations vec-
tors, respectively θ^a ($a = 1, \ldots, p$) and w^i ($i = 1, \ldots, q$), and work with polynomials
in these variables. The following definitions generalizes the ones given in (4.3.2)

$$\widehat{\mathcal{O}}_s^{a_1 \ldots a_j}(w, \vec{x}) \equiv w^{i_1} \ldots w^{i_s} \widehat{\mathcal{O}}^{a_1 \ldots a_j}{}_{i_1 \ldots i_s}(\vec{x}), \quad w \circ w = 0,$$
$$\widehat{\mathcal{O}}_s^{(j)}(w, \theta, \vec{x}) \equiv \theta^{a_1} \ldots \theta^{a_j} \widehat{\mathcal{O}}_s^{a_1 \ldots a_j}(w, \vec{x}), \quad \theta \bullet \theta = 0, \tag{4.A.1}$$

where the symbols $\circ$ and $\bullet$ represent, respectively, $SO(q)$-invariant and $SO(p)$-
invariant scalar products in real space.

The bulk-to-defect OPE of a scalar bulk operator $\Sigma(x)$ contains infinitely many
defect primaries $\widehat{\Sigma}_s$, scalars under $SO(p)$ and transforming as symmetric and traceless
tensors of $SO(q)$. If we neglect the contribution from defect descendants, we have
schematically

$$\Sigma(x) = \sum_{\widehat{\Sigma}, s} \frac{b_{\widehat{\Sigma}}^{\widehat{\Sigma}}}{|x_\perp|^{\Delta_\Sigma - \widehat{\Delta}_{\widehat{\Sigma}}}} (w \circ \hat{x})^s \, \widehat{\Sigma}_s(w, \vec{x}) + \ldots \tag{4.A.2}$$

In the expression above we introduced the unit vector $\hat{x}^i \equiv \frac{x^i}{|x_\perp|}$, orthogonal w.r.t.
the defect.[26] If we take the defect operators to be unit normalized, then the numbers

---

[26]To recover the operator's contribution in real space from the expression above it is sufficient to

$b_{\widehat{\Sigma}}^{\widehat{\Sigma}}$ are identified precisely with the bulk-to-defect couplings

$$\langle \Sigma(x)\widehat{\Sigma}_s(w,0)\rangle = \frac{b_{\Sigma}^{\widehat{\Sigma}}(w\circ\hat{x})^s}{|x_\perp|^{\Delta_\Sigma-\widehat{\Delta}_{\widehat{\Sigma}}}(x^2)^{\widehat{\Delta}_{\widehat{\Sigma}}}}. \tag{4.A.3}$$

The contribution from the defect descendants in (4.A.2) is completely encoded into (4.A.3). By comparing the bulk-to-defect OPE with (4.A.3) one finds [94]

$$\Sigma(x) = \sum_{\widehat{\Sigma},s}\sum_n \frac{b_{\Sigma}^{\widehat{\Sigma}}}{|x_\perp|^{\Delta_\Sigma-\widehat{\Delta}_{\widehat{\Sigma}}}} \frac{\left(-\frac{1}{4}|x_\perp|^2\vec{\nabla}_\parallel^2\right)^n}{n!\left(\widehat{\Delta}_{\widehat{\Sigma}}+1-\frac{p}{2}\right)_n}(w\circ\hat{x})^s\,\widehat{\Sigma}_s(w,\vec{x}). \tag{4.A.4}$$

We now specialize to the case where the bulk operator Σ is a free scalar, which we denote by ϕ, with defect modes ψ_s. As we have shown explicitly for co-dimension two defects in Section 4.2.2, the defect primaries that can couple to ϕ are selected by the free equation of motion. Requiring that the Laplacian annihilates (4.A.3) at separated points gives the following condition [94]

$$(\hat{\tau}-\Delta_\phi)(\Delta_\phi-\hat{\tau}+2-q-2s) = 0, \qquad \hat{\tau} = \widehat{\Delta}_{\widehat{\Sigma}}-s. \tag{4.A.5}$$

Assuming no further degeneracy, for each spin s at most two families of defect primaries are allowed in the bulk-to-defect OPE of ϕ. These two solutions, denoted as $\psi_s^{(\pm)}$, form a shadow pair on the defect

$$\psi_s^{(+)}: \quad \widehat{\Delta}_s^{(+)} = \Delta_\phi + s, \quad \text{or} \quad \psi_s^{(-)}: \quad \widehat{\Delta}_s^{(-)} = \Delta_\phi + 2 - q - s. \tag{4.A.6}$$

Crucially, the spin of the second family is restricted by unitarity (4.2.8) to the values $s \leq \frac{4-q}{2}$ (for $p > 1$) and $s \leq \frac{3-q}{2}$ (for $p = 1$). Note that for $q = p + 2$ there is a '$-$' mode of dimension zero and (as explained in the main text) by cluster decomposition we may assume it proportional to the defect identity $\mathbf{1}$. For $p > 2$ the primary that saturates the unitarity bound is a free field and must obey the Laplace equation, which is inconsistent with a non-zero two-point function with the bulk field ϕ. It can therefore be consistently removed from the spectrum. Altogether the unitary defect spectrum is summarized in table 4.1 in the main text.

4.B Two-point function in free theory for $q = 2$ defects

In this appendix we perform the computation of the two-point function of a free scalar in the presence of a twist defect. This computation was originally performed by the authors of [97], however we will obtain a slightly more general result. The

---

note that $(w\circ\hat{x})^s\,\widehat{\Sigma}_s(w,\vec{x})$ is mapped to $\hat{x}^{i_1}\dots\hat{x}^{i_s}\,\widehat{\Sigma}^{i_1\dots i_s}(\vec{x})$.

starting point is Green's equation (4.2.9), which we report here for convenience

$$-\Box G(x_1, x_2) = C_\phi\, \delta^{p+2}(x_1 - x_2), \quad C_\phi \equiv \frac{4\pi^{\frac{p}{2}+1}}{\Gamma\left(\frac{p}{2}\right)}. \qquad (4.B.1)$$

The normalization C_ϕ is chosen in such a way that

$$G(x_1, x_2) \underset{x_1 \to x_2}{\sim} \frac{1}{|x_1 - x_2|^{d-2}}. \qquad (4.B.2)$$

To solve Green's equation, it is convenient to Fourier transform to the p-dimensional momentum space along the defect and then adopt a basis of $SO(2)$ spherical harmonics. In terms of the complex coordinates $z_1 = |z_1|e^{i\varphi}$ and $z_2 = |z_2|$ we obtain

$$G(x_1, x_2) = \sum_s \int \frac{d^p k}{(2\pi)^p}\; e^{i\vec{k}\cdot\vec{x}_{12}} e^{is\varphi} a_s(|\vec{k}|, |z_1|, |z_2|), \qquad (4.B.3)$$

where the sum runs over all (half)-integers, depending on the choice of monodromy for ϕ. Denoting $|z_i| = r_i$ for simplicity of notation, we find that the modes a_s satisfy the following differential equation [27]

$$\left(|\vec{k}|^2 - \frac{\partial^2}{\partial r_1^2} - \frac{1}{r_1}\frac{\partial}{\partial r_1} + \frac{s^2}{r_1^2}\right) a_s(|\vec{k}|, r_1, r_2) = \frac{C_\phi}{2\pi}\frac{1}{r_1}\delta(r_1 - r_2). \qquad (4.B.4)$$

The homogeneous problem has a general solution given by $a_s(|\vec{k}|, r_1, r_2) = A(r_2)I_{|s|}(|\vec{k}|r_1) + B(r_2)K_{|s|}(|\vec{k}|r_1)$, where $I_s(x), K_s(x)$ are modified Bessel functions. Let us consider the region where $r_1 \geq r_2$. Then, regularity of the solution asymptotically far away from the defect, i.e. $r_1 \to \infty$, sets $A = 0$. In the region where $r_1 \leq r_2$, the $I_{|s|}(|\vec{k}|r)$ are regular while $K_{|s|}$ behave as

$$K_{|s|}(|\vec{k}|r) \underset{r \to 0}{\sim} |\vec{k}|^{-|s|}r^{-|s|} + |\vec{k}|^{|s|}r^{|s|},$$
$$K_0(|\vec{k}|r) \underset{r \to 0}{\sim} c\,\log(r|\vec{k}|) + c', \qquad (4.B.5)$$

for some constants c, c'. Due to the logarithmic singularity in the second line of the above, which is not allowed by conformal invariance, we are forced to set $B = 0$ for $s = 0$. For $|s| > 0$, on the other hand, there is no reason to impose regularity conditions at $r = 0$, since we do not expect the physics to be smooth in the proximity of the defect. In terms of the bulk-to-defect OPE, the singular modes in the first line of (4.B.5) take into account the presence of the defect primaries of dimensions $\Delta_\phi - |s|$. These singular solutions are compatible with unitarity as long as $p = 1$ or

---

[27]We used $\delta^2(x - x') = \frac{1}{r}\delta(\varphi - \varphi')\delta(r - r')$ and then $\delta(\varphi) = \frac{1}{2\pi}\sum_s e^{is\varphi}$.

$p > 1$ and $0 < |s| < 1$. Hence

$$a_s(|\vec{k}|, r_1, r_2) = \begin{cases} |s| \geq 0, & B_s^{\text{II}}(r_2)K_{|s|}(|\vec{k}|r_1), & r_1 \geq r_2, \\ |s| = 0 \text{ or } |s| \geq 1, & A_s^{\text{I}}(r_2)I_{|s|}(|\vec{k}|r_1), & r_1 \leq r_2, \\ 0 < |s| < 1, & A_s^{\text{I}}(r_2)I_{|s|}(|\vec{k}|r_1) + B_s^{\text{I}}(r_2)K_{|s|}(|\vec{k}|r_1), & r_1 \leq r_2. \end{cases}$$
(4.B.6)

For $p = 1$ the solution (4.B.5) is either a constant mode ($|s| = \frac{1}{2}$) or below the unitarity bound and we are free to set it to zero by choosing $B = 0$ for all s.[28] Let us now go back to the inhomogeneous problem and fix the solution (4.B.6) in order to reproduce the contact term in the r.h.s. of (4.B.4). To this end, we need to impose continuity of (4.B.6) at $r_1 = r_2$, and that the discontinuity of its first derivative at $r_1 = r_2$ equals precisely $\frac{C_\phi}{2\pi r_2}$. After some little algebra we find

$$a_s(|\vec{k}|, r_1, r_2) = \begin{cases} B_s^{\text{I}}(r_2)K_{|s|}(|\vec{k}|r_1) + \frac{C_\phi}{2\pi}I_{|s|}(|\vec{k}|r_2)K_{|s|}(|\vec{k}|r_1), & r_1 \geq r_2 \\ B_s^{\text{I}}(r_2)K_{|s|}(|\vec{k}|r_1) + \frac{C_\phi}{2\pi}I_{|s|}(|\vec{k}|r_1)K_{|s|}(|\vec{k}|r_2), & r_1 \leq r_2 \end{cases}$$
(4.B.7)

with the understanding that $B_s^{\text{I}}(r_2) \neq 0$ only for $p > 1$ and $0 < |s| < 1$. If we finally impose symmetry under exchange of the two external scalars, which are identical, we find the condition

$$B_s^{\text{I}}(r_1)K_{|s|}(|\vec{k}|r_2) = B_s^{\text{I}}(r_2)K_{|s|}(|\vec{k}|r_1),$$
(4.B.8)

which is satisfied by $B_s^{\text{I}}(r_2) = h_s K_{|s|}(|\vec{k}|r_2)$, for any real constant h_s. The final solution can be written as

$$G(x_1, x_2) = G^{(-)}(x_1, x_2) + G^{(+)}(x_1, x_2)$$
$$G^{(-)}(x_1, x_2) = \sum_{s=\pm\frac{1}{2}} \int \frac{d^p k}{(2\pi)^p} \, e^{i\vec{k}\cdot\vec{x}_{12}} e^{is\varphi} h_s K_{|s|}(|\vec{k}|r_1)K_{|s|}(|\vec{k}|r_2)$$
$$G^{(+)}(x_1, x_2) = \frac{C_\phi}{2\pi} \sum_{s\neq\pm\frac{1}{2}} \int \frac{d^p k}{(2\pi)^p} \, e^{i\vec{k}\cdot\vec{x}_{12}} e^{is\varphi} I_{|s|}(|\vec{k}|r_<)K_{|s|}(|\vec{k}|r_>),$$
(4.B.9)

where $r_< = \min(r_1, r_2)$ and $r_> = \max(r_1, r_2)$. Note that the expression above differs from the result of [97] by the additional contribution $G^{(-)}(x_1, x_2)$. One can explicitly

---

[28]Upon invoking cluster-decomposition principle, as we did in appendix 4.A.

perform the momentum-space integration in the first line of (4.B.9) to find

$$G^{(-)}(x_1, x_2) = \frac{2^{p-2} h_{\frac{1}{2}}}{(2\pi)^{\Delta_\phi - \frac{1}{2}}} \Gamma\left(\Delta_\phi - \frac{1}{2}\right) \frac{\cos\left(\frac{\varphi}{2}\right)}{(r_1 r_2)^{\Delta_\phi}} \frac{\left(\xi + \sqrt{\xi(\xi+4)} + 2\right)^{\Delta_\phi - \frac{1}{2}}}{\left(\xi + \sqrt{\xi(\xi+4)} + 4\right)^{2\Delta_\phi - 1}},$$

(4.B.10)

where we introduced the cross ratio

$$\xi = \frac{|\vec{x}_{12}|^2 + (r_1 - r_2)^2}{r_1 r_2}.$$

(4.B.11)

In real space, the spin s contribution to $G^{(+)}(x_1, x_2)$ is [97]

$$G_s^{(+)}(x_1, x_2) = \frac{\Gamma(\widehat{\Delta}_s^{(+)})}{\Gamma(\Delta_\phi)\,\Gamma\left(\widehat{\Delta}_s^{(+)} - \Delta_\phi + 1\right)} \frac{e^{is\varphi} \xi^{-\widehat{\Delta}_s^{(+)}}}{(r_1 r_2)^{\Delta_\phi}}$$

$$\times {}_2F_1\left(\widehat{\Delta}_s^{(+)}, \widehat{\Delta}_s^{(+)} - \frac{p-1}{2}; 2\widehat{\Delta}_s^{(+)} - p + 1; -\frac{4}{\xi}\right),$$

(4.B.12)

where $\widehat{\Delta}_s^{(+)} = \Delta_\phi + |s|$. Note that the result (4.B.12) is equivalent to (4.2.4) in virtue of the following identity

$$\xi^{-x} {}_2F_1\left(x, -\frac{p}{2} + x + \frac{1}{2}; -p + 2x + 1; -\frac{4}{\xi}\right) =$$

$$(\xi + 2)^{-x} {}_2F_1\left(\frac{x+1}{2}, \frac{x}{2}; -\frac{p}{2} + x + 1; \frac{4}{(\xi+2)^2}\right).$$

(4.B.13)

Note that if we impose trivial monodromy, the result (4.B.12) leads to the two-point function for a trivial defect:

$$\frac{1}{(x_1 - x_2)^{d-2}} = \sum_{s \in \mathbb{Z}} G_s^{(+)}(x_1, x_2).$$

(4.B.14)

For the twist defect in $p = 2$, we note that the generic solution (4.B.9) takes a simple form

$$G(x_1, x_2) = \frac{2\cos\left(\frac{\varphi}{2}\right)}{(x_1 - x_2)^2} \left(\frac{1}{\sqrt{\xi+4}} + \frac{h_{\frac{1}{2}}(1 - \cos\varphi + \xi/2)}{\sqrt{2}} \frac{\sqrt{2 + \xi + \sqrt{\xi(\xi+4)}}}{\left(4 + \xi + \sqrt{\xi(\xi+4)}\right)}\right),$$

(4.B.15)

which reduces to the result of [97] when we set $h_{\frac{1}{2}} = 0$.

Finally, by comparing (4.B.9) with the defect channel blocks (4.2.4) we can

extract the relevant bulk-to-defect OPE coefficients:

$$|b_\phi^{s,+}|^2 + (p-1)|b_\phi^{s,-}|^2 = \frac{(\Delta_\phi)_{|s|}}{|s|!},$$

$$|b_\phi^{s,-}|^2 = \delta_{|s|,\frac{1}{2}} \frac{h_{\frac{1}{2}}}{4\pi^{\Delta_\phi - \frac{1}{2}}} \Gamma\left(\Delta_\phi - \frac{1}{2}\right),$$

$$0 \le h_{\frac{1}{2}} \le \frac{4\pi^{p/2-1}}{\Gamma\left(\frac{p}{2}\right)}. \tag{4.B.16}$$

The inequality in the last line follows from $|b_\phi^{s,\pm}| \ge 0$, which is required by reflection-positivity.

4.C Three-point functions from the bulk-to-defect OPE

This appendix contains the derivations of the defect conformal blocks presented in section 4.3. In what follows we will keep p, q generic, for the sake of completeness. As a further generalization, we will take the bulk scalar to be generic, i.e. not necessarily free, and denote it as Σ (as we did in appendix 4.A).

Let us start from deriving the defect expansion of

$$\langle \Sigma(x_1) \widehat{\mathcal{O}}_{s_2}(w_2, \vec{x}_2) \widehat{T}_{s_3}^{(j)}(w_3, \theta, \infty) \rangle. \tag{4.C.1}$$

In the expression above, $\widehat{\mathcal{O}}$ and $\widehat{T}$ are symmetric and traceless tensors of $SO(q)$, respectively of spin s_2 and s_3. The dependence on the $SO(p) \times SO(q)$ is encoded into polynomials in the polarization vectors $\{w_i\}, \theta$, as explained in appendix 4.A.

The starting point is the three-point functions between the defect modes of Σ, denoted as $\widehat{\Sigma}$, and any other two defect operators:

$$\langle \widehat{\Sigma}_{s_1}(w_1, \vec{x}_1) \widehat{\mathcal{O}}_{s_2}(w_2, \vec{x}_2) \widehat{T}_{s_3}^{(j)}(w_3, \theta, \infty) \rangle = \frac{\hat{f}_{\widehat{\Sigma}\widehat{\mathcal{O}}\widehat{T}}}{|\vec{x}_{12}|^{\widehat{\Delta}_{\widehat{\Sigma}} + \widehat{\Delta}_{\widehat{\mathcal{O}}} - \widehat{\Delta}_{\widehat{T}}}} P_\perp^{(s_1,s_2,s_3)}(\{w_i\}) P_\parallel^{(j)}(\hat{x}_{12}, \theta). \tag{4.C.2}$$

The $SO(p)$ spin is encoded in the polynomials $P_\parallel^{(j)}$, which were already introduced in (4.3.6). The $SO(q)$ spin dependence is captured by the polynomials $P_\perp^{(s_1,s_2,s_3)}$, which are homogeneous of degree s_i in the transverse polarization vectors w_i

$$P_\perp^{(s_1,s_2,s_3)}(\{w_i\}) \equiv (w_1 \circ w_2)^{\frac{1}{2}(s_1+s_2-s_3)}(w_1 \circ w_3)^{\frac{1}{2}(s_1-s_2+s_3)}(w_2 \circ w_3)^{\frac{1}{2}(s_2-s_1+s_3)}, \tag{4.C.3}$$

where s_i are non-negative integers satisfying

$$s_1 + s_2 - s_3 = 2n_1, \quad s_1 - s_2 + s_3 = 2n_2, \quad s_2 - s_1 + s_3 = 2n_3, \qquad n_i \in \mathbb{N}. \tag{4.C.4}$$

Note that the w_1, w_2, w_3's cannot be linearly independent for $q = 2$, and as such the basis (4.C.3) becomes over-complete.

To compute (4.C.1), we apply the bulk-to-defect OPE (4.A.4) on the three-point functions (4.C.2). The derivatives in the parallel directions commute with the $SO(q)$ polynomials and, making use of the identity

$$\nabla^{2n}_{\vec{x}_{12}} \left(\frac{(-\vec{x}_{12} \bullet \theta)^j}{|\vec{x}_{12}|^{2t}} \right) = 4^n (t)_n \left(1 + t - j - \frac{p}{2} \right)_n \frac{(-\vec{x}_{12} \bullet \theta)^j}{|\vec{x}_{12}|^{2t+2n}}, \qquad (4.C.5)$$

we can find the following series representation

$$\langle \Sigma(x_1) \widehat{\mathcal{O}}_{s_2}(w_2, \vec{x}_2) \widehat{T}^{(j)}_{s_3}(w_3, \theta, \infty) \rangle =$$

$$\frac{P^{(j)}_{\parallel}(\hat{x}_{12}, \theta)}{|x_{1\perp}|^{\Delta_\Sigma + \widehat{\Delta}_{\widehat{\mathcal{O}}} - \widehat{\Delta}_{\widehat{T}}}} \sum_{\widehat{\Sigma}, s} b^{\widehat{\Sigma}}_{\widehat{\Sigma}} \, \hat{f}_{\widehat{\Sigma}\widehat{\mathcal{O}}\widehat{T}} \, P^{(s, s_2, s_3)}_{\perp}(\{w_i\})(w \circ \hat{x}_1)^s \times$$

$$\times \, \hat{\chi}^{\kappa_{\widehat{\Sigma}\widehat{\mathcal{O}}\widehat{T}} + \frac{j}{2}} \sum_n \frac{(-\hat{\chi})^{-n}}{n!} \frac{(-\kappa_{\widehat{\Sigma}\widehat{\mathcal{O}}\widehat{T}})_n \left(1 - \frac{p}{2} - j - \kappa_{\widehat{\Sigma}\widehat{\mathcal{O}}\widehat{T}} \right)_n}{\left(\widehat{\Delta}_{\widehat{\Sigma}} - \frac{p}{2} + 1 \right)_n}, \quad (4.C.6)$$

where we introduced the parameter

$$\kappa_{\widehat{\Sigma}\widehat{\mathcal{O}}\widehat{T}} = -\frac{1}{2}(\widehat{\Delta}_{\widehat{\Sigma}} + \widehat{\Delta}_{\widehat{\mathcal{O}}} - \widehat{\Delta}_{\widehat{T}} + j), \qquad (4.C.7)$$

as well as the cross-ratio (4.3.9). The sum over s is truncated to those values that satisfy $SO(q)$ selection rules (4.C.4). Finally, the sum over n can be performed for generic values of the parameters. The results is a beautiful Hypergeometric function

$$\mathcal{F}^{\widehat{\mathcal{O}}\widehat{T}}_{\widehat{\Sigma}}(\hat{\chi}) = \hat{\chi}^{\kappa_{\widehat{\Sigma}\widehat{\mathcal{O}}\widehat{T}} + \frac{j}{2}} \, {}_2F_1 \left(1 - \frac{p}{2} - j - \kappa_{\widehat{\Sigma}\widehat{\mathcal{O}}\widehat{T}}, -\kappa_{\widehat{\Sigma}\widehat{\mathcal{O}}\widehat{T}}, 1 - \frac{p}{2} + \widehat{\Delta}_{\widehat{\Sigma}}; -\frac{1}{\hat{\chi}} \right). \quad (4.C.8)$$

When we take the bulk operator to be a free scalar, the expression above gives precisely eq. (4.3.10). This result, can also be obtained by solving the relevant Casimir equation as done in [153].[29] Importantly, the defect blocks $\mathcal{F}$ are completely blind to the transverse directions. In particular they only depend on the parallel dimension p, and *not* on q.

Let us now consider the bulk-bulk-defect three-point function

$$\langle \Sigma(x_1) \Sigma(x_2) \widehat{T}^{(j)}_s(w, \theta, \infty) \rangle. \qquad (4.C.9)$$

Again, we will not require Σ to be a free scalar. The complete form of the expression

---

[29]We do not find perfect agreement with the block calculated in [153]. We obtained the same Casimir equation however our block is a different linear combination of solutions. The solution of [153] does not seem to be consistent with the OPE limit.

above can be obtained by applying once again the bulk-to-defect OPE to eq. (4.C.6) and then resum the descendants. In practise it is easier to start from the three-point functions

$$\langle\widehat{\Sigma}_{s_1}(w_1,\vec{x}_1)\widehat{\Sigma}'_{s_2}(w_2,\vec{x}_2)\widehat{T}_s^{(j)}(w,\theta,\infty)\rangle = \frac{\hat{f}_{\widehat{\Sigma}\widehat{\Sigma}'\widehat{T}}}{|\vec{x}_{12}|^{\widehat{\Delta}_{\widehat{\Sigma}}+\widehat{\Delta}_{\widehat{\Sigma}'}-\widehat{\Delta}_{\widehat{T}}}}P_\perp^{(s_1,s_2,s)}(\{w_i\})P_\parallel^{(j)}(\hat{x}_{12},\theta),$$

$$(4.C.10)$$

and apply twice on it the bulk-to-defect OPE (4.A.4). Making use twice of the identity (4.C.5) we obtain

$$\langle\Sigma(x_1)\Sigma(x_2)\widehat{T}_s^{(j)}(w,\theta,\infty)\rangle = \sum_{\widehat{\Sigma},\widehat{\Sigma}',s_1,s_2} b_\Sigma^{\widehat{\Sigma}} b_\Sigma^{\widehat{\Sigma}'}\,\hat{f}_{\widehat{\Sigma}\widehat{\Sigma}'\widehat{T}}$$

$$\times \sum_{m,n}\frac{(-1)^{m+n}}{m!n!}\frac{|x_{1\perp}|^{\widehat{\Delta}_{\widehat{\Sigma}}-\Delta_\Sigma+2n}|x_{2\perp}|^{\widehat{\Delta}_{\widehat{\Sigma}'}-\Delta_\Sigma+2m}}{|\vec{x}_{12}|^{-2\kappa_{\widehat{\Sigma}\widehat{\Sigma}'}+2m+2n-j}}$$

$$\times \frac{(-\kappa_{\widehat{\Sigma}\widehat{\Sigma}'})_m(-\kappa_{\widehat{\Sigma}\widehat{\Sigma}'}+m)_n\left(-\kappa_{\widehat{\Sigma}\widehat{\Sigma}'}-\hat{h}-j\right)_m\left(-\kappa_{\widehat{\Sigma}\widehat{\Sigma}'}+m-\hat{h}-j\right)_n}{\left(\widehat{\Delta}_{\widehat{\Sigma}}-\hat{h}\right)_n\left(\widehat{\Delta}_{\widehat{\Sigma}'}-\hat{h}\right)_m}$$

$$\times \underbrace{(w_1\circ\hat{x}_1)^{s_1}(w_2\circ\hat{x}_2)^{s_2}P_\perp^{(s_1,s_2,s)}(w_1,w_2,w)}_{\mathcal{W}_\perp^{(s_1,s_2,s)}(\hat{x}_1,\hat{x}_2,w)}P_\parallel^{(j)}(\hat{x}_{12},\theta),\qquad(4.C.11)$$

where we introduced

$$\kappa_{\widehat{\Sigma}\widehat{\Sigma}'}\equiv-\frac{1}{2}(\widehat{\Delta}_{\widehat{\Sigma}}+\widehat{\Delta}_{\widehat{\Sigma}'}-\widehat{\Delta}_{\widehat{T}}+j),\quad\hat{h}\equiv\frac{p}{2}-1.\qquad(4.C.12)$$

The integers s_1,s_2,s are constrained by the selection rules (4.C.4). Resumming this expression is expected to be hard since this configuration is characterized by three cross-ratios (compare to (4.2.3)),

$$\chi\equiv\frac{|\vec{x}_{12}|^2+|x_{1\perp}|^2+|x_{2\perp}|^2}{|x_{1\perp}||x_{2\perp}|},\quad t\equiv\frac{|x_{1\perp}|}{|x_{2\perp}|},\quad\cos\varphi\equiv\hat{x}_1\circ\hat{x}_2.\qquad(4.C.13)$$

For our purposes, which is studying the bulk OPE limit of (4.C.9), it will be sufficient to specialize (4.C.11) to the "cylindrical" configuration

$$x_1^i=|z|n_1^i,\quad x_2^i=|z|n_2^i,\quad n_1\circ n_2=\cos\varphi,\quad n\circ n=1,\quad t=1,\qquad(4.C.14)$$

where the resummation can be performed easily. In terms of the cross-ratio $\hat{\chi}$ defined

in (4.3.9) we find:

$$\mathcal{F}_{\widehat{\Sigma}\widehat{\Sigma}'}^{\widehat{T}}(\hat{\chi}) = \hat{\chi}^{-\frac{1}{2}(\widehat{\Delta}_{\widehat{\Sigma}}+\widehat{\Delta}_{\widehat{\Sigma}'}-\widehat{\Delta}_{\widehat{T}})}$$

$$_4F_3\left(\overline{\Delta}_{12} - \hat{h} - \frac{1}{2}, \overline{\Delta}_{12} - \hat{h}, -\kappa_{\widehat{\Sigma}\widehat{\Sigma}'}, -\kappa_{\widehat{\Sigma}\widehat{\Sigma}'} - j - \hat{h}; \widehat{\Delta}_{\widehat{\Sigma}} - \hat{h}, \widehat{\Delta}_{\widehat{\Sigma}'} - \hat{h}, 2\overline{\Delta}_{12} - 2\hat{h} - 1; -\frac{4}{\hat{\chi}}\right),$$

$$(4.C.15)$$

where we defined $\overline{\Delta}_{12} \equiv \frac{1}{2}(\widehat{\Delta}_{\widehat{\Sigma}} + \widehat{\Delta}_{\widehat{\Sigma}'})$. When we take Σ to be a free scalar we find precisely the blocks (4.3.20). Furthermore, from this result we can recover the blocks for the two-point function shown in eq.(4.2.4) by simply setting $\widehat{\Sigma} = \widehat{\Sigma}'$ and the third operator to be the identity. In this case, the functions $\mathcal{W}_\perp^{(s_1,s_1,0)}$ become Gegenbauer polynomials of $\cos\varphi$

$$\mathcal{W}_\perp^{(s,s)}(\hat{x}_1, \hat{x}_2) = (w_1\circ\hat{x}_1)^s (w_2\circ\hat{x}_2)^s (w_1\circ w_2)^s = \frac{s!}{2^s(\frac{q}{2}-1)_s}C_s^{(\frac{q}{2}-1)}(\cos\varphi). \quad (4.C.16)$$

Finally, after the hypergeometric transformation (4.B.13), the $_4F_3$ in (4.C.15) simply reduces to (4.2.4).

Chapter 5

Regge Trajectories for the (2,0) Theories

5.1 Introduction

The advent of Regge theory in the 1960s led to a profound improvement in our understanding of relativistic scattering amplitudes, relating in particular their high-energy behaviour to the spectrum of resonances and bound states. Holography led to expectations that a similar structure should exist in CFTs [34, 35, 154, 155], but it was only recently that these ideas became formalised non-perturbatively in a seminal paper by Caron-Huot [1].

The results of [1] indicate that a CFT spectrum organizes itself in *Regge trajectories* with spectra and OPE coefficients that are smooth functions of the spin ℓ. This picture elucidates the remarkable smoothness of numerically obtained OPE data, for example that of the three-dimensional Ising model analysed in [36, 156], and goes some way towards explaining the success of large spin perturbation theory [157, 158], see for example [159, 160]. As has become customary in the literature, we will use the expression "analyticity in spin" (of the OPE data) to refer to this circle of ideas.

It should be pointed out explicitly that so far analyticity in spin is at best an assumption with many supporting evidences. Caron-Huot's Lorentzian inversion formula in [1] has the potential to establish analyticity in spin down to the leading Regge trajectory. For this establishment to be rigorous one has to understand the scaling behaviour of the conformal correlators in both the Regge limit and the second-sheet lightcone limit, in which the Lorentzian inversion integral can potentially diverge. However, currently a rigorous calculation of the scaling behaviour in the second-sheet lightcone limit is still unknown. (See Section 5.4.3 for discussions in more details.) Moreover, even if the convergence of the Lorentzian inversion formula is understood, it is unclear how to extend analyticity in spin beyond the leading Regge trajectory. This is related to the fact that the OPE density function in the most

generic case is a complex function of two complex variables, scaling dimension and spin. There is also a priori no reason to assume all of the singularities in the OPE density function are just simple poles but not including other types of singularities such as branch cuts.

One important caveat concerns the behaviour for the lowest possible spins. For spins below some critical value $\ell^\star$ it becomes much harder to use analyticity in spin to extract concrete information about the spectrum of the theory, see for example [160, 161] for some attempts for the three-dimensional Ising and $O(2)$ models. According to the analysis in [1] the exact value of ℓ^* is related to the behaviour of the correlation function in the Regge limit. For a generic unitary CFT, it was deduced in [1] that $\ell^* \leqslant 1$ because its (suitably normalized) correlation functions are bounded by a constant in the Regge limit. A priori the spin 1 and spin 0 OPE data therefore do not need to smoothly connect to the higher spin OPE data.

In supersymmetric theories everything is better, and it is therefore worthwhile to investigate how analyticity in spin for conformal theories combines with supersymmetry. A first positive sign is that the analyticity in spin can extend also to lower spins in the theory, simply because a superconformal primary of spin $\ell \leqslant \ell^*$ can have conformal primary descendants of spin $\ell > \ell^*$ and OPE coefficients related by supersymmetry. Since the scaling dimensions of these descendants are simply integer-shifted compared to that of the primary, and the coefficients of each descendant conformal block are often equal to that of the primary times a simple rational function of Δ and ℓ, analyticity in spin of such a non-vanishing descendant trajectory would imply analyticity in spin of the primary trajectory[1] also below ℓ^*!

In this chapter we undertake a study of the non-perturbative implications of analyticity in spin for supersymmetric conformal field theories (SCFTs). We have chosen to focus on the six-dimensional $(2,0)$ theories, but at a qualitative level our results certainly extend to theories in lower dimensions and likely also to theories with less supersymmetry – we comment on this further in section 5.7.[2] The particular four-point function we analyse is that of the superconformal primary of the stress tensor multiplet. This is the same four-point function as was analysed holographically in [166, 167], and with numerical bootstrap methods in [18]. Perturbatively, in a large c expansion, this correlator was also studied in [162], taking as input the tree-level results of [168, 169]; and in [170–172]. The form of the superconformal Ward identities and superconformal blocks can be extracted from the more general analysis of [173].

---

[1]We caution the reader that this does not automatically ensure analyticity in spin of the full OPE data, *i.e.* including that of descendants, below ℓ^*. We will provide concrete counterexamples below.

[2]At a perturbative level the Lorentzian inversion formula of [1] has already been widely used for superconformal theories. For the $(2,0)$ theories there are for large c computations in [162], while $\mathcal{N} = 4$ SYM was studied in an expansion in $1/c$ in [163, 164]. An approximate spectrum for large, but finite ℓ was also studied through the inversion formula for certain $\mathcal{N} = 2$ theories in [165].

$$\mathscr{D}[2,0] \times \mathscr{D}[2,0] \sim \mathbf{1} + \underbrace{\mathscr{D}[2,0] + \mathscr{D}[4,0] + \mathscr{B}[2,0]_\ell} + \underbrace{\mathscr{D}[0,4] + \mathscr{B}[0,2]_\ell} + \mathscr{L}[0,0]_{\Delta,\ell}$$

$$\ell \to -4 \qquad (\Delta, \ell) \to (4, -2)$$
$$\ell \to -2 \qquad \ell \to -1$$
$$(\Delta, \ell) \to (2, -2)$$
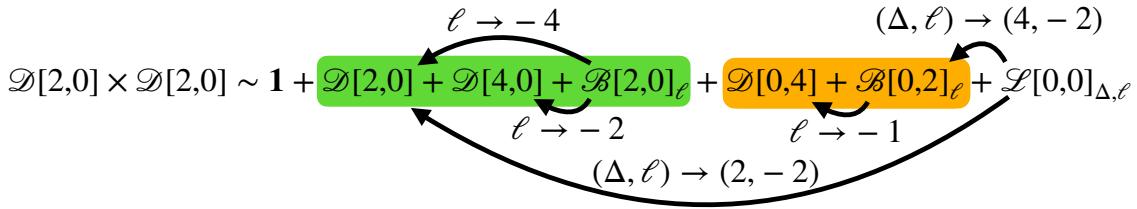
Figure 5.1. The self-OPE of the stress tensor multiplet. See the main text for further explanations.

5.1.1 Summary of results

Sections 5.3 and 5.6 contain our key results. The results of section 5.3 are summarized in figure 5.1. Unfortunately its explanation requires a minimal understanding of the rather technical superconformal block decomposition. We review this in section 5.2 and provide the essentials in the next paragraph.

We follow the notation of [18] and denote superconformal multiplets as $\mathcal{X}[p,q]_{\Delta,\ell}$ with (Δ, ℓ) and $[p, q]$ respectively corresponding to the conformal representation and the $\mathfrak{so}(5)$ R-symmetry Dynkin labels of the superconformal primary, and with $\mathcal{X} \in \{\mathcal{L}, \mathcal{A}, \mathcal{B}, \mathcal{C}, \mathcal{D}\}$ denoting the type of shortening condition. Long multiplets are denoted $\mathcal{L}$ and maximally short (half-BPS) multiplets are denoted $\mathcal{D}$. For short multiplets we do not write Δ because it is fixed by the other quantum numbers, and similarly we omit ℓ for the $\mathcal{D}$-type multiplets because it is always zero. Using this language the stress tensor multiplet is known to be a $\mathcal{D}[2,0]$ multiplet and in its self-OPE we find the six non-trivial multiplets shown in figure 5.1. (The Ward identities also allow for $\mathcal{B}[0,0]_\ell$ multiplets but these contain higher spin currents and appear only in the free theory, as well as for $\mathcal{D}[2,2]$ and $\mathcal{D}[0,2]$ multiplets which are excluded by Bose symmetry.) Out of the five types of short multiplets there are three, shaded in green, whose OPE coefficients are completely fixed by virtue of the chiral algebra construction of [174, 175]. For the other short multiplets, which are shaded in orange, the coefficients are generally not known. For the long multiplets we know neither the scaling dimensions nor the coefficients.

Given this rather involved structure of the superconformal OPE, it is a natural question to ask how the superconformal blocks organize themselves into Regge trajectories. The answer to this question turns out to be surprisingly involved. First of all, it is important to realize that a single Regge trajectory for superconformal primaries will induce many Regge trajectories corresponding to the conformal primary superdescendants. And because some of those descendant trajectories have higher spin, it becomes necessary to extend the superconformal trajectories to *negative spin* to get a complete picture. In doing so some obvious connections appear: the results that we review in section 5.2 (in particular table 5.1) indicate that the $\mathcal{D}[4, 0]$ and $\mathcal{D}[0, 4]$ multiplets find a natural place in the (straight) Regge trajectories of the $\mathcal{B}$-

type multiplets: the latter as the continuation of the $\mathcal{B}[0,2]_\ell$ multiplet to spin -1, and the former as the continuation of the $\mathcal{B}[2,0]_\ell$ multiplet to spin -2. What is less obvious, however, is that the $\mathcal{D}[2,0]$ multiplet itself does not fit into these trajectories. Instead, one finds that it is a combination of (i) the continuation to spin -2 of a long, unprotected Regge trajectory, and (ii) the continuation to spin -4 of the straight $\mathcal{B}[2,0]_\ell$ trajectory. Finally, the continuation of the $\mathcal{B}[0,2]_\ell$ trajectory to spin -3 induces unwanted (descendant) blocks which can be cancelled by the continuation to spin -2 of another unprotected long trajectory.

Altogether, then, analyticity in spin intertwines the straight and curved Regge trajectories in intricate ways, and multiplets with protected OPE coefficients or dimensions can appear on unprotected trajectories. This results in a non-trivial interplay between supersymmetry and analyticity in spin.[3]

As we also review in section 5.2, the unfixed OPE data for the four-point function of the $\mathcal{D}[2,0]$ multiplet is captured in a single function $a(z, \bar{z})$. This function shares many similarities with an ordinary CFT four-point function and in particular has a standard conformal block decomposition in the s-channel. It is therefore natural to try to apply the Lorentzian inversion formula of [1] directly to this function. In section 5.4 we will set up the inversion procedure. We analyse numerous subtleties, leading ultimately to a picture of the analytic structure of the corresponding spectral density as shown in figure 5.6 on page 173. In line with our previous discussion, the ℓ axis extends to *negative spins*: in fact, the rather soft Regge behaviour of $a(z, \bar{z})$ leads one to conclude that $\ell_* \leqslant -3$! In the figure we also observe two straight Regge trajectories corresponding to the two types of protected operators of figure 5.1, and the intersection of the leading long trajectory with a short trajectory at spin -2 as dictated by the analysis of section 5.3.

The observation that $\ell_* < 0$ means that, unlike in non-supersymmetric theories, *all* the physical supermultiplets appearing in the $\mathcal{D}[2,0]$ self-OPE are expected to be reachable via Regge trajectories. This leads one to the appealing prospect that this four-point function can (at least approximately) be bootstrapped: we iteratively apply the Lorentzian inversion formula to some initial trial spectrum until we hit a fixed point. Of course, with an OPE as in figure 5.1 the natural trial spectrum consists of the operators fixed by the chiral algebra.

In section 5.6 we present the initial results of such an approach. The first 'inversion' of the protected data in the t-channel yields an approximate s-channel spectrum whose long multiplets are of double-twist type, with anomalous dimensions that we

---

[3]A somewhat orthogonal result is presented in section 5.3.4: we find new constraints on the coefficients for the conformal block decomposition of the superconformal blocks themselves. These coefficient are of course already determined by the superconformal algebra, but our constraints arise from analyticity in spin and shadow symmetry, and we checked they are satisfied by the superblocks. Similar constraints should hold for the blocks in any SCFT as well as for the decomposition of an ordinary conformal block in lower-dimensional conformal blocks as in [176].

estimate. We then refine our estimate by inverting the *leading* Regge trajectory several times until we hit a fixed point. Although this procedure ignores the subleading Regge trajectories, for sufficiently large c the resulting scaling dimensions and OPE coefficients nicely track the numerical bootstrap bounds of [18] — see the numerous figures in section 5.6 starting on page 187. We therefore believe that a more complete iterative scheme would converge to the same 'extremal' solutions as those found with numerical bootstrap methods.

5.2 The four-point function

We consider the four-point function of the dimension four scalar which forms the bottom component of the $\mathcal{D}[2,0]$ stress tensor multiplet in the six-dimensional $(2,0)$ theories. Knowledge of this correlator allows for the computation of any four-point function involving only operators in the stress tensor superconformal multiplet [173], thus making it a natural object to study. Our conventions are exactly those of [18] from which we have lifted some of the equations and to which we refer the reader for more details. The essential summary is as follows. Our scalar transforms in the 14-dimensional $[2,0]$ representation of the $\mathfrak{so}(5)$ R-symmetry algebra. Since

$$[2,0] \otimes [2,0] = [0,0] \oplus [2,0] \oplus [0,2] \oplus [4,0] \oplus [0,4] \oplus [2,2] \,, \qquad (5.2.1)$$

the four-point function features six different R-symmetry channels $A_R(z,\bar{z})$ with R labelling the representations on the right-hand side. Our conventions for the four-point function and the R-symmetry projectors are given in appendix 5.A. As usual, conformal symmetry and the operator product expansion dictate that each of these admits a decomposition into ordinary conformal blocks:

$$A_R(z,\bar{z}) = \sum \lambda_{R\,\Delta,\ell}^2 \mathcal{G}_\Delta^{(\ell)}(z,\bar{z}) \,, \qquad (5.2.2)$$

but supersymmetry imposes far stricter constraints. First of all, for this correlator, the information in all six channels is completely encoded by two functions:

$$a(z,\bar{z}) \qquad \text{and} \qquad h(z) \,. \qquad (5.2.3)$$

As indicated, the second function is independent of $\bar{z}$. The relation is through simple second-order derivative operators. To fix ideas let us quote them here in full [173]:

$$A_{[4,0]}(z,\bar{z}) = \frac{1}{6}u^4\Delta_2\left[u^2 a(z,\bar{z})\right] \ ,$$

$$A_{[2,2]}(z,\bar{z}) = \frac{1}{2}u^4\Delta_2\left[u(v-1)a(z,\bar{z})\right] \ ,$$

$$A_{[0,4]}(z,\bar{z}) = \frac{1}{6}u^4\Delta_2\left[u(3(v+1)-u)a(z,\bar{z})\right] \ ,$$

$$A_{[0,2]}(z,\bar{z}) = \frac{1}{2}u^4\Delta_2\left[(v-1)\left((v+1)-\frac{3}{7}u\right)a(z,\bar{z})\right]$$
$$-u^2\left(\frac{(z-2)zh'(z)+(\bar{z}-2)\bar{z}h'(\bar{z})}{2(z-\bar{z})^2}+(z+\bar{z}-z\bar{z})\frac{h(z)-h(\bar{z})}{(z-\bar{z})^3}\right) \ ,$$

$$A_{[2,0]}(z,\bar{z}) = \frac{1}{2}u^4\Delta_2\left[\left((v-1)^2-\frac{1}{3}u(v+1)+\frac{2}{27}u^2\right)a(z,\bar{z})\right]$$
$$+u^2\left(z\bar{z}\frac{h(z)-h(\bar{z})}{(z-\bar{z})^3}-\frac{z^2h'(z)+\bar{z}^2h'(\bar{z})}{2(z-\bar{z})^2}\right) \ ,$$

$$A_{[0,0]}(z,\bar{z}) = \frac{1}{4}u^4\Delta_2\left[\left((v+1)^2-\frac{1}{5}(v-1)^2-\frac{3}{5}u(v+1)+\frac{3}{35}u^2\right)a(z,\bar{z})\right]$$
$$-u^2\frac{(5(1-z)+z^2)h'(z)+(5(1-\bar{z})+\bar{z}^2)h'(\bar{z})}{5(z-\bar{z})^2}$$
$$+u^2\left(2z\bar{z}+5(1-z)+5(1-\bar{z})\right)\frac{h(z)-h(\bar{z})}{5(z-\bar{z})^3} \ . \tag{5.2.4}$$

with the operator

$$\Delta_2 f(z,\bar{z}) := \left(\frac{\partial^2}{\partial z\partial\bar{z}}-\frac{2}{z-\bar{z}}\left(\frac{\partial}{\partial z}-\frac{\partial}{\partial\bar{z}}\right)\right)z\bar{z}f(z,\bar{z}) \ . \tag{5.2.5}$$

and with $u=z\bar{z}$ and $v=(1-z)(1-\bar{z})$ as usual.

Equation (5.2.4) automatically resolves all the constraints of the superconformal Ward identities and was first published in [173]. The deeper reason for the appearance of a meromorphic function $h(z)$ is the existence of a chiral algebra for the six-dimensional $(2,0)$ theories [174, 175].

5.2.1 Superconformal block decomposition

A related consequence of supersymmetry is the grouping of ordinary conformal blocks into superconformal blocks. In the OPE under consideration there can appear eight types of supermultiplets [166, 167, 177, 178]:

$$\mathcal{D}[2,0]\times\mathcal{D}[2,0] \sim \mathbf{1}+\mathcal{D}[2,0]+\mathcal{D}[4,0]+\mathcal{D}[0,4]+\mathcal{B}[2,0]_\ell+\mathcal{B}[0,2]_\ell+\mathcal{B}[0,0]_\ell+\mathcal{L}[0,0]_{\Delta,\ell} \ . \tag{5.2.6}$$

As indicated, some multiplets can have non-zero spin ℓ (which are necessarily odd for the $\mathcal{B}[0, 2]$ multiplets and even for the other multiplets by Bose symmetry). The last type of multiplets are the unprotected or 'long' multiplets and can also have arbitrary Δ (provided it lies above the unitarity bound, $\Delta > \ell + 6$). The $\mathcal{B}[0, 0]_\ell$ multiplets contain higher spin currents and will therefore no longer be considered in this work. The contribution of each multiplet to the four-point function is most easily captured by stating their contribution to $a(z, \bar{z})$ and $h(z)$; this is given in table 5.1 with the listed 'atomic' contributions given by [18]:

$$
\begin{aligned}
a_{\Delta,\ell}^{\text{at}}(z, \bar{z}) &= \frac{4}{z^6 \bar{z}^6 (\Delta - \ell - 2)(\Delta + \ell + 2)} \mathcal{G}_{\Delta+4}^{(\ell)}(\Delta_{12} = 0, \Delta_{34} = -2; z, \bar{z}) , \\
h_\beta^{\text{at}}(z) &= \frac{z^{\beta-1}}{1 - \beta} {}_2F_1[\beta - 1, \beta; 2\beta, z] ,
\end{aligned}
\tag{5.2.7}
$$

where $\mathcal{G}_{\Delta+4}^{(\ell)}(\Delta_{12} = 0, \Delta_{34} = -2; z, \bar{z})$ is an ordinary (non-supersymmetric) six-dimensional conformal block, but for a four-point function of operators with unequal scaling dimension $\Delta_{i=1,\ldots 4}$. We also introduced $\Delta_{ij} := \Delta_i - \Delta_j$. The explicit form of the block is given in (5.A.4). We also use the notation

$$
\mathcal{G}_\Delta^{(\ell)}(z, \bar{z})
\tag{5.2.8}
$$

for a block with $\Delta_{12} = \Delta_{34} = 0$. With (5.2.7) in hand one can verify, as was done in [18], that for each line in table 5.1 the application of the operators in equation (5.2.4) yields a finite sum of ordinary conformal blocks with the expected quantum numbers in each of the six R-symmetry channels — see the figures in the next section for examples.

$\mathcal{X}$	Δ	$a^{\mathcal{X}}(z, \bar{z})$	$h^{\mathcal{X}}(z)$	comments
$\mathcal{L}[0, 0]_{\Delta,\ell}$	Δ	$a_{\Delta,\ell}^{\text{at}}(z, \bar{z})$	0	generic long multiplet, $\Delta > \ell + 6$
$\mathcal{B}[0, 2]_{\ell-1}$	$\ell + 7$	$a_{\ell+6,\ell}^{\text{at}}(z, \bar{z})$	0	$\ell > 0$
$\mathcal{D}[0, 4]$	8	$a_{6,0}^{\text{at}}(z, \bar{z})$	0	
$\mathcal{B}[2, 0]_{\ell-2}$	$\ell + 6$	$a_{\ell+4,\ell}^{\text{at}}(z, \bar{z})$	$2^{-\ell} h_{\ell+4}^{\text{at}}(z)$	$\ell > 0$
$\mathcal{D}[4, 0]$	8	$a_{4,0}^{\text{at}}(z, \bar{z})$	$h_4^{\text{at}}(z)$	
$\mathcal{B}[0, 0]_\ell$	$\ell + 4$	0	$h_{\ell+4}^{\text{at}}(z)$	higher spin currents, $\ell \geqslant 0$
$\mathcal{D}[2, 0]$	4	0	$h_2^{\text{at}}(z)$	stress tensor multiplet
$\mathbf{1}$	0	0	$h_0^{\text{at}}(z)$	identity

Table 5.1. Superconformal blocks contribution from all superconformal multiplets appearing in the OPE of two stress tensor multiplets. The contributions are determined from the atomic building blocks. Bose symmetry requires that ℓ is an even integer. Here Δ is the dimension of the superconformal primary.

5.2.2 OPE coefficients from the chiral algebra

The chiral algebra [174] underlying the $(2,0)$ theories [175] completely fixes the function $h'(z)$ in terms of a single parameter which one may take to be the c central charge.[4] This fixes

$$h(z) = -\left(\frac{z^3}{3} - \frac{1}{z-1} - \frac{1}{(z-1)^2} - \frac{1}{3(z-1)^3} - \frac{1}{z}\right) - \frac{8}{c}\left(z - \frac{1}{z-1} + \log(1-z)\right) + \beta\,, \tag{5.2.9}$$

where β is an unphysical integration constant that does not appear in the correlation function, as is clear from equation (5.2.4). We fix it as $\beta = -1/6 + 8/c$ such that the atomic decomposition of $h(z)$ reads

$$h(z) = h_0^{at}(z) + \sum_{\substack{\ell=-2,\\ \ell \text{ even}}}^{\infty} b_\ell\, h_{\ell+4}^{at}(z)\,, \tag{5.2.10}$$

with[5]

$$b_\ell = \frac{(\ell+1)(\ell+3)(\ell+2)^2\frac{\ell}{2}!\left(\frac{\ell}{2}+2\right)!!\left(\frac{\ell}{2}+3\right)!!(\ell+5)!!}{18(\ell+2)!!(2\ell+5)!!}$$
$$+\frac{8}{c}\frac{\left(2^{-\frac{\ell}{2}-1}(\ell(\ell+7)+11)(\ell+3)!!\Gamma\left(\frac{\ell}{2}+2\right)\right)}{(2\ell+5)!!}\,.$$

One can now use the block decomposition of $h(z)$ to also completely fix the coefficients of the $\mathcal{D}[2,0]$, $\mathcal{D}[4,0]$ and $\mathcal{B}[2,0]_\ell$ multiplets in terms of c. According to table 5.1 the latter two multiplets also give a contribution to $a(z,\bar{z})$. It is then useful to split off this 'chiral' contribution and write

$$a(z,\bar{z}) = a^\chi(z,\bar{z}) + a^u(z,\bar{z})\,, \tag{5.2.11}$$

with $a^\chi(z,\bar{z})$ capturing the completely known contribution of the $\mathcal{D}[4,0]$ and $\mathcal{B}[2,0]_\ell$ multiplets,

$$a^\chi(z,\bar{z}) := \sum_{\substack{\ell=0,\\ \ell \text{ even}}}^{\infty} 2^\ell b_\ell\, a_{\ell+4,\ell}^{at}(z,\bar{z})\,, \tag{5.2.12}$$

---

[4]This central charge is determined by the two-point function of the stress tensor, given, e.g., in [179]. We normalize it such that a single free tensor multiplet has $c=1$, and thus it is related to the canonically normalized C_T of [179] by $C_T = \frac{84}{\pi^6}c$.

[5]Here b_{-2} should be thought of as the limit of the given expression as $\ell \to -2$, which gives $b_{-2} = 8/c$.

and with an 'unknown' part $a^u(z, \bar{z})$ of the form

$$a^u(z, \bar{z}) = \sum_{\Delta \geqslant \ell+6, \ell} \lambda^2_{\Delta, \ell} a^{\mathrm{at}}_{\Delta, \ell}(z, \bar{z}) \,. \tag{5.2.13}$$

The blocks that saturate the inequality correspond to the $\mathcal{D}[0, 4]$ or $\mathcal{B}[0, 2]_\ell$ multiplets, and all other blocks correspond to $\mathcal{L}[0, 0]_{\Delta, \ell}$ multiplets.

5.2.3 Crossing symmetry equations

The crossing symmetry equations which arise from permuting the external operators lead to a set of linear algebraic relations for the functions $A_R(z, \bar{z})$. Substituting (5.2.4) into these relations, one finds that all the derivatives can be eliminated and (assuming the above form of $h(z)$) one also finds simple algebraic crossing equations for the function $a(z, \bar{z})$ [18]. These read:

$$a(z, \bar{z}) = \frac{1}{(1 - z)^5 (1 - \bar{z})^5} a \left(\frac{z}{z - 1}, \frac{\bar{z}}{\bar{z} - 1} \right)$$
$$z\bar{z}\, a(z, \bar{z}) = (1 - z)(1 - \bar{z}) a(1 - z, 1 - \bar{z}) + \mathcal{C}_h(1 - z, 1 - \bar{z}) - \mathcal{C}_h(z, \bar{z}) \tag{5.2.14}$$

where

$$\mathcal{C}_h(z, \bar{z}) = \frac{1}{(z - \bar{z})^3} \frac{h(z) - h(\bar{z})}{z\bar{z}} \,. \tag{5.2.15}$$

The first of the crossing equations relates the t- and u-channel and is solved by demanding that the s-channel block decomposition (equations (5.2.12) and (5.2.13)) only contains even spin operators. The second one is less trivial as it relates the block decompositions in different channels. It will be used extensively below.

5.3 Regge trajectories and supersymmetry

As we mentioned in the introduction, a given superconformal multiplet contains several conformal primary operators whose Regge trajectories are naturally related by supersymmetry. It might then appear natural to focus on the Regge trajectories of the superconformal multiplets as a whole, and to ignore the trajectories of the superconformal descendants. For the $\mathcal{D}[2, 0]$ correlator one can do so by analysing the Regge trajectories for all spins directly for the function $a(z, \bar{z})$ instead of those for the six functions $A_R(z, \bar{z})$. Perhaps surprisingly, doing so would only paint an incomplete picture: for several superconformal Regge trajectories the arrangement of the conformal descendants, which is dictated by supersymmetry, is *not* automatically correct. Instead, the combined demands of analyticity in spin together with supersymmetry lead to non-trivial constraints for superconformal Regge trajectories.

The aim of this section is to exhibit these constraints and argue for a particular structure of the superconformal trajectories that resolves them. We will first consider

the contributions of the short multiplets, which lie on straight trajectories, and then move on to the long multiplets whose twist is not fixed by supersymmetry. The next two subsections detail the issues and are unavoidably a bit technical. The hasty reader may want to skip to subsection 5.3.3 for a summary of the issues we uncovered and their potential resolution.

All of the issues we discuss below will happen for low spins where, as mentioned in the introduction, the operators do not always manifestly lie on Regge trajectories. The threshold value ℓ_* is claimed to be determined by the Regge behaviour of the correlation function. In section 5.4.3 we will show that the Regge behaviour of the six functions $A_R(z, \bar{z})$ is actually quite a bit softer than in a non-supersymmetric theory, leading to extended manifest analyticity in spin. Let us here already quote the upshot, which is that:

$$
\begin{aligned}
&A_{[4,0]} \text{ has analyticity in spin for } \ell > -3\,, \\
&A_{[2,2]} \text{ has analyticity in spin for } \ell > -2\,, \\
&A_{[2,0]} \text{ has analyticity in spin for } \ell > -1\,, \\
&A_{[0,4]} \text{ has analyticity in spin for } \ell > -1\,, \\
&A_{[0,2]} \text{ has analyticity in spin for } \ell > 0\,, \\
&A_{[0,0]} \text{ has analyticity in spin for } \ell > 1\,.
\end{aligned}
\tag{5.3.1}
$$

5.3.1 Short multiplets and straight trajectories

Short multiplets with unknown coefficients

We start our exploration with the $\mathcal{B}[0, 2]_{\ell-1}$ multiplets (for even $\ell > 0$), which are short multiplets whose coefficients are not fixed by the chiral algebra. Since their dimensions are fixed, they lie on straight Regge trajectories. We begin by plotting the conformal primary descendants and their trajectories for a few low-lying spins for each of the R-symmetry channels. This yields the black dots and solid black lines in figure 5.2.

Note that we have added a small horizontal split to overlapping Regge trajectories for presentational purposes: the twist of all trajectories are really even integers. For space reasons we have only added a (partial) legend to the $[4, 0]$ channel: the black half-line connects the $\mathcal{B}[0, 2]_1$, $\mathcal{B}[0, 2]_3$, $\mathcal{B}[0, 2]_5$, ... multiplets, and the corresponding primary operators are always the first three black dots on this half-line. (In other words, in each R-symmetry channel the operator content of the $\mathcal{B}[0, 2]_1$ multiplet is given by those black dots that lie on the endpoint of a black half-line, and so on for the remaining multiplets.)

The most interesting feature of these trajectories now follows from the dashed lines, which indicate the continuation of this trajectory to unphysical spins of the superconformal primary. We are forced to draw this continuation because analyticity in spin dictates that Regge trajectories cannot just end in the middle of the
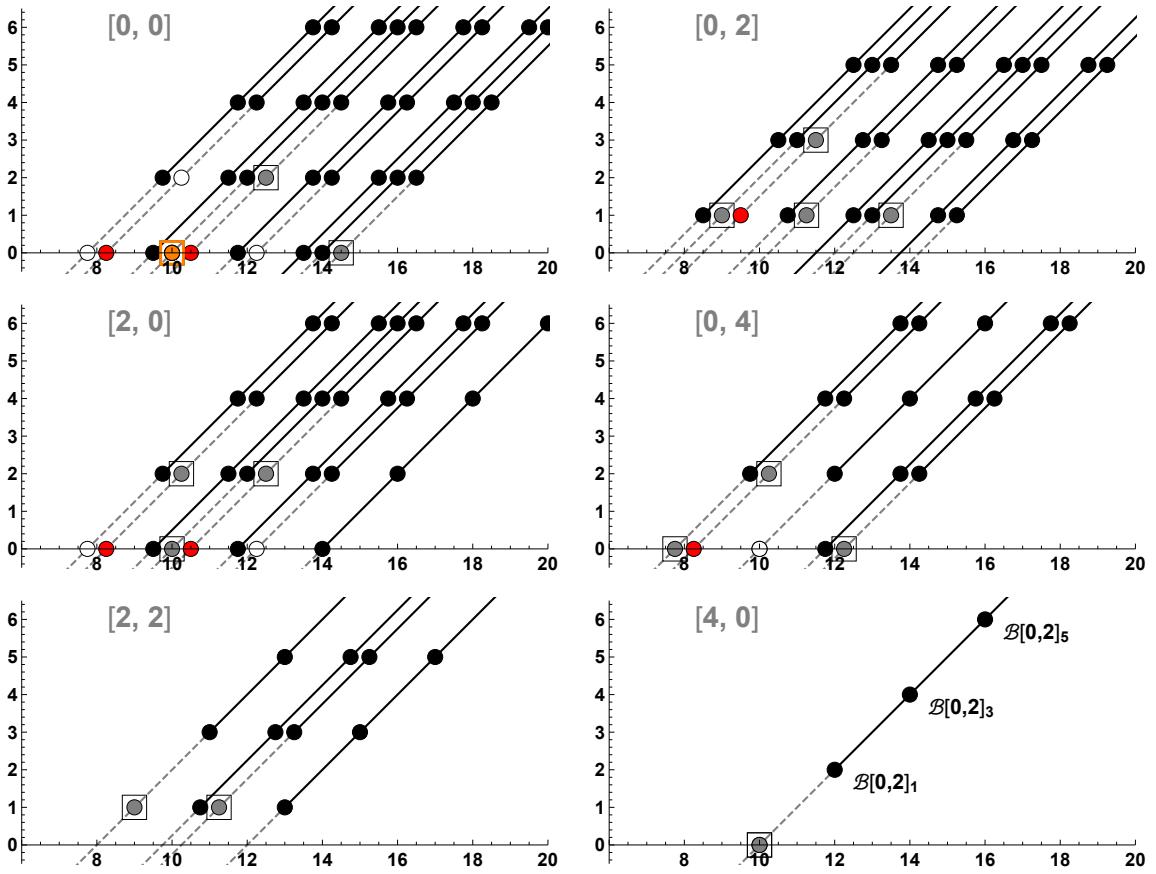
Figure 5.2. (Δ, ℓ) planes: $\mathcal{B}[0,2]_{\ell-1}$ trajectories (lines and dots) and $\mathcal{D}[0,4]$ operators (squares)

(Δ, ℓ) plane. After going down two units in spin along this dashed line we find the hypothetical "$\mathcal{B}[0,2]_{-1}$" multiplet and going down four units yields the "$\mathcal{B}[0,3]_{-3}$" multiplet. Neither of these multiplets exist, so what are we to make of them?

Let us first consider the "$\mathcal{B}[0,2]_{-1}$" multiplet. In the plots we show grey, orange and white dots at the putative locations of its conformal primary operators. The white dots are easiest to explain: they correspond to the absence of an operator due to a kinematical zero. For example, the twist ten trajectory in the $[0,4]$ channel gives a contribution of the form

$$\lambda^2_{\mathcal{B}[0,2]_{\ell-1}} \frac{\ell(4+\ell)(5+\ell)(9+\ell)}{12(1+\ell)(3+\ell)(6+\ell)(8+\ell)} \mathcal{G}^{(\ell)}_{10+\ell}(z, \bar{z}), \qquad (5.3.2)$$

with $\lambda^2_{\mathcal{B}[0,2]_{\ell-1}}$ the contribution of this superconformal multiplet to (5.2.13). We see that this contribution vanishes at $\ell = 0$ and this explains the corresponding white dot. The orange and the grey dots are then actual conformal primary blocks that, barring a dynamical zero in the overall OPE coefficient, need to be accommodated

by other supermultiplets.

As the reader might have expected from table 5.1, the multiplet that comes to the rescue is the $\mathcal{D}[0,4]$ multiplet. The operator contents of the latter is indicated by the squares in the figure and we see a nice one-to-one match between these and the grey and orange dots of the "$\mathcal{B}[0,2]_{-1}$" multiplet. Although this is not obvious from the figure, *almost* all the coefficients work out as well. For example, in the $[2,0]$ channel there is a twist 8 trajectory of the form:

$$\lambda^2_{\mathcal{B}[0,2]_{\ell-1}} \frac{(\ell+5)^2(\ell+9)}{3(\ell+8)(2\ell+9)(2\ell+11)} \mathcal{G}^{(2+\ell)}_{10+\ell}(z,\bar{z}), \tag{5.3.3}$$

and in the limit $\ell \to 0$ this precisely matches a contribution to the $\mathcal{D}[0,4]$ multiplet of the form:

$$\lambda^2_{\mathcal{D}[0,4]} \frac{25}{3 \cdot 8 \cdot 11} \mathcal{G}^{(2)}_{10}(z,\bar{z}). \tag{5.3.4}$$

Similarly we find that the coefficients agree for all the other grey dot/square combinations. It is therefore natural to postulate that

$$\lim_{\ell \to -1} \lambda^2_{\mathcal{B}[0,2]_\ell} = \lambda^2_{\mathcal{D}[0,4]}, \tag{5.3.5}$$

where taking the limit of course only makes sense because of analyticity in spin.

Surprisingly, assuming equation (5.3.5) does not resolve everything: there is a strange mismatch which occurs for the scalar of dimension 10 in the $[0,0]$ channel. In the $\mathcal{B}[0,2]_{\ell-1}$ supertrajectory we obtain:

$$\lim_{\ell \to 0} \lambda^2_{\mathcal{B}[0,2]_{\ell-1}} \frac{3(\ell+4)(\ell+5)(\ell(\ell+9)(4\ell(\ell+9)+59)-360)}{280(\ell+1)(\ell+3)(\ell+6)(\ell+8)(2\ell+7)(2\ell+11)} \mathcal{G}^{(\ell)}_{10+\ell}(z,\bar{z})$$
$$= -\frac{15}{2156} \lambda^2_{\mathcal{D}[0,4]} \mathcal{G}^{(0)}_{10}(z,\bar{z}), \tag{5.3.6}$$

where we used equation (5.3.5). Although the $\mathcal{D}[0,4]$ multiplet should indeed have a block with these quantum numbers, its coefficient is different and should actually be:

$$\frac{1}{308} \lambda^2_{\mathcal{D}[0,4]} \mathcal{G}^{(0)}_{10}(z,\bar{z}). \tag{5.3.7}$$

This mismatch is why we coloured this combination orange rather than grey in the figure.[6] Let us call this **issue 1**. We note that this issue is only present if we

---

[6]One may wonder how the issue arises, given that everything is clearly analytic in spin at the level of the function $a(z,\bar{z})$. The problem is that the $\mathcal{B}[0,2]_{\ell-1}$ multiplet induces a block $\mathcal{G}^{(\ell-4)}_{\ell+10}(z,\bar{z})$ in the $[0,0]$ channel which has negative spin for $\ell = 0, 2$. As we send $\ell \to 2$ this becomes a spin -2 block, which one may check vanishes identically in six dimensions and therefore does not contribute. But for $\ell \to 0$ we find a spin -4 block, which happens to be equal to (16/3 times) a spin 0 block of the same dimension. This yields an additional contribution to the coefficient of the spin 0 block of dimension 10 in the $\mathcal{D}[0,4]$ multiplet and causes the non-analyticity in spin.

have analyticity down to spin 0 in the $[0,0]$ R-symmetry channel, which does not rigorously follow from the Regge limit analysis summarized in (5.3.1).

Let us now go down two more units in spin and investigate the "$\mathcal{B}[0,2]_{-3}$" multiplet which is indicated by the red dots in the figure. (Perhaps surprisingly, there is no kinematical zero that prevents any of these operators from appearing.) According to (5.3.1) we expect to have analyticity of the CFT data at all the red points except the scalars in the $[0,0]$ channel, but these blocks do not correspond to the operator content of any other superconformal multiplet. They are therefore genuinely unwanted contributions, and the fact that they do not vanish automatically is what we call **issue 2**. Of course, this issue would be resolved immediately if the overall coefficient vanishes, so if $\lim_{\ell \to -2} \lambda^2_{\mathcal{B}[0,2]_{\ell-1}} = 0$, but we emphasize that this would be a *dynamical* constraint. We will find another potential dynamical resolution below.

Short multiplets with known coefficients

Our next set of multiplets contains short multiplets with a contribution to the chiral algebra: the $\mathcal{B}[2,0]_{\ell-2}$ and the $\mathcal{D}[4,0]$ multiplets. We can repeat the above analysis for these operators, but with the one change that here the OPE coefficients are completely fixed:

$$\lambda^2_{\mathcal{B}[2,0]_{\ell-2}} = 2^{\ell} b_{\ell}, \qquad \lambda^2_{\mathcal{D}[4,0]} = \lim_{\ell \to 0} \lambda^2_{\mathcal{B}[2,0]_{\ell-2}} = 2 b_0 \,. \qquad (5.3.8)$$

and therefore the analogue of equation (5.3.5) is manifestly true. For the six functions $A_R(z, \bar{z})$ these multiplets give the picture shown in figure 5.3.

The white and grey dots now indicate the operator content of a "$\mathcal{B}[2,0]_{-2}$" multiplet and, as expected, match almost perfectly with the squares that correspond to a $\mathcal{D}[4,0]$ multiplet. Yet there is again one exception: the scalar of dimension 8 in the $[0,0]$ channel. For this operator we have

$$\lim_{\ell \to 0} \lambda^2_{\mathcal{B}[2,0]_{\ell-2}} \frac{9(\ell - 1)(\ell + 8)}{1400(\ell + 1)(\ell + 6)} \mathcal{G}^{(\ell)}_{8+\ell}(z, \bar{z}) = -\frac{3}{350} \lambda^2_{\mathcal{D}[4,0]} \mathcal{G}^{(0)}_8(z, \bar{z}) \,, \qquad (5.3.9)$$

whereas the $\mathcal{D}[4,0]$ multiplet does not have such a scalar. We call this **issue 3**, although we must note once again that analyticity is not guaranteed from (5.3.1) for spin zero.

We have two more issues to discuss. First, as for the previous figure, the further continuation down to a "$\mathcal{B}[2,0]_{-4}$" multiplet induces another unwanted scalar operator of dimension 8 in the $[2,0]$ channel with coefficient

$$\lim_{\ell \to -2} \lambda^2_{\mathcal{B}[2,0]_{\ell-2}} \frac{(\ell + 4)^2 (\ell + 5)^2 (\ell + 8)}{8(\ell + 6)(2\ell + 7)(2\ell + 9)^2(2\ell + 11)} \mathcal{G}^{(2+\ell)}_{10+\ell}(z, \bar{z}) = \lambda^2_{\mathcal{B}[2,0]_{-4}} \frac{9}{700} \mathcal{G}^{(0)}_8(z, \bar{z}) \,. \qquad (5.3.10)$$
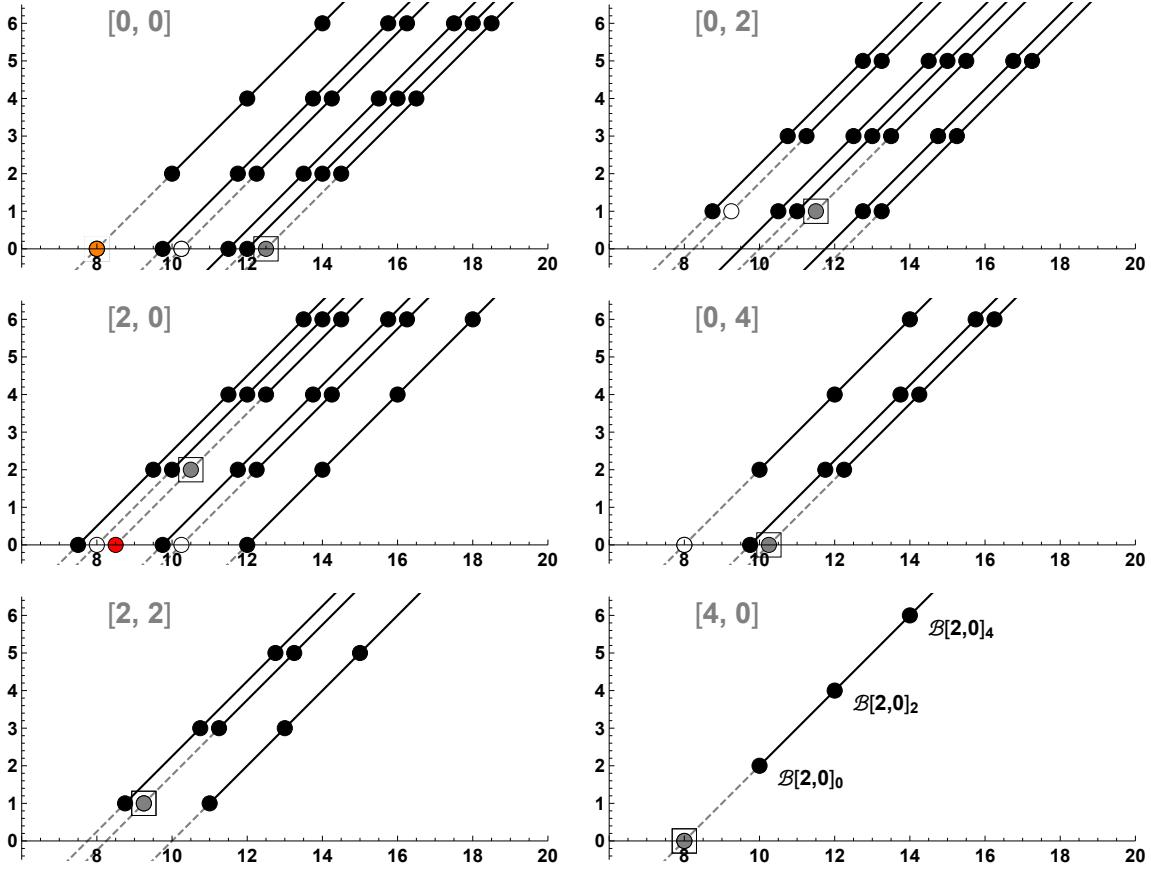
Figure 5.3. (Δ, ℓ) planes: $\mathcal{B}[2,0]_{\ell-2}$ trajectories (lines and dots) and $\mathcal{D}[4,0]$ operators (squares)

This isolated operator once more cannot fit in a superconformal multiplet and so the block must somehow cancel: this is **issue 4**. Notice that in this case the OPE coefficient is known,

$$\lambda^2_{\mathcal{B}[2,0]_{-4}} = \frac{1}{4}b_{-2} = \frac{2}{c}. \tag{5.3.11}$$

The putative resolution of issue 2 therefore cannot work in this case, since $2/c > 0$ in all but the generalized free theory.

The last issue for this set of blocks is the $\mathcal{D}[2,0]$ multiplet itself. It contributes three conformal blocks:

$$\begin{aligned}
[0,0] &: \frac{6}{175}\mathcal{G}_6^{(2)}(z,\bar{z})\,, \\
[2,0] &: \frac{1}{2}\mathcal{G}_4^{(0)}(z,\bar{z})\,, \\
[0,2] &: \frac{1}{5}\mathcal{G}_5^{(1)}(z,\bar{z})\,,
\end{aligned} \tag{5.3.12}$$

which we recognize as the contributions from the stress tensor, the superconformal primary, and the R-symmetry current. This block has an OPE coefficient equal to $b_{-2} = 8/c$ as determined by the chiral algebra and so is present in any bona fide theory. It is however clear that neither of these three operators fits into any of the Regge trajectories we have drawn so far, and this is **issue 5**.

5.3.2 Long multiplets

Now let us analyse the Regge trajectories for the long multiplets $\mathcal{L}[0,0]_{\Delta,\ell}$. For these multiplets the scaling dimensions are unknown, and likewise there is no a priori proof that the Regge trajectories $\ell(\Delta)$ have a particularly simple form. We can nevertheless explore the consequences if we *assume* that there exists a trajectory that extends to low spins. Just as for the protected multiplets, we will find issues corresponding to non-analyticity in the induced trajectories for the $A_R(z, \bar{z})$ as soon as any Regge trajectory for a supermultiplet crosses the lines with $\ell = 0$, $\ell - 2$, or $\ell = -4$. For efficiency of presentation we would like to capture all the issues in one plot, and to do so we simply invented an otherwise random trajectory[7] that crosses all these three lines as shown in figure 5.4. We however stress that the issues we are about to list are *local*, in the sense that they hold for any trajectory crossing these low spins, and do not depend on the global shape of the trajectory. For example, in our view it would have been perfectly possible for a trajectory that intersects the $\ell = -4$ line to be disconnected from a trajectory that extends to positive spins.

The legend in the $[4,0]$ channel indicates the scaling dimension that we have chosen for the first four long multiplets on our hypothetical trajectories. (Recall that $\Delta > \ell + 6$ for an $\mathcal{L}[0,0]_{\Delta,\ell}$ multiplet by unitarity which is easily obeyed here.) Unlike the previous plots there are no exactly overlapping induced trajectories for any of the $A_R(z, \bar{z})$ and therefore there was no need to add a horizontal split by hand.

At low spins we encounter our first issue at spin 0. We see some kinematical zeroes, indicated by the white dots, which are analytic in spin and nothing to worry about. However the red dot indicates a problem: for a long supermultiplet with quantum numbers (Δ, ℓ) and ℓ generic there exists a conformal primary R-symmetry singlet of the form:

$$\lambda^2_{\mathcal{L}[0,0]_{\Delta,\ell}} \xi(\ell, \Delta) \mathcal{G}^{(\ell)}_{\Delta+4}(z, \bar{z}) \,, \tag{5.3.13}$$

with $\xi(\ell, \Delta)$ a rational function of Δ and ℓ that is too ugly to include here. In the limit $\ell \to 0$ we find:

$$\lim_{\ell \to 0} \xi(\ell, \Delta) = -\frac{3(\Delta - 2)(\Delta + 4)(\Delta(\Delta + 2) - 6)}{448(\Delta - 3)(\Delta + 1)^2(\Delta + 5)} \,, \tag{5.3.14}$$

---

[7]The sketched trajectory is not *entirely* random: we picked a convex shape and an asymptotic twist of 12, meaning we can think of it as the second double-twist trajectory after the leading one (which asymptotes to twist 8).
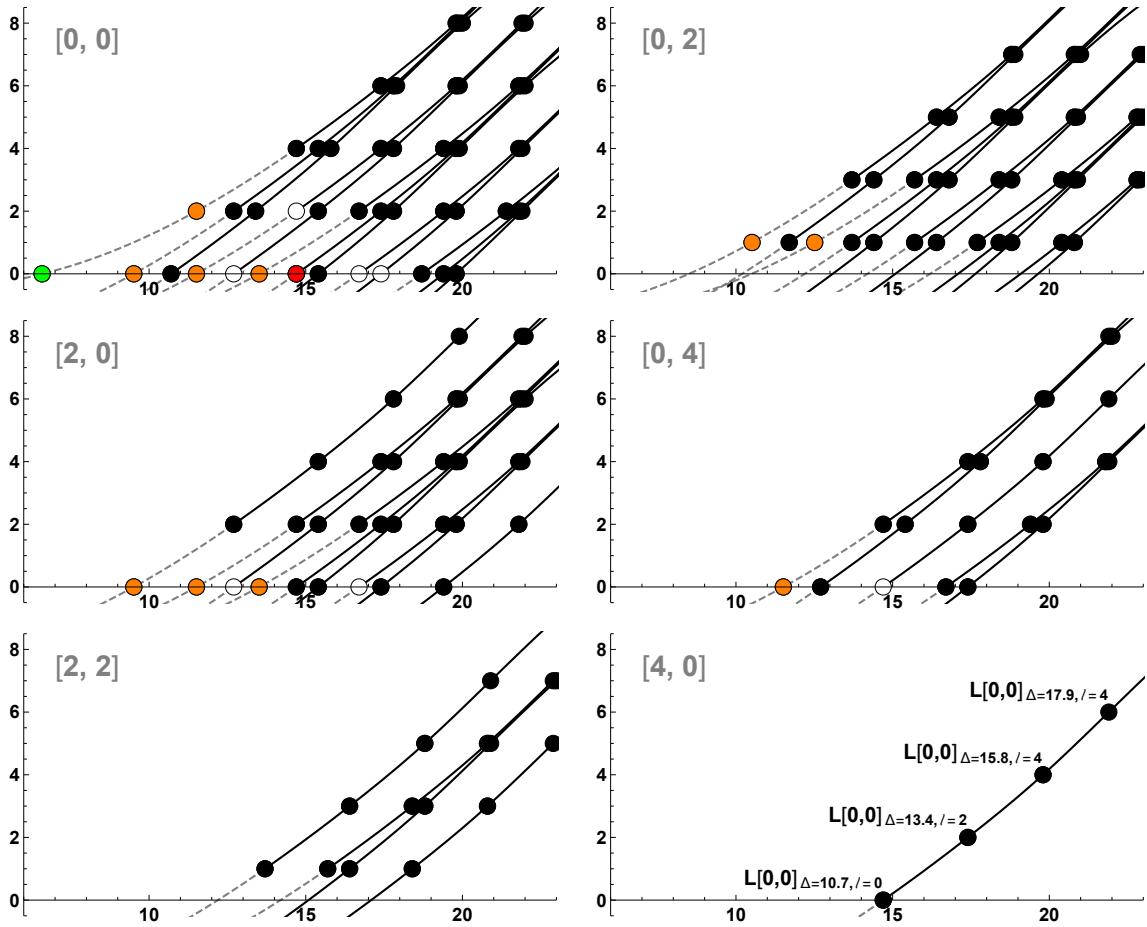
Figure 5.4. (Δ, ℓ) planes: a randomly chosen $\mathcal{L}[0,0]_{\Delta,\ell}$ trajectory extending down to spin -4.

which is not the correct expression for a spin zero long multiplet, which instead has a contribution of the form:[8]

$$\lambda^2_{\mathcal{L}[0,0]_{\Delta,0}} \frac{9(\Delta-4)(\Delta-2)(\Delta+4)(\Delta+6)}{1792(\Delta-3)(\Delta-1)(\Delta+3)(\Delta+5)} \mathcal{G}^{(0)}_{\Delta+4}(z,\bar{z}). \qquad (5.3.15)$$

We can call this **issue 6**. We stress that it exists for *any* long multiplet trajectory that crosses the $\ell = 0$ line, provided analyticity holds down to spin zero in the singlet channel.[9]

Going down in spin, we reach the orange points at spin -2, which correspond to **issue 7**. Again, a "$\mathcal{L}[0,0]_{\Delta,-2}$" multiplet does not exist and so generically the combination of orange points should not actually be present in a physical theory.

---

[8]The discrepancy is again due to a spin $\ell - 4$ block in the supermultiplet — see the footnote 6.

[9]Note that while the difference between (5.3.14) and (5.3.15) vanishes for $\Delta = 2$, this value is not allowed for $\ell = 0$ by unitarity.

Notice that we have shown the situation for generic Δ; much like the function $\xi(\ell, \Delta)$ vanishes at $\Delta = 2$ there are some zeroes in the coefficients for specific values of Δ and then some of the orange points may disappear. This will be important below.

Finally if a long supertrajectory hits spin -4 then we induce a single scalar of dimension $\Delta + 4$ in the $[0, 0]$ channel. This is the green dot and **issue 8**, which once more is only an issue if analyticity holds down to spin zero in this channel.

5.3.3 Resolving the issues

Let us recap. The issues we have collected are:

1. The limit $\ell \to 0$ of the $\mathcal{B}[0, 2]_{\ell-1}$ multiplet should be a $\mathcal{D}[0, 4]$ multiplet but gives the wrong coefficient for a dimension 10 scalar in the $[0, 0]$ channel.

2. The limit $\ell \to -2$ of the $\mathcal{B}[0, 2]_{\ell-1}$ multiplet gives unwanted operators in several channels.

3. The limit $\ell \to 0$ of the $\mathcal{B}[2, 0]_{\ell-2}$ multiplet should be a $\mathcal{D}[4, 0]$ multiplet but gives the wrong coefficient for a dimension 8 scalar in the $[0, 0]$ channel.

4. The limit $\ell \to -2$ of the $\mathcal{B}[2, 0]_{\ell-2}$ multiplet gives an unwanted dimension 8 scalar in the $[2, 0]$ channel with coefficient $9/(350c)$.

5. The operators in the $\mathcal{D}[2, 0]$ multiplet do not fit in a short Regge trajectory.

6. The limit $\ell \to 0$ of a generic $\mathcal{L}[0, 0]_{\Delta, \ell}$ multiplet should be an $\mathcal{L}[0, 0]_{\Delta, 0}$ multiplet but gives the wrong coefficient for a dimension $\Delta + 4$ scalar in the $[0, 0]$ channel.

7. The limit $\ell \to -2$ of a generic $\mathcal{L}[0, 0]_{\Delta, \ell}$ multiplet gives unwanted operators in several channels.

8. The limit $\ell \to -4$ of a generic $\mathcal{L}[0, 0]_{\Delta, \ell}$ multiplet gives an unwanted scalar of dimension $\Delta + 4$ in the $[0, 0]$ channel.

We see that issues 1, 3, 6 and 8 all pertain only to scalars in the R-symmetry singlet channel. It is not entirely clear that we need to take them seriously: according to equation (5.3.1) analyticity in spin for $A_{[0,0]}(z, \bar{z})$ is guaranteed only down to spin $\ell > 1$. Although this would be one way to resolve the issues (or at least provide us with a license to ignore them), there is another option: issue 8 has the potential to resolve the other 3 issues. More precisely we simply postulate the existence of otherwise unknown unprotected Regge trajectories that cross the $\ell = -4$ line at $\Delta = 6$ (to resolve issue 1), at $\Delta = 4$ (to resolve issue 3) and at $\Delta = \hat{\Delta}$ with $\hat{\Delta}$ the dimension of any generic long multiplet that crosses the $\ell = 0$ line (to resolve issue 6). Whether this is the correct resolution, or whether there is another mechanism

at play, is not something we can hope to address with our current knowledge of the $(2,0)$ theories.

More interesting resolutions can be found for the other issues. The first observation is a perfect cancellation between a special case of issue 7 and issue 2: if a long multiplet trajectory crosses $\ell = -2$ exactly at $\Delta = 4$ then it induces precisely the same set of blocks as the "$\mathcal{B}[0,2]_{-3}$" multiplet. We can write that

$$\mathcal{L}[0,0]_{\Delta=4,\ell=-2} = \mathcal{B}[0,2]_{-3}, \tag{5.3.16}$$

where, as always, the evaluation at negative spin is understood to be defined through analytic continuation. This means that issue 2 can be resolved not only by demanding that the $\mathcal{B}[0,2]_{-3}$ multiplet has zero coefficient (as we hypothesized above), but also by a long trajectory hitting spin -2 exactly at $\Delta = 4$ with the right coefficient. Just as for the spin -4 long multiplets, at present our understanding of the $(2,0)$ theories is insufficient to know which of these two potential resolutions is realized. We do note, however, that hitting spin -2 at $\Delta = 4$ would not be entirely unreasonable for the first subleading trajectory. This trajectory asymptotes to $\Delta = \ell + 10$ but according to a large spin analysis is expected to slope towards lower Δ at lower spins. Again with our current knowledge of $(2,0)$ theories we cannot tell if this or other mechanisms are in place to resolve these issues.

This leaves us with issue 5 which is arguably the most interesting. Our suggested resolution comes about by another special case of issue 7: an "$\mathcal{L}[0,0]_{\Delta=2,\ell=-2}$" long supermultiplet, or more precisely the analytic continuation of a regular long multiplet to $\ell = -2$ and $\Delta = 2$, gives the contribution:

$$
\begin{aligned}
[0,0] &: -\frac{24}{175}\mathcal{G}_6^{(2)}(z,\bar{z}), \\
[2,0] &: -2\mathcal{G}_4^{(0)}(z,\bar{z}) + \frac{9}{700}\mathcal{G}_8^{(0)}(z,\bar{z}), \\
[0,2] &: -\frac{4}{5}\mathcal{G}_5^{(1)}(z,\bar{z}).
\end{aligned}
\tag{5.3.17}
$$

Therefore, if we add this multiplet with a (negative) coefficient $-2/c$ then we reproduce all the stress tensor multiplet blocks with the right coefficient. The one mismatch is an additional scalar block of dimension 8 in the $[2,0]$ channel, but its coefficient $-9/(350c)$ is precisely such that it cancels the unwanted conformal block of issue 4, which is thereby also resolved! It is therefore entirely natural to conjecture the following observation:

Claim 1. *The leading long $\mathcal{L}[0,0]_{\Delta,\ell}$ multiplet trajectory extends to $\ell = -2$ where it hits $\Delta = 2$ and has a residue corresponding to an OPE coefficient of $-2/c$. This yields the conformal blocks of the stress tensor multiplet in the different $A_R(z,\bar{z})$.*
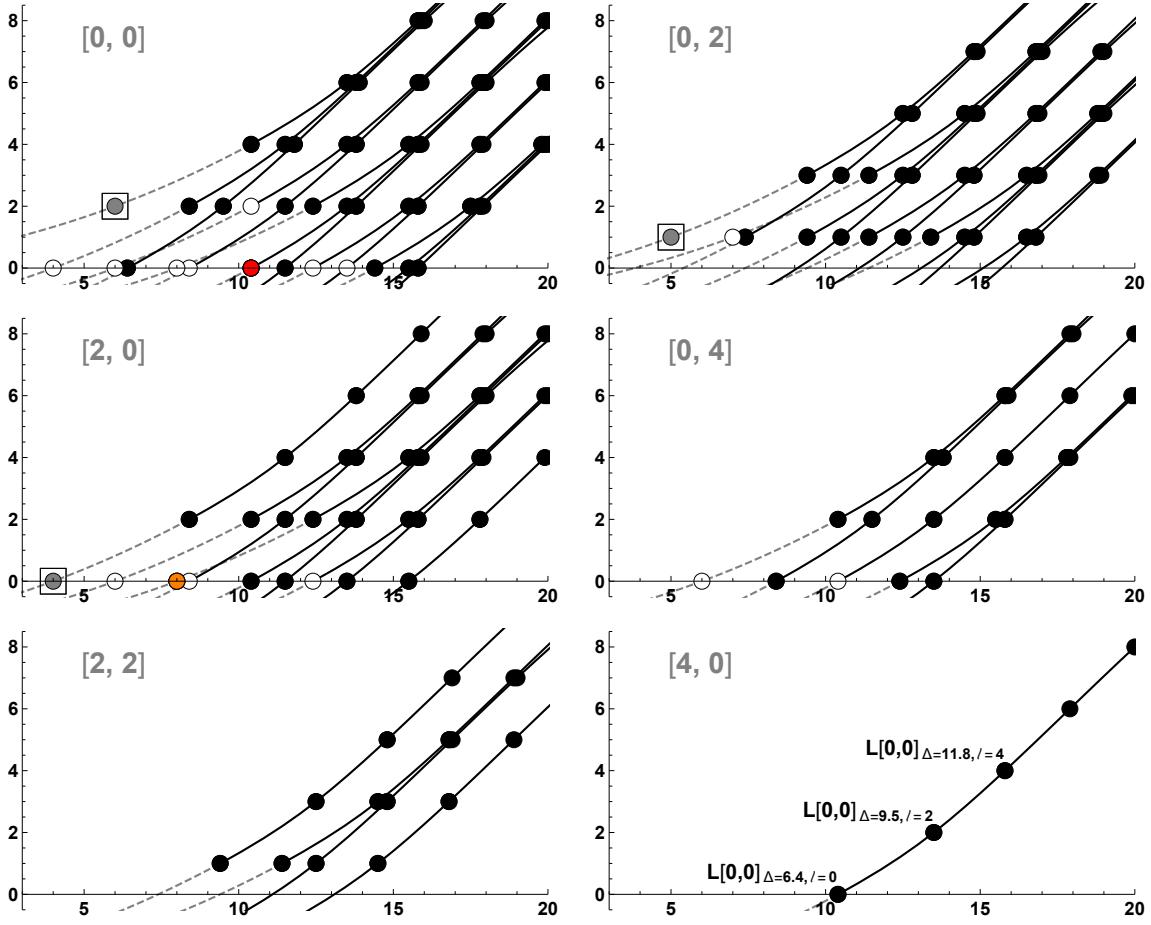
Figure 5.5. (Δ, ℓ) planes: leading $\mathcal{L}[0,0]_{\Delta,\ell}$ trajectory (lines and dots) and $\mathcal{D}[2,0]$ operators (squares)

The observation that the stress tensor multiplet lies on an unprotected trajectory implies a remarkable interplay between the long and protected multiplets that we could not have observed without appealing to analyticity in spin of descendants. It leads to the improved picture for the leading long trajectory in the $(2,0)$ theories shown in figure 5.5.

This picture is again heuristic: to draw the trajectory we took some reasonable guesses for the scaling dimensions of the first few long multiplets based on the numerical bootstrap results of [18] at $c = 25$. We then included the point $\Delta = 2$ at spin -2 and drew an otherwise arbitrary curve through all these points. As before, the solid part of the curve corresponds to long multiplets with physical spins $\ell \geqslant 0$ and the dotted part is the continuation to negative spin. The grey and orange dots correspond to respectively the resolution of issue 5 and 4. As for any long multiplet there is still an instance of issue 8 which is indicated by the red dot.

From the picture we also observe that the very leading Regge trajectory in the

$[0, 0]$ channel is given by a specific conformal primary descendant of dimension $\Delta + 4$ and spin $\ell + 4$ if the superconformal primary has dimension Δ and spin ℓ. (This trajectory asymptotes to the line $\Delta = \ell + 8$ which means that it is indeed more leading than any of the short trajectories.) According to our observation this is the trajectory that the stress tensor lies on. In this sense the $(2, 0)$ theories would then be similar to a non-supersymmetric theory like the Ising or $O(N)$ models where there is ample numerical evidence that the stress tensor lies on the leading (non-straight) Regge trajectory.

Resolution in generalized free field theory

We can now investigate how the issues are resolved in theories whose spectrum and OPE coefficients we know exactly. There are only two such options: the theory of N free tensor multiplets, and generalized free field theory. However, the former is qualitatively different from the cases considered in this work since it is free, and will thus have an extra family of short multiplets $(\mathcal{B}[0, 0]_{\ell \geqslant 0})$, which contain conserved currents of spin larger than two. These multiplets give rise to various new conformal primary trajectories and change the aforementioned issues. In particular, the stress tensor fits as the continuation to $\ell = -2$ of this trajectory.

We will then consider only the case of generalized free field theory. The corresponding four-point function is obtained just by Wick contractions, and solves the crossing equations with $c = \infty$. The function $a(z, \bar{z})$ for this theory reads:

$$a(z, \bar{z}) = \frac{z^3(\bar{z} - 1)^3 - 3z^2(\bar{z} - 1)^3 + 3z(\bar{z} - 1)^3 - (\bar{z} - 2)((\bar{z} - 1)\bar{z} + 1)}{3(z - 1)^3 z^2(\bar{z} - 1)^3 \bar{z}^2} . \quad (5.3.18)$$

An added advantage of this function is its very soft behaviour in the Regge limit and in the second-sheet light-cone limit, which per the analysis of section 5.4.3 leads to an improvement over the generic behaviour of equation (5.3.1): for this function we have analyticity for all physical spins in all channels. This means all eight issues must be resolved. Issues 4 and 5 are automatically resolved since $c = \infty$, and in what follows we will see how the remaining issues are resolved for the leading trajectories. We note that the superconformal block decomposition of this correlator is easily found, and besides the protected multiplets we find towers of unprotected multiplets at the double twist values $\Delta = 8 + \ell + 2n$, $n \in \mathbb{N}_0$. The corresponding coefficients can be found by applying the supersymmetric inversion formula of section 5.4.

Let us start with the leading trajectory of the R-symmetry singlet channel, which has twist $\tau = \Delta - \ell = 8$. Operators on this trajectory get contributions from the two short trajectories as well as the leading long trajectory with $\Delta = 8 + \ell$, $\ell \geqslant 0$. Taking the OPE coefficients of these operators we can reconstruct the leading trajectory of $A_{[0,0]}(z, \bar{z})$ using the superconformal blocks. Altogether we find the

following conformal primaries

$$A_{[0,0]}(z,\bar{z})\Big|_{\tau=8} = \sum_{\substack{\ell\geqslant 0, \\ \ell \text{ even}}} 2^{\ell+2} b_{\ell+2} c_{2,2}^{\mathcal{B}[2,0]_\ell} \mathcal{G}_{\ell+10}^{(\ell+2)}(z,\bar{z})$$

$$+ \sum_{\substack{\ell\geqslant 1, \\ \ell \text{ odd}}} \lambda_{\mathcal{B}[0,2]_\ell}^2 \left(c_{1,1}^{\mathcal{B}[0,2]_\ell} \mathcal{G}_{\ell+9}^{(\ell+1)}(z,\bar{z}) + c_{3,3}^{\mathcal{B}[0,2]_\ell} \mathcal{G}_{\ell+11}^{(\ell+3)}(z,\bar{z}) \right)$$

$$+ \sum_{\substack{\Delta=8+\ell, \\ \ell\geqslant 0, \\ \ell \text{ even}}} \lambda_{\mathcal{L}[0,0]_{\Delta,\ell}}^2 \left(c_{4,4}^{\mathcal{L}[0,0]_{\Delta,\ell}} \mathcal{G}_{\Delta+4}^{(\ell+4)}(z,\bar{z}) + c_{2,2}^{\mathcal{L}[0,0]_{\Delta,\ell}} \mathcal{G}_{\Delta+2}^{(\ell+2)}(z,\bar{z}) + c_{0,0}^{\mathcal{L}[0,0]_{\Delta,\ell}} \mathcal{G}_{\Delta}^{(\ell)}(z,\bar{z}) \right),$$

$$(5.3.19)$$

where $c_{\bullet,\bullet}^{\bullet}$ are the coefficients of the expansion of the superconformal block of the respective supermultiplet in conformal blocks. We chose not to spell them out here, but they are completely known rational functions of Δ and ℓ. Analyticity in spin of the leading Regge trajectory for $\ell \geqslant 0$ requires the above to be identical to

$$A_{[0,0]}(z,\bar{z})\Big|_{\tau=8} = \sum_{\substack{\Delta=8+\ell, \\ \ell\geqslant 0, \\ \ell \text{even}}} \left(2^\ell b_\ell c_{2,2}^{\mathcal{B}[2,0]_{\ell-2}} + \lambda_{\mathcal{B}[0,2]_{\ell-1}}^2 c_{1,1}^{\mathcal{B}[0,2]_{\ell-1}} + \lambda_{\mathcal{B}[0,2]_{\ell-3}}^2 c_{3,3}^{\mathcal{B}[0,2]_{\ell-3}} \right.$$

$$\left. + \lambda_{\mathcal{L}[0,0]_{\Delta-4,\ell-4}}^2 c_{4,4}^{\mathcal{L}[0,0]_{\Delta-4,\ell-4}} + \lambda_{\mathcal{L}[0,0]_{\Delta-2,\ell-2}}^2 c_{2,2}^{\mathcal{L}[0,0]_{\Delta-2,\ell-2}} + \lambda_{\mathcal{L}[0,0]_{\Delta,\ell}}^2 c_{0,0}^{\mathcal{L}[0,0]_{\Delta,\ell}} \right) \mathcal{G}_{\Delta}^{(\ell)}(z,\bar{z}),$$

$$(5.3.20)$$

such that the OPE coefficients are an analytic function of ℓ. Indeed these two expressions agree due to the following relations between OPE coefficients and the superconformal block coefficients:

$$\lambda_{\mathcal{L}[0,0]_{6,-2}} = 0, \qquad c_{1,1}^{\mathcal{B}[0,2]_{-1}} = 0, \qquad \lambda_{\mathcal{B}[0,2]_{-3}} = 0, \qquad c_{4,4}^{\mathcal{L}[0,0]_{4,-4}} \lambda_{\mathcal{L}[0,0]_{4,-4}}^2 = -b_0 c_{2,2}^{\mathcal{B}[2,0]_{-2}}.$$

$$(5.3.21)$$

The last equation means issues 3 and 8 (for the leading long trajectory) cancel out, while issue 2 and 7 (for the leading long trajectory) are resolved by the OPE coefficients vanishing. The same exercise can be done for the twist 10 conformal primaries in the R-symmetry singlet channel, and this time a relation between (a) the spin -4 long multiplet of the sub-leading trajectory ($\Delta = 10+\ell$), (b) the $\mathcal{D}[0,4]$ multiplet, and (c) the short trajectory $\mathcal{B}[2,0]_\ell$ at spin -1 conspire to solve issues 1 and 8 (for the subleading long trajectory). Carrying out these checks for higher twists, one finds that the OPE coefficients continue to conspire to resolve all issues; for example issue 6 for the leading long trajectory ($\Delta = 8+\ell$) is cancelled by issue 8 for the sub-sub-leading long trajectory ($\Delta = 12+\ell$).

5.3.4 Shadow symmetry in all channels

We have seen that a single Regge trajectory at the level of supermultiplets induces several Regge trajectories for the $A_R(z, \bar{z})$ which have integer shifts in ℓ and Δ and OPE coefficients determined by the super-Regge trajectory. What is not at all obvious is then whether *shadow symmetry* is automatically realized. To see that it is, let us focus on the long multiplets. Consider a long trajectory where the spin of the superconformal primary is given by a function $\ell_{s.c.p.}(\Delta)$. To deduce the shadow symmetry of this function consider first the $[4, 0]$ channel. There we see that the super-trajectory induces a single regular conformal trajectory that is shifted by four units, so

$$\ell_{[4,0]}(\Delta) = \ell_{s.c.p.}(\Delta - 4). \tag{5.3.22}$$

This is a regular bosonic trajectory and therefore obeys ordinary shadow symmetry: $\ell_{[4,0]}(6 - \Delta) = \ell_{[4,0]}(\Delta)$. The shadow symmetry of the super-trajectory is therefore

$$\ell_{s.c.p.}(\Delta) = \ell_{s.c.p.}(-2 - \Delta), \tag{5.3.23}$$

and in particular the shadow-symmetric point at the level of the super-trajectory lies at $\Delta = -1$. Now consider the coefficient of the $[4, 0]$ descendant. In our conventions it equals

$$\lambda_{[4,0]}^2(\Delta + 4, \ell) = \frac{(\Delta - \ell - 2)(\Delta + \ell + 2)}{(\Delta - \ell - 6)(\Delta + \ell - 2)} \lambda_{s.c.p.}^2(\Delta, \ell), \tag{5.3.24}$$

with $\lambda_{s.c.p.}^2(\ell, \Delta)$ denoting the coefficient of the block corresponding to the superconformal primary (in the $[0, 0]$ channel). The ordinary shadow symmetry [1] reads

$$\frac{\lambda_{[4,0]}^2(6 - \Delta, \ell)}{K_{6-\Delta,\ell}^{0,0}} = \frac{\lambda_{[4,0]}^2(\Delta, \ell)}{K_{\Delta,\ell}^{0,0}}, \tag{5.3.25}$$

where $K_{\Delta,\ell}^{0,0}$ is a kinematical factor defined in equation (5.4.17) below, and implies a slightly modified shadow symmetry for the superconformal primary:

$$\frac{\lambda_{s.c.p.}^2(\Delta, \ell)}{K_{\Delta+4,\ell}^{0,0}} = \frac{(\ell - \Delta)(-\Delta + \ell + 6)(\Delta + \ell - 2)(\Delta + \ell + 4)}{(-\Delta + \ell - 4)(-\Delta + \ell + 2)(\Delta + \ell + 2)(\Delta + \ell + 8)} \frac{\lambda_{s.c.p.}^2(-2 - \Delta, \ell)}{K_{2-\Delta,\ell}^{0,0}}. \tag{5.3.26}$$

Next, let us consider another trajectory, for example the superconformal primary itself in the $[0, 0]$ channel. How can the above equations be compatible with ordinary shadow symmetry in this channel, which would send $\Delta \to 6 - \Delta$ and not $\Delta \to -2 - \Delta$? The answer is that another superconformal descendant comes to the rescue, as follows. To restore shadow symmetry we need a 'shadow superconformal primary' trajectory $\ell_{s.s.c.p.}(\Delta)$ given by the shadow of the shadow:

$$\ell_{s.s.c.p.}(\Delta) := \ell_{s.c.p.}(6 - \Delta) = \ell_{s.c.p.}(\Delta - 8). \tag{5.3.27}$$

This trajectory does indeed exist in the supermultiplet: it is the top component of the long multiplet with dimension $\Delta + 8$. Compared to the superconformal primary, its coefficient is the messy expression:

$$\lambda^2_{s.s.c.p.}(\Delta + 8, \ell) = \frac{\Delta(\Delta + 6)(-\Delta + \ell + 2)(\Delta - \ell)(\Delta - \ell + 2)^2(\Delta - \ell + 4)}{65536(\Delta + 2)(\Delta + 4)(-\Delta + \ell - 3)(-\Delta + \ell + 1)(-\Delta + \ell + 6)(\Delta - \ell + 1)^2}$$
$$\times \frac{(\Delta + \ell + 2)(\Delta + \ell + 4)(\Delta + \ell + 6)^2(\Delta + \ell + 8)}{(\Delta + \ell - 2)(\Delta + \ell + 3)(\Delta + \ell + 5)^2(\Delta + \ell + 7)} \lambda^2_{s.c.p.}(\Delta, \ell) ,$$

(5.3.28)

but it is precisely the one necessary to recover shadow symmetry between these two multiplets in the $[0, 0]$ channel: with a little computation one finds that

$$\frac{\lambda^2_{s.s.c.p.}(6 - \Delta, \ell)}{K^{0,0}_{6-\Delta, \ell}} = \frac{\lambda^2_{s.c.p.}(\Delta, \ell)}{K^{0,0}_{\Delta, \ell}} .$$

(5.3.29)

We have checked that similar relations exist between other superconformal descendants and that therefore the entire set of Regge trajectories in each of the six R-symmetry channels is shadow symmetric provided the relation (5.3.26) holds. To the best of our knowledge, the corresponding identities involving the coefficients of the different conformal blocks inside the superconformal multiplet have not been observed before. We expect it to be a very general property, valid for any superconformal algebra, that can for example be used as an additional verification in the computations of superconformal blocks, and perhaps provide extra constraints on the superconformal blocks of non-BPS operators.[10] It would be interesting to see if this property can be deduced more directly from properties of the superconformal algebra.

5.4 Supersymmetric inversion

The demonstration of analyticity in spin of the OPE data for any CFT proceeds via the so-called Lorentzian inversion formula of [1]. For the four-point function under consideration one could in principle apply the formula to the six different functions $A_R(z, \bar{z})$ and combine the data from these operations in order to get a complete picture for the Regge trajectories of the superconformal multiplets. A more elegant approach is to work directly with the function $a(z, \bar{z})$. As we will discuss below, this function essentially has all the right properties for the Euclidean and Lorentzian

---

[10]In fact, we naturally would expect that a similar identity holds if we decompose ordinary conformal blocks into lower-dimensional conformal blocks. This would ensure that, if we for example analyse a correlation function of a three-dimensional theory with two-dimensional conformal blocks, the shadow symmetry of each three-dimensional trajectory separately suffices to ensure shadow symmetry of the (generically infinitely many) two-dimensional trajectories it induces. It would be interesting to verify this.

inversion formulas to apply, and its block decomposition will give us direct access to all the OPE coefficients of operators that contribute to it.

5.4.1 Inversion formula for $a(z, \bar{z})$

As can be seen from equations (5.2.7), (5.2.12) and (5.2.13), the function $a(z, \bar{z})$, multiplied by $(z\bar{z})^6$, admits a conformal block decomposition as follows:

$$
\begin{aligned}
(z\bar{z})^6 a(z, \bar{z}) &= (z\bar{z})^6 a^\chi(z, \bar{z}) + (z\bar{z})^6 a^u(z, \bar{z}), \\
(z\bar{z})^6 a^\chi(z, \bar{z}) &= \sum_{\ell=0,\,\ell\,\text{even}}^{\infty} \frac{2^\ell b_\ell}{\ell+3} \mathcal{G}_{\ell+8}^{(\ell)}(\Delta_{12} = 0, \Delta_{34} = -2; z, \bar{z}), \\
(z\bar{z})^6 a^u(z, \bar{z}) &= \sum_{\substack{\Delta \geqslant \ell+6, \\ \ell \geqslant 0,\,\ell\,\text{even}}} \frac{4\lambda_{\Delta,\ell}^2}{(\Delta - \ell - 2)(\Delta + \ell + 2)} \mathcal{G}_{\Delta+4}^{(\ell)}(\Delta_{12} = 0, \Delta_{34} = -2; z, \bar{z}).
\end{aligned}
$$

(5.4.1)

It is therefore most natural to apply the inversion formula of [1] to $(z\bar{z})^6 a(z, \bar{z})$. The inversion formula results in a function $c(\Delta, \ell)$ whose meromorphic structure captures the OPE data. Normally one evaluates $c(\Delta, \ell)$ at integer ℓ and, for generic values of Δ, a pole in $c(\Delta, \ell)$ at some value Δ^* signifies the presence of a conformal block in the OPE decomposition, whose coefficient is simply given by (minus) the residue of the pole. In our case there is a small offset to take into account: a pole at generic Δ^* signifies the presence of a supermultiplet contributing as $a_{\Delta^*-4,\ell}^{\text{at}}$ (for a long multiplet this means the primary has dimension $\Delta_{\text{s.c.p.}} = \Delta^* - 4$ according to table 5.1), and whose OPE coefficient is related to the residue by the factor $4/(\Delta^*-\ell-6)/(\Delta^*+\ell-2)$.

The decomposition (5.4.1) shows that we should treat $(z\bar{z})^6 a(z, \bar{z})$ as a four-point function of non-identical scalar operators with $\Delta_{12} = 0$ and $\Delta_{34} = -2$. Furthermore, all the spins in its block decomposition are even integers and therefore there is no distinction between the t- and the u-channel contributions. The singularities of $(z\bar{z})^6 a(z, \bar{z})$ are also those of a four-point function of non-identical scalars, as can be seen from its conformal block decomposition (5.4.1) and its crossing equation (5.2.14). All in all, the associated spectral density is computable through the Lorentzian inversion formula [1] as[11]

$$
c(\Delta, \ell) = 2^{\Delta-5+\ell} \frac{(1 + (-1)^\ell)}{4} \kappa_{\Delta+\ell}^{0,-2} \int_0^1 dz\,d\bar{z}\,\mu(z, \bar{z})\,\mathcal{G}_{\ell+5}^{(\Delta-5)}(0, -2; z, \bar{z})\,\text{dDisc}_t\left[(z\bar{z})^6 a(z, \bar{z})\right],
$$

(5.4.2)

---

[11]The factor $2^{\Delta-5+\ell}$ follows from our normalization of conformal blocks. It is spelled out in appendix 5.A and differs from that of [1] by a factor 2^ℓ.

where the most important factor involves the *double discontinuity* operation, which for a generic four-point function $g(z, \bar{z})$ reads:

$$\text{dDisc}_t\left[g(z, \bar{z})\right] = \cos\left(\pi\frac{\Delta_{34} - \Delta_{12}}{2}\right) g(z, \bar{z}) - \frac{1}{2}e^{i\pi\frac{\Delta_{34}-\Delta_{12}}{2}} g(z, 1 - (1-\bar{z})e^{2\pi i})$$
$$- \frac{1}{2}e^{-i\pi\frac{\Delta_{34}-\Delta_{12}}{2}} g(z, 1 - (1-\bar{z})e^{-2\pi i}) . \tag{5.4.3}$$

where the $e^{2\pi i}$ factors indicate an analytic continuation onto a secondary sheet, in this case around $\bar{z} = 1$. The other factors are given by:

$$\kappa_{\Delta+\ell}^{\Delta_{12},\Delta_{34}} = \frac{\Gamma(\frac{\Delta+\ell+\Delta_{12}}{2})\Gamma(\frac{\Delta+\ell-\Delta_{12}}{2})\Gamma(\frac{\Delta+\ell+\Delta_{34}}{2})\Gamma(\frac{\Delta+\ell-\Delta_{34}}{2})}{2\pi^2\Gamma(\Delta+\ell-1)\Gamma(\Delta+\ell)} , \tag{5.4.4}$$

$$\mu(z, \bar{z}) = \left|\frac{z-\bar{z}}{z\bar{z}}\right|^{d-2} \frac{((1-z)(1-\bar{z}))^{\frac{\Delta_{34}-\Delta_{12}}{2}}}{(z\bar{z})^2} , \tag{5.4.5}$$

and we recall that $\mathcal{G}_\Delta^{(\ell)}(\Delta_{12}, \Delta_{34}; z, \bar{z})$ is an ordinary bosonic conformal block. For our case one should set $\Delta_{12} = 0$ and $\Delta_{34} = -2$ in all of the above formulas.

5.4.2 Single-valuedness

In the derivations of the Lorentzian inversion formula [1, 33] it is usually assumed that the function to be 'inverted' is a proper CFT four-point function. Here this is not exactly the case: although $a(z, \bar{z})$ has a nice decomposition into s-channel conformal blocks, it has slightly awkward t-channel behaviour. To see this, recall the crossing symmetry equation (5.2.14) and take $z, \bar{z} \to 1$. The functions $a(1-z, 1-\bar{z})$ and $\mathcal{C}_h(1-z, 1-\bar{z})$ are nicely behaved in that limit, but $\mathcal{C}_h(z, \bar{z})$ has a logarithmic term not seen in an ordinary four-point function. Loosely speaking we can write that:[12]

$$(z\bar{z})^6 a(z, \bar{z}) \supset \frac{8(z\bar{z})^4}{c(z-\bar{z})^3}\left(\log(1-z) - \log(1-\bar{z})\right) . \tag{5.4.6}$$

The problem with this term is that it spoils Euclidean single-valuedness of $a(z, \bar{z})$: when setting $\bar{z} = z^*$ and taking z around 1 in the complex plane the function does not return to itself.

It would be nice to investigate the true importance of Euclidean single-valuedness around 1 (and around ∞) for the validity of the Lorentzian inversion formula more generally. We can however show that it is unimportant in our case in a simpler way.

---

[12]This equation attempts to highlight the logarithmic singularity but in doing so is a bit misleading, because it also shows an apparent singularity at $z = \bar{z}$. The latter cancels in the full $a(z, \bar{z})$.

We consider the function

$$a^{\text{free}}(z,\bar{z}) := \frac{(z^3(\bar{z}-1)^3 - 3z^2(\bar{z}-1)^3 + 3z(\bar{z}-1)^3 - (\bar{z}-2)((\bar{z}-1)\bar{z}+1))}{3(z-1)^3 z^2 (\bar{z}-1)^3 \bar{z}^2}$$
$$+ \frac{4(-(z-\bar{z})(z+\bar{z}-2) + 2(z-1)(\bar{z}-1)\log(1-z) - 2(z-1)(\bar{z}-1)\log(1-\bar{z}))}{c(z-1)z^2(\bar{z}-1)\bar{z}^2(z-\bar{z})^3} \,.$$

$$(5.4.7)$$

This function was introduced in [167] as the four-point function obtained by simple Wick contractions in the theory of N free tensor multiplets, with $c = N$ (and it is also a fairly natural object from the holographic perspective). The conformal block decomposition of this function is rather easy to find. Furthermore, if we ignore its non-single-valuedness and blindly substitute it into the Lorentzian inversion formula (5.4.2) we get the right answer.[13] So at least for $a^{\text{free}}(z,\bar{z})$ the non-single valuedness is not an issue.

The argument for the validity of the Lorentzian inversion formula for generic $a(z,\bar{z})$ is then as follows. Let us define:

$$\tilde{a}(z,\bar{z}) = a(z,\bar{z}) - a^{\text{free}}(z,\bar{z}) \,. \tag{5.4.8}$$

Then $(z\bar{z})^6 \tilde{a}(z,\bar{z})$ is single-valued and has a good conformal block decomposition (albeit without positive coefficients), so the Lorentzian inversion formula should be applicable. Of course we get a different density $\tilde{c}(\Delta,\ell)$ which includes the spectrum of $a^{\text{free}}(z,\bar{z})$ in addition to the physical spectrum of $a(z,\bar{z})$. But the Lorentzian inversion formula is fundamentally a linear operation that in itself does not require single-valuedness. So we can split $\tilde{a}(z,\bar{z})$ again and apply the Lorentzian inversion formula to each term separately. Since we verified that the inversion of $a^{\text{free}}(z,\bar{z})$ works and the corresponding $c^{\text{free}}(\Delta,\ell)$ yields the correct conformal block decomposition, it must be that the inversion of $a(z,\bar{z})$ gives

$$\tilde{c}(\Delta,\ell) + c^{\text{free}}(\Delta,\ell) \,, \tag{5.4.9}$$

and this function has the right analyticity properties to recover the conformal block decomposition of $a(z,\bar{z})$ and nothing more.

5.4.3 Behaviour on the second sheet

As we stated above, the results of [1] tie the Regge behaviour of correlation functions to the minimal spin for which the OPE data is guaranteed to be analytic in spin. Non-analyticity happens when the contributions to the integrals from 'arcs at infinity' are non-zero [1, 33, 180]. These arcs correspond to the case where $\bar{z} \to 0$ on the secondary

---

[13]We have explicitly checked this for the operators of twist 4, 6, 8 and 10 but strongly suspect this to be true for all other operators as well.

sheets reached by going around $\bar{z} = 1$. If one sends $z \to 0$ at the same rate as $\bar{z}$ then this is the Regge limit. It is customary to parametrise this limit as:

$$z = w\,\sigma\,, \quad \bar{z} = \frac{w}{\sigma}\,, \quad w \to 0\,, \quad \sigma \text{ fixed}\,. \tag{5.4.10}$$

For a general function $g(z,\bar{z})$ the arguments of [1] imply that with a Regge behaviour of the form

$$g \sim w^{1-\ell_*}\,, \tag{5.4.11}$$

the 'arcs at infinity' contributions from the Regge limit vanish if the integral $\oint_0 dw\, w^{\ell-\ell_*-1}$ converges, so if $\ell > \ell_*$. In this way softer Regge behaviour implies a larger domain of analyticity in spin.

Let us investigate the behaviour of our correlation function in this limit. We begin by noting that the functions $A_R(z,\bar{z})$ have a decomposition into ordinary bosonic blocks, including an identity operator for the singlet channel. The non-supersymmetric arguments of [1] then go through: the $A_R(z,\bar{z})$ must be bounded by a constant in the Regge limit and analyticity in spin holds at least for any spin $\ell > 1$. Supersymmetry allows us to do better. We can see this by eliminating the derivatives in (5.2.4) to find an expression for $a(z,\bar{z})$ in terms of (z and $\bar{z}$ dependent) linear combinations of the $A_R(z,\bar{z})$ and $h(z)$. Since we know $h(z)$ exactly and can also bound the $A_R(z,\bar{z})$, it is not hard to deduce that

$$(z\bar{z})^6 a(z,\bar{z}) \sim \frac{3A_{[2,0]} + A_{[0,4]}}{3} w^2\,, \qquad \text{as } w \to 0\,. \tag{5.4.12}$$

in the Regge limit. This is a softer behaviour in the Regge limit with respect to a bosonic correlator that grows as w^0, ensuring analyticity in spin down to spin $\ell > -1$. However, we expect analyticity to hold all the way down to spin $\ell > -3$. One partial argument for this are the conformal primary trajectories in the R-symmetry singlet channel: as shown in section 5.3 a superconformal primary of spin ℓ has a descendant of spin $\ell + 4$ in this channel. The $\ell > -3$ result for the superconformal primaries then immediately follows from the non-supersymmetric result that analyticity in spin holds down to spin 1 for any conformal family.

This expectation can be proven by bounding the growth of $a(z,\bar{z})$ in the Regge limit directly, as done in [1], using the fact that the t- and u-channel OPEs converge in that limit. In appendix 5.B we use the t- and u-channel OPEs in an expansion in the z and $\bar{\bar{z}}$ variables to bound the growth of $a(z,\bar{z})$ as

$$(z\bar{z})^6 a(z,\bar{z}) \sim w^4\,; \qquad \text{as } w \to 0\,, \tag{5.4.13}$$

along almost any direction in the complex w-plane, confirming analyticity in spin of

$c(\Delta, \ell)$ all the way for all spins greater than $-3!$[14]

We note that the non-single-valuedness of $a(z, \bar{z})$ is not important: since $a^{\text{free}}(z, \bar{z})$ behaves like w^5 in this limit, equation (5.4.13) also gives the leading behaviour for the single-valued correlator $\tilde{a}(z, \bar{z})$.

Let us finally discuss the Regge behaviour of the six functions $A_R(z, \bar{z})$. A naive estimate arises by plugging the behaviour (5.4.13) into equation (5.2.4), but the latter contains derivatives and if a function vanishes at least as fast w^4 then it is not mathematically guaranteed that its derivative vanishes at least as fast as w^3. In appendix 5.B we therefore explain how to bound the derivatives of $a(z, \bar{z})$ directly, leading to the Regge behaviour:

$$A_{[4,0]} \sim w^4, \qquad A_{[2,2]} \sim w^3, \qquad A_{[2,0]} \sim w^2,$$
$$A_{[0,4]} \sim w^2, \qquad A_{[0,2]} \sim w^1, \qquad A_{[0,0]} \sim w^0. \tag{5.4.14}$$

This directly leads to the results quoted in equation (5.3.1) at the beginning of section 5.3.

The lightcone limit

Another potential contribution from the 'arcs at infinity' comes from a lightcone limit on the second sheet that corresponds to $\bar{z} \to 0$ holding z fixed. In this limit the convergence of the Lorentzian inversion formula depends on Δ and ℓ; more precisely, if $g(z, \bar{z}) \sim \bar{z}^{\tau^*/2}$ in that limit, then we need

$$\Delta - \ell < \tau^*, \qquad \text{and} \qquad d - \Delta - \ell < \tau^*. \tag{5.4.15}$$

It is not immediately clear what the correct value of τ^* could be. On the first sheet τ^* is equal to the lowest twist in the s-channel spectrum. In that case $\tau^* \geq d/2 - 1$ would be appropriate for a generic CFT, because the s-channel identity operator needs to be subtracted, while in our case $\tau^* = 8$. As discussed in [33], this value again leads to analyticity in spin for $\ell > 1$ because we can set $\Delta = d/2$, and in our case it would not spoil $\ell > -3$. On the secondary sheets this is not necessarily true because the s-channel block decomposition no longer converges – instead one uses the t-channel conformal block decomposition (and unitarity) to bound the full correlator by its behaviour on the first sheet. The best possible bound that can be rigorously proven in this way corresponds to $\tau^* \geq 0$. This value is however unlikely: it would imply non-convergence of the Lorentzian inversion formula for $\Delta < \ell$ and invalidate the analyses of the first Regge trajectory in the literature. (In our case we can show that $\tau^* \geq 4$ instead of zero from (5.B.3) and (5.B.8), but the effect is similar.)

---

[14]To be precise, the z and $\bar{z}$ expansion can be used to show the given behaviour along any direction with $\arg(w) \neq \pi/2$. Using the ρ variables it might be possible to show the bound is valid also exactly along the imaginary axis. See appendix 5.B for details.

It would be interesting to have a better handle on the lightcone behaviour on the secondary sheets, but we will not consider possible lightcone contributions further in the remainder of this chapter. See [19, 33, 144, 181] for previous discussions on the second sheet lightcone limit.

5.4.4 Analyticity properties of $c(\Delta, \ell)$

As we explained in the previous subsection, conformal blocks in the decomposition of $a(z, \bar{z})$ correspond to poles in the function $c(\Delta, \ell)$. These are however not the only poles: there are also kinematical singularities. It is therefore worthwhile to take a look at the analytic structure of $c(\Delta, \ell)$, which we will do in this subsection. In contrast with most other studies we will also be interested in what happens at *negative* spins ℓ. The result of our analysis is summarized in figure 5.6.

Kinematical singularities

Recall that the shadow symmetry of the OPE density is embodied in the following equation

$$\frac{c(\Delta, \ell)}{K_{\Delta, \ell}^{\Delta_{12}, \Delta_{34}}} = \frac{c(d - \Delta, \ell)}{K_{d-\Delta, \ell}^{\Delta_{12}, \Delta_{34}}}, \tag{5.4.16}$$

where

$$K_{\Delta, \ell}^{\Delta_{12}, \Delta_{34}} = \frac{\Gamma(\Delta - 1)}{\Gamma(\Delta - d/2)} \kappa_{\Delta+\ell}^{\Delta_{12}, \Delta_{34}}. \tag{5.4.17}$$

The shadow symmetry for $c(\Delta, \ell)$ follows automatically from $c(\Delta, \ell)$ as defined through eqs. (5.4.2) and (5.4.1), and from shadow symmetry in the $[4, 0]$ channel given in (5.3.25). For this reason we choose to analyse the kinematical singularities of $c(\Delta, \ell)/K_{\Delta, \ell}^{0, -2}$ and one can recover the kinematical singularities of $c(\Delta, \ell)$ by removing the K factor. From (5.4.2) we see that these singularities are encoded in the kernel block times a prefactor, more precisely $2^{\Delta-5} \frac{\Gamma(\Delta-3)}{\Gamma(\Delta-1)} \mathcal{G}_{\ell+5}^{(\Delta-5)}(0, -2; z, \bar{z})$. Using (5.5.11) it can be easily checked that this combination is shadow symmetric.

The generic pole structure of conformal blocks was discussed in [81, 182], but it does not apply to even spacetime dimensions where we can also encounter double poles. In our case $d = 6$ and thus we will analyse the pole structure using the closed form of the six-dimensional conformal blocks directly.

We are only interested in the pole locations and below in table 5.2 we tabulate both the simple and double poles in $\frac{\Gamma(\Delta-3)}{\Gamma(\Delta-1)} \mathcal{G}_{\ell+5}^{(\Delta-5)}(0, -2; z, \bar{z})$. We have written these as poles in spin because we will soon be interested in the setup with fixed Δ and negative ℓ.

pole locations in ℓ	simple poles	double poles
$(\Delta - 3) - 4 - 2n$	$n \in \mathbb{Z}_{\geq 0}$	$\Delta \in \mathbb{Z}_{\leq 3}, n \in \mathbb{Z}_{\geq 0}$
-3		$\Delta = 2, 4$
$-(\Delta - 3) - 4 - 2n$	$n \in \mathbb{Z}_{\geq 0}$	$\Delta \in \mathbb{Z}_{\geq 4}, n \in \mathbb{Z}_{\geq 0}$

Table 5.2. Simple and double poles of $\frac{\Gamma(\Delta-3)}{\Gamma(\Delta-1)} \mathcal{G}_{\ell+5}^{(\Delta-5)}(0, -2; z, \bar{z})$

Dynamical poles and analyticity in spin

Finally we have to take into account the dynamical poles in $c(\Delta, \ell)$. The conformal block decomposition of $(z\bar{z})^6 a(z, \bar{z})$ was given in equation (5.4.1). The short multiplets induce two straight Regge trajectories: one with known OPE coefficients at $\Delta = \ell + 8$ and one with unknown OPE coefficients at $\Delta = \ell + 10$. The long multiplets have unknown scaling dimensions, but as we discussed in the previous subsection we expect the leading long trajectory to smoothly continue to the stress tensor. If we take the various offsets into account this means that it must cross through the point $\Delta = 6$ and $\ell = -2$ in $c(\Delta, \ell)$. The numerical results of [18] further suggest that this trajectory asymptotes to the leading double twist trajectory, which here implies that its asymptotic twist equals 12.

In section 5.4.3 we analysed the Regge behaviour of the function $a(z, \bar{z})$ and found that it behaves rather smoothly; if $z = \sigma w$ and $\bar{z} = w/\sigma$ then $(z\bar{z})^6 a(z, \bar{z}) \sim w^4$ as $w \to 0$ on the secondary sheets. The integral in (5.4.2) therefore converges in that region as long as $\ell > -3$, and the contributions from the 'arcs at infinity' in the Regge limit must also vanish for this range of spins.

An impression of the interplay of kinematic and dynamical poles is shown in figure 5.6. We omitted the subleading unprotected Regge trajectories in the figure. Note that the claim 1 implies the short $\mathcal{B}[2, 0]$ trajectory and the leading long trajectory intersect at spin -2 and $\Delta = 6$ in figure 5.6. The OPE coefficients of the two trajectories are such that the residue of $c(\Delta, -2)$ at $\Delta = 4$ vanishes.

5.5 Practical supersymmetric inversion

In this section we will discuss some practical aspects of working with the inversion formula (5.4.2) for $a(z, \bar{z})$. We will first discuss the use of the crossing equation and the simplifications that occur after substitution of the t-channel conformal block decomposition. This provides sufficient background for a small (and crude) numerical test of convergence for negative spins which we perform in subsection 5.5.2. It will be convenient to consider the small z expansion of the integrand of equation (5.4.2),
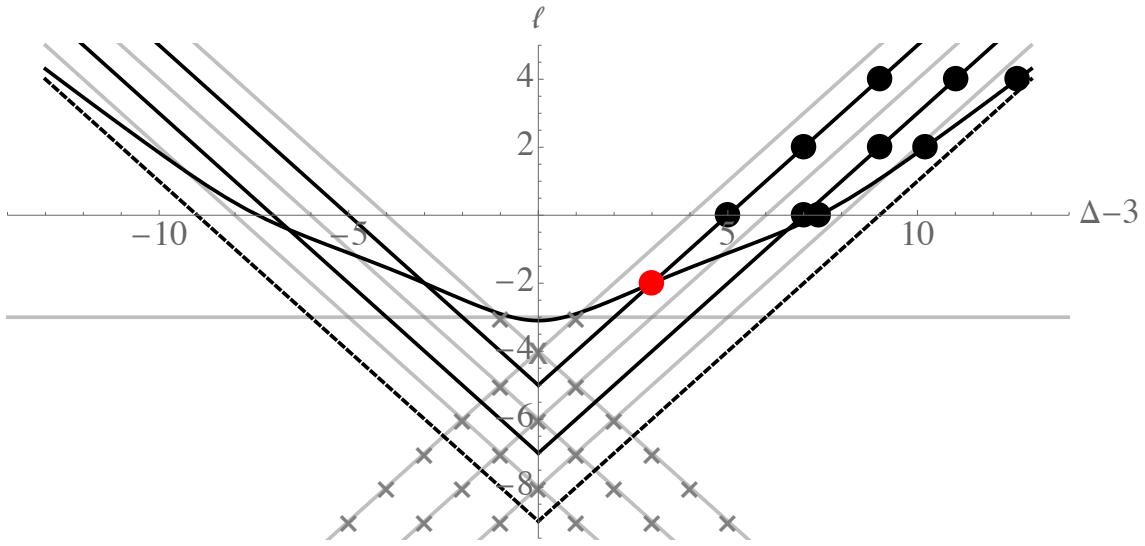
Figure 5.6. Regge trajectories (black) and kinematical poles (grey) of $c(\Delta, \ell)/K_{\Delta, \ell}^{0, -2}$ for $a(z, \bar{z})$. The dots indicate physical operators with the red one corresponding to the the stress tensor multiplet. The dashed line indicates the asymptotic double twist behaviour of the leading long multiplets. The grey crosses indicate double poles.

and in subsection 5.5.3 we explain how this works and use it to recover the OPE coefficients of the short multiplets that contribute to the chiral algebra. This all provides sufficient background for more serious numerical experiments in section 5.6.

One subtle but important point of the inversion formula (5.4.2) is relegated to appendix 5.C. In that appendix we discuss how to regulate divergences that arise in the $z \to 1$ limit of the integral. Roughly speaking these divergences arise because the scaling dimensions are integers, and in practice we find badly divergent integrals of the type $\int^{1} dz \, (1 - z)^{-n}$. Although such divergences are invisible in the small z expansion discussed in subsection 5.5.3, it is of course of fundamental importance that we are able to tame them since otherwise the entire inversion formula would stop making sense.

5.5.1 The t-channel decomposition

The double discontinuity (5.4.3) vanishes for each s-channel block separately and the integral in (5.4.2) does not commute with the decomposition into these blocks. Instead one can employ crossing symmetry and consider the t-channel block decomposition. In typical 'experiments' one approximates the four-point function on the right-hand side of (5.4.2) with a finite sum of t-channel blocks and investigates the resulting approximation to $c(\Delta, \ell)$.

Let us recall that the crossing equation (5.2.14) for $a(z, \bar{z})$ reads:

$$z\bar{z}\, a(z, \bar{z}) = (1 - z)(1 - \bar{z}) \left(a^{u}(1 - z, 1 - \bar{z}) + a^{\chi}(1 - z, 1 - \bar{z}) \right)$$
$$+ \mathcal{C}_h(1 - z, 1 - \bar{z}) - \mathcal{C}_h(z, \bar{z}) \,, \tag{5.5.1}$$

where

$$\mathcal{C}_h(z, \bar{z}) = \frac{1}{(z - \bar{z})^3} \frac{h(z) - h(\bar{z})}{z\bar{z}}. \tag{5.5.2}$$

Notice that we now split $a(1 - z, 1 - \bar{z}) = a^\chi(1 - z, 1 - \bar{z}) + a^u(1 - z, 1 - \bar{z})$ on the right-hand side to highlight that one part of this function is known and fixed by the chiral algebra as discussed in section 5.2.

The Lorentzian inversion formula instructs us to take the double discontinuity of the right-hand side of equation (5.5.1). It is well-known that, in general conformal field theories, the contribution to the double discontinuity vanishes for the t-channel operators with double-twist quantum numbers. In our case even more cancellations occur than the "double-twists" of the inverted correlator $(z\bar{z})^6 a(z, \bar{z})$, although they do correspond to double-twists in the different R-symmetry channels.

First consider $a^u(1 - z, 1 - \bar{z})$. Its block decomposition was given in equation (5.2.13) which we repeat here:

$$a^u(1 - z, 1 - \bar{z}) = \sum_{\Delta \geqslant \ell+6, \ell} \lambda^2_{\Delta, \ell} a^{\mathrm{at}}_{\Delta, \ell}(1 - z, 1 - \bar{z}). \tag{5.5.3}$$

It is not hard to verify that the blocks with $\Delta = \ell + 6$ that saturate the inequality, which we recall correspond to the $\mathcal{D}[0, 4]$ multiplet (for $\ell = 0$) and the $\mathcal{B}[0, 2]_\ell$ multiplets (for $\ell > 0$), have vanishing integrated double discontinuity. Therefore only the long multiplets can contribute, and:

$$\mathrm{dDisc}_t \left[(1 - z)(1 - \bar{z}) a^u(1 - z, 1 - \bar{z}) \right] = \sum_{\Delta > \ell+6, \ell} \lambda^2_{\Delta, \ell} \, \mathrm{dDisc}_t \left[(1 - z)(1 - \bar{z}) a^{\mathrm{at}}_{\Delta, \ell}(1 - z, 1 - \bar{z}) \right] .$$

$$\tag{5.5.4}$$

so the inequality constraint for Δ has become strict. The double discontinuity of a single t-channel conformal block is

$$\mathrm{dDisc}_t \left[\mathcal{G}^{(\ell)}_\Delta(0, -2; 1 - z, 1 - \bar{z}) \right] = -2 \sin^2 \left(\frac{\Delta + \ell}{2} \pi \right) \mathcal{G}^{(\ell)}_\Delta(0, -2; 1 - z, 1 - \bar{z}),$$

$$\tag{5.5.5}$$

where we have used the fact that ℓ is an even integer.

Next we consider $a^\chi(1 - z, 1 - \bar{z})$. This is a known function whose block decomposition was given in equation (5.2.12). For these blocks the double discontinuity is not vanishing, but instead it cancels almost entirely against the contribution from

$\mathcal{C}_h(1-z, 1-\bar{z})$. In fact we may write:

$$\text{dDisc}_t \left[(1-z)(1-\bar{z})a^{\chi}(1-z, 1-\bar{z}) + \mathcal{C}_h(1-z, 1-\bar{z})\right] =$$

$$\text{dDisc}_t \left[\frac{\tilde{h}(1-z) - \tilde{h}(1-\bar{z})}{(\bar{z}-z)^3(1-z)(1-\bar{z})}\right], \quad (5.5.6)$$

with $\tilde{h}(z)$ defined as the 'truncation' of $h(z)$ to just the identity and the stress tensor block:

$$\tilde{h}(z) = h_0^{\text{at}}(z) + b_{-2}h_2^{\text{at}}(z) = -\frac{1}{2} + \frac{1}{z} + \frac{24}{c}\left(1 - \frac{2}{z} + \frac{2\log(1-z)}{z} - \frac{2\log(1-z)}{z^2}\right).$$
$$(5.5.7)$$

Notice that the identity and the stress tensor are the only multiplets that do not contribute to $a^{\chi}(1-z, 1-\bar{z})$.

The previous two paragraphs imply that, out of the all t-channel data, *only the identity, the stress tensor multiplet, and the long multiplets contribute to the double discontinuity.* The contribution of all the other short multiplets simply drops out. Notice that there is furthermore a contribution to the double discontinuity from $\mathcal{C}_h(z, \bar{z})$ which is non-vanishing and not subject to the above cancellations. In equations:

$$\text{dDisc}_t \left[(z\bar{z})^6 a(z, \bar{z})\right]$$

$$= \sum_{\Delta > \ell+6, \ell} \lambda_{\Delta,\ell}^2 \text{dDisc}_t \left[(z\bar{z})^5(1-z)(1-\bar{z})a_{\Delta,\ell}^{\text{at}}(1-z, 1-\bar{z})\right]$$

$$+ \text{dDisc}_t \left[\frac{(z\bar{z})^5\left(\tilde{h}(1-z) - \tilde{h}(1-\bar{z})\right)}{(\bar{z}-z)^3(1-z)(1-\bar{z})} - (z\bar{z})^5\mathcal{C}_h(z, \bar{z})\right]$$

$$= \sum_{\Delta > \ell+6, \ell} \frac{-8\lambda_{\Delta,\ell}^2}{(\Delta-\ell-2)(\Delta+\ell+2)}\left(\frac{z\bar{z}}{(1-z)(1-\bar{z})}\right)^5 \sin^2\left(\frac{\Delta+\ell}{2}\pi\right)\mathcal{G}_{\Delta+4}^{(\ell)}(0, -2; 1-z, 1-\bar{z})$$

$$+ \text{dDisc}_t \left[\left(\frac{2z^4}{(1-z)^3} + \frac{8z^4\left(1 - 6z + 3z^2 + 2z^3 - 6z^2\log(z)\right)}{c(1-z)^6}\right)\frac{1}{1-\bar{z}}\right.$$

$$\left. - \frac{4z^4}{3(1-z)^3}\frac{1}{(1-\bar{z})^2} + \frac{z^4}{3(1-z)^3}\frac{1}{(1-\bar{z})^3} + \frac{8z^4}{c(1-z)^3}\log(1-\bar{z})\right],$$
$$(5.5.8)$$

where in passing to the final expression we have only kept the terms with non-vanishing double discontinuity.

175
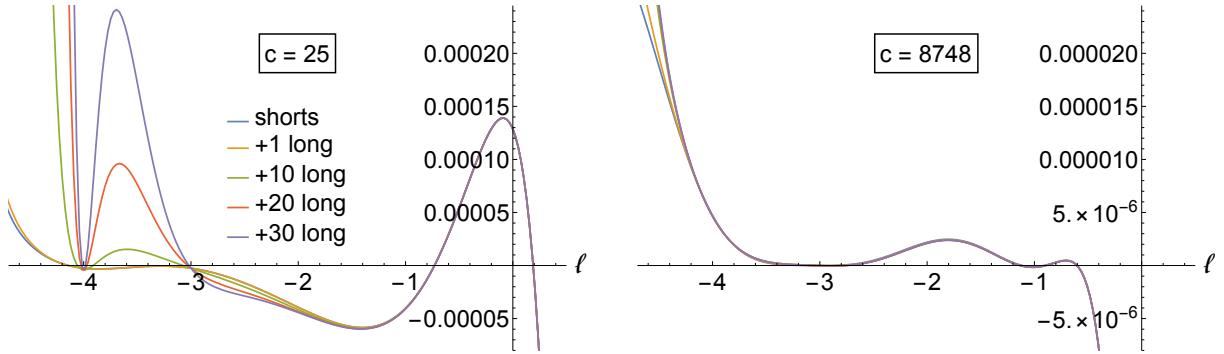
Figure 5.7. We plot a crude estimate of $c(\Delta, \ell)|_{\text{phys}}$ as a function of ℓ with $\Delta = 3 + 10^{-5}$ and with $c = 25$ (left) and $c = 8748$ (right). The slight displacement from the shadow symmetric line at $\Delta = 3$ is simply for faster numerics. Here $c(\Delta, \ell)|_{\text{phys}} = (\ell + 3) c(\Delta, \ell) / [\kappa_{\Delta + \ell} \Gamma((\ell + \Delta + 1)/2) \Gamma((\ell + 6 - \Delta + 1)/2)]$ is just the $c(\Delta, \ell)$ with all spurious poles divided out. The long blocks are scalars from increasingly large twist trajectories $(8, 10, 12, ...)$. Their OPE coefficients are taken from supergravity results for $c = 25$ and mean field theory results for $c = 8748$. The anomalous dimensions are all set to -1.

5.5.2   Convergence along shadow-symmetric line

As a first experiment we can try to see if we can numerically observe convergence for negative spins as predicted by the Regge behaviour discussed in section 5.4.3. To do so we can start with (5.5.8) and plug in increasingly many t-channel blocks. Since we do not know the exact spectrum (and are only interested in a quick numerical check of the convergence properties anyway) we took a maximally crude approximation: apart from the leading Regge trajectory, for which we used some input from the numerical bootstrap results of [18], we took a 'shifted' mean-field-like spectrum of scalar operators where all the dimensions were shifted from their mean field values by 1. This was done to maximize their contribution to the dDisc, because with the shift the prefactor $\sin^2(\pi(\Delta + \ell)/2) = 1$. For the OPE coefficients we took the values obtained from the supergravity computation of [167] extrapolated to finite c. We did not add spinning operators since these numerically would have contributed much less to the double discontinuity anyway. We then inverted this spectrum using (5.4.2) and plot the resulting function $c(\Delta, J)$ at the shadow-symmetric point where $\Delta = d/2 + 10^{-5}$, taking care to regulate the $z \to 1$ divergences as discussed in appendix 5.C. The results are shown in figure 5.7.

Note that we have divided out unphysical poles analysed in subsection 5.4.4. Although our estimate is extremely crude, we do see convergence for negative spins and a breakdown not until spin -3 for $c = 25$ and around -4 for $c = 8748$. Note that the pole at $\ell = -5$ is expected: it is the intercept of the leading short trajectory which we also show in figure 5.6.

5.5.3 Small z expansion

We would like to use the inversion formula (5.5.8) to extract anomalous dimensions and OPE coefficients. A practical way to do so is to use the small z expansion [1], which works as follows. We first define

$$h = \frac{\Delta - \ell}{2}, \qquad \bar{h} = \frac{\Delta + \ell}{2}, \tag{5.5.9}$$

and rewrite (5.4.2) as

$$c(h, \bar{h}) = \int_0^1 \frac{dz}{2z} z^{-h} \left(2^{2\bar{h}-5} 2\kappa_{2\bar{h}}^{0,-2} z^{h+1} \int_z^1 d\bar{z}\, \mu(z, \bar{z})\, \mathcal{G}_{\bar{h}-h+5}^{(\bar{h}+h-5)}(0, -2; z, \bar{z})\, \mathrm{dDisc}_t \left[(z\bar{z})^6 a(z, \bar{z}) \right] \right). \tag{5.5.10}$$

Here we have restricted the range of $\bar{z}$ integration to $z < \bar{z} < 1$ which brings in a factor of 2. We are also considering only the even spin $c(h, \bar{h})$ and thus replaced $1 + (-1)^\ell = 2$. In the limit $z \to 0$ the bracketed expression above can be expanded in powers of z and then the outer integral simply converts these powers into poles of h. The OPE coefficients are then given by the coefficients of this power series expansion — up to a Jacobian to transform from $(h, \bar{h})$ back to (Δ, ℓ).

When away from shadow symmetric line we can simplify (5.5.10) by discarding "half" of the kernel block. This follows from the fact that one can split a conformal block into two parts:

$$\mathcal{G}_{\ell+d-1}^{(\Delta+1-d)}(\Delta_{12}, \Delta_{34}; z, \bar{z}) = (\mathcal{G}^{\mathrm{pure}})_{\ell+d-1}^{(\Delta+1-d)}(\Delta_{12}, \Delta_{34}; z, \bar{z})$$
$$+ 2^{d-2\Delta} \frac{\Gamma(\Delta-1)\Gamma\left(-\Delta+\frac{d}{2}\right)}{\Gamma\left(\Delta-\frac{d}{2}\right)\Gamma(-(\Delta+1-d))} (\mathcal{G}^{\mathrm{pure}})_{\ell+d-1}^{(-\Delta+1)}(\Delta_{12}, \Delta_{34}; z, \bar{z}), \tag{5.5.11}$$

where each of the $\mathcal{G}^{\mathrm{pure}}$ can be expanded into pure power terms in the limit $z \ll \bar{z} \ll 1$ [1]. For example, the contribution from the first $\mathcal{G}^{\mathrm{pure}}$ to the $\bar{z}$ integral kernel in (5.5.10) has the following expansion

$$2^{\bar{h}+h+1-d} z^{h+1} \mu(z, \bar{z})(\mathcal{G}^{\mathrm{pure}})_{\bar{h}-h+d-1}^{(\bar{h}+h+1-d)}(\Delta_{12}, \Delta_{34}; z, \bar{z})$$
$$= \frac{(1-\bar{z})^{\frac{\Delta_{34}-\Delta_{12}}{2}}}{\bar{z}^2} \sum_{n=0}^{\infty} z^n \sum_{j=-n}^{n} B_{n,j}^{\Delta_{12},\Delta_{34}}(h, \bar{h}) k_{2(\bar{h}+j)}^{\Delta_{12},\Delta_{34}}(\bar{z}), \tag{5.5.12}$$

where the constant prefactor is inserted to simplify notation, and

$$k_{2\bar{h}}^{\Delta_{12},\Delta_{34}}(z) := z^{\bar{h}}\, {}_2F_1\left(\bar{h} - \frac{\Delta_{12}}{2}, \bar{h} + \frac{\Delta_{34}}{2}, 2\bar{h}; z\right). \tag{5.5.13}$$

Similar manipulations can be done for the second pure power term, with one notable difference that the second expansion scales as $z^{\Delta - d/2}(1 + O(z))$ which we can ignore when we are to the right of the shadow symmetric line.

The expansion coefficients in (5.5.12) are easy to fix[15] and the first few coefficients with $d = 6$, $\Delta_{12} = 0$, $\Delta_{34} = -2$ are

$$
\begin{aligned}
B_{0,0}(h, \bar{h}) &= 1 \,, \\
B_{1,1}(h, \bar{h}) &= -\frac{\left(\bar{h}^2 - 1\right)(h - \bar{h} - 2)}{2(2\bar{h} - 1)(2\bar{h} + 1)(h - \bar{h} - 3)} \,, \\
B_{1,0}(h, \bar{h}) &= 1 - \frac{h}{2} \,, \\
B_{1,-1}(h, \bar{h}) &= -\frac{2(h + \bar{h} - 3)}{h + \bar{h} - 4} \,.
\end{aligned}
\tag{5.5.15}
$$

After substituting the inverted block with $\mathcal{G}^{\text{pure}}$ and using the expansion (5.5.12), we can define a generating function as

$$
C(z, \bar{h} + j) = 2^{\bar{h} - h + 1} \kappa_{2\bar{h}}^{0,-2} \int_z^1 \frac{d\bar{z}}{\bar{z}^2 (1 - \bar{z})} k_{2(\bar{h}+j)}^{0,-2}(\bar{z}) \, \text{dDisc}_t \left[(z\bar{z})^6 a(z, \bar{z}) \right] \,, \tag{5.5.16}
$$

such that (5.5.10) can be rewritten as

$$
\begin{aligned}
c(h, \bar{h}) &= \int_0^1 \frac{dz}{2z} z^{-h} \left(\sum_{n,j} z^n B_{n,j}(h, \bar{h}) C(z, \bar{h} + j) \right) \\
&\equiv \int_0^1 \frac{dz}{2z} z^{-h} \widetilde{C}(z, h, \bar{h}) \,.
\end{aligned}
\tag{5.5.17}
$$

In the existing literature the small z expansion of the inversion formula is generally used to extract CFT data of the leading trajectory from the generating function. For such a case we would only need the leading ($n = j = 0$) term. We may write

$$
C(z, \bar{h}) \approx P(\bar{h}) z^{h(\bar{h})} \,, \tag{5.5.18}
$$

and the OPE data for the leading trajectory can then be extracted as

$$
h(\bar{h}) = \lim_{z \to 0} \frac{z \partial_z C(z, \bar{h})}{C(z, \bar{h})} \,, \qquad P(\bar{h}) = \lim_{z \to 0} \frac{C(z, \bar{h})}{z^{h(\bar{h})}} \,, \tag{5.5.19}
$$

---

[15]For this it is useful to use the identity [1]

$$
\frac{1}{\bar{z}} k_{2\bar{h}}(\bar{z}) = k_{2\bar{h}-2}(\bar{z}) + \left(\frac{1}{2} + \frac{\Delta_{12}\Delta_{34}}{8\bar{h}(\bar{h}-1)} \right) k_{2\bar{h}}(\bar{z}) + \frac{\left(\Delta_{12}^2 - 4\bar{h}^2\right)\left(\Delta_{34}^2 - 4\bar{h}^2\right)}{64\bar{h}^2 \left(4\bar{h}^2 - 1\right)} k_{2\bar{h}+2}(\bar{z}) \,. \tag{5.5.14}
$$

where $h(\bar{h}) = h_\infty + \delta h(\bar{h})$ with h_∞ the double-trace value and $\delta h(\bar{h}) \to 0$ as $\bar{h} \to \infty$. The anomalous dimension can be determined by solving the equation

$$\delta h(\bar{h}) = \bar{h} - \ell - h_\infty\,. \tag{5.5.20}$$

and the squared OPE coefficient can be calculated through

$$\lambda_{\Delta,\ell}^2 = \left(1 - \frac{\partial h(\bar{h})}{\partial \bar{h}}\right)^{-1} \cdot P(\bar{h})\,, \tag{5.5.21}$$

where the Jacobian factor is needed because $\lambda_{\Delta,\ell}^2$ is the residue of $c(\Delta, \ell)$ with respect to Δ at fixed ℓ.

In our case the setup is slightly different. A quick look at figure 5.6 shows that for all non-negative spins the leading two trajectories are expected to be straight: they correspond respectively to the short multiplets belonging to the chiral algebra (with known coefficients) and the short multiplets at the unitarity bound of the long multiplet (with unknown coefficients). After that we find the leading unprotected trajectory. In equations this means that, if we write the generic power expansion ansatz,

$$\widetilde{C}(z, h, \bar{h}) \approx \sum_k P_k(h, \bar{h}) z^{h_k(\bar{h})}\,, \tag{5.5.22}$$

then in our case

$$\widetilde{C}(z, h, \bar{h}) \approx P_4(h, \bar{h}) z^4 + P_5(h, \bar{h}) z^5 + \sum_k P_k(h, \bar{h}) z^{h_k(\bar{h})}\,, \tag{5.5.23}$$

with the sum running over all the unprotected Regge trajectories.

Consistency with the conformal block decompositions

Let us now offer some comments on the consistency of (5.5.23) with the conformal block decompositions. Firstly, it agrees (as it should) with the s-channel expansion of $a(z, \bar{z})$: taking all the prefactors into account it is easy to see that the contributions from $a_{\ell+4,\ell}^{\text{at}}$ begin at z^4, those from $a_{\ell+6,\ell}^{\text{at}}$ at z^5, and those from the long multiplets at even higher powers; for example, in mean field theory the leading unprotected trajectory begins to contribute at the z^6 term.

Next, let us try to discern the origin of the various powers in (5.5.23) from the t-channel perspective. (In the footnote below we discuss the obvious issue of convergence.) To do so we have to remember the inhomogeneous crossing symmetry equation for $\text{dDisc}_t\left[(z\bar{z})^6 a(z, \bar{z})\right]$, which concretely speaking leads to the extra terms displayed in equation (5.5.8). These (known) terms already result in z^4 and z^5 terms (without logarithms) at small z, and in the next subsection we will show that the z^4 term precisely reproduces the OPE coefficients of the short multiplets that contribute

to the chiral algebra. This leaves us with the sum over t-channel blocks corresponding to the unknown operators. At small z, a single t-channel block looks like:

$$
\left(\frac{z\bar{z}}{(1-z)(1-\bar{z})} \right)^5 \mathcal{G}_\Delta^{(\ell)}(0, -2; 1-z, 1-\bar{z}) =
$$

$$
\sum_{n=0}^{\infty} z^{n+5} H_{\Delta,\ell}^{(1),n}(1-\bar{z}) + \sum_{n=0}^{\infty} z^{n+6} \log(z) H_{\Delta,\ell}^{(2),n}(1-\bar{z}) , \quad (5.5.24)
$$

where the prefactor on the left-hand side matches that of the crossing equation (5.5.8) and the explicit form of the H functions will not be important for us. Remarkably, this is precisely the structure that we would expect from equation (5.5.23): no contribution to the z^4 term, which is therefore determined entirely by the inhomogeneous terms in the crossing symmetry equation, a non-zero z^5 term, which means a non-zero contribution to the short multiplets with undetermined coefficients, and a logarithm signifying an anomalous dimension starting only at order z^6.[16]

In the next subsection we will first invert the z^4 term in order to recover the known OPE coefficients of the chiral algebra. In section 5.6 we will numerically estimate some of the unknown OPE data corresponding to the z^5 term and beyond.

Recovering the chiral algebra shorts

In agreement with the previous discussion we will take the coefficient of z^4 from the inhomogeneous terms in the crossing equation (5.5.8) and ignore any contribution from the unprotected multiplets. Substituting this into equation (5.5.16) for the generating function, the integral to do is then:

$$
\left. C(z, \bar{h}) \right|_{z^4} = 2^{\bar{h}-h+1} \kappa_{2\bar{h}}^{0,-2} \int_0^1 \frac{d\bar{z}}{\bar{z}^2(1-\bar{z})} k_{2\bar{h}}^{0,-2}(\bar{z})
$$

$$
\times \mathrm{dDisc}_t \left[\frac{1}{3} \frac{1}{(1-\bar{z})^3} - \frac{4}{3} \frac{1}{(1-\bar{z})^2} + \left(2 + \frac{8}{c} \right) \frac{1}{1-\bar{z}} + \frac{8}{c} \log(1-\bar{z}) \right] ,
$$

$$
(5.5.25)
$$

---

[16] An important caveat to the above analysis is that an infinite sum over t-channel blocks need not have the same behaviour as a single block, and so using equation (5.5.24) in the crossing symmetry equation does not constitute a completely reliable estimate for the small z limit of $a(z, \bar{z})$. In fact, a comparison of the (known) z^4 term on both sides of the crossing equations does show that the t-channel blocks must sum up to give non-zero z^4 and z^5 terms in $(z\bar{z})^6 a(z, \bar{z})$. However, it is also easy to see that these terms have vanishing double discontinuity and are therefore unimportant in the Lorentzian inversion formula. Also, each t-channel block only contributes with $\log(z)$ and integer z powers, while finite anomalous dimensions (with respect to exact double-twist dimensions) require higher powers of the $\log(z)$.

Using the factor $4/(\Delta_{\text{s.c.p.}} - \ell - 2)(\Delta_{\text{s.c.p.}} + \ell + 2)$ to convert to physical OPE coefficient, we have

$$C(z, \bar{h} = \ell + 4)\Big|_{z^4} = \frac{\lambda^2_{\mathcal{B}[2,0]_{\ell-2}}}{\ell + 3}. \tag{5.5.26}$$

and with a bit of algebra one then finds

$$\lambda^2_{\mathcal{B}[2,0]_{\ell-2}} = \frac{\sqrt{\pi}\, 2^{-\ell-7}(\ell+1)(\ell+2)(\ell+3)\Gamma(\ell+7)}{9\,\Gamma\left(\ell+\frac{7}{2}\right)} + \frac{\sqrt{\pi}\, 2^{-\ell-2}\left(\ell^2 + 7\ell + 11\right)\Gamma(\ell+4)}{c\,\Gamma\left(\ell+\frac{7}{2}\right)}. \tag{5.5.27}$$

It is easy to check that the result matches $2^\ell b_\ell$ for all even spins, but is a nicer function of ℓ.

5.6 Numerical approximations

In this section we will use the small z expansion of subsection 5.5.3 for some numerical experiments. Our main question is whether the input of some limited t-channel OPE data can produce a reliable approximation of the s-channel OPE data. We will mostly focus on the low-spin operators in the leading Regge trajectory which will allow us to make comparisons to the numerical bootstrap results of [18].

5.6.1 Inversion for higher-twist trajectories

In this section we generalize (5.5.19), which states how to extract the leading-twist data from the inversion formula, to higher-twist trajectories. This amounts to extracting the coefficient and powers of the z^5 and higher terms in $\widetilde{C}(z, h, \bar{h})$ shown in equation (5.5.23). These terms get contributions from the long multiplets, which we do not know exactly, and so we use an approximation scheme where we input only finitely many long t-channel blocks. For the z^5 term the scheme is obvious: we just sum the coefficients of all the z^5 terms of whatever t-channel blocks we put into the inversion formula. The resulting coefficient in the generating function directly provides an estimate for the OPE coefficients of the $\mathcal{D}[0,4]$ and $\mathcal{B}[0,2]_\ell$ short multiplets. The integrals to be done are detailed in subsection 5.6.1 below.

For the unprotected multiplets the ansatz (5.5.23) in principle dictates that we should compute:

$$h_n(\bar{h}) = \lim_{z\to 0} \frac{z\partial_z \widetilde{C}_n^{\text{sub.}}(z, h, \bar{h})}{\widetilde{C}_n^{\text{sub.}}(z, h, \bar{h})}, \qquad P_n(h, \bar{h}) = \lim_{z\to 0} \frac{\widetilde{C}_n^{\text{sub.}}(z, h, \bar{h})}{z^{h_n(\bar{h})}}. \tag{5.6.1}$$

where the 'sub.' superscript indicates that we should subtract the contribution of the more leading terms in the small z expansion before taking the limit. This prescription however runs into the familiar problem that each t-channel block contributes only a

$\log(z)z^6$ term as $z \to 0$, and such terms need to exponentiate to recover the expected $z^{\bar{h}(h)}$ behaviour, signalling that the t-channel sum does not commute with taking $z \to 0$ term by term. In order to remedy this we will evaluate the right-hand sides of (5.6.1) at finite but small z.

Finite z inversion

The essence of the "finite-z inversion" method [36, 159, 161] is to replace equation (5.6.1) with an estimate at small but finite z_0

$$
\begin{aligned}
h_n(\bar{h}) &\simeq h_{z_0,n}(h,\bar{h}) = \left.\frac{z\partial_z \widetilde{C}_n^{\text{sub.}}(z,h,\bar{h})}{\widetilde{C}_n^{\text{sub.}}(z,h,\bar{h})}\right|_{z=z_0}, \\
P_n(h,\bar{h}) &\simeq P_{z_0,n}(h,\bar{h}) = \left.\frac{\widetilde{C}_n^{\text{sub.}}(z,h,\bar{h})}{z^{h_{z_0,n}(h,\bar{h})}}\right|_{z=z_0}.
\end{aligned}
\tag{5.6.2}
$$

Notice that at finite z_0 higher order terms in the expansion (5.5.23) also contribute and this introduces h-dependence into the approximation of $h_n(\bar{h})$ which is therefore now denoted as $h_{z_0,n}(h,\bar{h})$. Equation (5.5.20) is modified into

$$
h_{z_0,n}(h(\bar{h}),\bar{h}) = h_{z_0,n}(\bar{h} - \ell, \bar{h}) = \bar{h} - \ell.
\tag{5.6.3}
$$

Since the exact answer is independent of h, a weak h-dependence of $h_{z_0,n}$ should be a sign of its good approximation to $h(\bar{h})$. Note also that now we have distinct equations to solve for each spin ℓ – a significant difference compared to the more common (practical) analyses of the leading Regge trajectory.

The value of z_0 in (5.6.2) is crucial to the approximation results we get, but before discussing the determination of z_0, let us first introduce another variable y which turns out to be useful for the inversion calculation. The y variable is defined such that the inversion of the "generalized free" part in (5.5.8), i.e., the protected part of $a(z,\bar{z})$ in the limit $c \to \infty$, gives exactly zero anomalous dimensions *even when* using the finite-z inversion (5.6.2). Denoting the inversion result as $\widetilde{C}_n^{\text{sub.}}(z,h,\bar{h})|_{\text{gf}}$, we have

$$
y^n(z,h,\bar{h}) := \widetilde{C}_n^{\text{sub.}}(z,h,\bar{h})|_{\text{gf}},
\tag{5.6.4}
$$

and by construction this gives

$$
\frac{y\partial_y \widetilde{C}_n^{\text{sub.}}(z,h,\bar{h})|_{\text{gf}}}{\widetilde{C}_n^{\text{sub.}}(z,h,\bar{h})|_{\text{gf}}} = n,
\tag{5.6.5}
$$

for any z_0. This also gives reliable results for anomalous dimensions of operators with large spin which asymptote to generalized free operators. The switch from z to

y introduces a Jacobian factor and (5.6.2) becomes

$$
\begin{aligned}
h_{y_0,n}(h,\bar{h}) &= \left.\frac{y\partial_y \widetilde{C}_n^{\text{sub.}}(z(y),h,\bar{h})}{\widetilde{C}_n^{\text{sub.}}(z(y),h,\bar{h})}\right|_{y=y_0} = \left(\left.\frac{y\partial_y z}{z}\right|_{z=z_0}\right)\cdot h_{z_0,n}(h,\bar{h}) \\
&= \left.\frac{ny^n(z,h,\bar{h})}{\partial_z y^n(z,h,\bar{h})}\frac{\partial_z \widetilde{C}_n^{\text{sub.}}(z,h,\bar{h})}{\widetilde{C}_n^{\text{sub.}}(z,h,\bar{h})}\right|_{z=z_0},
\end{aligned}
\tag{5.6.6}
$$

where the Jacobian is calculated by taking a derivative on both sides of (5.6.4), and[17]

$$
P_{y_0,n}(h,\bar{h}) = \left.\frac{\widetilde{C}_n^{\text{sub.}}(z,h,\bar{h})}{z^{h_{y_0,n}(h,\bar{h})}}\right|_{z=z_0}.
\tag{5.6.7}
$$

Although y is conceptually a nicer variable, from (5.6.4) we see that it depends on $z, h, \bar{h}$, which makes it practically more complicated. Therefore, we will write $y_0 = y(z_0, h, \bar{h})$ and all the finite-y inversions in this chapter will be performed at fixed z_0 rather than y_0.

To find the suitable value of z_0 (or y_0), we will plot both $h_{z_0,n}(h,\bar{h})$ (or $h_{y_0,n}(h,\bar{h})$) and $P_{z_0,n}(h,\bar{h})$ (or $P_{y_0,n}(h,\bar{h})$) as functions of z and look for a plateau, similar to the approach in [161]. Because of the relatively small amount of unprotected OPE data available to us, we will first pick a value for z_0 based on inversion of only the protected part of $a(z,\bar{z})$ (called *short inversion*). After extracting the unprotected CFT data (see next paragraph for details) we will check if the selected z_0 still sits on a plateau when inverting both protected and unprotected part of $a(z,\bar{z})$ (called *long inversion*). This is illustrated in figure 5.8 where we consider the leading long scalar multiplet with $c = 98$. By repeating this procedure for other values of central charge and spin, one will find different suitable values for z_0.

Iterative inversion procedure

To test whether we can bootstrap the CFT data out of the protected sector we will adopt an iterative procedure. First we invert only the short multiplets to obtain a set of estimated data, denoted as $iter_0$, for the multiplets on the leading long trajectory up to spin $\ell_{\max} = 16$.[18] Then we invert these long multiplets from $iter_0$ to obtain a new set of CFT data, $iter_1$, again for the leading long trajectory again up to $\ell_{\max}$. Then we iterate for several times until the data converges and $iter_n$ will

---

[17]Notice that we extract the coefficient of $z^{h_{y_0,n}}$ instead of $y^{h_{y_0,n}}$, because, as can be seen from (5.6.4), y is defined to include the "generalized free" OPE coefficient. One could also have defined y dividing the right-hand side of (5.6.4) by the OPE coefficient, and then we would extract the coefficient of $y^{h_{y_0,n}}$.

[18]It is straightforward to extend to higher $\ell_{\max}$, but we find that this does not noticeably change the results. We do expect, however, that including higher-twist long trajectories can improve the results significantly (see subsection 5.6.2).
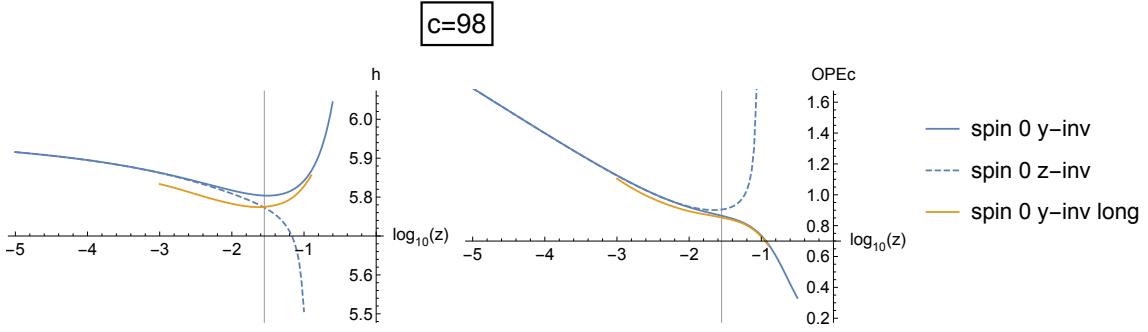
Figure 5.8. Short and long (up to spin 16) inversion results for spin 0 long multiplet with $c = 98$. The vertical lines on both plots pass through $\log_{10} z = -1.55$, and this is our choice for the finite y inversion. The orange curves indicate that the plateau regions remain largely unchanged after adding the long multiplet contribution. We also included plots using the z variable for comparison.

be our final numerical estimate. In practice we found that $2 \leqslant n \leqslant 5$ is sufficient, depending on the central charge. As mentioned before the value of z_0 for finite-$y(z)$ inversion should be determined separately for each spin. However, for large spins the anomalous dimensions are highly suppressed and vary little as we change z_0, thus in practice we can use the same z_0 for spins $\ell \geqslant 2$ or 4 depending on the central charge.

Extract the OPE coefficients of the shorts at bound

With an estimate for the long multiplets in hand we can invert for the OPE coefficients of the non-chiral algebra short multiplets.[19] This can be done similarly as in section 5.5.3. The main differences are that we need to extract the coefficient of z^5 term rather than the z^4 term, and invert both protected and unprotected operators.

In equations we have

$$\left. \widetilde{C}(z, h = 5, \bar{h} = \ell + 5) \right|_{z^5} = \frac{\lambda^2_{\mathcal{B}[0,2]_{\ell-1}}}{2\ell + 8} = \frac{\left(\lambda^{\text{short}}\right)^2_{\mathcal{B}[0,2]_{\ell-1}} + \left(\lambda^{\text{long}}\right)^2_{\mathcal{B}[0,2]_{\ell-1}}}{2\ell + 8} , \quad (5.6.8)$$

and $\lambda^2_{\mathcal{D}[0,4]} = \lim_{\ell \to -1} \lambda^2_{\mathcal{B}[0,2]_\ell}$. Inverting the protected part in a similar manner as before yields the contribution from the short multiplets in the t-channel:

$$\begin{aligned}
\left(\lambda^{\text{short}}\right)^2_{\mathcal{B}[0,2]_{\ell-1}} =& \frac{\sqrt{\pi} 2^{-\ell-9}(\ell+1)(\ell+2)(\ell+4)(\ell+7)(\ell+8)\Gamma(\ell+6)}{9\Gamma\left(\ell+\frac{9}{2}\right)} \\
& - \frac{5\sqrt{\pi} 2^{-\ell-4}(\ell+4)(\ell(\ell+9)+17)\Gamma(\ell+6)}{c(\ell+3)(\ell+6)\Gamma\left(\ell+\frac{9}{2}\right)} .
\end{aligned} \quad (5.6.9)$$

---

[19]Recall that the t-channel non-chiral algebra short multiplets have vanishing double discontinuity and therefore they do not participate in the iteration procedure, as discussed in section 5.5.1.

As for the long multiplets, using the double discontinuity expression (5.5.8) and the expression generating function (5.5.16), we find that they contribute:

$$
\left(\lambda^{\text{long}}\right)^2_{\mathcal{B}[0,2]_{\ell-1}} = 2^\ell(2\ell+8) \sum_{\Delta'_{\text{s.c.p.}}>\ell'+6,\ell'} \frac{-8\lambda^2_{\Delta'_{\text{s.c.p.}},\ell'}\sin^2\left((\Delta'_{\text{s.c.p.}}+\ell')\pi/2\right)}{(\Delta'_{\text{s.c.p.}}-\ell'-2)(\Delta'_{\text{s.c.p.}}+\ell'+2)}
$$

$$
\times\, 2\kappa^{0,-2}_{2(\ell+5)}\int_0^1 d\bar{z}\,\frac{1}{\bar{z}^2(1-\bar{z})}k^{0,-2}_{2(\ell+5)}(\bar{z})\left(\frac{\bar{z}}{1-\bar{z}}\right)^5 \mathcal{G}^{(\ell')}_{\Delta'_{\text{s.c.p.}}+4}(0,-2;1,1-\bar{z})\,,
$$

$$(5.6.10)$$

where we have used primed notation for t-channel quantum numbers. Note that the t-channel block is evaluated at $z=0$, which gives a finite linear combination of eight hypergeometric functions $_2F_1(\ldots,1-\bar{z})$. Therefore, for each 6d conformal block the $\bar{z}$ integral breaks down into eight atomic integrals and they can be performed analytically using the method in [159].

Equation (5.6.10) presents a kind of 'supersymmetric sum rule' for the OPE data. We see no reason why it could not be absolutely convergent for all spins. One interesting application could then be the vanishing OPE coefficient of the $\mathcal{D}[0,4]$ multiplet for the A_1 theory with $c=25$ which was discussed already in [18]. In that case the positive contribution from equation (5.6.9) needs to be offset by the uniformly negative contributions from the long multiplets in equation (5.6.10). More generally, taking only finitely many t-channel blocks into account would provide an upper bound on the OPE coefficients.

5.6.2   Numerical results

In this subsection we present the numerical estimates for the following unknown CFT data:[20]

- conformal dimensions of the leading long multiplets Δ_ℓ, $\ell=0,2,4,6$,

- OPE coefficients of the leading long multiplets $\lambda^2_{\mathcal{L}[0,0]_{\Delta_\ell,\ell}}$, $\ell=0,2,4,6$,

- OPE coefficients of non-chiral algebra short multiplets $\lambda^2_{\mathcal{D}[0,4]}$ and $\lambda^2_{\mathcal{B}[0,2]_{\ell-1}}$ with $\ell=2,4,6$.

We will plot all of this data as a function of the central charge c. As a reminder, we note that for the A_{N-1} and D_N theories

$$
c(A_{N-1})=4N^3-3N-1\,, \qquad c(D_N)=16N^3-24N^2+9N\,. \tag{5.6.11}
$$

In each of the three cases we will take as our initial input the inhomogeneous contribution to the crossing equation, *i.e.*, the last two lines on the right-hand side

---

[20]Estimates for higher spins (up to $\ell=16$) are available from the authors on request.

of (5.5.8). At first order in the iteration this yields something that bears qualitative similarities to the supergravity answer, but with the important difference that we work at finite c and finite z – so the familiar derivatives of conformal blocks now get replaced with an approximation consisting of regular conformal blocks. We then feed the answers for the leading Regge trajectory into the right-hand side of (5.5.8) and iterate a few times as described in the previous subsection.

Besides this straightforward iteration scheme, we have also attempted to improve our results for the A_1 theory with $c = 25$ with a small variation where we input the following numerical bootstrap data [18]:

$$\Delta_0 \lesssim 6.4\,, \quad \lambda^2_{\mathcal{L}[0,0]_{\ell=0}} \lesssim 1.3\,, \quad \Delta_2 \lesssim 9.4\,. \tag{5.6.12}$$

These are respectively the dimension and coefficient of the first scalar and the dimension of the first spin 2 operator. These values are rough extrapolations of the bootstrap bounds of [18] which are believed to be saturated for the (2, 0) theory with $c = 25$. To incorporate these values we have simply replaced the corresponding OPE data in the output of an iteration with (5.6.12) before feeding it back into the next iteration.

Dimensions of leading long multiplets

In figure 5.9 we present the conformal dimensions of the multiplets in the leading long Regge trajectory for the first few spins as functions of $c^{-1/3}$.[21] We include both the results from *short inversion* (the starting point of the iteration) and *long inversion* (the fixed point of the iterated inversion for the leading long trajectory).

The shaded regions in the plots correspond to the numerical upper bounds from [18] which are available for $\ell = 0, 2, 4$.[22] We also plot some holographic results: firstly the two-derivative supergravity solution [166, 167], which agrees with large-spin perturbation theory, secondly the $c^{-5/3}$ correction for the A_n and D_n theories obtained in [162] which arises from higher-derivative terms in the bulk, and thirdly the c^{-2} and $c^{-8/3}$ corrections which arise from bulk loops and which were determined from the tree-level data also in [162].[23] Although these curves only correspond to the first few terms in the large c expansion, we have nevertheless plotted them down

---

[21]The reason of using $c^{-1/3}$ is that this helps separate the large c results further than using c^{-1}, and $c^{-1/3}$ is proportional to N^{-1} in the large N limit.

[22]Note that the upper bound for leading long scalar at $c = 25$ in figure 5.9 is around 7.1 instead of 6.4 as shown in (5.6.12), because these grey shaded bounds are obtained with $\mathcal{D}[0, 4]$ multiplet present while the upper bound $\Delta_0 \lesssim 6.4$ is obtained by removing $\mathcal{D}[0, 4]$ by hand. See [18] for more details. Also, the steps occurring in the spin 4 bound are simply a numerical artifact due to an early termination of the binary search.

[23]The computation in [162] left some coefficients undetermined. We only show a comparison with this data for higher spins where these coefficients have no effect.
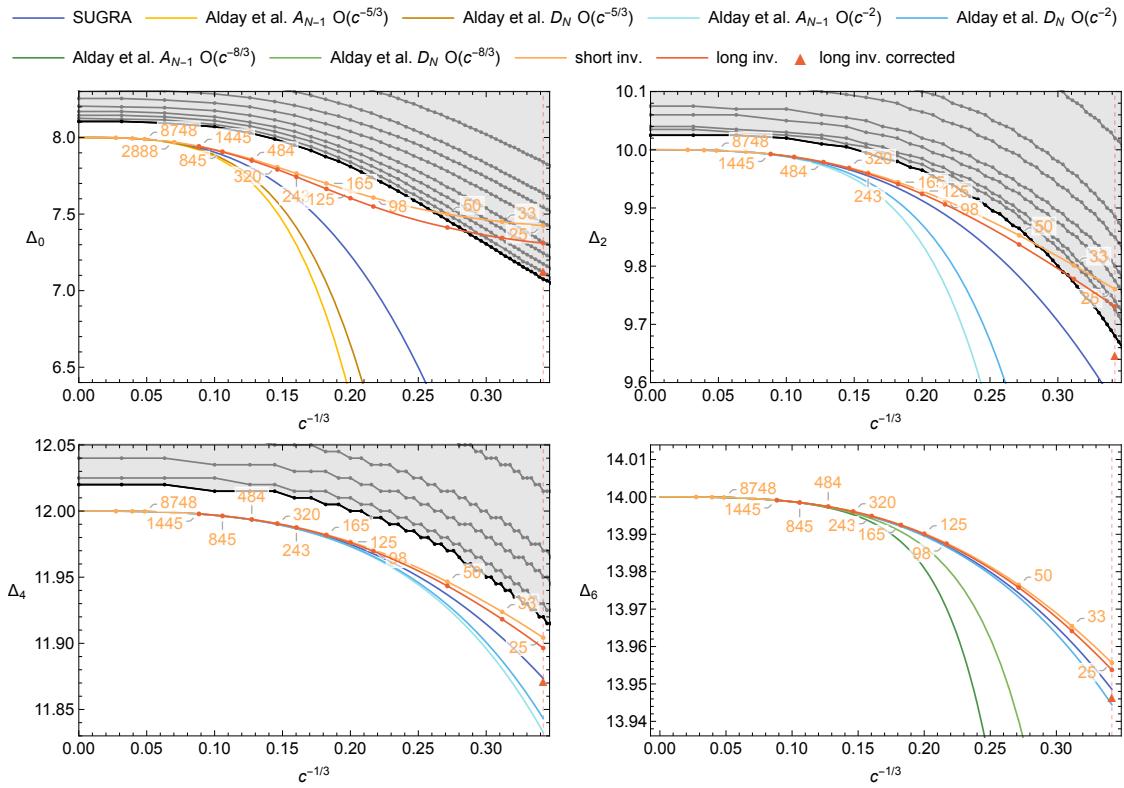
Figure 5.9. Dimensions of the leading long multiplets with spin 0, 2, 4, 6, against $c^{-1/3}$. The grey shaded regions are numerical upper bounds (available for spin 0, 2, 4) from [18]. The orange numbers are central charges (a strict subset of the chosen values correspond to physical theories). The orange curves correspond to short inversions and the red curves correspond to stabilized iterative long inversions up to spin 16 (see text for a detailed explanation). For $c = 25$, we also perform a corrected iterative long inversion, taking into account the numerical results of [18], and the result is indicated by a triangular point. We also show $1/c$ results from two-derivative supergravity and higher order c^α corrections (denoted as $O(c^\alpha)$ in the plot legend) from [162, 171] whenever available.

to finite values of c.[24]

Our best results are those for intermediate values of c where we differ significantly from the supergravity results and more closely trace the numerical bounds. For example, for $10^2 \lesssim c \lesssim 10^3$ the numerics indicate the existence of an extremal solution to the crossing equations with a fairly large Δ_0. The holographic results significantly underestimate this gap, but our repeated inversion formula tracks it much more reliably. Our iteration scheme is less successful for the only non-trivial theory with $c < 98$, which is the A_1 theory with $c = 25$: at this point our estimates sometimes even exceed the numerical bounds. This likely happens because the anomalous dimensions are too large and recovering them correctly in the s-channel requires the

---

[24]We do not expect a large c expansion to converge, and the regime where finite c answers qualitatively agree with (non-resummed) holographic computations might end up being very small.

input of (many) more conformal blocks in the t-channel.[25] For comparison: in the three-dimensional Ising model the largest anomalous dimension for a physical operator on the leading Regge trajectory is approximately 0.036 (the stress tensor), whereas for $c = 25$ the the scalar (with dimension Δ_0) has an anomalous dimension of about 1.6.

As shown in the plot, the $c^{-5/3}$ corrections are different for the A_n and D_n series of theories. This raises the interesting question whether our iterative inversion scheme could potentially also recover this difference. There might, for example, be different fixed points of our procedure which one could try to find by starting with different initial conditions, for example by an additional input of the $c^{-5/3}$ corrections. In this way we could hope to iterate towards solutions that the numerical bootstrap cannot find. It would be very interesting to try this in future work.

OPE coefficients of leading long multiplets

In figure 5.10 we present the OPE coefficients of the leading long multiplets for the first few lowest spins as functions of $c^{-1/3}$. Similar to before, we show results from short inversion, the corrected and uncorrected long inversions, together with supergravity results and numerical estimates.[26] The picture is rather similar: for intermediate central charges we much more accurately trace the numerical bounds (especially in the scalar sector) than the supergravity result. This corroborates our viewpoint that our iterative procedure converges towards the extremal solution.

5.6.3 OPE coefficients of non-chiral algebra short multiplets

In figure 5.11 we present estimates for the OPE coefficients of the short multiplets not fixed by the chiral algebra, for the first few lowest spins and as functions of $c^{-1/3}$.[27] Here the short inversion produces the same results as the one from supergravity and therefore we only need to show the long inversion results. We also show the results

---

[25]We have also attempted to include one more Regge trajectory in the t-channel but this did not significantly change the results. At a superficial level this is because anomalous dimensions and OPE coefficients go to zero quickly for higher trajectories, yielding suppressions in the Lorentzian inversion formula. This leads us to suspect that one may need to include more than just the double-twist Regge trajectories (of the external operators) in the t-channel, but we have not investigated this further.

[26]The numerical results are unpublished results from [18]. They correspond to upper bounds for the squared OPE coefficients *under the assumption that the corresponding conformal dimensions saturate their own bounds*. They are therefore similar to those shown in figure 12 of [18]. Since the inversion procedure does not produce exactly the same conformal dimensions, these upper bounds on OPE coefficients are not entirely applicable, but we do expect them to provide decent estimates. The bounds appear jittery due to an imprecise determination of the long dimensions following from an early termination of the binary search – see footnote 22, and also due to insufficient numerical precision as noted in [18].

[27]The numerical bounds displayed appear jittery due to "failed searches" which occur because the numerical precision used is barely sufficient to obtain these bounds as noted in [18].
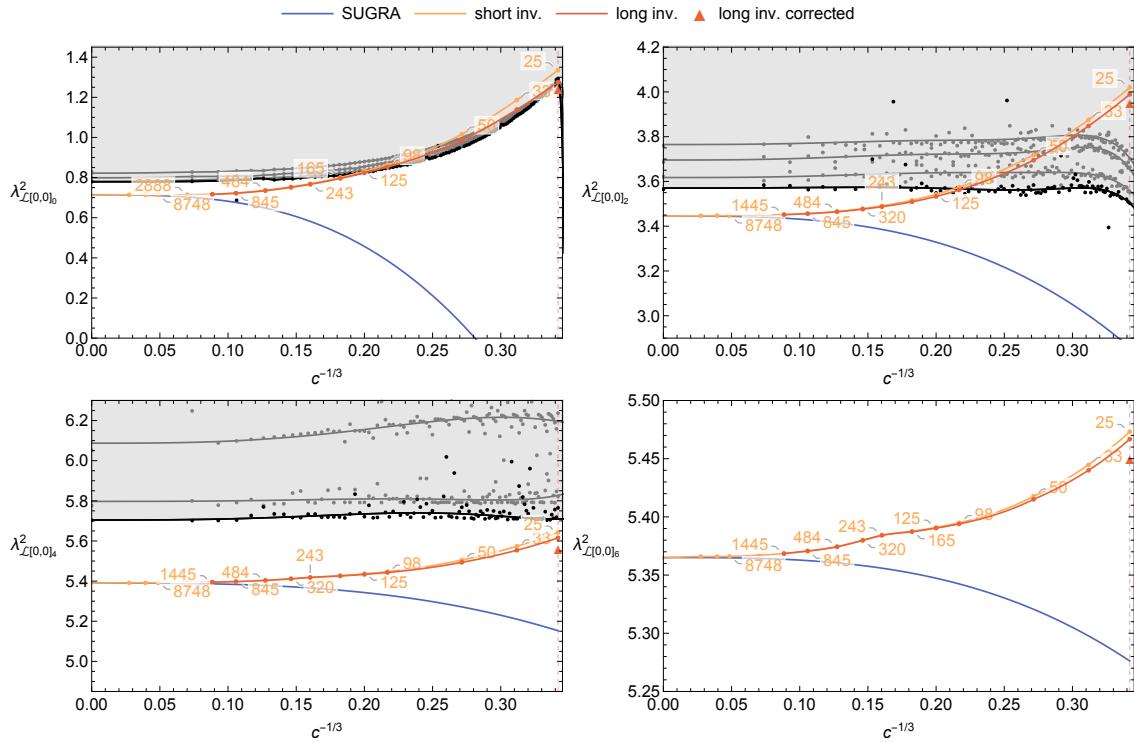
Figure 5.10. OPE coefficients of leading long multiplets with spin 0, 2, 4, 6, against $c^{-1/3}$. The grey shaded regions are unpublished numerical upper bounds (available for spin 0, 2, 4) from [18]. The orange numbers are central charges (a strict subset of the chosen values correspond to physical theories). The orange curves correspond to short inversions and the red curves correspond to stabilized iterative long inversions up to spin 16 (see text for detailed explanation). For $c = 25$, we also perform a corrected (triangular point) iterative long inversion using the numerical results of [18].

from [162] whenever applicable. The relative normalizations between that work and ours are as follows:

$$\frac{\left(\lambda^{\text{there}}\right)^2_{\mathcal{D}[0,4]}}{\left(\lambda^{\text{here}}\right)^2_{\mathcal{D}[0,4]}} = \frac{3}{8}, \qquad \frac{\left(\lambda^{\text{there}}\right)^2_{\mathcal{B}[0,2]_{\ell-1}}}{\left(\lambda^{\text{here}}\right)^2_{\mathcal{B}[0,2]_{\ell-1}}} = \frac{2^{-\ell-1}\ell(\ell+3)}{(\ell+1)(\ell+4)}. \qquad (5.6.13)$$

Here we find only marginal improvement over the supergravity answers.

Note that for A_1 theory ($c = 25$), $\lambda^2_{\mathcal{D}[0,4]}$ should vanish [18], but we were not able to recover this result from any estimate that involves only a single trajectory. Indeed, if we use (i) the numerical upper bounds on $\Delta_{0,2,4}$, $\lambda^2_{\mathcal{L}[0,0]_{\ell=0,2,4}}$ from [18], (ii) the assumption that large spin perturbation theory is reliable for $\ell \geqslant 6$, and (iii) convexity of the leading long trajectory then one cannot recover $\lambda^2_{\mathcal{D}[0,4]} = 0$ at $c = 25$ by just inverting the data on the leading Regge trajectory. The difficulty of recovering this vanishing OPE coefficient is also confirmed by an analysis we present in appendix 5.D, which shows that we need unrealistically large OPE coefficients if
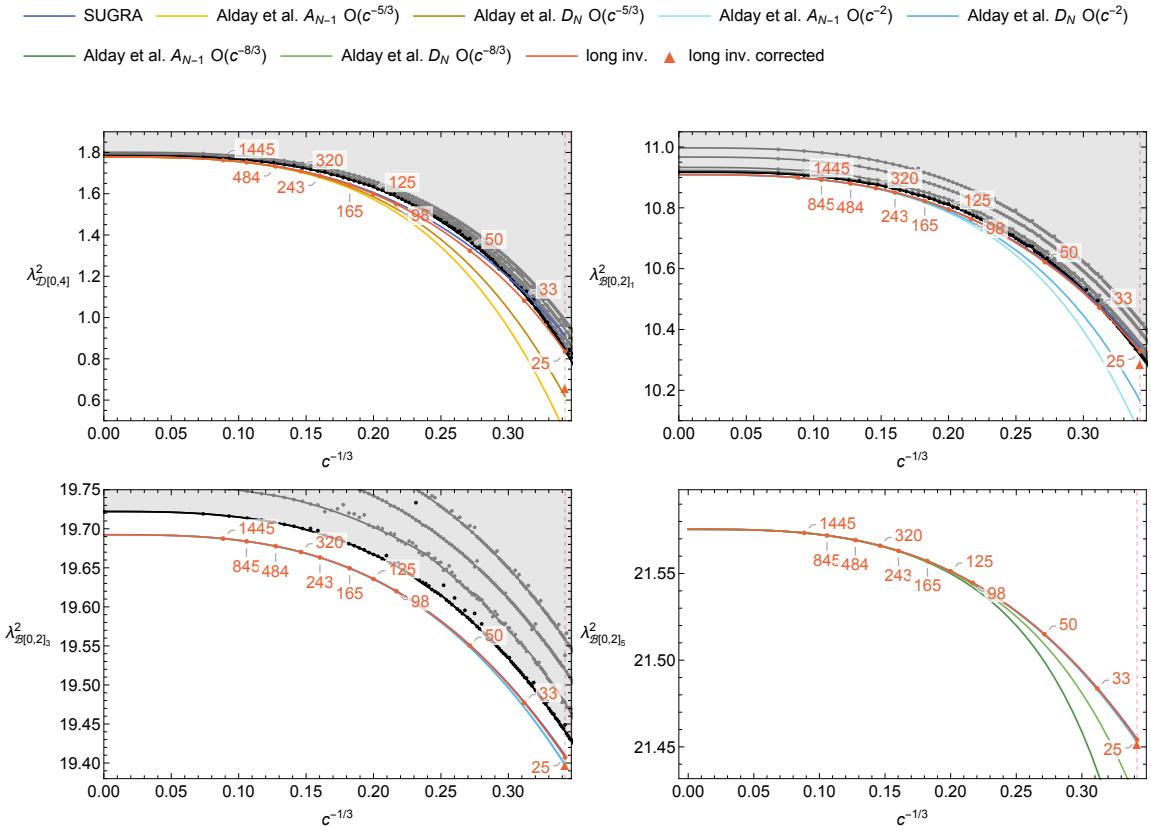
Figure 5.11. OPE coefficients of non-chiral algebra short multiplets with spin 0, 2, 4, 6, against $c^{-1/3}$. The grey shaded regions are numerical upper bounds (available for spin 0, 2, 4) from [18]. The red numbers are central charges (a strict subset of the chosen values correspond to physical theories). Short inversions produce the same results as the supergravity ones. The red curves correspond to stabilized iterative long inversions up to spin 16 (see text for detailed explanation). For $c = 25$, we also perform a corrected (triangular point) iterative long inversion using numerical data from [18]. We also show higher order c^α corrections (denoted as $O(c^\alpha)$ in the plot legend) from [162, 171] whenever available.

we only use a few t-channel blocks.[28]

Finally, let us mention that a similar negative result holds for the recovery of the stress tensor multiplet. Recall that we argued in section 5.3 that the leading unprotected Regge trajectory should cross the stress tensor point at $(\Delta, \ell) = (2, -2)$, which would correspond to an anomalous dimension equal to 4. In practice we observed that the finite y estimates rapidly stopped being sensible already at smaller negative spins: for example, we find a zero in the function $y(z, h, \bar{h})$ which leads to a singularity in $h_{y_0}(h, \bar{h})$. It is then not sensible to try even lower spins without adding

---

[28]On the other hand, as explained in subsection 5.6.1, the fact that $\lambda^2_{\mathcal{D}[0,4]} = 0$ translates into a specific sum rule for the other OPE data and one can ask whether this datum can be used as an input in order to improve our other estimates for this theory. We leave this as an interesting open question for future work.

many more t-channel blocks.

5.7 Outlook

We have explored the consequences of analyticity in spin for the six-dimensional $(2,0)$ theories and found an interesting interplay between supersymmetry and Regge trajectories. Some numerical experiments allowed us to approximately bootstrap the four-point function of the stress tensor multiplet. Let us mention a few possibilities for further explorations.

First, our numerical experiments can be extended. We can certainly consider other correlators or other theories, in different dimensions and with varying amounts of supersymmetry. Other possibilities include the incorporation of subleading Regge trajectories for the correlator at hand, or perhaps a multi-correlator study to improve the estimates. A related direction is the incorporation of known results into the numerics. For example, for the leading trajectory we claim to know both its location and coefficient at spin -2 and it would be nice to somehow use this information.

It would be especially nice if we could use the $c^{-5/3}$ results because it would allow us to distinguish between the A- and D-type theories at large c. Perhaps this can be done by finding different fixed points for very large c and then tracing them as c gradually decreased.

Second, it would be interesting to have a better idea of the Regge trajectories in supersymmetric theories for negative or non-integer spins. There should also be supersymmetric versions of the light-ray operators of [38] and it would be interesting to study their properties. Also, is there a more direct argument for the improved Regge behaviour (and larger analyticity in spin) in supersymmetric theories or do we have to analyse individual multiplets for each correlator separately? Furthermore, the softer Regge behaviour of supersymmetric correlators means the dispersion relations of [83, 183], which reconstruct a correlator from its double-discontinuity should apply directly without any subtractions. It would be interesting to consider the convergent sum-rules of [183] in the case of the $\mathcal{N} = (2,0)$ theories, and to solidify our understanding of the Regge intercept by resolving the questions we discussed in section 5.4.

Different amounts of supersymmetry and different dimensions

Much of what was discussed here in the context of six-dimensional $\mathcal{N} = (2,0)$ SCFTs is not unique to these theories. Four-point functions of BPS operators often enjoy an extended analyticity in spin due to a softer Regge behaviour of the correlator that is inverted. Roughly, in dimensions $d > 2$ one expects analyticity in spin for $\ell > \ell^\star$, with $\ell^\star = 1 - \frac{d-2}{2}\mathcal{N}$ for $d \neq 5$, and $\ell^\star = -1$ for $d = 5$, from the fact that supersymmetry relates conformal primaries of spin one to conformal primaries with

spin $\ell^\star$.[29] As a result, Regge trajectories of the superprimaries exchanged in such OPEs are more constrained than their bosonic counterparts, with analyticity in spin imposing constraints on short and long trajectories. We leave a detailed study of the interplay between analyticity in spin and supersymmetry for future work, and simply conclude with a few general comments on how the stress tensor fits into superconformal primary Regge trajectories in interacting theories.

In the case of SCFTs with more than eight supercharges we expect the stress tensor to fit into the leading long trajectory at a *negative spin*, similarly to what was discussed here. For maximally supersymmetric theories it corresponds to the spin -2 continuation of the leading long superprimary trajectory, which should have dimension 0 (-1) in four (three) dimensions. This follows from examining the half-BPS superblocks for the stress tensor supermultiplet correlator given in, *e.g.*, [66, 173, 185–187], and we expect this structure to hold for other half-BPS correlators. This fits well with the results for planar $\mathcal{N} = 4$ Super-Yang-Mills, where complete Regge trajectories can be obtained numerically, for any value of the 't Hooft coupling, from the quantum spectral curve approach [188]. The Regge trajectory obtained in [188] is that of the leading unprotected single-trace conformal primary operators, in the $\mathbf{20'}$ R-symmetry representation, that appear in the stress tensor superprimary's self-OPE.[30] For spin greater than two, the operators in this trajectory are genuinely unprotected long operators, but at spin zero one finds the superprimary of the stress tensor multiplet itself. As pointed out in [188], the fact that the spin is an even function of the dimension, for this Regge trajectory, follows from shadow symmetry of the Regge trajectories in the $\mathbf{105}$ R-symmetry channel. We expect shadow symmetry in this channel (and all others) will follow from the structure of the superconformal blocks, as we observed in section 5.3.4 for the $(2,0)$ theories.

Just like in the $\mathcal{N} = (2,0)$ case, the stress tensor supermultiplet OPE in $\mathcal{N} = 4$ features various short multiplets whose OPE coefficients are completely fixed from the chiral algebra of [174], see [186] for details. As argued in [164], the superprimary Regge trajectories are analytic for all spins greater than -3, and we expect other connections between long and short trajectories to follow from imposing simultaneously analyticity in spin and supersymmetry.

Analyticity in spin demands SCFTs with eight supercharges, or less, have a structure of superconformal Regge trajectories that looks closer to the non-supersymmetric case – the stress tensor supermultiplet should fit at *non-negative* spin in the leading long trajectory. For SCFTs with eight supercharges, we expect that the stress

---

[29]This can be seen from the structure of the superconformal multiplets in [184]. However, a precise statement requires an analysis of the Regge behaviour of the correlator whose conformal block decomposition is being inverted. As far as we know this has been only done in four dimensions for chiral operators in the non-chiral channel [165], and $\mathcal{N} = 4$ half-BPS operators [164].

[30]Note, however, that the leading singe-trace trajectory is not necessarily the leading Regge trajectory of the full non-perturbative CFT. This trajectory is also analysed in [35].

tensor superprimary (a scalar and singlet [184]) should fit into the leading super-Regge trajectory, which will have the first *unprotected long* operator at spin two. The stress tensor itself would fall in the leading Regge conformal primary trajectory, which has the first unprotected operator at spin four. At the level of kinematics this expectation can be checked from the known superblocks of half-BPS flavour current multiplets which were written down explicitly, for arbitrary dimensions, in [189, 190]. The chiral algebra of [174] provides a check at the level of *dynamics* for the four-point function of flavour current multiplets in four-dimensional $\mathcal{N} = 2$ SCFTs. Requiring the stress tensor to fit into the leading unprotected Regge trajectory fixes the OPE coefficient and scaling dimension of this trajectory at zero spin – see the blocks given in [66, 191]. These values turn out to be precisely what is needed to ensure analyticity down to spin zero of the function $(z\bar{z})^2 \mathcal{G}(z, \bar{z})$ defined in [191], which admits a block decomposition and has a softer Regge growth (ensuring analyticity for $\ell > -1$) similarly to $(z\bar{z})^6 a(z, \bar{z})$ here. Once again, more interconnections between short and long trajectories will likely follow from analyticity in spin.

5.A   (Super)conformal blocks and projectors

We consider the four-point function of the superprimary of the stress tensor multiplet $\Phi^{\{IJ\}}(x)$, where I, J are fundamental $so(5)$ indices. Contracting the $\mathfrak{so}(5)$ indices with null vectors Y^I as $\Phi(x, Y) = Y_I Y_J \Phi^{\{IJ\}}(x)$, we can write the four-point function as

$$\langle \Phi(x_1, Y_1)\Phi(x_2, Y_2)\Phi(x_3, Y_3)\Phi(x_4, Y_4) \rangle = 16 \frac{(Y_1 \cdot Y_2)^2 (Y_3 \cdot Y_4)^2}{x_{12}^8 x_{34}^8} \sum_R A_R(z, \bar{z}) P^R(\alpha, \bar{\alpha}) \,,$$
(5.A.1)

with

$$
\begin{aligned}
\frac{1}{\alpha\bar{\alpha}} &:= \frac{(Y_1 \cdot Y_2)(Y_3 \cdot Y_4)}{(Y_1 \cdot Y_3)(Y_2 \cdot Y_4)} \,, & \frac{(\alpha - 1)(\bar{\alpha} - 1)}{\alpha\bar{\alpha}} &:= \frac{(Y_1 \cdot Y_4)(Y_2 \cdot Y_3)}{(Y_1 \cdot Y_3)(Y_2 \cdot Y_4)} \,, \\
z\bar{z} &:= \frac{x_{12}^2 x_{34}^2}{x_{13}^2 x_{24}^2} \,, & (1 - z)(1 - \bar{z}) &:= \frac{x_{14}^2 x_{23}^2}{x_{13}^2 x_{24}^2} \,.
\end{aligned}
$$
(5.A.2)

Here P^R are the projectors onto each of the representations R appearing in the tensor product of two $[2,0]$ representations in (5.2.1) and are given by [173]

$$Y^{[4,0]}(\alpha, \bar\alpha) = (\alpha\bar\alpha)^2 + (\alpha - 1)^2(\bar\alpha - 1)^2 + 4\alpha\bar\alpha(\alpha - 1)(\bar\alpha - 1) - \frac{8(\alpha\bar\alpha + (\alpha - 1)(\bar\alpha - 1))}{9} + \frac{8}{63},$$

$$Y^{[2,2]}(\alpha, \bar\alpha) = (\alpha\bar\alpha)^2 - (\alpha - 1)^2(\bar\alpha - 1)^2 - \frac{4(\alpha\bar\alpha - (\alpha - 1)(\bar\alpha - 1))}{7},$$

$$Y^{[0,4]}(\alpha, \bar\alpha) = (\alpha\bar\alpha)^2 + (\alpha - 1)^2(\bar\alpha - 1)^2 - 2\alpha\bar\alpha(\alpha - 1)(\bar\alpha - 1) - \frac{2(\alpha\bar\alpha + (\alpha - 1)(\bar\alpha - 1))}{3} + \frac{1}{6},$$

$$Y^{[0,2]}(\alpha, \bar\alpha) = \alpha + \bar\alpha - 1,$$

$$Y^{[2,0]}(\alpha, \bar\alpha) = \alpha\bar\alpha + (\alpha - 1)(\bar\alpha - 1) - \frac{2}{5},$$

$$Y^{[0,0]}(\alpha, \bar\alpha) = 1.$$

$$(5.A.3)$$

We denote the six-dimensional (non-supersymmetric) conformal blocks appearing the de decomposition of a four-point function of operators with dimensions $\Delta_{i=1,\dots 4}$ by $\mathcal{G}_\Delta^{(\ell)}(\Delta_{12}, \Delta_{34}; z, \bar z)$, where $\Delta_{ij} = \Delta_i - \Delta_j$. Here and throughout this chapter we omit the first two arguments (Δ_{12}, Δ_{34}) whenever they are vanishing. Their explicit form reads [66, 192] [31]

$$\mathcal{G}_\Delta^{(\ell)}(\Delta_{12}, \Delta_{34}; z, \bar z) = \mathcal{F}_{00} - \frac{\ell + 3}{\ell + 1}\mathcal{F}_{-11} + \frac{(\Delta - 4)(\ell + 3)}{16(\Delta - 2)(\ell + 1)}$$
$$\frac{(\Delta - \ell - \Delta_{12} - 4)(\Delta - \ell + \Delta_{12} - 4)(\Delta - \ell + \Delta_{34} - 4)(\Delta - \ell - \Delta_{34} - 4)}{(\Delta - \ell - 5)(\Delta - \ell - 4)^2(\Delta - \ell - 3)}\mathcal{F}_{02}$$
$$- \frac{\Delta - 4}{\Delta - 2}\frac{(\Delta + \ell - \Delta_{12})(\Delta + \ell + \Delta_{12})(\Delta + \ell + \Delta_{34})(\Delta + \ell - \Delta_{34})}{16(\Delta + \ell - 1)(\Delta + \ell)^2(\Delta + \ell + 1)}\mathcal{F}_{11}$$
$$+ \frac{2(\Delta - 4)(\ell + 3)\Delta_{12}\Delta_{34}}{(\Delta + \ell)(\Delta + \ell - 2)(\Delta - \ell - 4)(\Delta - \ell - 6)}\mathcal{F}_{01},$$

$$(5.A.4)$$

where

$$\mathcal{F}_{nm}(z, \bar z) = \frac{(z\bar z)^{\frac{\Delta - \ell}{2}}}{(z - \bar z)^3}\left(\left(\frac{z}{2}\right)^\ell z^{n+3}\bar z^m {}_2F_1\left(\frac{\Delta + \ell - \Delta_{12}}{2} + n, \frac{\Delta + \ell + \Delta_{34}}{2} + n, \Delta + \ell + 2n, z\right)\right.$$
$${}_2F_1\left(\frac{\Delta - \ell - \Delta_{12}}{2} - 3 + m, \frac{\Delta - \ell + \Delta_{34}}{2} - 3 + m, \Delta - \ell - 6 + 2m, \bar z\right) - (z \longleftrightarrow \bar z)\bigg).$$

$$(5.A.5)$$

---

[31]With respect to [18, 66, 192] we removed an overall factor of $(-1)^\ell$.

5.B Regge bound of $a(z, \bar{z})$

In this appendix we show that the function $a(z, \bar{z})$ is bounded in the Regge limit as (5.4.13). This limit corresponds to going around the branch cut starting at $\bar{z} = 1$ and sending w, defined in (5.4.10), to zero along any direction in the complex-w plane.[32] Following [1], we do so by bounding the function on the secondary sheets (obtained by going around the branch cut in either direction according to the phase of w) by its (positive) value on the first sheet with real values of the cross-ratios.

The function $a(z, \bar{z})$ admits a decomposition in powers of z and $\bar{z}$ following from its s-channel OPE, given in equations (5.2.11), (5.2.12) and (5.2.13), as

$$(z\bar{z})^6 a(z, \bar{z}) = \sum_{\Delta' \geqslant 8 + |\ell|, \ell} b_{\Delta', \ell} \, z^{\frac{\Delta' - \ell}{2}} \bar{z}^{\frac{\Delta' + \ell}{2}} \, , \tag{5.B.1}$$

where $\Delta' \geqslant 8 + |\ell|$ follows from the decomposition of $a(z, \bar{z})$ in the blocks given in eq. (5.2.7), with the prime in Δ to remind us the sum runs over both conformal primaries and descendants, and where ℓ runs over positive and negative spins of any parity. To bound $a(z, \bar{z})$ on the second sheet we now need to show the coefficients $b_{\Delta', \ell}$ are non-negative. The function $a(z, \bar{z})$ is only related to a physical correlator through the inverse of the differential operator Δ_2 as given in equation (5.2.5), so we do not know of a direct way to use reflection positivity to show positivity of the coefficients $b_{\Delta', \ell}$. However, reflection positivity would also follow from positivity of the coefficients of the decomposition of $a(z, \bar{z})$ in blocks as given in (5.2.12) and (5.2.13), so all that remains is to show the blocks $a_{\Delta, \ell}^{\mathrm{at}}(z, \bar{z})$ in (5.2.7) have a positive decomposition in powers of z and $\bar{z}$. We have checked this to be the case for all relevant scaling dimensions and for various spins in a series expansion in small z and $\bar{z}$, but do not have a proof, due to the convoluted form of six-dimensional conformal blocks (5.A.4). We will proceed using the z and $\bar{z}$ coordinates and not the ρ variable of [67] since the expansion of z and $\bar{z}$ in powers of ρ and $\bar{\rho}$ is not positive.[33]

Bounding $a(z, \bar{z})$

The expansion (5.B.1) converges for $|z|, |\bar{z}| < 1$. Using the second crossing symmetry equation (5.2.14) we can use instead the t-channel decomposition to compute

$$a(z, \bar{z}) = \frac{1}{((1 - z)(1 - \bar{z}))^5 z\bar{z}} \sum_{\Delta' \geqslant 8 + |\ell|, \ell} b_{\Delta', \ell} (1 - z)^{\frac{\Delta' - \ell}{2}} (1 - \bar{z})^{\frac{\Delta' + \ell}{2}} + \frac{\mathcal{C}_h(1 - z, 1 - \bar{z}) - \mathcal{C}_h(z, \bar{z})}{z\bar{z}} \, ,$$
$$\tag{5.B.2}$$

---

[32]Compared to [1] we have re-scaled w such that $4w_{\mathrm{there}} = w_{\mathrm{here}}$.

[33]While $(z\bar{z})^6 a(z, \bar{z})$ does not have an expansion in positive powers of ρ and $\bar{\rho}$ it is still possible that $(z\bar{z})^6 a(z, \bar{z})/(1 - z)/(1 - \bar{z})$ does, which given the form of the crossing equations would be a sufficient condition. However, due to the convoluted form of the blocks, we could only check this to a rather low order in the ρ and $\bar{\rho}$ expansion. If the expansion is indeed positive, then following the same reasoning as below would yield the bound (5.4.13) for all values of $\arg(w)$.

where the sum now converges for $|1-z|, |1-\bar{z}| < 1$. This representation of $a(z,\bar{z})$ allows us to continue to the secondary sheets by going around the cut starting at $\bar{z} = 1$, provided $|1-\bar{z}| < 1$. For $|1-\bar{z}| > 1$ we will use the u-channel below. Going around the branch cut amounts to introducing phases in the scaling-block expansion above, and we get

$$
|a^{\circlearrowright/\circlearrowleft}(z,\bar{z})| \leqslant \frac{|1-z||1-\bar{z}|}{|z\bar{z}|} \frac{z'\bar{z}'}{(1-z')(1-\bar{z}')} a(z',\bar{z}') + \left| \frac{\mathcal{C}^{\circlearrowright/\circlearrowleft}{}_h(1-z, 1-\bar{z}) - \mathcal{C}^{\circlearrowright/\circlearrowleft}{}_h(z,\bar{z})}{z\bar{z}} \right|
$$
$$
- \frac{\mathcal{C}_h(1-z', 1-\bar{z}') - \mathcal{C}_h(z',\bar{z}')}{(1-z')(1-\bar{z}')} \frac{|1-z||1-\bar{z}|}{|z\bar{z}|} ,
\tag{5.B.3}
$$

where we used the second crossing equation again, and defined

$$
1 - z' \equiv |1-z| < 1 , \qquad 1 - \bar{z}' \equiv |1-\bar{z}| < 1
\tag{5.B.4}
$$

We can now take the limit of $w \to 0$, using

$$
z \sim \sigma w , \qquad \bar{z} \sim \frac{1}{\sigma} w , \qquad z' \sim \sigma |w| \cos(\arg(w)) , \qquad \bar{z}' \sim \frac{1}{\sigma} |w| \cos(\arg(w)) .
\tag{5.B.5}
$$

The behaviour of $a(z',\bar{z}')$ as $w \to 0$ is controlled by the lowest dimensional operator appearing in its decomposition. which is the superprimary of the $\mathcal{D}[4,0]$ supermultiplet with $\Delta' = 8$, while the behaviour of the remaining terms can be found from the explicit form of $\mathcal{C}_h(z,\bar{z})$ given in eq. (5.2.15). All in all we find

$$
|a^{\circlearrowright/\circlearrowleft}(z,\bar{z})| \leqslant \frac{\sec^6(\arg(w)) + 1}{3|w|^8} , \qquad \text{as } w \to 0 ,
\tag{5.B.6}
$$

where the leading contribution comes from the terms involving $\mathcal{C}_h$ only. This bound is valid for $|\arg(w)| < \pi/2$ which corresponds to the region of convergence of the t-channel decomposition. To obtain a bound for $|\arg(w)| > \pi/2$ we now turn to a u-channel decomposition.

Combining both equations in (5.2.14) we write now an expansion valid for $|1-z|, |1-\bar{z}| > 1$

$$
a(z,\bar{z}) = \frac{(1-z)(1-\bar{z})}{z\bar{z}} \sum_{\Delta' \geqslant 8 + |\ell|, \ell} b_{\Delta',\ell} \left(\frac{1}{1-z}\right)^{\frac{\Delta'-\ell}{2}} \left(\frac{1}{1-\bar{z}}\right)^{\frac{\Delta'+\ell}{2}}
$$
$$
+ \frac{1}{z(1-z)^4} \frac{1}{\bar{z}(1-\bar{z})^4} \left(\mathcal{C}_h\left(\frac{1}{1-z}, \frac{1}{1-\bar{z}}\right) - \mathcal{C}_h\left(\frac{z}{z-1}, \frac{\bar{z}}{\bar{z}-1}\right) \right) .
\tag{5.B.7}
$$

Going around the branch-cut starting at $\bar{z} = 1$ in either direction once again intro-

duces just phases in the expansion, while $\mathcal{C}_h$ is a known function, and so we write

$$
\begin{aligned}
|a^{\circlearrowright/\circlearrowleft}(z,\bar{z})| &\leqslant \frac{(1-z')^5(1-\bar{z}')^5(z'\bar{z}')}{|1-z|^5|1-\bar{z}|^5|z\bar{z}|}a(z',\bar{z}') \\
&+ \left| \frac{1}{z(1-z)^4}\frac{1}{\bar{z}(1-\bar{z})^4}\left(\mathcal{C}^{\circlearrowright/\circlearrowleft}{}_h\left(\frac{1}{1-z},\frac{1}{1-\bar{z}}\right) - \mathcal{C}^{\circlearrowright/\circlearrowleft}{}_h\left(\frac{z}{z-1},\frac{\bar{z}}{\bar{z}-1}\right)\right)\right| \\
&- \left(\mathcal{C}_h\left(\frac{1}{1-z'},\frac{1}{1-\bar{z}'}\right) - \mathcal{C}_h\left(\frac{z'}{z'-1},\frac{\bar{z}'}{\bar{z}'-1}\right)\right)\frac{(1-z')^6(1-\bar{z}')^6}{|1-z|^5|1-\bar{z}|^5|z\bar{z}|}\,.
\end{aligned}
$$
(5.B.8)

Just as before we find that the Regge behaviour of $a(z,\bar{z})$ is bounded by

$$
|a^{\circlearrowright/\circlearrowleft}(z,\bar{z})| \leqslant \frac{\sec^6(\arg(w))+1}{3|w|^8}, \quad \text{as } w \to 0\,,
$$
(5.B.9)

thus showing eq. (5.4.13) for $|\arg(w)| \neq \pi/2$.

Bounding $A_R(z,\bar{z})$

Finally, we need to bound the behaviour of the $A_R(z,\bar{z})$ in the Regge limit. These functions are obtained from $a(z,\bar{z})$ and its first z and $\bar{z}$ derivatives through equation (5.2.4). Taking a derivative with respect to z and/or $\bar{z}$ in equation (5.B.1) does not spoil positivity of the expansion coefficients. We can then can repeat the above computation bound directly $\partial_z a(z,\bar{z})$, $\partial_{\bar{z}} a(z,\bar{z})$ and $\partial_{\bar{z}}\partial_z a(z,\bar{z})$. The bounds obtained then imply the Regge behaviour of $A_R(z,\bar{z})$ quoted in (5.4.14), for $|\arg(w)| \neq \pi/2$.

5.C Regulating the divergence of $c(\Delta,\ell)$ near $z \to 1$

In this appendix we discuss the regularization of integrals in the Lorentzian inversion formula (5.4.2) and explicitly work out the case of four-dimensional mean field theory as an example.

The integrals over z (and $\bar{z}$) in $c(\Delta,\ell)$ diverge when the integrand scales in the limit $z \to 1$ as $O\left((1-z)^{-p}\right)$ with $p \geqslant 1$. In general this divergence can be resolved by analytic continuation of p from the convergent region $p < 1$ to its actual value, but when p is an integer such analytic continuation fails because of factors like $\Gamma(-p+n)$ where n is a positive integer. In the $\bar{z}$ variable there are additional sine functions from the double discontinuity operation and they produce compensating zeros to yield finite answers; this is why we encountered no divergences in the inversion of the z^4 term that we performed in section 5.5.3. This leaves us with the divergence from the z-integral when p is a large enough integer. As was already discussed in [1, 33], one can either regulate the z-integral by setting a cutoff $1-\epsilon$ and then drop the divergent terms in the limit $\epsilon \to 0$; or one can keep p generic for integration,

then series expand p around the actual integral value and discard divergent terms. Here we apply the second approach.

Let us consider the split of the double discontinuity as in equation (5.5.8). It is easy to verify that the contribution from the long multiplets always converges, but the contribution from the short multiplets behaves as $(1 - z)^{-4}$ and needs to be regulated. The way to do so is to write $c(\Delta, \ell)$ as

$$c(\Delta, \ell) = \frac{c^{(-2)}(\Delta, \ell)}{(p - 4)^2} + \frac{c^{(-1)}(\Delta, \ell)}{p - 4} + c^{(0)}(\Delta, \ell) + \mathcal{O}(p - 4), \qquad (5.C.1)$$

and then simply drop $c^{(-2)}(\Delta, \ell)$ and $c^{(-1)}(\Delta, \ell)$.

Two follow-up checks are needed: first, $c^{(0)}(\Delta, \ell)$ should give the correct residues at physical poles; second, the subtracted parts which are (the principal series integral of) $c^{(-2)}(\Delta, \ell)$ and $c^{(-1)}(\Delta, \ell)$ should not have a conformal block decomposition to make sure that nothing physical is subtracted.

The first check is straightforward. We simply calculate $c^{(0)}(\Delta, \ell)$ for the short multiplets and find that the residues at twist 8 and 10 in the sense of $(z\bar{z})^6 a(z, \bar{z})$ match (5.5.27) and (5.6.9) respectively. The second check is however technically more involved because conformal blocks in 6d are complicated functions. Therefore we will instead do a simpler check to illustrate the essential idea.

Example: mean field theory in 4d

Let us now consider the four-point function $\langle \phi\phi\phi\phi \rangle$ of mean field theory in 4d. We first use the inversion formula to reproduce the CFT data, and then focus on the cases with integral external dimensions. In this section the normalization of the conformal blocks is the same as that in [1].

For MFT we only need to invert the t-channel identity operator, and we get

$$c(\Delta, \ell) = \frac{1 + (-1)^\ell}{4} \kappa_{\Delta + \ell} \int_0^1 dz d\bar{z} \mu(z, \bar{z}) \mathcal{G}_{\ell+3}^{(\Delta-3)}(z, \bar{z}) \mathrm{dDisc} \left[\left(\frac{z\bar{z}}{(1 - z)(1 - \bar{z})} \right)^{\Delta_\phi} \right]$$

$$= \frac{(1 + (-1)^\ell)(\Delta - 2)(\ell + 1)}{4\pi^2} \sin^2(\pi \Delta_\phi) \Gamma(1 - \Delta_\phi)^2 \Gamma(2 - \Delta_\phi)^2$$

$$\times \frac{\Gamma\left(\frac{1}{2}(\Delta + \ell)\right)^2 \Gamma(-\Delta + \ell + 4) \Gamma\left(\frac{1}{2}(-\Delta + \ell + 2\Delta_\phi)\right) \Gamma\left(\frac{1}{2}(-4 + \Delta + \ell + 2\Delta_\phi)\right)}{\Gamma\left(\frac{1}{2}(-\Delta + \ell + 4)\right)^2 \Gamma(\Delta + \ell - 1) \Gamma\left(\frac{1}{2}(-\Delta + \ell - 2\Delta_\phi + 8)\right) \Gamma\left(\frac{1}{2}(\Delta + \ell - 2\Delta_\phi + 4)\right)} .$$

$$(5.C.2)$$

It it straightforward to check that when ℓ is an even integer, the residue of $-c(\Delta, \ell)$ at $\Delta = 2\Delta_\phi + \ell + 2n$ indeed gives the OPE coefficient of MFT given in [193].

When $\Delta_\phi \in \mathbb{Z}_{\geqslant 2}$ it can be seen from the second line of (5.C.2) that $c(\Delta, \ell)$ is divergent, since there is a fourth-order pole and only a second-order zero. To regulate

poles in Δ $(n = 0, 1, 2, \ldots)$	origin	comment
$\Delta = -\ell - 2n$	$\Gamma\left(\frac{1}{2}(\Delta + \ell)\right)^2$	κ-factor poles, not picked up
$\Delta = \ell + 5 + 2n$	$\dfrac{\Gamma(-\Delta + \ell + 4)}{\Gamma\left(\frac{1}{2}(-\Delta + \ell + 4)\right)^2}$	kernel block poles, cancelled by block poles
$\Delta = 2\Delta_\phi + \ell + 2n$	$\Gamma\left(\frac{1}{2}(-\Delta + \ell + 2\Delta_\phi)\right)$	double-twist poles, zero residue
$4 - \Delta = 2\Delta_\phi + \ell + 2n$	$\Gamma\left(\frac{1}{2}(-4 + \Delta + \ell + 2\Delta_\phi)\right)$	shadow double-twist poles, not picked up

Table 5.3. Poles in Δ of $c^{(-2)}(\Delta, \ell; \Delta_\phi)$

$c(\Delta, \ell)$ for any integer Δ_ϕ we expand

$$c(\Delta, \ell; \Delta_{\text{ex}}) = \frac{c^{(-2)}(\Delta, \ell; \Delta_\phi)}{(\Delta_{\text{ex}} - \Delta_\phi)^2} + \frac{c^{(-1)}(\Delta, \ell; \Delta_\phi)}{\Delta_{\text{ex}} - \Delta_\phi} + c^{(0)}(\Delta, \ell; \Delta_\phi) + O(\Delta_{\text{ex}} - \Delta_\phi),$$

$$(5.\text{C}.3)$$

where we have kept the dependence on external dimension explicit. The residues are

$$c^{(-2)}(\Delta, \ell; \Delta_\phi) = \frac{(1 + (-1)^\ell)(\Delta - 2)(\ell + 1)}{2\Gamma(\Delta_\phi - 1)^2 \Gamma(\Delta_\phi)^2}$$

$$\times \frac{\Gamma\left(\frac{1}{2}(\Delta + \ell)\right)^2 \Gamma(-\Delta + \ell + 4)\Gamma\left(\frac{1}{2}(-\Delta + \ell + 2\Delta_\phi)\right)\Gamma\left(\frac{1}{2}(-4 + \Delta + \ell + 2\Delta_\phi)\right)}{\Gamma\left(\frac{1}{2}(-\Delta + \ell + 4)\right)^2 \Gamma(\Delta + \ell - 1)\Gamma\left(\frac{1}{2}(-\Delta + \ell - 2\Delta_\phi + 8)\right)\Gamma\left(\frac{1}{2}(\Delta + \ell - 2\Delta_\phi + 4)\right)},$$

$$(5.\text{C}.4)$$

and

$$c^{(-1)}(\Delta, \ell; \Delta_\phi) = \Bigg[-2\psi(\Delta_\phi - 1) - 2\psi(\Delta_\phi) + \psi\left(\frac{-\Delta + \ell + 2\Delta_\phi}{2}\right) + \psi\left(\frac{-4 + \Delta + \ell + 2\Delta_\phi}{2}\right)$$

$$+ \psi\left(\frac{-\Delta + \ell - 2\Delta_\phi + 8}{2}\right) + \psi\left(\frac{\Delta + \ell - 2\Delta_\phi + 4}{2}\right) \Bigg] \times c^{(-2)}(\Delta, \ell; \Delta_\phi).$$

$$(5.\text{C}.5)$$

Now we check the poles of Δ in $c^{(-2)}(\Delta, \ell; \Delta_\phi)$. There are four sets of poles and they all come from the Γ-functions in the numerator of (5.C.4). From left to right,

the first set of poles originate from the κ-factor. In general this factor reads

$$\kappa_{\Delta+\ell}^{\Delta_{12},\Delta_{34}} = \frac{\Gamma(\frac{1}{2}(\Delta+\ell+\Delta_{12})\Gamma(\frac{1}{2}(\Delta+\ell-\Delta_{12})\Gamma(\frac{1}{2}(\Delta+\ell+\Delta_{34})\Gamma(\frac{1}{2}(\Delta+\ell-\Delta_{34})}{2\pi^2\Gamma(\Delta+\ell)\Gamma(\Delta+\ell-1)},$$

(5.C.6)

and has poles at

$$\Delta = -\ell \pm \Delta_{12} - 2n, \quad \Delta = -\ell \pm \Delta_{34} - 2n, \quad n = 0, 1, 2, \ldots. \quad (5.C.7)$$

As discussed in [33] these poles are on the left hand side of the Δ-integration contour when the *external* dimensions are in the principal series and therefore not picked up. When we analytically continue external dimensions to physical (and real) values, although some of the poles may move to the right of contour integration, the contour should be deformed such that the poles remain to the left and not picked up. The second set of poles are the spurious poles similar to the ones listed in the last row of table 5.2. These poles will be picked up in the principal-series integration

$$g(z, \bar{z}) = \int_{d/2-i\infty}^{d/2+i\infty} \frac{d\Delta}{2\pi i} c(\Delta, \ell)\mathcal{G}_\Delta^{(\ell)}(z, \bar{z}) + (\text{non-norm.}), \quad (5.C.8)$$

but as shown in [33] they will be cancelled exactly by the poles of the block $\mathcal{G}_\Delta^{(\ell)}(z, \bar{z})$, thus nothing physical is subtracted. The third and fourth set of poles are physical double-twist poles and their shadows. One can check that the residues of the third set of poles vanish when $\Delta_\phi \in \mathbb{Z}_{\geq 2}$ and the fourth set of poles are never picked up. We summarize these results in table 5.3 and note in passing that the check related to physical poles is the most important one.

Turning to $c^{(-1)}(\Delta, \ell)$, it is straightforward to check that it does not contain any poles other than those in $c^{(-2)}(\Delta, \ell)$. Therefore, we conclude that $c^{(-2)}(\Delta, \ell)$ and $c^{(-1)}(\Delta, \ell)$ do not have a block decomposition and can be safely subtracted.

5.D   Exploring the required t-channel contributions

In this appendix we explore the issues with the A_1 theory a bit further. In particular, we would like to know whether the vanishing of the $\mathcal{D}[0, 4]$ OPE coefficient at $c = 25$ can be recovered at all from a sum over t-channel blocks, and if so what properties such a block decomposition has. Therefore we take the rather crude ansatz where we pack the contribution of the entire unprotected part of $a(z, \bar{z})$ into the first few t-channel long blocks with some (unrealistically) large anomalous dimensions and OPE coefficients. Demanding then that $\lambda_{\mathcal{D}[0,4]}^2 = 0$ might give us an idea of what this implies for the unprotected data.

Concretely we experimented with approximating the entire unprotected contribution in the t-channel by the following three groups of data:

1 block: $\quad \Delta_0 = 6.4, \quad \lambda^2_{\mathcal{L}[0,0]_0} = 11.4071,$

2 blocks: $\quad \Delta_0 = 6.4, \quad \lambda^2_{\mathcal{L}[0,0]_0} = 1.59017, \quad \Delta_2 = 8.4, \quad \lambda^2_{\mathcal{L}[0,0]_2} = 4.21943,$

(5.D.1)

2+2 blocks: $\quad \Delta_0 = 6.4, \quad \lambda^2_{\mathcal{L}[0,0]_0} = 1.44136, \quad \Delta_2 = 8.4, \quad \lambda^2_{\mathcal{L}[0,0]_2} = 3.84518,$

$\Delta_{0'} = 8.86, \quad \lambda^2_{\mathcal{L}[0,0]_{0'}} = 6.08945, \quad \Delta_{2'} = 10.86, \quad \lambda^2_{\mathcal{L}[0,0]_{0'}} = 8.74061,$

where the first two groups consider only multiplets on the leading long trajectory while the last one also takes into account of the subleading long trajectory, which we distinguish by adding a prime in the spin. The inversion results are shown in table 5.4. For all of these sets we have imposed $\lambda^2_{\mathcal{D}[0,4]} = 0$. From the table we can draw some qualitative conclusions:

- The OPE coefficient of the non-chiral algebra short multiplets are relatively stable across all three sets of input data.

- The dimensions of the long multiplets in all columns are lower than the inversion results in figure 5.9.

- Distributing the contributions to double discontinuity into more blocks on the leading long trajectory lowers the dimensions and OPE coefficients of the leading long multiplets. However, notice that in the "2 blocks" column Δ_0 is still higher while Δ_2 is already lower than the numerical bootstrap's prediction $\Delta_0 \simeq 6.4, \Delta_2 \simeq 9.4$. All the OPE coefficients decrease after the redistribution.

- Distributing the contribution to double discontinuity into both leading and subleading long trajectories further slightly lowers Δ_0 and increases Δ_2, which moves the results closer to numerical predictions. From the OPE coefficients, $\lambda^2_{\mathcal{L}[0,0]_0}$ receives the most significant change, a decrease that is also consistent with our expectation. Therefore, we again see evidence that we should include contributions from the subleading long trajectory to fully recover the unprotected CFT data.

	1 block	2 blocks	2+2 blocks
$\lambda^2_{\mathcal{B}[0,2]_{\ell-1}}$ $\ell = 2, 4, 6$	10.1005	10.1009	10.1127
	19.3475	19.3476	19.3518
	21.4387	21.4387	21.4399
Δ_ℓ $\ell = 0, 2, 4, 6$	7.0681	6.9434	6.9405
	9.4951	9.3667	9.3783
	11.8086	11.7476	11.7559
	13.9220	13.8990	13.9029
$\lambda^2_{\mathcal{L}[0,0]_\ell}$ $\ell = 0, 2, 4, 6$	1.9259	1.5510	1.5282
	4.1565	3.8376	3.8343
	5.5590	5.2950	5.3085
	5.4229	5.3212	5.3312

Table 5.4. Crude estimates of unprotected CFT data of A_1 theory for the first few lowest spins. The results are obtained by imposing $\lambda^2_{\mathcal{D}[0,4]} = 0$ and approximating the entire unprotected part of $a(z, \bar{z})$ by: a single scalar block on the leading long trajectory ("1"), one block of spin 0 and one block of spin 2 on the leading long trajectory ("2"), and blocks of spin 0 and spin 2 both on the leading and subleading long trajectories ("2+2"). The input CFT data are listed in (5.D.1).

List of Figures

List of Tables

Bibliography

[1] S. Caron-Huot, *Analyticity in Spin in Conformal Theories*, *JHEP* **09** (2017) 078, [arXiv:1703.00278].

[2] S. Komatsu, M. F. Paulos, B. C. Van Rees, and X. Zhao, *Landau diagrams in AdS and S-matrices from conformal correlators*, *JHEP* **11** (2020) 046, [arXiv:2007.13745].

[3] E. Lauria, P. Liendo, B. C. Van Rees, and X. Zhao, *Line and surface defects for the free scalar field*, *JHEP* **01** (2021) 060, [arXiv:2005.02413].

[4] M. Lemos, B. C. van Rees, and X. Zhao, *Regge trajectories for the (2,0) theories*, *accepted by JHEP* (12, 2021) [arXiv:2105.13361].

[5] J. M. Maldacena, *The Large N limit of superconformal field theories and supergravity*, *Adv. Theor. Math. Phys.* **2** (1998) 231–252, [hep-th/9711200].

[6] E. Witten, *Anti-de Sitter space and holography*, *Adv. Theor. Math. Phys.* **2** (1998) 253–291, [hep-th/9802150].

[7] S. S. Gubser, I. R. Klebanov, and A. M. Polyakov, *Gauge theory correlators from noncritical string theory*, *Phys. Lett. B* **428** (1998) 105–114, [hep-th/9802109].

[8] L. Susskind and E. Witten, *The Holographic bound in anti-de Sitter space*, hep-th/9805114.

[9] T. Banks, M. R. Douglas, G. T. Horowitz, and E. J. Martinec, *AdS dynamics from conformal field theory*, hep-th/9808016.

[10] J. Polchinski, *Scale and Conformal Invariance in Quantum Field Theory*, *Nucl. Phys. B* **303** (1988) 226–236.

[11] I. Heemskerk, J. Penedones, J. Polchinski, and J. Sully, *Holography from Conformal Field Theory*, *JHEP* **10** (2009) 079, [arXiv:0907.0151].

[12] S. El-Showk and K. Papadodimas, *Emergent Spacetime and Holographic CFTs*, *JHEP* **10** (2012) 106, [arXiv:1101.4163].

[13] M. F. Paulos, J. Penedones, J. Toledo, B. C. van Rees, and P. Vieira, *The S-matrix bootstrap. Part I: QFT in AdS*, *JHEP* **11** (2017) 133, [arXiv:1607.06109].

[14] E. Witten, *Some comments on string dynamics*, in *STRINGS 95: Future Perspectives in String Theory*, 7, 1995. hep-th/9507121.

[15] E. Witten, *Baryons and branes in anti-de Sitter space*, *JHEP* **07** (1998) 006, [hep-th/9805112].

[16] O. Aharony, Y. Oz, and Z. Yin, *M theory on AdS(p) x S(11-p) and superconformal field theories*, *Phys. Lett. B* **430** (1998) 87–93, [hep-th/9803051].

[17] L. F. Alday, D. Gaiotto, and Y. Tachikawa, *Liouville Correlation Functions from Four-dimensional Gauge Theories*, *Lett. Math. Phys.* **91** (2010) 167–197, [arXiv:0906.3219].

[18] C. Beem, M. Lemos, L. Rastelli, and B. C. van Rees, *The (2, 0) superconformal bootstrap*, *Phys. Rev. D* **93** (2016), no. 2 025016, [arXiv:1507.05637].

[19] P. Kravchuk, J. Qiao, and S. Rychkov, *Distributions in CFT II. Minkowski Space*, arXiv:2104.02090.

[20] I. Bertan, *Quantum scalar field theory in AdS and the AdS/CFT correspondence*. PhD thesis, Munich U., 2019.

[21] C. G. Callan and F. Wilczek, *Infrared behavior at negative curvature*, *Nuclear Physics B* **340** (1990), no. 2 366–386.

[22] O. Aharony, D. Marolf, and M. Rangamani, *Conformal field theories in anti-de Sitter space*, *JHEP* **02** (2011) 041, [arXiv:1011.6144].

[23] D. Carmi, L. Di Pietro, and S. Komatsu, *A Study of Quantum Field Theories in AdS at Finite Coupling*, *JHEP* **01** (2019) 200, [arXiv:1810.04185].

[24] D. Harlow and D. Stanford, *Operator Dictionaries and Wave Functions in AdS/CFT and dS/CFT*, arXiv:1104.2621.

[25] L. Susskind, *Holography in the flat space limit*, *AIP Conf. Proc.* **493** (1999), no. 1 98–112, [hep-th/9901079].

[26] J. Polchinski, *S matrices from AdS space-time*, hep-th/9901076.

[27] S. B. Giddings, *Flat space scattering and bulk locality in the AdS / CFT correspondence*, *Phys. Rev. D* **61** (2000) 106008, [hep-th/9907129].

[28] S. B. Giddings, *The Boundary S matrix and the AdS to CFT dictionary*, *Phys. Rev. Lett.* **83** (1999) 2707–2710, [hep-th/9903048].

[29] I. R. Klebanov and E. Witten, *AdS / CFT correspondence and symmetry breaking*, *Nucl. Phys. B* **556** (1999) 89–114, [hep-th/9905104].

[30] D. Z. Freedman, S. D. Mathur, A. Matusis, and L. Rastelli, *Correlation functions in the CFT(d) / AdS(d+1) correspondence*, *Nucl. Phys. B* **546** (1999) 96–118, [hep-th/9804058].

[31] D. Pappadopulo, S. Rychkov, J. Espin, and R. Rattazzi, *OPE Convergence in Conformal Field Theory*, *Phys. Rev. D* **86** (2012) 105043, [arXiv:1208.6449].

[32] V. K. Dobrev, V. B. Petkova, S. G. Petrova, and I. T. Todorov, *Dynamical derivation of vacuum operator-product expansion in euclidean conformal quantum field theory*, *Phys. Rev. D* **13** (Feb, 1976) 887–912.

[33] D. Simmons-Duffin, D. Stanford, and E. Witten, *A spacetime derivation of the Lorentzian OPE inversion formula*, *JHEP* **07** (2018) 085, [arXiv:1711.03816].

[34] L. Cornalba, *Eikonal methods in AdS/CFT: Regge theory and multi-reggeon exchange*, arXiv:0710.5480.

[35] M. S. Costa, V. Goncalves, and J. Penedones, *Conformal Regge theory*, *JHEP* **12** (2012) 091, [arXiv:1209.4355].

[36] D. Simmons-Duffin, *The Lightcone Bootstrap and the Spectrum of the 3d Ising CFT*, *JHEP* **03** (2017) 086, [arXiv:1612.08471].

[37] M. Correia, A. Sever, and A. Zhiboedov, *An Analytical Toolkit for the S-matrix Bootstrap*, arXiv:2006.08221.

[38] P. Kravchuk and D. Simmons-Duffin, *Light-ray operators in conformal field theory*, *JHEP* **11** (2018) 102, [arXiv:1805.00098].

[39] S. Caron-Huot and J. Sandor, *Conformal Regge Theory at Finite Boost*, *JHEP* **05** (2021) 059, [arXiv:2008.11759].

[40] J. Penedones, "2018 Bootstrap School: Regge Physics, Lecture 3." https://www.youtube.com/watch?v=KbBi8DNVPnc&list=PLcxG181Xrg95ikWn7tH7Lcd31rzb53GBN&index=14.

[41] M. Gary, S. B. Giddings, and J. Penedones, *Local bulk S-matrix elements and CFT singularities*, *Phys. Rev. D* **80** (2009) 085005, [arXiv:0903.4437].

[42] T. Okuda and J. Penedones, *String scattering in flat space and a scaling limit of Yang-Mills correlators*, *Phys. Rev.* **D83** (2011) 086001, [arXiv:1002.2641].

[43] J. Penedones, *Writing CFT correlation functions as AdS scattering amplitudes*, *JHEP* **03** (2011) 025, [arXiv:1011.1485].

[44] V. Goncalves, *Four point function of $\mathcal{N} = 4$ stress-tensor multiplet at strong coupling*, *JHEP* **04** (2015) 150, [arXiv:1411.1675].

[45] M. F. Paulos, J. Penedones, J. Toledo, B. C. van Rees, and P. Vieira, *The S-matrix bootstrap II: two dimensional amplitudes*, *JHEP* **11** (2017) 143, [arXiv:1607.06110].

[46] M. F. Paulos, J. Penedones, J. Toledo, B. C. van Rees, and P. Vieira, *The S-matrix bootstrap. Part III: higher dimensional amplitudes*, *JHEP* **12** (2019) 040, [arXiv:1708.06765].

[47] A. Homrich, J. Penedones, J. Toledo, B. C. van Rees, and P. Vieira, *The S-matrix Bootstrap IV: Multiple Amplitudes*, *JHEP* **11** (2019) 076, [arXiv:1905.06905].

[48] O. Aharony, M. Berkooz, D. Tong, and S. Yankielowicz, *Confinement in Anti-de Sitter Space*, *JHEP* **02** (2013) 076, [arXiv:1210.5195].

[49] O. Aharony, M. Berkooz, and S.-J. Rey, *Rigid holography and six-dimensional $\mathcal{N} = (2,0)$ theories on $AdS_5 \times S^1$*, *JHEP* **03** (2015) 121, [arXiv:1501.02904].

[50] S. Giombi and H. Khanchandani, *CFT in AdS and boundary RG flows*, arXiv:2007.04955.

[51] S. Giombi, R. Roiban, and A. A. Tseytlin, *Half-BPS Wilson loop and AdS_2/CFT_1*, *Nucl. Phys. B* **922** (2017) 499–527, [arXiv:1706.00756].

[52] M. Beccaria and A. A. Tseytlin, *On boundary correlators in Liouville theory on AdS_2*, *JHEP* **07** (2019) 008, [arXiv:1904.12753].

[53] E. Hijano, *Flat space physics from AdS/CFT*, *JHEP* **07** (2019) 132, [arXiv:1905.02729].

[54] S. Dubovsky, V. Gorbenko, and M. Mirbabayi, *Asymptotic fragility, near AdS_2 holography and $T\overline{T}$*, *JHEP* **09** (2017) 136, [arXiv:1706.06604].

[55] J. Penedones, J. A. Silva, and A. Zhiboedov, *Nonperturbative Mellin Amplitudes: Existence, Properties, Applications*, arXiv:1912.11100.

[56] J. Maldacena, D. Simmons-Duffin, and A. Zhiboedov, *Looking for a bulk point*, *JHEP* **01** (2017) 013, [arXiv:1509.03612].

[57] K. Skenderis, *Lecture notes on holographic renormalization*, *Class. Quant. Grav.* **19** (2002) 5849–5876, [hep-th/0209067].

[58] M. Beccaria, S. Giombi, and A. A. Tseytlin, *Correlators on non-supersymmetric Wilson line in $\mathcal{N} = 4$ SYM and AdS_2/CFT_1*, *JHEP* **05** (2019) 122, [arXiv:1903.04365].

[59] M. Beccaria and G. Landolfi, *Toda theory in AdS_2 and $\mathcal{W}A_n$-algebra structure of boundary correlators*, *JHEP* **10** (2019) 003, [arXiv:1906.06485].

[60] M. Beccaria, H. Jiang, and A. A. Tseytlin, *Non-abelian Toda theory on AdS_2 and $AdS_2/CFT_2^{1/2}$ duality*, *JHEP* **09** (2019) 036, [arXiv:1907.01357].

[61] M. Beccaria, H. Jiang, and A. A. Tseytlin, *Supersymmetric Liouville theory in AdS_2 and AdS/CFT*, *JHEP* **11** (2019) 051, [arXiv:1909.10255].

[62] M. Beccaria, H. Jiang, and A. A. Tseytlin, *Boundary correlators in WZW model on AdS_2*, *JHEP* **05** (2020) 099, [arXiv:2001.11269].

[63] K. Skenderis and B. C. van Rees, *Real-time gauge/gravity duality*, *Phys. Rev. Lett.* **101** (2008) 081601, [arXiv:0805.0150].

[64] K. Skenderis and B. C. van Rees, *Real-time gauge/gravity duality: Prescription, Renormalization and Examples*, *JHEP* **05** (2009) 085, [arXiv:0812.2909].

[65] F. A. Dolan and H. Osborn, *Conformal four point functions and the operator product expansion*, *Nucl. Phys.* **B599** (2001) 459–496, [hep-th/0011040].

[66] F. Dolan and H. Osborn, *Conformal partial waves and the operator product expansion*, *Nucl. Phys. B* **678** (2004) 491–507, [hep-th/0309180].

[67] M. Hogervorst and S. Rychkov, *Radial Coordinates for Conformal Blocks*, *Phys. Rev.* **D87** (2013) 106004, [arXiv:1303.1111].

[68] F. Aprile and P. Vieira, *Large p explorations. From SUGRA to big STRINGS in Mellin space*, arXiv:2007.09176.

[69] L. Cornalba, M. S. Costa, J. Penedones, and R. Schiappa, *Eikonal Approximation in AdS/CFT: From Shock Waves to Four-Point Functions*, JHEP **08** (2007) 019, [hep-th/0611122].

[70] D. J. Gross and P. F. Mende, *String Theory Beyond the Planck Scale*, Nucl. Phys. B **303** (1988) 407–454.

[71] J. A. Minahan, *Holographic three-point functions for short operators*, JHEP **07** (2012) 187, [arXiv:1206.3129].

[72] G. Mack, *D-independent representation of Conformal Field Theories in D dimensions via transformation to auxiliary Dual Resonance Models. Scalar amplitudes*, arXiv:0907.2407.

[73] E. Hijano, P. Kraus, E. Perlmutter, and R. Snively, *Witten Diagrams Revisited: The AdS Geometry of Conformal Blocks*, JHEP **01** (2016) 146, [arXiv:1508.00501].

[74] L. Landau, *On analytic properties of vertex parts in quantum field theory*, Nucl. Phys. **13** (1960), no. 1 181–192.

[75] S. Coleman and R. Norton, *Singularities in the physical region*, Nuovo Cim. **38** (1965) 438–442.

[76] J. D. Bjorken and S. D. Drell, *Relativistic quantum fields*. McGraw-Hill, 1965.

[77] R. J. Eden, P. V. Landshoff, D. I. Olive, and J. C. Polkinghorne, *The analytic S-matrix*. Cambridge University Press, 2002.

[78] G. Sterman, *An introduction to quantum field theory*. Cambridge university press, 1993.

[79] A. Fitzpatrick, J. Kaplan, J. Penedones, S. Raju, and B. C. van Rees, *A Natural Language for AdS/CFT Correlators*, JHEP **11** (2011) 095, [arXiv:1107.1499].

[80] M. F. Paulos, *Towards Feynman rules for Mellin amplitudes*, JHEP **10** (2011) 074, [arXiv:1107.1504].

[81] F. Kos, D. Poland, and D. Simmons-Duffin, *Bootstrapping Mixed Correlators in the 3D Ising Model*, JHEP **11** (2014) 109, [arXiv:1406.4858].

[82] D. Mazac and M. F. Paulos, *The analytic functional bootstrap. Part I: 1D CFTs and 2D S-matrices*, JHEP **02** (2019) 162, [arXiv:1803.10233].

[83] D. Carmi and S. Caron-Huot, *A Conformal Dispersion Relation: Correlations from Absorption*, arXiv:1910.12123.

[84] M. Dodelson and H. Ooguri, *High-energy behavior of Mellin amplitudes*, Phys. Rev. D **101** (2020), no. 6 066008, [arXiv:1911.05274].

[85] P. Haldar and A. Sinha, *Froissart bound for/from CFT Mellin amplitudes*, SciPost Phys. **8** (2020) 095, [arXiv:1911.05974].

[86] S. Weinberg, *Infrared photons and gravitons*, *Phys. Rev.* **140** (1965) B516–B524.

[87] T. He, V. Lysov, P. Mitra, and A. Strominger, *BMS supertranslations and Weinberg's soft graviton theorem*, *JHEP* **05** (2015) 151, [arXiv:1401.7026].

[88] A. Strominger, *Lectures on the Infrared Structure of Gravity and Gauge Theory*, arXiv:1703.05448.

[89] E. Hijano and D. Neuenfeld, *Soft photon theorems from CFT Ward identites in the flat limit of AdS/CFT*, arXiv:2005.03667.

[90] N. Kobayashi and T. Nishioka, *Spinning conformal defects*, *JHEP* **09** (2018) 134, [arXiv:1805.05967].

[91] M. F. Paulos, S. Rychkov, B. C. van Rees, and B. Zan, *Conformal Invariance in the Long-Range Ising Model*, *Nucl. Phys. B* **902** (2016) 246–291, [arXiv:1509.00008].

[92] C. Behan, L. Di Pietro, E. Lauria, and B. C. van Rees, *Bootstrapping boundary-localized interactions*, arXiv:2009.03336.

[93] V. Procházka and A. Söderberg, *Composite operators near the boundary*, *JHEP* **03** (2020) 114, [arXiv:1912.07505].

[94] M. Billò, V. Gonχcalves, E. Lauria, and M. Meineri, *Defects in conformal field theory*, *JHEP* **04** (2016) 091, [arXiv:1601.02883].

[95] A. Söderberg, *Anomalous Dimensions in the WF O(N) Model with a Monodromy Line Defect*, *JHEP* **03** (2018) 058, [arXiv:1706.02414].

[96] P. Liendo, L. Rastelli, and B. C. van Rees, *The Bootstrap Program for Boundary CFT$_d$*, *JHEP* **07** (2013) 113, [arXiv:1210.4258].

[97] D. Gaiotto, D. Mazac, and M. F. Paulos, *Bootstrapping the 3d Ising twist defect*, *JHEP* **03** (2014) 100, [arXiv:1310.5078].

[98] F. Gliozzi, P. Liendo, M. Meineri, and A. Rago, *Boundary and Interface CFTs from the Conformal Bootstrap*, *JHEP* **05** (2015) 036, [arXiv:1502.07217].

[99] F. Gliozzi, *Truncatable bootstrap equations in algebraic form and critical surface exponents*, *JHEP* **10** (2016) 037, [arXiv:1605.04175].

[100] P. Liendo and C. Meneghelli, *Bootstrap equations for $\mathcal{N} = 4$ SYM with defects*, *JHEP* **01** (2017) 122, [arXiv:1608.05126].

[101] M. Lemos, P. Liendo, M. Meineri, and S. Sarkar, *Universality at large transverse spin in defect CFT*, *JHEP* **09** (2018) 091, [arXiv:1712.08185].

[102] M. Hogervorst, *Crossing Kernels for Boundary and Crosscap CFTs*, arXiv:1703.08159.

[103] A. Bissi, T. Hansen, and A. Söderberg, *Analytic Bootstrap for Boundary CFT*, *JHEP* **01** (2019) 010, [arXiv:1808.08155].

[104] A. Kaviraj and M. F. Paulos, *The Functional Bootstrap for Boundary CFT*, arXiv:1812.04034.

[105] D. Mazáč, L. Rastelli, and X. Zhou, *An analytic approach to BCFT$_d$*, *JHEP* **12** (2019) 004, [arXiv:1812.09314].

[106] P. Liendo, Y. Linke, and V. Schomerus, *A Lorentzian inversion formula for defect CFT*, arXiv:1903.05222.

[107] D. M. McAvity and H. Osborn, *Conformal field theories near a boundary in general dimensions*, *Nucl. Phys.* **B455** (1995) 522–576, [cond-mat/9505127].

[108] D. M. McAvity and H. Osborn, *Energy momentum tensor in conformal field theories near a boundary*, *Nucl. Phys.* **B406** (1993) 655–680, [hep-th/9302068].

[109] A. Gadde, *Conformal constraints on defects*, *JHEP* **01** (2020) 038, [arXiv:1602.06354].

[110] E. Lauria, M. Meineri, and E. Trevisani, *Radial coordinates for defect CFTs*, *JHEP* **11** (2018) 148, [arXiv:1712.07668].

[111] S. Guha and B. Nagaraj, *Correlators of Mixed Symmetry Operators in Defect CFTs*, *JHEP* **10** (2018) 198, [arXiv:1805.12341].

[112] E. Lauria, M. Meineri, and E. Trevisani, *Spinning operators and defects in conformal field theory*, *JHEP* **08** (2019) 066, [arXiv:1807.02522].

[113] M. Isachenkov, P. Liendo, Y. Linke, and V. Schomerus, *Calogero-Sutherland Approach to Defect Blocks*, *JHEP* **10** (2018) 204, [arXiv:1806.09703].

[114] T. Dimofte, D. Gaiotto, and N. M. Paquette, *Dual boundary conditions in 3d SCFT's*, *JHEP* **05** (2018) 060, [arXiv:1712.07654].

[115] S. Giombi and H. Khanchandani, *O(N) Models with Boundary Interactions and their Long Range Generalizations*, arXiv:1912.08169.

[116] C. P. Herzog and K.-W. Huang, *Boundary Conformal Field Theory and a Boundary Central Charge*, *JHEP* **10** (2017) 189, [arXiv:1707.06224].

[117] R. Kumar Gupta, C. P. Herzog, and I. Jeon, *Duality and Transport for Supersymmetric Graphene from the Hemisphere Partition Function*, arXiv:1912.09225.

[118] C. P. Herzog, K.-W. Huang, I. Shamir, and J. Virrueta, *Superconformal Models for Graphene and Boundary Central Charges*, *JHEP* **09** (2018) 161, [arXiv:1807.01700].

[119] M. Gaberdiel and A. Recknagel, *Conformal boundary states for free bosons and fermions*, *JHEP* **11** (2001) 016, [hep-th/0108238].

[120] C. Cordova, D. Gaiotto, and S.-H. Shao, *Surface Defects and Chiral Algebras*, *JHEP* **05** (2017) 140, [arXiv:1704.01955].

[121] L. Bianchi and M. Lemos, *Superconformal surfaces in four dimensions*, arXiv:1911.05082.

[122] D. Gaiotto, G. W. Moore, and A. Neitzke, *Wall-Crossing in Coupled 2d-4d Systems*, *JHEP* **12** (2012) 082, [arXiv:1103.2598].

[123] D. Gaiotto, L. Rastelli, and S. S. Razamat, *Bootstrapping the superconformal index with surface defects*, *JHEP* **01** (2013) 022, [arXiv:1207.3577].

[124] O. J. Ganor, *Six-dimensional tensionless strings in the large n limit*, *Nuclear Physics B* **489** (Mar, 1997) 95–121.

[125] M. Henningson and K. Skenderis, *Weyl anomaly for wilson surfaces*, *Journal of High Energy Physics* **1999** (Jun, 1999) 012–012.

[126] M. Henningson, *Surface observables and the weyl anomaly*, 1999.

[127] A. Gustavsson, *On the weyl anomaly of wilson surfaces*, *Journal of High Energy Physics* **2003** (Dec, 2003) 059–059.

[128] A. Gustavsson, *Conformal anomaly of wilson surface observables - a field theoretical computation*, *Journal of High Energy Physics* **2004** (Jul, 2004) 074–074.

[129] N. Drukker, M. Probst, and M. Trépanier, *Surface operators in the 6d $\mathcal{N} = (2,0)$ theory*, arXiv:2003.12372.

[130] M. Mezei, S. S. Pufu, and Y. Wang, *Chern-Simons theory from M5-branes and calibrated M2-branes*, *JHEP* **08** (2019) 165, [arXiv:1812.07572].

[131] E. Witten, *SL(2,Z) action on three-dimensional conformal field theories with Abelian symmetry*, hep-th/0307041.

[132] D. Gaiotto and E. Witten, *S-Duality of Boundary Conditions In N=4 Super Yang-Mills Theory*, *Adv. Theor. Math. Phys.* **13** (2009), no. 3 721–896, [arXiv:0807.3720].

[133] N. Seiberg, T. Senthil, C. Wang, and E. Witten, *A Duality Web in 2+1 Dimensions and Condensed Matter Physics*, *Annals Phys.* **374** (2016) 395–433, [arXiv:1606.01989].

[134] L. Di Pietro, D. Gaiotto, E. Lauria, and J. Wu, *3d Abelian Gauge Theories at the Boundary*, *JHEP* **05** (2019) 091, [arXiv:1902.09567].

[135] M. Billó, M. Caselle, D. Gaiotto, F. Gliozzi, M. Meineri, and R. Pellegrini, *Line defects in the 3d Ising model*, *JHEP* **07** (2013) 055, [arXiv:1304.4110].

[136] T. Dimofte and D. Gaiotto, *An E7 Surprise*, *JHEP* **10** (2012) 129, [arXiv:1209.1404].

[137] D. Gaiotto, *Boundary F-maximization*, arXiv:1403.8052.

[138] L. Bianchi, M. Meineri, R. C. Myers, and M. Smolkin, *Rényi entropy and conformal defects*, *JHEP* **07** (2016) 076, [arXiv:1511.06713].

[139] M. S. Costa, J. Penedones, D. Poland, and S. Rychkov, *Spinning Conformal Correlators*, *JHEP* **11** (2011) 071, [arXiv:1107.3554].

[140] C. Behan, L. Rastelli, S. Rychkov, and B. Zan, *A scaling theory for the long-range to short-range crossover and an infrared duality*, *J. Phys.* **A50** (2017), no. 35 354002, [arXiv:1703.05325].

[141] C. Behan, L. Rastelli, S. Rychkov, and B. Zan, *Long-range critical exponents near the short-range crossover*, *Phys. Rev. Lett.* **118** (2017), no. 24 241601, [`arXiv:1703.03430`].

[142] C. Behan, *Bootstrapping the long-range Ising model in three dimensions*, *J. Phys.* **A52** (2019), no. 7 075401, [`arXiv:1810.07199`].

[143] G. J. Turiaci and A. Zhiboedov, *Veneziano amplitude of vasiliev theory*, *Journal of High Energy Physics* **2018** (Oct, 2018).

[144] T. Hartman, S. Jain, and S. Kundu, *Causality Constraints in Conformal Field Theory*, *JHEP* **05** (2016) 099, [`arXiv:1509.00014`].

[145] A. Bissi, P. Dey, and T. Hansen, *Dispersion Relation for CFT Four-Point Functions*, *JHEP* **04** (2020) 092, [`arXiv:1910.04661`].

[146] J. Cardy, *Scaling and Renormalization in Statistical Physics*. Cambridge University Press, 1996.

[147] A. Petkou and K. Skenderis, *A Nonrenormalization theorem for conformal anomalies*, *Nucl. Phys.* **B561** (1999) 100–116, [`hep-th/9906030`].

[148] B. C. van Rees, *Irrelevant deformations and the holographic Callan-Symanzik equation*, *JHEP* **10** (2011) 067, [`arXiv:1105.5396`].

[149] Z. Komargodski and D. Simmons-Duffin, *The Random-Bond Ising Model in 2.01 and 3 Dimensions*, *J. Phys.* **A50** (2017), no. 15 154001, [`arXiv:1603.04444`].

[150] C. Behan, *Conformal manifolds: ODEs from OPEs*, *JHEP* **03** (2018) 127, [`arXiv:1709.03967`].

[151] T. Dimofte, N. Garner, M. Geracie, and J. Hilburn, *Mirror symmetry and line operators*, *JHEP* **02** (2020) 075, [`arXiv:1908.00013`].

[152] E. Kozik and B. Svistunov, *Vortex-phonon interaction*, *Physical Review B* **72** (Nov, 2005).

[153] A. Karch and Y. Sato, *Conformal Manifolds with Boundaries or Defects*, *JHEP* **07** (2018) 156, [`arXiv:1805.10427`].

[154] R. C. Brower, J. Polchinski, M. J. Strassler, and C.-I. Tan, *The Pomeron and gauge/string duality*, *JHEP* **12** (2007) 005, [`hep-th/0603115`].

[155] L. Cornalba, M. S. Costa, and J. Penedones, *Eikonal Methods in AdS/CFT: BFKL Pomeron at Weak Coupling*, *JHEP* **06** (2008) 048, [`arXiv:0801.3002`].

[156] L. F. Alday and A. Zhiboedov, *An Algebraic Approach to the Analytic Bootstrap*, *JHEP* **04** (2017) 157, [`arXiv:1510.08091`].

[157] A. Fitzpatrick, J. Kaplan, D. Poland, and D. Simmons-Duffin, *The Analytic Bootstrap and AdS Superhorizon Locality*, *JHEP* **12** (2013) 004, [`arXiv:1212.3616`].

[158] Z. Komargodski and A. Zhiboedov, *Convexity and Liberation at Large Spin*, *JHEP* **11** (2013) 140, [`arXiv:1212.4103`].

[159] S. Albayrak, D. Meltzer, and D. Poland, *More Analytic Bootstrap: Nonperturbative Effects and Fermions*, *JHEP* **08** (2019) 040, [arXiv:1904.00032].

[160] J. Liu, D. Meltzer, D. Poland, and D. Simmons-Duffin, *The Lorentzian inversion formula and the spectrum of the 3d O(2) CFT*, *JHEP* **09** (2020) 115, [arXiv:2007.07914].

[161] S. Caron-Huot, Y. Gobeil, and Z. Zahraee, *The leading trajectory in the 2+1D Ising CFT*, arXiv:2007.11647.

[162] L. F. Alday, S. M. Chester, and H. Raj, *6d (2,0) and M-theory at 1-loop*, arXiv:2005.07175.

[163] L. F. Alday and S. Caron-Huot, *Gravitational S-matrix from CFT dispersion relations*, *JHEP* **12** (2018) 017, [arXiv:1711.02031].

[164] S. Caron-Huot and A.-K. Trinh, *All tree-level correlators in $AdS_5 \times S_5$ supergravity: hidden ten-dimensional conformal symmetry*, *JHEP* **01** (2019) 196, [arXiv:1809.09173].

[165] M. Cornagliotto, M. Lemos, and P. Liendo, *Bootstrapping the (A_1, A_2) Argyres-Douglas theory*, *JHEP* **03** (2018) 033, [arXiv:1711.00016].

[166] G. Arutyunov and E. Sokatchev, *Implications of superconformal symmetry for interacting (2,0) tensor multiplets*, *Nucl. Phys. B* **635** (2002) 3–32, [hep-th/0201145].

[167] P. Heslop, *Aspects of superconformal field theories in six dimensions*, *JHEP* **07** (2004) 056, [hep-th/0405245].

[168] L. Rastelli and X. Zhou, *Holographic Four-Point Functions in the (2, 0) Theory*, *JHEP* **06** (2018) 087, [arXiv:1712.02788].

[169] X. Zhou, *On Superconformal Four-Point Mellin Amplitudes in Dimension $d > 2$*, *JHEP* **08** (2018) 187, [arXiv:1712.02800].

[170] P. Heslop and A. E. Lipstein, *M-theory Beyond The Supergravity Approximation*, *JHEP* **02** (2018) 004, [arXiv:1712.08570].

[171] S. M. Chester and E. Perlmutter, *M-Theory Reconstruction from (2,0) CFT and the Chiral Algebra Conjecture*, *JHEP* **08** (2018) 116, [arXiv:1805.00892].

[172] T. Abl, P. Heslop, and A. E. Lipstein, *Recursion relations for anomalous dimensions in the 6d $(2,0)$ theory*, *JHEP* **04** (2019) 038, [arXiv:1902.00463].

[173] F. A. Dolan, L. Gallot, and E. Sokatchev, *On four-point functions of 1/2-BPS operators in general dimensions*, *JHEP* **09** (2004) 056, [hep-th/0405180].

[174] C. Beem, M. Lemos, P. Liendo, W. Peelaers, L. Rastelli, and B. C. van Rees, *Infinite Chiral Symmetry in Four Dimensions*, *Commun. Math. Phys.* **336** (2015), no. 3 1359–1433, [arXiv:1312.5344].

[175] C. Beem, L. Rastelli, and B. C. van Rees, *$\mathcal{W}$ symmetry in six dimensions*, *JHEP* **05** (2015) 017, [arXiv:1404.1079].

[176] M. Hogervorst, *Dimensional Reduction for Conformal Blocks*, *JHEP* **09** (2016) 017, [arXiv:1604.08913].

[177] B. Eden, S. Ferrara, and E. Sokatchev, *(2,0) superconformal OPEs in D = 6, selection rules and nonrenormalization theorems*, *JHEP* **0111** (2001) 020, [hep-th/0107084].

[178] S. Ferrara and E. Sokatchev, *Universal properties of superconformal OPEs for 1/2 BPS operators in $3 \leqslant D \leqslant 6$*, *New J.Phys.* **4** (2002) 2, [hep-th/0110174].

[179] H. Osborn and A. C. Petkou, *Implications of conformal invariance in field theories for general dimensions*, *Annals Phys.* **231** (1994) 311–362, [hep-th/9307010].

[180] D. Rutter and B. C. Van Rees, *Applications of Alpha Space*, *JHEP* **12** (2020) 048, [arXiv:2003.07964].

[181] M. Kologlu, P. Kravchuk, D. Simmons-Duffin, and A. Zhiboedov, *Shocks, Superconvergence, and a Stringy Equivalence Principle*, *JHEP* **11** (2020) 096, [arXiv:1904.05905].

[182] F. Kos, D. Poland, and D. Simmons-Duffin, *Bootstrapping the $O(N)$ vector models*, *JHEP* **06** (2014) 091, [arXiv:1307.6856].

[183] S. Caron-Huot, D. Mazac, L. Rastelli, and D. Simmons-Duffin, *Dispersive CFT Sum Rules*, arXiv:2008.04931.

[184] C. Cordova, T. T. Dumitrescu, and K. Intriligator, *Multiplets of Superconformal Symmetry in Diverse Dimensions*, *JHEP* **03** (2019) 163, [arXiv:1612.00809].

[185] M. Nirschl and H. Osborn, *Superconformal Ward identities and their solution*, *Nucl. Phys. B* **711** (2005) 409–479, [hep-th/0407060].

[186] C. Beem, L. Rastelli, and B. C. van Rees, *More $\mathcal{N} = 4$ superconformal bootstrap*, *Phys. Rev. D* **96** (2017), no. 4 046014, [arXiv:1612.02363].

[187] S. M. Chester, J. Lee, S. S. Pufu, and R. Yacoby, *The $\mathcal{N} = 8$ superconformal bootstrap in three dimensions*, *JHEP* **09** (2014) 143, [arXiv:1406.4814].

[188] N. Gromov, F. Levkovich-Maslyuk, and G. Sizov, *Quantum Spectral Curve and the Numerical Solution of the Spectral Problem in AdS5/CFT4*, *JHEP* **06** (2016) 036, [arXiv:1504.06640].

[189] C.-M. Chang and Y.-H. Lin, *Carving Out the End of the World or (Superconformal Bootstrap in Six Dimensions)*, *JHEP* **08** (2017) 128, [arXiv:1705.05392].

[190] N. Bobev, E. Lauria, and D. Mazac, *Superconformal Blocks for SCFTs with Eight Supercharges*, *JHEP* **07** (2017) 061, [arXiv:1705.08594].

[191] C. Beem, M. Lemos, P. Liendo, L. Rastelli, and B. C. van Rees, *The $\mathcal{N} = 2$ superconformal bootstrap*, *JHEP* **03** (2016) 183, [arXiv:1412.7541].

[192] F. A. Dolan and H. Osborn, *Conformal Partial Waves: Further Mathematical Results*, arXiv:1108.6194.

[193] A. L. Fitzpatrick and J. Kaplan, *Unitarity and the Holographic S-Matrix, JHEP* **10** (2012) 032, [arXiv:1112.4845].

Titre : Aspects des théories de champs conformes et champs quantiques en AdS

Mots clés : Théorie des champs, Théories conformes, Supersymétrie

Résumé : Nous étudions des aspects des théories quantiques et conformes, qui sont utiles pour décrire des systèmes comme les particules élémentaires et les transitions de phase dans les fluides et les aimants. Nos principaux résultats sont triples.

Premièrement, nous montrons que l'étude des théories quantiques des champs dans l'espace courbe peut être un moyen utile d'obtenir sa matrice S, qui fournit une description des processus de diffusion.

Deuxièmement, nous considérons les théories quantiques des champs sans interactions, et nous nous demandons si nous pouvons ajouter des interactions uniquement localisées sur un défaut de l'espace-temps. Nous montrons que de telles configurations ne peuvent pas être conformes de manière invariante.

Troisièmement, nous considérons des théories importantes pour la théorie des cordes et qui décrivent la gravité quantique. Nous expliquons comment les états avec un spin différent peuvent être regroupés en trajectoires, et montrons que ces trajectoires s'étendent beaucoup plus loin que dans la plupart des théories.

Title : Aspects of conformal field theories and quantum fields in AdS

Keywords : Quantum and conformal field theories, supersymmetry

Abstract : We study aspects of quantum and conformal theories, which are useful to describe systems as diverse as elementary particles and phase transitions in fluids and magnets. Our main results are threefold.

First, we show that studying quantum field theories in curved space can be a useful way to obtain its S-matrix, which provides a description scattering processes.

Second, we consider quantum field theories without interactions, and ask ourselves whether we can add interactions only localized on a defect in space-time. We show that such setups cannot be conformally invariant.

Third, we consider theories that are important in string theory and describe quantum gravity. We explain how states with a different spin can be grouped in trajectories, and show that these trajectories extend much further than in most theories.

Institut Polytechnique de Paris
91120 Palaiseau, France